UNIVERSITY OF SOUTHAMPTON

FACULTY OF MEDICINE

Cancer Sciences

Volume 1 of 1

In vivo manipulation of Fc gamma Receptor expression and activity through macrophage polarization

by

Lang Dou

Thesis for the degree of Doctor of Philosophy

October 2017

UNIVERSITY OF SOUTHAMPTON

ABSTRACT

FACULTY OF MEDICINE

Cancer Sciences

Thesis for the degree of Doctor of Philosophy

IN VIVO MANIPULATION OF FC GAMMA EXPRESSION AND ACTIVITY THROUGH MACROPHAGE POLARIZATION

Lang Dou

Over the last few years, it has become clear that immunotherapy has the potential to eliminate cancer. Macrophages have been shown to play a central role in tumour immunotherapy, especially direct targeting therapy with monoclonal antibodies (mAb). In tumours, macrophage populations are particularly heterogeneous, with several subpopulations of macrophage co-existing in the microenvironment. It has been documented that tumour associated macrophages can contribute to tumour progression and likely impact on the efficacy of immunotherapy.

In this project, we have combined various reagents, including toll-like receptor (TLR) agonists and stimulator of interferon genes (STING) ligands with anti-CD20 mAb in an attempt to polarise macrophages towards a pro-inflammatory phenotype to augment mAb efficacy. We found that the TLR3 agonist poly(I:C) polarized macrophages to a pro-inflammatory phenotype, and significantly promoted B cell depletion in vitro and in vivo by greatly increased the Fc gamma receptors (FcγR) activatory to inhibitory ratio on F4/80+ macrophages. We also demonstrated that B cell depletion using a murine version (Ritm2a) of the anti-human CD20 mAb rituximab is inhibited in the BCL_1 lymphoma model. Using the potent IRF3 activator and STING ligand DMXAA we were able to overcome tumour mediated suppression and recover mAb activity. Consistent with these data, DMXAA combined with anti-mouse CD20 mAb 18B12 markedly enhanced survival in the BCL_1 lymphoma model leading to cures in ~80-90% of mice.

Finally, we demonstrated that mAb against the co-stimulatory molecule 4-1BB (CD137) were able to inhibit tumour growth in an isotype dependent manner via two distinct mechanisms; agonism through activating CD8+ T cells and direct targeting by deleting intratumoural CD4+Foxp3+ regulatory T (Treg) cells. The activity of anti-4-1BB mAb was lost in FcγR deficient mice demonstrating that both mechanisms of action are dependent on FcγR. Further, compared to anti-4-1BB mIgG2a (LOB12.0 mIgG2a) alone, mAb administered in combination with poly(I:C) further suppressed tumour growth leading to earlier regression.

Thus, we would surmise that polarizing macrophages to a pro-inflammatory phenotype can be used as a general strategy to promote direct target anti-CD20 mAb and dual mechanism anti-4-1BB mAb activity via manipulation of FcγR expression on F4/80 high tissue resident macrophages. Our results suggest that in addition to modifying mAb to interact better with effector cells, enhancing the function of effector cells such as macrophages may represent a good strategy to improve anti-cancer mAb therapy. (383 words)

Table of Contents

List of Figures

DECLARATION OF AUTHORSHIP

I, Lang Dou declare that this thesis and the work presented in it are my own and has been generated by me as the result of my own original research.

In vivo manipulation of Fc gamma Receptor expression and activity through macrophage polarization I confirm that:

1. This work was done wholly or mainly while in candidature for a research degree at this University;
2. Where any part of this thesis has previously been submitted for a degree or any other qualification at this University or any other institution, this has been clearly stated;
3. Where I have consulted the published work of others, this is always clearly attributed;
4. Where I have quoted from the work of others, the source is always given. With the exception of such quotations, this thesis is entirely my own work;
5. I have acknowledged all main sources of help;
6. Where the thesis is based on work done by myself jointly with others, I have made clear exactly what was done by others and what I have contributed myself;

Parts of this work (part of figure 21, 30b, 35, 38, 40) have been published as:

White, A.L., et al., Fcγ Receptor Dependency of Agonistic CD40 Antibody in Lymphoma Therapy Can Be Overcome through Antibody Multimerization. The Journal of Immunology, 2014. 193(4): p. 1828-1835.

Dahal, L. N., L. Dou, K. Hussain, R. Liu, A. Earley, K. L. Cox, S. Murinello, I. Tracy, F. Forconi, A. J. Steele, P. J. Duriez, D. Gomez-Nicola, J. L. Teeling, M. J. Glennie, M. S. Cragg and S. A. Beers (2017). "STING Activation Reverses Lymphoma-Mediated Resistance to Antibody Immunotherapy." Cancer Research 77(13): 3619-3631.

Parts of this work (part of figure 42, 44, 46, 47b, 49b) have been submitted for publication as:

L.Dou.,et al., 4-1BB antibodies can eliminate tumors through depletion or agonism and are enhanced by engineering dual-activity mAb.

Signed: Lang Dou

Date: 19/08/2017

Acknowledgements

I would like to take this opportunity to express my gratitude to everyone who supported me throughout this project. I am thankful for their aspiring guidance, invaluably constructive criticism and friendly advice during the project work.

I express my warm thanks to Claude H.T Claude, Matthew J. Carter， Alison L. Tutt, Thomas R.W. Tipton, Lekh N. Dahal, Mark S. Cragg, everyone in the Antibody and Vaccine Group and the animal house. Special thanks to my supervisors Stephen Beers and Martin Glennie.

At last, I want to thank my parents, Jingyuan Yang and Yingming Dou for all kinds of sacrifice they made to let me finish this PhD.

Abbreviations

2-ME= 2-Mercaptoethanol

ADCC= Antibody-dependent cell-mediated cytotoxicity

ADCP= Antibody dependent cellular phagocytosis

ALCL= anaplastic large cell lymphoma

A : I= Activatory to inhibitory ratio

Akt = Protein Kinase B

APC= Antigen-presenting cell

Arg1= Arginase I

BCL_1= B-cell lymphoma 1

BCR= B-cell receptor

BM= Bone marrow

BMDM= Bone marrow derived macrophage

BTK= Bruton's tyrosine kinase

CARs=Chimeric T cell receptors

CCR= C-C chemokine receptor type

CCL= CC chemokine ligand

CD= Cluster of differentiation

CDR= Complementarity determining region

CFSE=Carboxyfluorescein succinimidyl ester

CHOP= Cyclophosphamide+Hydroxydaunorubicin+Oncovin+ Prednisone

CpG-ODN= 5'-C-phosphate-G-3' Oligodeoxynucleotide

CR= complete response

CRDs=C-type carbohydrate recognition domains

CSF-1= Colony-stimulation factor-1

CSF-1R= Colony-stimulation factor-1 receptor

CT26= Colon Tumor #26

CTSB= Cathepsin B

CTSS= Cathepsin S

CTLA-4= Cytotoxic T-lymphocyte-associated protein 4

CX3CR1= CX3C chemokine receptor 1

DC= Dendritic cell

DC-Sign= Dendritic cell-specific ICAM-3–grabbing nonintegrin

DMXAA= 5,6-Dimethylxanthenone-4-acetic acid

Fc= Fragment crystallisable

FcγR= Fc gamma receptor

FDA= Food and Drug Administration

FITC= Fluorescein Isothiocyanate

GAPDH=Glyceraldehyde 3-phosphate dehydrogenase

GM-CSF=granulocyte-macrophage colony stimulating factor

GPI= Glycosylphosphatidylinositol

H_2O_2= Hydrogen Peroxide

HER2= Receptor tyrosine-protein kinase erbB-2

HPRT= Hypoxanthine-guanine phosphoribosyltransferase

HSC= Hematopoietic stem cell

IC= Immune complex

Ig= immunoglobulin

IKK= IκB kinase

IL= Interleukin

iPLA2= calcium independent PLA phospholipase A2

IRF= Interferon regulatory factor

ITAM= Immunoreceptor tyrosine-based activation motif

ITIM= Immunoreceptor tyrosine-based inhibition motif

iNOS= inducible nitric oxide synthase

IFN= interferon

kDA = kDalton

KO = knockout

mAb= Monoclonal antibody

MAPK= mitogen-activated protein kinases

MCP-1= Monocytes chemoattractant protein-1

MCSF= Macrophage colony-stimulating factor

MDM= Human monocyte-derived macrophages

MDSC= myeloid-derived suppressor cell

MHC= Major histocompatibility complex

MMPs= matrix metalloproteinases

mRNA= Message RNA

MyD88= myeloid-differentiation factor 88

NFκB =nuclear factor kappa-light-chain-enhancer of activated B cells

NFAT= nuclear factor of activated T cells

NHL= non-Hodgkins lymphomas

NK= Natural killer

NOD= nucleotide-binding oligomerization domain

NSCLC= Non-small cell lung cancer

P53= Tumor protein p53

PAMPs= pathogen-associated molecular patterns

PAP=Prostatic acid phosphatase

PCD= Programmed Cell Death

PDAC= pancreatic ductal adenocarcinoma

PH= pleckstrin homology

PI3K= phosphatidalyinositol-3-kinase

PKC= protein kinase C

PLC-γ2= phospholipase C-γ2 PLC-γ2

Poly(I:C)= Polyinosinic-polycytidylic acid

PRRs= Pattern recognition receptors

PyMT= Polyoma Virus middle T antigen

Rab5= GTPase rab5

RIG-I=retinoid acid-inducible gene I

SCLC= small cell lung cancer

SCID= Severe combined immunodeficiency

Src= sarcoma

STING= stimulator of interferon genes

SHIP= Src homology 2 domain-containing inositol 5-phosphatases

TIRAP= TIR domain–containing adapter protein

TRIF=TIR-domain-containing adapter-inducing interferon-β

TRAF= TNF receptor associated factor

TRAM= TRIF-related adaptor molecule

Treg= Regulatory T cell

TRIF= TIR domain–containing adapter protein inducing IFN-b

TNFR= tumor necrosis factor receptor

SHP=protein tyrosine phosphatases

Src= Proto-oncogene tyrosine-protein

SRC-1=steroid receptor coactivator 1

SPARC=secreted protein acidic and rich in cysteine

Syk= Spleen tyrosine kinase

TAM= Tumour-associated macrophage

TBK1= TANK-binding kinase 1

TIE-2= Angiopoietin receptor Tie2

TLR= Toll-like receptor

T : NT= Target : non target

VEGF= vascular endothelial growth factor

WT= Wild type

Chapter I - Introduction

1.1 The roles of macrophages in innate and adaptive immunity

Macrophages are large phagocytic mononuclear cells. Recently, it has been demonstrated that mouse macrophages have two origins [1, 2]. Hematopoietic stem cell (HSC) derived macrophages are differentiated from circulating myeloid precursor cells from the bone marrow (BM) [1]. The differentiation of HSC to macrophage is mediated by colony stimulating factor 1 (CSF1). HSC derived macrophages are absent in osteopetrotic (op/op) mutant mice which possess an inactivating mutation in the CSF-1 gene [3]. The majority of tissue resident macrophages however develop from the yolk sac before the appearance of HSC [2]. Transcription factor myb has been shown to be crucial for developing HSC and hence HSC dependent macrophages [2]. In myb-/- mice, the HSC derived macrophages were absent in the skin, kidney, pancreas, spleen and lung [2]. On the contrary, myb is dispensable for the development of yolk sac derived macrophages. Yolk sac derived macrophages developed normally in myb-/- mice [2].

Several specific markers have been used to identified macrophages, in mouse F4/80, cluster of differentiation(CD)11b and colony-stimulation factor-1 receptor(CSF-1R), in human, CD64, CD68, CD163 and CD16 [4]. Combination of these markers allows us to distinguish macrophages from other myeloid lineage cells, such as neutrophils and basophils. For example, bone marrow derived macrophage (BMDM) were CD11b bright, F4/80 low, however, yolk sac derived macrophages were CD11b low and F4/80 bright [2].

Macrophages play an important role in innate and adaptive immunity (Figure 1). In innate immune responses, both human and mouse macrophages recognise pathogen-associated molecular patterns (PAMPs) on microorganisms through pattern recognition receptors (PRRs) (Figure 1), including macrophage mannose receptor (CD206) [5],

multiple Toll-like receptors (TLR) [6], nucleotide-binding oligomerization domain (NOD)-like receptors [7] and retinoid acid-inducible gene I (RIG-I)-like receptors [8]. The Mannose receptor does not possess signalling motifs on its cytoplasmic tail [5], microorganisms, such as Pneumocystis carinii [9] and C. albicans [10] are recognised by the C-type carbohydrate recognition domains (CRDs) on the mannose receptor extracellular domains, the bound microorganism is then internalised and transported to lysosomes for degradation [5, 9, 10]. Cytosolic dsRNA or 5′ -triphosphate ssRNA is recognized by C-terminal domains on RIG-I-like receptors, ultimately activating nuclear factor kappa-light-chain-enhancer of activated B cells (NFκB), and Interferon regulatory factor (IRF)3 [11]. Bacteria with peptidoglycan motifs, such as gram-negative bacteria can be recognised by NOD-like receptors, resulting in NFκB activation via the IKK pathway [7, 11]. TLRs are able to recognise a wide range of molecules derived from microbes [6]. Ligands binding to TLRs trigger the myeloid differentiation primary response gene 88 (MyD88) pathway which ultimately activates NFκB [6, 11]. In addition, stimulating TLRs also triggers a MyD88-independent, TIR-domain-containing adapter-inducing interferon-β (TRIF)-dependent pathway, result in IRF3 activation [6, 11]. Activating the NFκB pathway by PRRs induces production of several mediators, including pro-inflammatory cytokine IL1, IL6, IL12 [12] and chemokines CXCL8, CCL2 and CCL4 [13]. These cytokines and chemokines released by macrophages induce local inflammation and can activate Natural Killer (NK) cells [12, 13]. Additionally, activated mice BMDM produce a variety of toxic mediators that help kill microorganisms for example Nitric Oxide (NO), hydrogen peroxide (H_2O_2) and superoxide anion (O2-) [13]. Taken together, macrophages play a central role in innate immunity eliminating invading pathogens via phagocytosis, releasing inflammatory cytokines and the production of toxic mediators.

In adaptive immune responses, human and mouse macrophages can act as antigen-presenting cells (APC) [14] (Figure 1). Microorganisms or necrotic and apoptotic cells

can be recognised by macrophages, engulfed and then degraded into peptides in phagosomes. At the same time, ingestion of these materials stimulates the expression of major histocompatibility complex (MHC) class II. When phagosomes fuse with lysosomes, the degraded peptides are bound to the MHC II molecule in phagolysosomes, this MHC class II-peptide complex then moves to the plasma membrane and the peptides presented to T helper(T_h) cells [14]. T cells require three signals for full activation; antigen presentation provides the first signal to T_h cells, followed by a second co-stimulatory signal, for example the ligation of CD28 with B7 family protein [15]. The activated T_h cells start proliferating and releasing IL2, which binds to the same T_h cells in an autocrine manner or nearby T_h cells in a paracrine manner leading to full activation. Ligation by IL2 induces clonal expansion and enhances the proliferation of T_h cells [15].

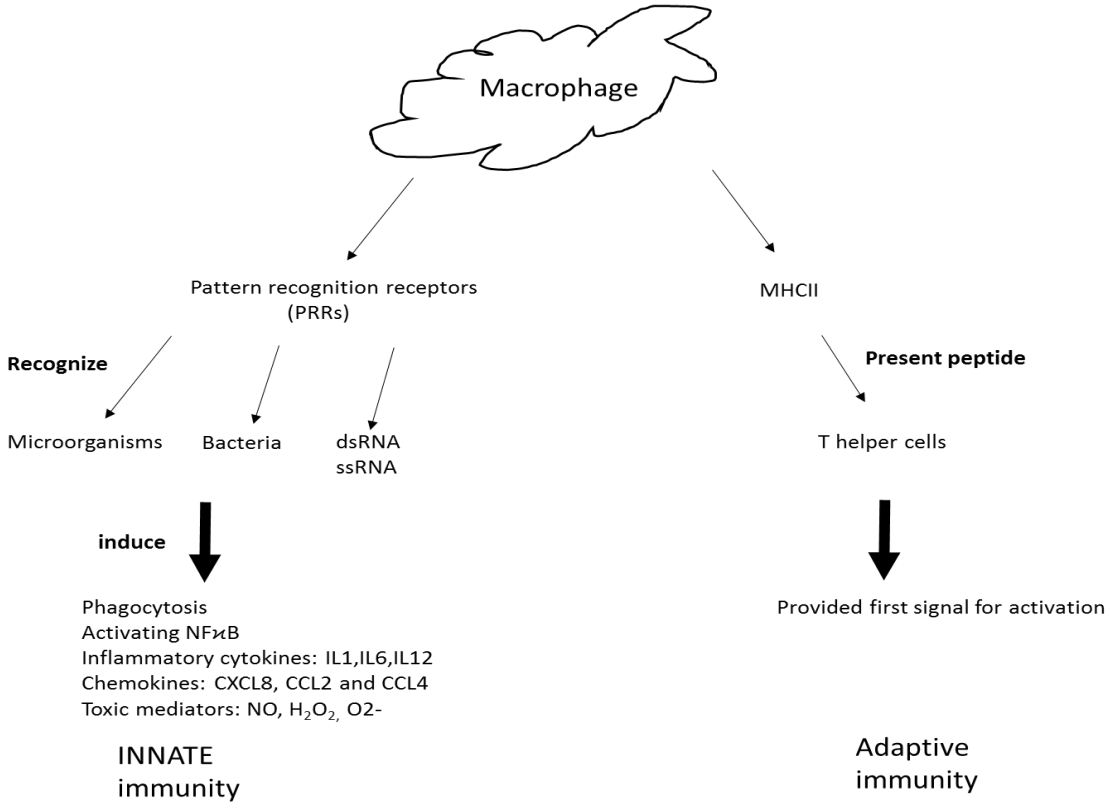

Figure 1: Macrophages in innate and adaptive immune response. In innate immune responses, PRRs, such as macrophage mannose receptors, Toll-like receptors, NOD-like receptors and RIG-I like receptors enable macrophages to recognise and respond to a wide range of pathogens. Binding with pathogen activates the NFκB pathway leading to the release of inflammatory cytokines and chemokines. In addition, activating PRRs on macrophages induces phagocytosis and the production of toxic mediators. In adaptive immune responses, macrophages can present phagocytosed peptide fragments to Th cells, thus providing an important signal for Th cells activation. In addition, inflammatory cytokines, such as IL12 released by macrophages can promote Th1 cell differentiation, thus enhance Th1 response.

1.2 Macrophages kill microorganisms by phagocytosis

Human and mouse macrophages are able to remove dead cells and cellular debris, eliminate pathogens such as bacteria and virus through a cellular process, known as phagocytosis. Phagocytosis is defined as the ingestion of large (≥0.5-μm) particles by cells and is important in maintaining tissue homeostasis [16]. Unlike other endocytic processes, such as micropinocytosis, phagocytosis is a receptor-regulated event [16]. In mouse system, PAMPs expressed on foreign particles, for example fungi, bacteria and parasites can be recognised by PRRs on macrophages and form membrane-bound vacuoles called phagosomes [16]. Once separated from the surface membrane, the

newly formed phagosome will undergo the phagosome maturation process that changes the composition of the phagosome [17]. During early maturation, nascent phagosomes fuse with early endosomes to form the early phagosome, which is characterised by recruitment of the GTPase rab5 (Rab5)[16]. Rab5 exerts its effects by recruiting and activating several effector proteins, for example, the mVps34 [18] and early endosomal antigen 1 (EEA1) [19]. Vps34 belongs to the Phosphatidylinositol-4,5-bisphosphate 3-kinase (PI3K) family. During early phagosome maturation, Vps34 is able to catalyze formation of the signalling lipid phosphatidylinositol 3-phosphate (PI(3)P) from phosphatidylinositol [18]. EEA1 binding to PI(3)P enhances docking and fusion of early endosomes [19]. The ablation of Vps34 by specific inhibitory mAb remarkably impairs phagosome maturation [18]. Finally, the early phagosome switches to a more mature, late phagosome that is characterised by the acquisition of different biochemical markers, including the small GTPase Rab7, and loss of early markers such as Rab5 [16]. The other key difference is that late phagosomes are more acidic than early phagosomes, as late phagosomes possess additional proton pumps that translocate H^+ from the cytosol to phagosomes [16].Late phagosomes can fuse with lysosomes forming the phagolysosome, this organelle is defined by its noticeable acidity (pH 4.5–5.0) [20]. Firstly, this acidic environment suppresses microbial growth [16]. Secondly, phagolysosome acidification itself can induce target degradation directly [16]. Finally, acidity can indirectly enhance phagolysosome degradative activity through the stimulation of proteolytic enzymes such as cathepsins D and L [21].Foreign bodies can be recognized by small soluble molecules found in the blood known as opsonins these include complement proteins; C3b, C4b, and iC3b, antibodies, and mannose-binding lectin [22]. Foreign bodies coated by opsonins are able to bind to opsonic receptors on macrophages and induce phagocytosis [20]. Immunoglobulin (Ig) G- Fc gamma receptor (FcγR) interaction is the best studied model. IgG recognise target antigen are bound to FcγRs on macrophages, this induces clustering of the FcγR, and activate a signalling

cascade (Section 1.4, page 8). Eventually the macrophage internalises the particle evoking phagocytosis and degradation of the target antigen.

1.3 Antibody

Antibody is also known as immunoglobulin, there are two types of Igs; membrane and soluble and they are produced by B cells. The membrane bound form is expressed on the surface of B cells as the B-cell receptor (BCR) [23]. Antigen binding to the BCR activates multiple downstream pathways, for example Bruton's tyrosine kinase (BTK), phospholipase C-γ2 (PLC-γ2) and phosphatidalyinositol-3-kinase (PI3K) [24], ultimately stimulating NFκB and nuclear factor of activated T cells (NFAT) [24]. These transcription factors are important in controlling B cell survival, proliferation, cytokine production and class switching, a process which allows B cells to generate different isotypes of antibody to perform particular tasks in the immune response [24]. The soluble form of Ig is primarily produced by a type of fully-differentiated B cell called a plasma cell [25]. Briefly, antigen-binding B cells are retained in the T-cell zone of the spleen, where they present antigen to CD4+ T helper cells. This process activates the CD4+ T helper cells, which then produce Tumour necrosis factor (TNF) superfamily member CD40 ligand and Interleukin (IL) 4 [25]. These mediators induce B cell proliferation and allow B cell differentiation into plasma cells [25]. To date, five isotypes of antibody have been identified in placental mammals, known as IgA, IgD, IgE, IgG, and IgM [15, 26] (Figure 2). They differ in their structure, biological properties and locations [15, 26]. IgG is the most abundant antibody isotype found in the circulation, accounting for 70-85% of the total Ig pool [26]. The molecule weight of IgG is approximately 150 kilo Dalton (kDa). IgG consists of two identical heavy chains and two identical light chains, these polypeptide chains are linked by disulphide bonds and form a “Y” shaped structure [15, 26] (Figure 2). The top part of the antibody contains two F(ab) regions which are responsible for antigen binding, while the bottom part, known as Fragment crystallisable (Fc) region, mediates effector engagement [15, 26]. The antigen binding site is located on the tip of the F(ab)

region, an area called the complementarity determining regions (CDR), which bind to a particular antigen, thus determining antibody specificity and avidity [15, 26]. There are four IgG subclasses in human: IgG1, 2, 3 and 4 [27] and five subclasses in mice: IgG1, 2a, 2b, 2c and 3 [28]. IgG is able to remarkably enhance phagocytosis through opsonisation. In addition, IgG can also activate complement. Briefly, antibody-pathogen immune complexes bind to C1q triggering the classical complement pathway. As a result, C5b, C6, C7, C8, and polymeric C9 are recruited to the pathogen surface, generating the membrane attack complex. These complexes form transmembrane channels and induce the osmotic lysis of the target pathogen [15].Similar to IgG, monomeric IgA consists of two heavy chains and two light chains. IgA is the most important antibody in mucous secretions, such as tears, saliva, sweat and secretions from the gastrointestinal tract [15, 26]. In the mucosa, IgA exists in the dimeric form with a J chain linking two identical molecules together (Figure 2). The function of IgA is to stop microbes binding to mucous membranes, and this isotype represents 5%-15% of the total Ig pool [15, 26]. Unlike IgG, IgM contains an additional constant domain in its Fc region (Figure 2). In serum, IgM is present as a pentamer joined by the J chain (Figure 2) and represents 5%-10% total antibody pool [15, 26]. IgM is the first antibody to reach the site of infection, because IgM has not undergone class switching, thus is fast to produce and provides immediate protection [15, 26]. IgD accounts for 1% of total Ig pool and the precise function of IgD is still unknown [15]. IgE is the least abundant isotype, it only accounts for 0.05% of total Ig in blood serum. The major role of IgE is to generate immunity against parasites, for example Fasciola hepatica and Trichinella spiralis [29]. Additionally, IgE also mediates type I hypersensitivity where mast cells become activated against harmless antigen [29]. Type I hypersensitivity induces several allergic diseases such as food allergies, allergic asthma and allergic rhinitis [29].

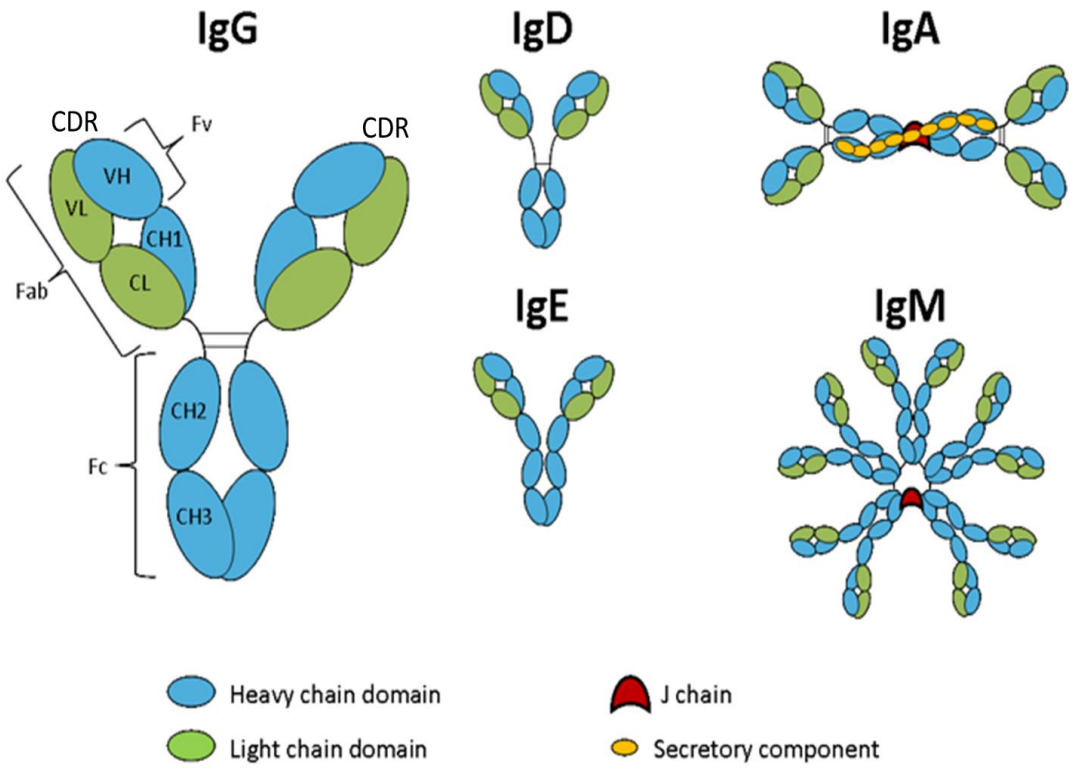

Figure 2: The structure of different isotypes of immunoglobulin. There are five isotypes of antibodies: IgG accounts for 70-85% total immunoglobulin pool and is important in activating phagocytosis and complement. IgA represent 5%-15% of total antibody pool is the predominant Ig for mucous immunity. IgM plays an essential role in the primary immune response and represent 5%-10% of total Ig. The least abundant IgE is crucial for parasite immunity and allergic reactions. The precise function of IgD is unknown. (Image is cited from [26])

1.4 Fc gamma Receptors

FcγRs act to link the adaptive humoral immune response mediated by antibodies to innate immune effector cell function. In mouse and human systems, FcγRs are expressed on a wide range of immune cells, for example B cells, dendritic cells (DC), natural killer (NK) cells, macrophages, monocytes, neutrophils, eosinophils and basophils. The expression of FcγRs on these effector cells is essential in regulating their function. For instance, multiple FcγRs expressed on macrophages mediate antibody dependent cellular phagocytosis (ADCP) [15]. NK cells eliminate target cells via

antibody-dependent cell-mediated cytotoxicity (ADCC) [30], this process is regulated by FcγRIII. In addition, the activation of B cell is negatively regulated by FcγRII [30].

To date, four subclasses of FcγRs have been identified in mouse: FcγRI (CD64), FcγRII (CD32), FcγRIII (CD16) and FcγRIV (Figure 3) [30]. Due to the presence of allelic FcγR variants, human FcγRs are more complex. Based on genomic localization and gene sequence analysis human FcγRIA corresponds to mouse FcγRI, human FcγRIIB to mouse FcγRII, human FcγRIIA to mouse FcγRIII and human FcγRIIIA to mouse FcγRIV [30]. To avoid confusion, FcγRII will be used to represent either mouse or human FcγRII/FcγRIIB in the rest of content. Both human and mouse FcγRs have different affinities to IgG isotypes [27, 28]. For example, Human IgG1(hIgG1) and hIgG3 bind to all human FcγRs, hIgG2 binds only to human FcγRIIA and the V158 polymorphic form of FcγRIIIA (there are two polymorphic alleles of the gene-encoding FcγRIIIA which confer differential mAb binding V_{158} has a higher affinity and F_{158} a lower affinity) [31]. Mouse IgG1(mIgG1) can bind to mFcγRII and mFcγRIII, mIgG2a and mIgG2b are able to bind to all mouse activatory FcγRs, mFcγRI, mFcγRIII and mFcγRIV [31], whilst mIgG3 can only bind to mFcγRI [31]. Notably, mIgG2a also interacts with mFcγRII but only at low avidity [31].

The majority of FcγRs are multi-subunit complexes, with an extracellular α chain and, intracellular γ chain. The function of the α chain is to recognize and bind immunoglobulin, and the γ chain is required for signal transduction through its Immunoreceptor tyrosine-based activation motif (ITAM) signalling motif [32]. The exceptions to this rule are mouse FcγRII, human FcγRIIA and FcγRII, these receptors are single chain receptors, in which the γ chain signalling function is replaced by signalling competent cytoplasmic domain of their α chains containing ITAM for human FcγRIIA or Immunoreceptor tyrosine-based inhibition motif (ITIM) for both mouse and human FcγRII respectively (Figure 3) [30]. Glycosylphosphatidylinositol (GPI)-linked receptor FcγRIIIB has no cytoplasmic domain, it has been proposed that FcγRIII acts via synergizing with other FcγRs [30]. FcγRs can

be classified into activatory FcγRs and inhibitory FcγRs. Activatory FcγRs, such as mouse FcγR I, III and FcγR IV interact with the common γ chain which possesses an ITAM in the intracellular domain [33, 34]. Crosslinking FcγRs with immunoglobulin leads to the activation of sarcoma (Src) family kinases, such as Hck, Fgr and Lyn, which then phosphorylate tyrosine residues on the ITAM. Experiments using Hck−/−, Fgr−/−, and Lyn−/− triple-deficient phagocytes led to delayed phagocytosis [35]. The phosphorylated ITAM motif then becomes a docking site for the SH-2 domains of Spleen tyrosine kinase (Syk). Activated Syk then triggers downstream pathways, such as protein kinase C (PKC), phosphatidylinositol-4,5-bisphosphate 3-kinase (PI3K) and calcium independent phospholipase A_2 ($iPLA_2$) [33, 34], resulting in the enhancement of macrophage mediate phagocytosis and pro-inflammatory cytokine release. The importance of $iPLA_2$ in FcγR dependent phagocytosis was demonstrated by studies where they administered bromoenol lactone, a selective inhibitor of $iPLA_2$, to macrophage resulting in the arrest of phagocytosis [36]. In addition, treating FcγR transfected COS-l cells, a fibroblast/epithelial-like cell line, with the PI3K specific inhibitor wortmannin also reduced phagocytosis [37]. Although the precise role of PKC in phagocytosis is still elusive, it has been observed that PKC accumulates in macrophage phagosomes during phagosome maturation [38].

FcγRII is the only inhibitory FcγR and was first identified as expressed on B cells, but subsequent research has revealed that FcγRII is widely expressed on hematopoietic cells providing negative feedback [34]. FcγRII-/- mice spontaneously develop autoimmune glomerulonephritis in a strain-specific manner [39], suggesting that FcγRII is crucial in tuning immune responses. FcγRII carries an immunoreceptor tyrosine-based inhibition motif (ITIM) in its cytoplasmic domain. Crosslinking of FcγRII with activating receptors, for example the activated BCR, induces ITIM phosphorylation, which then becomes the docking site for protein tyrosine phosphatases (SHP)-1 and -2. These two phosphatases dephosphorylate tyrosines on the stimulated BCR, which in turn leads to

the dephosphorylation of several protein-tyrosine kinases that are important in activating PLC-γ2 pathway, including Spleen tyrosine kinase (SYK) and BTK. These signalling events eventually supress the early activatory signalling events counteracting the stimulation [32, 34].

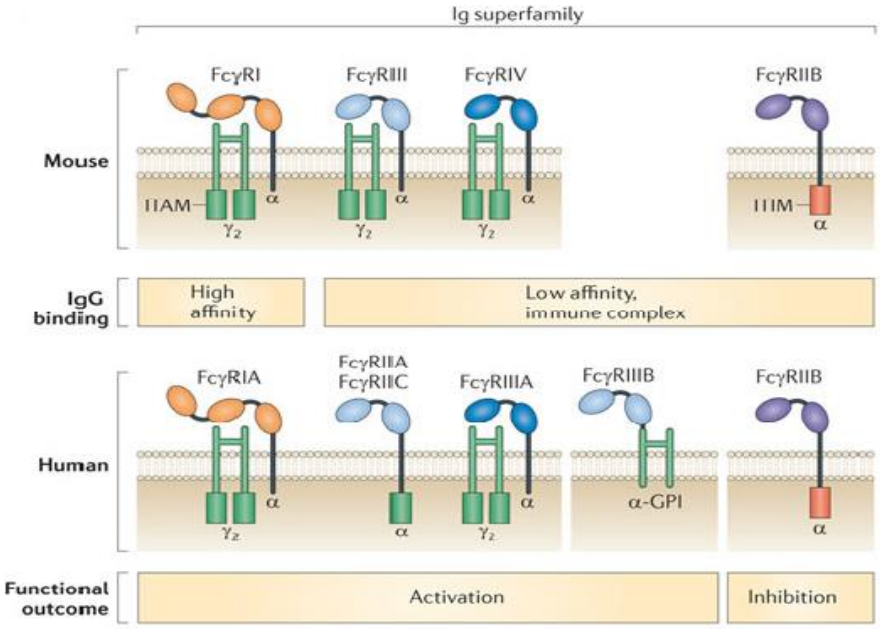

Figure 3: The family of Fc gamma receptors. The difference between mouse and human FcγRs. Three mouse activatory FcγRs have been identified. These activatory FcγRs contain α chain to recognize and bind immunoglobulin, and a γ chain for signal transduction. There are four activatory FcγRs in human: FcγRIA, FcγRIIA/IIC, FcγRIIIA and FcγRIIIB. Similar to mouse activatory FcγRs, human FcγRIA and FcγRIIIA have an α chain and γ chain in their cytoplasmic domains. FcγRIIA/IIC only contain an α chain in the cytoplasmic domain. FcγRIIIB is a GPI-linked receptor, thus has no cytoplasmic domain. Both human and mouse have a single chain inhibitory receptor FcγRII. Additionally, FcγRI is the only high affinity FcγR expressed on mouse and human effector cells (Figures are cited from [40]).

1.5 The plasticity of macrophage

Phenotypically, macrophages are considered to be highly plastic cells, which means that they can be polarised to different activation states in response to external stimuli. This plasticity is reflected in the fact that macrophages have the most complex cellular transcriptome described to date [41]. According to their activation state, both human and mice macrophages can broadly be classified into pro-inflammatory M1 macrophages [42],

also known as classically activated macrophages and anti-inflammatory M2 macrophages, also called alternatively activated macrophages [43-45].

Stimulation by the TLR 4 agonist Lipopolysaccharides (LPS) and the pro-inflammatory cytokine IFN-γ skews macrophages towards an M1 phenotype characterised by the release of inflammatory cytokines, such as IL12, and TNFα. These inflammatory cytokines induce local inflammation and promote T helper cell 1 dominant T lymphocyte responses [41, 44]. Pro-inflammatory macrophages also increase their production of inducible nitric oxide synthase (iNOS), which catalyses the production of nitric oxide (NO) from L-arginine. NO has broad biological functions, including helping to control infections, relaxing muscle and regulating tumour growth [46, 47]. NO is able to induce microbe DNA damage through production of the metabolite peroxynitrite [47]. iNOS-deficient mice have been shown to have increased susceptibility to Listeria monocytogenes [48]. Importantly, NO rapidly binds to ferrous iron with high affinity inducing the production of cyclic-GMP, which then causes calcium re-uptake, ultimately lead to muscle relaxation [46]. The role of NO in cancer is controversial, in Apc(Min/+)Nos2(-/-) mice, the absence of iNOS promoted adenoma tumorigenesis [49]. DNA damage induced by NO, triggered accumulation of tumour protein p53 (p53), which initiated apoptosis and stopped tumour growth [46]. In contrast, Jenkins et al transfected a murine iNOS cDNA cassette into human carcinoma cell line DLD-1 to allow tumour cells to generate NO continuously [50]. They found engineered tumours grew faster than wild type tumours in nude mice [50].

T helper cell 2 cytokines IL4 and IL13 polarise macrophages to an M2 phenotype [43]. Stimulation with IL4 and IL13 activates Janus kinases1,3(JAK1, JAK3) and phosphatidalyinositol-3-kinase(PI3K) pathway, ultimately leading to phosphorylate Signal transducer and activator of transcription 6 (STAT6)[45]. The phosphorylated STAT6 then migrates to cell nucleus, and binds to promoters of genes, including genes regulate cell proliferation and expression of IL10 [51].Unlike the M1 phenotype, M2 macrophages express no or low levels of inflammatory mediators and have enhanced arginase

production, in support of their role in tissue repair [52] and regulation of the immune response [43, 45]. M2 macrophages also produce insulin-like growth factor-1 that helps sustain M2 activation and tissue regeneration [53]. Several surface markers are used to distinguish M2 macrophages, including: CD206 (C-Type Mannose Receptor 1) and CD163 (Hemoglobin-Haptoglobin Scavenger Receptor). In injured muscle, CD206 positive macrophages have been shown to generate hepatocyte growth factor that can promote muscle fibre regeneration [54]. In a rat model, CD163 expressing macrophages are present in the liver after birth and are maintained throughout adulthood, implying that M2 macrophages may also be involved in embryonic and postnatal development [55]. In addition, M2 macrophages are poor antigen presenting cells, they predominately release anti-inflammatory cytokines IL10, which can inhibit Th1 cytokines released by CD4+ T cells [51].

1.6 Tumour associated macrophages

1.6.1 Macrophages are essential components of tumour microenvironment

The function of macrophages in tumour initiation, progression and metastases is controversial [56]. Tumour-associated macrophages (TAM) are an important component of the tumour microenvironment [43]. In late stage solid tumours, for example breast cancer, TAM represent an anti-inflammatory, pro-angiogenic population, and therefore promote tumour progression and metastasis [43]. Genetic ablation of macrophage colony stimulating factor 1 (CSF1) in the Polyoma Virus middle T antigen (PyMT) mouse model of breast cancer, significantly inhibited tumour progression [57]. In the same PyMT model, Segall and colleagues showed that TAM are required for breast cancer cell migration [58]. Results from clinical studies also support this contention; there is a strong negative correlation between macrophage number and patient relapse-free survival from lung [56] and thyroid [59] tumours. Additionally, in Hodgkin's lymphoma increased TAM numbers were significantly associated with shortened survival in patients [60]. In contrast, one

study in non-small cell lung cancer (NSCLC) demonstrated that patients with a higher percentage of islet macrophages survived longer [61]. Moreover, two recent studies on follicular lymphoma reported that patients with higher content of TAMs had a more favourable response to rituximab containing immunochemotherapy [62, 63]. Suzuki and colleagues used deep sequencing techniques to measure the transcription state of the THP-1, human acute monocytic leukemia cell line through a time course and demonstrated that human macrophages have the most complicated transcriptome known [41]. Together, these data suggest that TAM are highly heterogeneous populations and that although subpopulations of TAM may have many features in common it is highly likely that certain TAM subpopulations are organ and tumour specific [64].

1.6.2 The role of tumour associated macrophages switches along with tumour progression

It has been well documented that human tumours are infiltrated by inflammatory cells, for example effector T cells, B cells, NK cells and macrophages [65]. The presence of these inflammatory cells has been taken as evidence that our body does not ignore a growing tumour, instead it attempts to prevent tumour progression. The primary goal of inflammation is to eliminate invading foreign bodies, for instance bacteria and virus [66]. However, compared to infections, tumour cells only evoke weak cellular and humoral responses [67]. This may be because most tumour-associated antigens are considered as self-antigens [67]. To avoid damage to “self” tissue, the host recruits regulatory cell populations, such as regulatory T cell (Treg) [68] and myeloid-derived suppressor cell (MDSC) [69] to downregulate the immune response thereby suppressing its own response to the tumour. These mediators establish a chronic inflammatory environment that has been widely agreed to favour tumour development and progression [65].

Initially the inflammatory tumour environment skews macrophages into a pro-inflammatory (M1-like) phenotype that is characterised by production of IL12 and increased expression of co-stimulatory molecules CD80/86 and MHC II (Figure 4)[64]. These cytokines and receptors are important in Th1 cell differentiation and activation, suggesting that pro-inflammatory macrophages can stop tumours developing indirectly by stimulating T-cell mediated immunity [70]. Accumulation of suppressor populations, such as Treg and MDSC, allows TAMs in concert with other immune cells to form a chronic inflammatory environment [71], which is defined by the release of inflammatory mediators TNF-α and iNOS [64, 65]. NO is an essential cellular signalling molecule, which can act to promote survival of cancer and enhance tumour angiogenesis [72, 73]. The role of TNF-α in tumour progression is paradoxical. Balkwill demonstrated that physiologic and pathologic levels of TNF-α may promote tumour growth [74]. Additionally, it has been suggested that deletion of TNF-α by specific mAb might be therapeutically useful for renal cell carcinoma [75]. However, in contrast TNF-α has also been shown to be able to induce apoptosis of the LNCaP human prostate adenocarcinoma cell-line in a dose dependent manner [76]. The different roles of TNF-α in tumour growth may depend on the dose of cytokine and the context of the experiment [77]. For example, at low concentrations (0.5–50 ng/mL) TNF-α induces angiogenesis in vitro, characterised by the formation of capillary-tube-like structures [77]. This effect is supressed by using high concentration (500 ng/mL) of TNF-α [77]. As tumours become more established, the macrophage phenotype switches from pro-inflammatory to anti-inflammatory, with decreased expression of TNFα and iNOS [78] and increased production of the immunomodulatory cytokine IL10 [79] and arginase 1 [80] (Figure 4). The latter impairing T cell responses by reducing the expression of the T-cell receptor CD3 zeta chain [80].

IL4 released by CD4+ T cells or the tumour cells themselves can skew macrophages toward an invasive phenotype that is characterised by the generation of epidermal

growth factor (EGF) [79]. In the PyMT mouse model, macrophage promoted tumour invasion and migration is significantly decreased in the absence of IL4 [79]. Invasive macrophage mediated tumour migration is regulated by EGF [58]. CSF-1 released by tumours cells stimulates invasive macrophages, in response to this stimulation macrophages start to produce EGF, which then activates tumour cells and enhances tumour migration [58]. Several experiments have shown that macrophage activated migration can be recapitulated in vitro, using different systems, such as the collagen overlay [81] and the mammary epithelial organoid culture model [79]. In contrast, knocking out the steroid receptor coactivator 1 (SRC-1) which mediates CSF-1 release, reduced tumour migration in the PyMT tumour model [82].

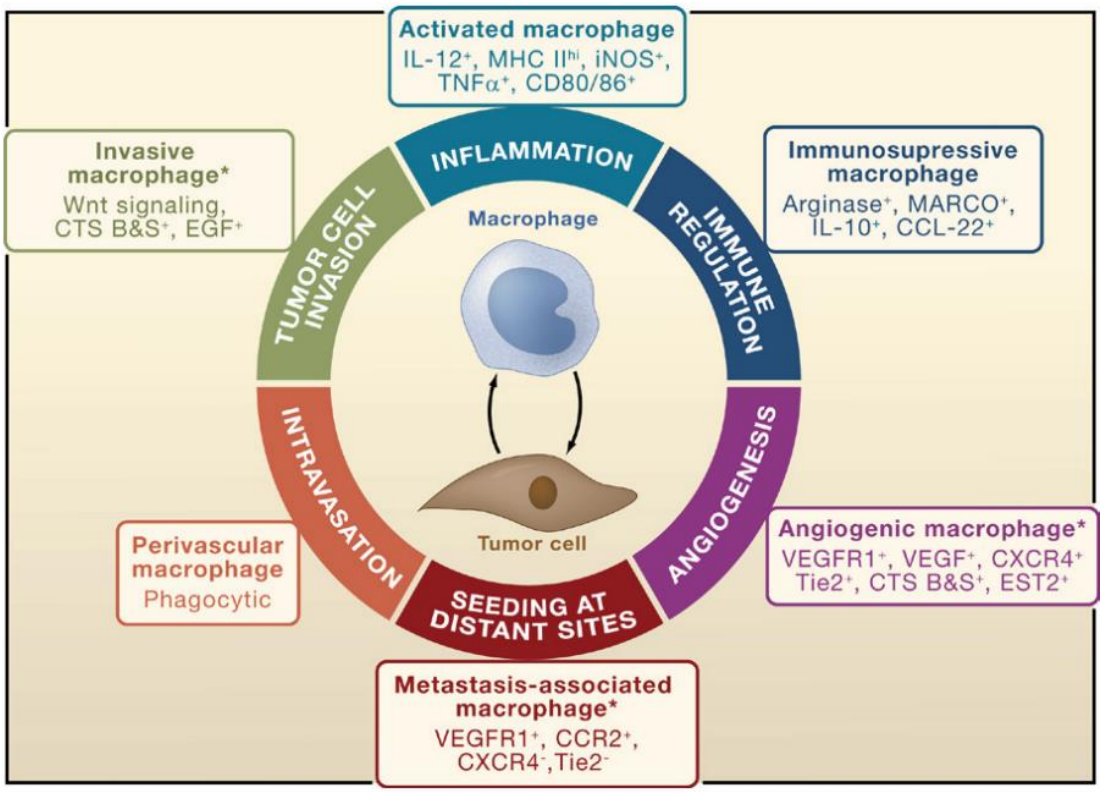

Figure 4: Macrophage phenotypes and tumourigenesis. CD11b+, F4/80+ macrophages are educated by the tumour microenvironment and may result in the formation of six tumour associated macrophage sub-populations. In early stage cancer, the inflammatory environment skews macrophages into an inflammatory phenotype that defined by expression of CD80/CD86, MHC II and the production of IL12. Accumulation of suppressor cells lead to a chronic inflammatory environment, where macrophage start producing TNF-α and iNOS. As tumour burden increases further, macrophages switch to an anti-inflammatory phenotype, characterised by releasing arginase 1 and IL10. In addition, IL4 derived from the tumour environment skews macrophage to an invasive phenotype, this phenotype characterised by the expression of EGF, Cathepsins and matrix metalloproteinases. Angiogenic macrophages express vascular endothelial growth factor, angiopoietin receptor Tie2 and matrix metalloproteinases 9. Metastasis-associated macrophages produce versican that help to promote tumour metastatic efficiency. This phenotype is defined by the expression of CXCR4, CCR2 and VEGFR1. (Figure is cited from [64]).

In addition, macrophages have been shown to be important in developing extracellular matrix (ECM) via synthesis of osteonectin, also known as secreted protein acidic and rich in cysteine (SPARC) [83]. Osteonectin is a 40 kDa calcium-binding glycoprotein that plays an important role in cell-matrix interactions and collagen binding [83]. Overexpression of osteonectin in human pancreatic ductal adenocarcinoma (PDAC) correlates with disease progression and poor prognosis [83]. Sangaletti and colleagues demonstrated that osteonectin is required for spontaneous metastasis from primary tumours [84]. Invasive macrophages also produce a series of proteases, which break down the basement membrane matrix and this process is suggested to free tumour cells from basement membrane restriction allowing tumour migration [85]. These proteases

include, Cathepsins and matrix metalloproteinases (MMPs). Cathepsin B (CTSB) and S (CTSS) are cysteine proteases. Depletion of CTSB or CTSS using knockout mice, PyMT;ctsb−/− [86] , ctss−/−RT2 [87] reduced tumour invasion and metastasis. MMPs are endopeptidases, which break peptide bonds in a zinc dependent manner. According to substrate specificity, MMPs can be divided into four subgroups. The Kitamura group showed that MMP2, MMP9 and CC-chemokine receptor 1 (CCR1) expressed on CD34+ immature myeloid cells are required for tumour invasion in a colon model. Deletion of CCR1 stopped CD34+ cells migrating towards tumour epithelium that expressed CCR1 ligand CC chemokine ligand 9 (CCL9), this prevented accumulation of CD34+ immature myeloid cells at the invasion front and suppressed tumour invasion [88].

During tumour development, the balance between pro- and anti-angiogenic factors moves towards a pro-angiogenic outcome, which plays a role in switching the tumour from a dormant to malignant form [89]. This angiogenic switch is a hallmark of the benign-to-malignant transition in most tumours [89]. Several cells have been shown to be involved in this complicated transition, in particular tumour associated macrophages, which are central to this process [90] (Figure 4). Lin and colleagues used mice carrying the homozygous null allele for CSF-1 (*Csf1*^{op}). They found that depletion of macrophages delays the angiogenic switch [91]. In contrast, overexpression of CSF-1 in PyMT mice increased the infiltration of macrophages and dramatically accelerated the formation of vessel networks [91]. Additionally, in the Lewis lung carcinoma model, depletion of macrophage via liposome-encapsulated clodronate result in angiogenesis suppression [92]. These angiogenesis promoting macrophage sub-populations are characterized by expression of the angiopoietin receptor Tie2 (TIE-2) and production of vascular endothelial growth factor (VEGF) (Figure 4). Upon activation by angiopoietins, TIE-2 has been demonstrated to promote angiogenesis. In the PyMT model, two subpopulations of macrophage expressing distinct levels of TIE-2 have been identified [93]. At the same time, macrophages are able to generate MMP9, which then releases VEGF from

extracellular depots. The bisphosphonate, zoledronic acid, can stop metalloprotease activity in macrophages [94]. In a cervical carcinogenesis model, mice treated with zoledronic acid showed inhibited MMP9 expression on macrophages, this reduced VEGF production and impaired tumour angiogenesis [94].

In the metastatic process cells released from primary tumours travel to distant sites via the circulatory or lymphatic systems, after which these cells need to extravasate and then survive long enough in the tissue to successfully seed at metastatic sites [93]. Thus metastasis is not an efficient process, primary tumours require production of helping factors to promote metastatic efficiency, for example, versican [93]. Versican is a tumour-derived extracellular matrix protein. In the Lewis lung carcinoma model, versican binds to TLR2 and TLR6 triggering IL6 and TNFα release. These two cytokines are indispensable for the development of tumour metastases in the Lewis lung carcinoma model [95]. Several experiments have demonstrated that the accumulation of myeloid cells in a distant site, also called the premetastatic site, are important to improve the efficiency of metastases [96]. Myeloid cells at premetastatic sites indirectly secrete matrix-bound VEGF via production of MMP9. The VEGF induced by MMP9 has been shown to promote efficiency of lung-specific metastasis [97]. Indeed, at these premetastatic sites myeloid cells have not yet been fully characterised. Data from Kappan et al. suggest that these myeloid cells are mononuclear phagocytic cells and CD11b, VEGF positive [96]. Thus, it is possible that at these premetastatic sites the accumulating myeloid cells are a subpopulation of TAM [93]. When tumour cells arrive at the metastatic site and start to extravasate, they start recruiting macrophages. In the PyMT mouse model, depletion of these premetastatic macrophages by liposome encapsulated clodronate significantly decreased extravasation efficiency and subsequent metastatic growth [98]. Studies characterising prometastatic macrophages suggest they are F4/80+CSF-1R+CD11b+Gr1- CX3C chemokine receptor 1^{high} ($CX3CR1^{high}$) $CCR2^{high}$ and $VEGFR1^{high}$ [98]. Using a diptheria transgene approach to ablate CD11b+ macrophage in a lung

metastasis model dramatically decreased tumour cell metastatic potential, with both seeding and persistent growth impaired [98].

1.7 Toll-like Receptors

Macrophage function is mediated by PRRs that recognise foreign bodies and initiate subsequent signalling events (Section 1.1, page 1)[6]. One well characterised PRR family are the TLR.TLRs are type I transmembrane proteins, which recognise and bind to PAMP through leucine-rich repeat ectodomains [6]. Depending on the cellular location, TLRs can be divided broadly into two subgroups. The first group composes TLRs expressed on the cell surface, including TLR1, TLR2, TLR4, TLR5, TLR6 and TLR11 (Figure 5) [6]. The other group consists of TLR3, TLR7, TLR8 and TLR9 and these receptors are expressed intracellularly, variously in endosomes, lysosomes and the endoplasmic reticulum (Figure 5) [6]. Different ligands of TLRs have been discovered, including for TLR1/2: Di/triacyl lipopeptides, TLR3: polyinosinic:polycytidylic acid (Poly(I:C)) and double-strand RNA; TLR4: LPS; TLR5: flagellin; TLR7/TLR8: single strand RNA and TLR9: CpG Oligodeoxynucleotide (CpG ODN) [99]. See list below:

Receptors	Ligands	Locations
TLR 1	Di/triacyl lipopeptides	Cell surface
TLR 2	Di/triacyl lipopeptides	Cell surface
TLR 3	Polyinosinic:polycytidylic acid (Poly(I:C)) and double-strand RNA	Cell compartment
TLR 4	Lipopolysaccharide	Cell surface
TLR 5	Flagellin and profilin	Cell surface
TLR 6	multiple diacyl lipopeptides	Cell surface
TLR 7	single strand RNA	Cell compartment

TLR 8	single strand RNA	Cell compartment
TLR 9	CpG Oligodeoxynucleotide	Cell compartment

Upon activation by ligand, TLR1, TLR2, TLR7 and TLR9 signal through the adapter molecule myeloid-differentiation factor 88 (MyD88), while TLR3 transduces signals through TIR domain–containing adapter protein inducing IFN-β (TRIF)-dependent pathway [6, 100] (Figure 5). It is noteworthy that stimulating TLR4 with LPS triggers both MyD88 and TRIF dependent pathways [6, 100].

TLR1, TLR2 and TLR4 stimulate MyD88 dependent pathway through TIR domain–containing adapter protein (TIRAP), which ultimately activates NFκB through the IKK pathway. Briefly, inhibitor of kappa B protein suppresses NFκB via masking of its nuclear localization signal. Stimulating IKK specifically phosphorylates the inhibitor of kappa B protein, which then dissociates from NFκB. This results in NFκB nuclear translocation and activation [6, 100]. NFκB has a broad range of functions, including controlling cell proliferation, maintaining cell survival and producing inflammatory cytokines [101]. However TIRAP is not required for TLR7 and TLR9 to trigger the MyD88 pathway [100]. TIRAP-deficient LPS-induced splenocytes demonstrate remarkably decreased proliferation and IL-6, TNF-α and IL-12 cytokine production [102]. Additionally, in response to stimulation with the TLR9 ligand CpG, Wild-type and TIRAP-deficient macrophages produced comparable amounts of IL-6, TNF-α and IL-12 [102].

Activation of TLR3 or TLR4 triggers the TRIF pathway, which allows IkB kinases IKKε and TANK-binding kinase 1 (TBK1) to phosphorylate IRF3. IRF3 then translocates to the nucleus and activates interferon (IFN) β gene expression [6, 99] (Figure 5). It has been shown that TRIF-related adaptor molecule (TRAM) is necessary for TLR4 triggered TRIF-dependent responses, while it's dispensable for TLR3 induced responses [103]. Masahiro et al found that in response to LPS stimulation, the gene encoding for IFNβ *Ifit2*

was strongly impaired in TRAM-deficient mice peritoneal macrophages [103]. Whereas WT and TRAM-deficient peritoneal macrophages revealed similar amounts of *Ifit2* expression when stimulated by TLR3 ligand poly(I:C) [103]. TRIF can also induce NFκB activation through TNF receptor associated factor (TRAF)6 [6, 103] (Figure 5).

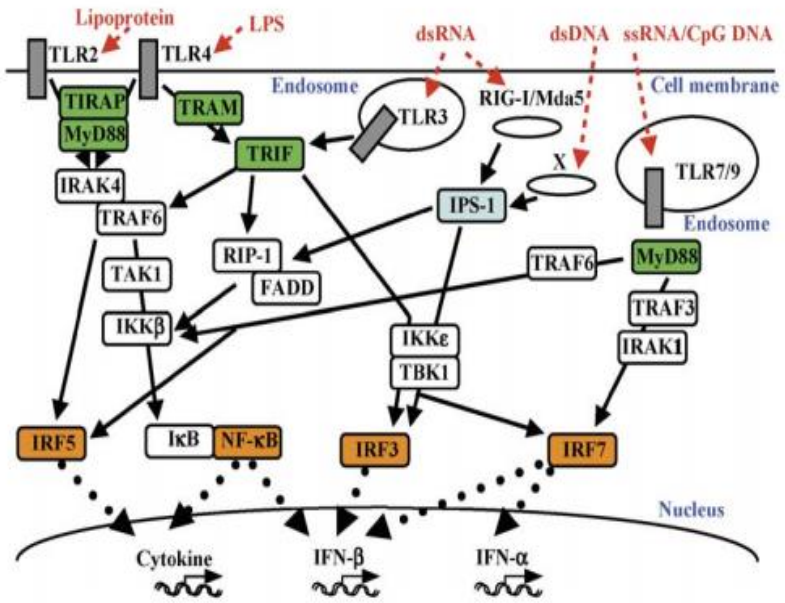

Figure 5: TLR signal pathway. TLR 2, TLR 7 and TLR 9 stimulation triggers a MyD88 dependent pathway through the IKK axis, resulting in NFκB activation. TLR 3 stimulation induces a TRIF dependent pathway, ultimately activating IRF3. Stimulation by the TLR4 agonist LPS triggers both MyD88 dependent and TRIF dependent pathways (Figure is cited from [6]).

1.8 Toll-like Receptors in cancer

In the 18th century, Coley found that injecting heat-killed bacteria, for example species of Streptococcus pyogenes and Serratia marcescens ('Coley's toxin') caused tumour regression [104]. Later, research found that one component of Coley's toxin is the TLR4 agonist LPS. Stimulation by LPS activated antigen presentation cells, particularly dendritic cells (DC), which in turn activated cytotoxic T lymphocytes (CTL) and natural killer (NK) cells in a type I IFN-dependent manner [105]. Once activated, NK cells are able to induce tumour cell death directly by releasing granzyme B and perforin [106]. These two proteinases eliminate tumour cells through lysing the plasma-membrane and

inducing apoptosis [106]. Similar to NK cells, activated CTL destroy tumour cells via the release of granzymes [107].

To date, advances in TLR biology have demonstrated that the role of TLR in cancer is controversial. Stimulating TLR3, TLR7/TLR8 or TLR9 have been shown predominantly to suppress tumour growth through activating myeloid DC which induce NK cell activation [108]. In a genetic model of prostate cancer overexpressing the transgenic adenocarcinoma of the mouse prostate (TRAMP) transgene, administration of the TLR3 agonist poly(I:C) suppressed tumour growth [109]. Additionally, treatment with poly(I:C) increased NK cell infiltration and reduced tumour growth in a mouse model transplanted with highly aggressive hepatocellular carcinoma [110].

TLR7/TLR8 agonist imiquimod is the most successful TLR agonist for cancer treatment currently. Imiquimod predominately binds TLR7, and is used topically to treat basal cell carcinoma and melanoma [111]. Mechanistically, TLR7/TLR8 agonists are able to activate NK and DC in a type I interferon dependent manner [112, 113]. In two phase III clinical trials, imiquimod (5%) cream was used to treat superficial basal cell carcinoma, and achieved a 75% clearance rate [114]. In a phase II clinical trial, topical imiquimod was administered to breast cancer patients with cutaneous metastases and the result reported that 20% of patients achieved a partial response [115].

Another well studied Toll-like receptor is TLR9. The anti-tumour effects of TLR9 are highlighted by the fact that TLR9 synthetic oligodeoxynucleotide agonists (CpG-ODN) have been shown to induce anti-tumour effects in xenograft models of murine neuroblastoma and colon cancer [116, 117]. In addition, CpG-ODN conjugated with siRNA that targets the immune suppressor gene Stat3 promoted anti-tumour effects against subcutaneously implanted melanoma [118].TLR9 agonists have been shown to induce the generation of type I interferons that in turn activate DC, NK and CD8 T cells

[119]. TLR9 agonists CpG-ODN 2006 can induce tumour cell death in Burkitt's lymphoma in vitro in a MyD88 dependent manner [120].

Although a large number of studies have demonstrated that TLR agonists exert anti-tumour function [108], a few studies have suggested the contrary with TLRs promoting tumours in some settings. Treatment with the TLR4 agonist LPS accelerated the development of pancreatic neoplasia in p48Cre; $Kras^{G12D}$ mice [121]. In the same model, genetic knock out TLR4 markedly inhibited tumour growth [121]. A recent publication demonstrated that microRNA miR-21 and miR-29a released from tumour cells binds to TLR7 in mice and TLR8 in humans, induced TLR-mediated NFκB activation and promoted the production of prometastatic inflammatory cytokines, including TNF-α and IL-6 [122]. These inflammatory cytokines are able to enhance tumour growth and metastasis [122]. Additionally, TLR7 expression was increased in murine and human pancreatic adenocarcinoma and stimulating TLR7 with ssRNA40 in p48Cre;$Kras^{G12D}$ mouse promoted tumour growth [123].

1.9 STING

Stimulator of Interferon Genes (STING) is a transmembrane protein that is localised to the endoplasmic reticulum [124]. STING is expressed in a wide range of immune cells including, T cells, NK cells, and various myeloid populations including macrophages [124]. Human STING consists of four transmembrane domains and one C-terminal region [124]. Recent work has demonstrated that activation of STING by its ligand cytosolic double-stranded DNA triggers the IRF3 pathway [125]. In vitro experiments demonstrated that C-terminal region on STING is crucial for IRF3 activation [125]. His_6-STING(181-379) that lack all transmembrane domains was enough to activate the IRF3 pathway [125]. Protein fragments purified from deletion mutants of STING(281-379) that contains the C-terminal domain but absence of the transmembrane domains can activate

IRF3 when incubated with cytosolic extracts from HeLa cells [125]. Upon activation, STING recruits IRF3 and TBK1 to the C-terminal region, this process facilitates IRF3 phosphorylation by TBK1 [125]. Phosphorylated IRF3 then translocates to the nucleus and triggers interferon (IFN) β gene expression[125]. The mutation of STING at S366A or L374A retain the recruitment and activation of TBK1, but impairs the interaction between IRF3 and STING, prevent IRF3 activation [125].

In 1997, Baguley and Ching described a potent xanthenone derivative, 5,6-Dimethylxanthenone-4-acetic acid (DMXAA) as a vascular disrupting agent that was shown to possess anti-tumour activity in mouse models [126]. Lately it has been demonstrated that the vascular disrupting effects noted by them may be specific for poorly and immaturely vascularised tumours [127]. For example, vascular disrupting effects of DMXAA observed on the subcutaneous 344SQ-ELuc tumours did not extend to spontaneously arising tumours in the K-ras$^{LA1/+}$ GEMM model of NSCLC [127]. Recent work has found that DMXAA is able to induce CD8+ T cell infiltrating into tumour cells via activating DC [128] in mice and that this was as a direct result of STING binding and activation. In EG7 thymoma [128], AB12 mesothelioma [129] and L1C2 bronchoalveolar carcinoma [129] models, DMXAA can induce an effective CD8+ T cell response and inhibit tumour growth. In severe combined immunodeficiency (SCID) models that mice do not have the ability to develop T and B lymphocytes, DMXAA failed to control tumour growth [128] supporting an immune effect beyond vascular disruption. Administration of DMXAA has been shown to trigger production of IFNβ via activating the IRF3 pathway [130]. It has been demonstrated that IFNβ is important in priming tumour-infiltrated T cells [105]. Compared to WT mice, the tumour specific killing ability is absent from of splenocytes of mice lacking the IFN-α/β receptor(Ifnar1$^{-/-}$) [105]. In addition, WT mice that received IFN-α/β receptor-specific blocking mAb MAR1-5A3 failed to reject the H31m1 MCA sarcoma (immunogenic sarcomas derived from 3'-methylcholanthrene–treated Rag2$^{-/-}$ mice) compared to mice that received isotype control GIR-208 mAb [105].

To sum up, although it has been documented that the STING ligand DMXAA eliminates tumours by targeting endothelial cells and pericytes of the already established tumour vasculature, this effect may be limited to immaturely vascularised tumours[127]. Most recent evidence indicates that the predominate anti-tumour activity of STING ligand DMXAA is derived from IFNβ that is produced after activating IRF3 pathway.

1.10 Cancer Immunotherapy

The term cancer immunotherapy refers to treatments that harness or enhance immunological processes to fight cancer. The immune system is extraordinarily powerful with its specificity and capacity to produce memory responses [15]. These unique characteristics could allow immunotherapy to achieve long-lasting remissions, with few side effects, and for any cancer, for example lung cancer [131], leukaemia [132], breast cancer [133] and lymphoma [134]. Briefly, cancer immunotherapy can be classified into four types; vaccines, cytokines, cellular therapy and mAb therapy. Cancer treatment vaccines elicit and boost immune response to eliminate tumour cells [135]. Among different cancer vaccines, DNA vaccines represent a promising strategy to induce immune responses. DNA vaccines contain flexible designs of DNA vectors that encode a wide range of tumour associated antigens and immunoenhancing proteins [136]. One example of an immunoenhancing protein is IL-12, it has been reported that co-injection of plasmids encoding IL-12 and human carcinoembryonic antigen strongly boost Th1 and cytotoxic T lymphocyte response against Lewis lung carcinoma [137]. The principle of DNA vaccines is based on inserting a bacterial plasmid DNA that encodes a tumour associated antigen under the control of a mammalian promoter into the host's tissues, the plasmids are subsequently transfected into the myocytes allowing for in vivo production and expression by the host's own protein expression systems [135]. The double stranded DNA is able to activate the IRF3 pathway and induce expression of Type-I IFNs by binding to TLR3 [138]. In addition, TLR9 recognises unmethylated CpG

DNA in the plasmid also triggering production of Type-I IFNs [138]. At the same time, DNA vaccines can elicit cytotoxic T cell responses through the cross-presentation pathway [138]. Tumour associated antigens generated in myocytes are taken up by DCs and cross-presented to CD8+ T cells through MHC class I [139]. In a phase I trial, human gp100 plasmid DNA was injected intramuscularly and only mild toxicity was observed [140]. Although, DNA vaccines are stable and safe, they have had limited success in generating therapeutic effects against most tumours due to poor immunogenicity [138]. The most successful cytokine therapy for cancer is IL-2 therapy. IL-2 is a 15.5-kDa cytokine produced predominately by CD8+ T cells, NK cells, activated DC and activated CD4+ T cells [141]. IL-2 is important in mediating T cell proliferation and differentiation [15]. In 1992, FDA approved Proleukin, a human recombinant version of IL-2 for treatment of metastatic renal carcinoma [142].

Cellular immunotherapy enhances immunity against tumour cells through the introduction of modified APCs or effector cells. Provenge (Sipuleucel-T) is the only US-approved cell-based therapy for the treatment of prostate cancer [143]. DCs extracted from patients' blood were incubated with a fusion protein (PA2024) that consists of two parts, antigen prostatic acid phosphatase (PAP) and granulocyte-macrophage colony stimulating factor (GM-CSF). PAP is expressed on 95% of prostate carcinomas, treating isolated DCs with PAP promotes immunogenicity [144]. GM-CSF is essential for DC maturation and homeostasis [145]. After incubation, the activated product was re-infused into patients. The Median survival time increased from 21.7 months for placebo-treated patients to 25.8 months for sipuleucel-T patients [143]. Chimeric T cell receptors (CARs) expressing T cells are engineered T cells that consist of a single-chain variable fragment fused with CD3-zeta transmembrane and endodomain, in addition, chimeric 4-1BB, OX40 and CD28 can be incorporated with CD3-zeta endodomain to enhance proliferative/survival signals [146]. In a phase I study, adoptive transfer CAR-modified T cells targeting CD19 and containing the CD3-zeta activation domain and 4-1BB costimulatory domain

(CTL019 cells) into 30 patients with relapsed/refractory acute lymphoblastic leukemia achieved 90% complete response (CR) rate [147].

Monoclonal antibody (mAb) mediated immunotherapy has become one of the most successful treatment strategies for patients with haematological malignancies and solid tumours over the past 15 years [148]. One of the most important characteristics of mAb is their ability to recognize antigen specifically [148]. Based on this unique ability of mAb, three different mAb mediated treatment strategies have been developed, direct targeting mAb, antibody-drug conjugates both of which primarily act to delete targets, often tumour, cells, and immunomodulatory mAb which in contrast bind to immune cells and aim to stimulate the immune system to induce anti-tumour response.

1.10.1 Direct targeting antibodies

The first mechanism of action for a direct targeting mAb is to simply block the target antigen from interacting with it natural binding partner by the binding of the mAb F(ab) region and thereby inhibit subsequent activity. For instance, trastuzumab (Herceptin), a HER2 receptor blocking mAb. Normally, activation of the HER2 receptor induces dimerization that triggers downstream signaling and leads to cell proliferation and division [149]. The overexpression of HER2 receptor has been observed in 20-25% of breast cancers [150]. Several mechanisms of action have been proposed for the mechanism of action of anti-HER2 mAb, one potential mechanism demonstrated for trastuzumab is directly to prevent HER2 dimerization via binding to HER2 subdomain IV [151, 152]. In addition, it has been reported that type II anti-CD20 mAb can induce cell arrest in different B cell lines in a Fc independent mechanism [153]. Subsequent research showed that type II anti-CD20 mAb binding is able to directly trigger intracellular signals in the target cell, and leading to programmed cell death (Figure 6), a mechanism distinct from classical apoptosis, as DNA fragmentation and nuclear condensation were not observed [154, 155]. It was reported that enlarged lysosomes are present in the

cytoplasm of dying cells, and that cell death induced was dependent upon subsequent reactive oxygen species release and therefore type II anti-CD20 may induce PCD, via a non-apoptotic lysosomal and reactive oxygen species dependent pathway[156, 157]. Thus, apart from blocking target receptors, engagement of F(ab) fragments is enough to trigger downstream pathways and induce direct cell death.

Direct targeting mAb bind to antigens as exemplified by those expressed on tumour cells can also recruit effector cells and complement components to mAb Fc region. This recruitment of effector function to the antigen target allows the mAb to induce several potential killing mechanisms; FcγR dependent antibody dependent cellular cytotoxicity (ADCC) or phagocytosis (ADCP), and complement mediated lysis [156] (Figure 6). These mechanisms alone or together can eliminate tumour cells in vivo [156]. In ADCP, antibody-antigen complexes are bound by FcγR expressing effector cells such as macrophages, allowing the macrophage to engulf tumour cells into phagosomes, eventually digesting tumour cells in a pH dependent manner [148] (section 1.2, page 4).

In addition, antibody antigen complexes can also bind to FcγRIIIA expressed on NK cells. The activation and cytotoxicity of NK cells are regulated by a balance between activatory receptors, inhibitory receptors and co-receptors [158]. In brief, absence of inhibitory signals, for example ligation of killer-cell immunoglobulin-like receptors and Ly49 together with activatory signal from FcγRIIIA engagement triggers NK cells activation and the release of perforin and granzymes that are able to lyse tumour cells [158]. Co-engagement of other activating NK receptors, for instance natural cytotoxicity receptors, NKG2D, DNAX Accessory Molecule-1 and 2B4 may enhance NK cell activation in a synergistic manner [159]. Using a xenograft breast carcinoma model, a study has demonstrated that an anti-human epidermal growth factor receptor 2(HER2) mAb engineered to prevent Fc binding to FcγRIIIA failed to stop tumour growth [160]. Additionally, in subcutaneous xenograft models the genetic deletion of the common

signaling gamma chain required for activatory FcγR function ablated the therapeutic activity of direct targeting anti-cancer mAb [160].

Ligation of C1q to antibody antigen complex can trigger the classical complement pathway, releasing anaphylatoxins (C3a, C4a and C5a), as well as opsonins [156]. These products from complement activation can promote phagocytosis or form membrane attack complexes that are able to form pores in the target cell membrane and cause lysis [156]. In SCID mice, treatment with cobra venom factor to inactivate complement led to a strong reduction in the therapeutic activity of anti-CD20 mAb 1F5 and rituximab [154]. Recent research, using a syngeneic mice model demonstrated that rituximab activity is not impaired in complement deficient (C1q-/- and C3-/-) mice [161]. This suggests that complement may not be important in rituximab treatment.

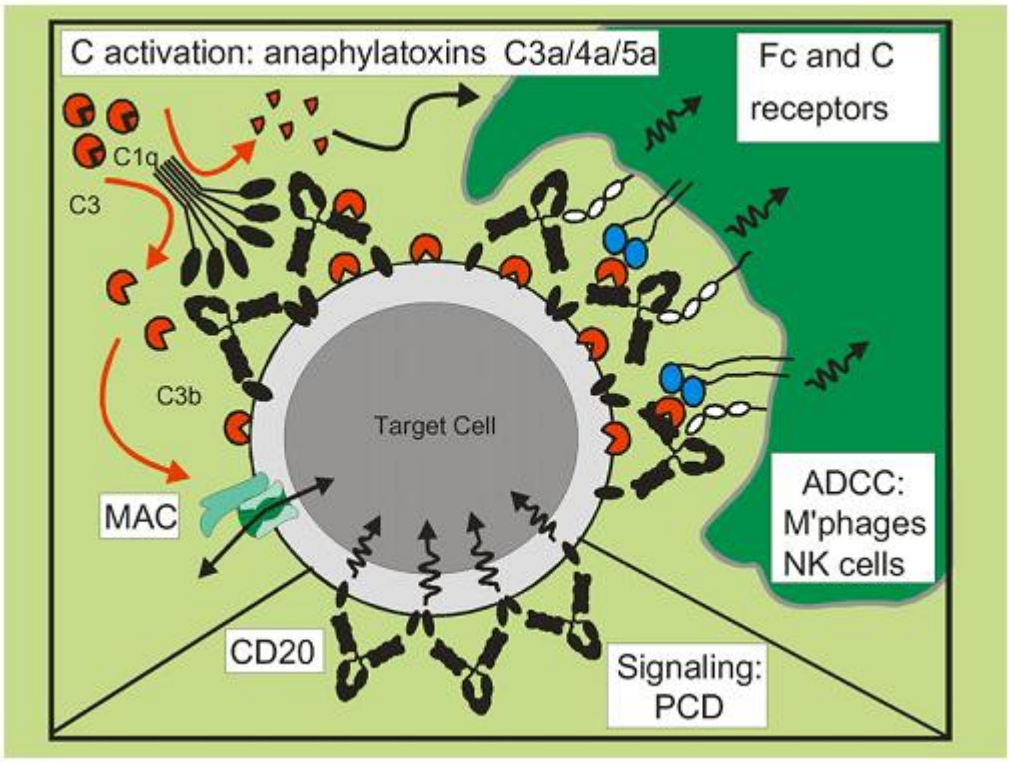

Figure 6: Mechanisms of action of direct targeting mAb rituximab. Rituximab eliminates tumour cells through four potential mechanisms, including macrophage mediate antibody dependent cellular phagocytosis (ADCP), NK cells mediate antibody dependent cellular cytotoxicity(ADCC), programmed cell death(PCD) and complement mediated lysis. In the complement, antibody antigen complex can bind to C1q and activate the classical complement pathway, which causes target cell lysis by generating membrane attack complexes (MAC) in the plasma membrane. Anti-CD20 mAb binds to target cells can trigger programme cell death singling that eliminates target cells by inducing apoptosis (Figure is cited from [135]).

One well studied direct targeting mAb family is the anti-CD20 mAb. CD20 is a plasma membrane resident phosphoprotein [162]. To date, no known natural ligand has been identified for CD20 [162]. Experiments have demonstrated that calcium influx was decreased in CD20 knock out mice, which suggests that CD20 may play an important role in controlling calcium influx [163]. It has been documented that BCR is required for CD20 evoked calcium influx [164]. Using a Ramos cell line that does not express BCR, Clare et al. have showed that type I anti-CD20 mAb induced calcium influx was strongly reduced [164]. One potential mechanism has been proposed that upon ligating with Type I anti-CD20 mAb, CD20 and BCR are co-localized in lipid rafts, this led to the clustering of BCR ITAM and causing protein-tyrosine kinase, PLC-γ activation, inositol trisphosphate release, eventually induced calcium flux [164].

CD20 is expressed on all normal B cells from the pre-B cell stage to plasma cell differentiation and importantly for cancer therapy on almost all malignant B cells [165, 166]. This fact allows rituximab to target tumour cells efficiently without impacting antibody production in the long term [167]. Anti-CD20 mAb can be classified into type I (rituximab-like) or type II (tositumomab-like) [154, 156, 168]. Type I anti-CD20 mAb are able to redistribute CD20 into lipid rafts and induce potent complement activation [154]. This may be because that CD20 redistribution leads to mAb clustering which provides an ideal density for Fc region binding to C1q, thus facilitating the triggering of the classical complement pathway [154]. Rituximab was approved by the US Food and Drug Administration (FDA) in 1997 to treat B cell malignancies [169]. In contrast, type II anti-CD20 mAb can't trigger complement, because they lack the ability to induce CD20 lipid raft redistribution [168]. Instead type II anti-CD20 mAb have been shown to induce a non-classical apoptosis that is independent of mitochondria and caspases [153]. CD20 mediated cell death is maintained when treated with different caspases inhibitors, for example serpin molecule crmA (inhibitor of initiator caspases-8 and -10), VDVAD (specific caspase-2 inhibitor) and ZVAD-FMK (inhibitor of all caspases other than caspases-2,-8 and -10) [153]. In addition, anti-CD20 mAb are able to induce death in cytoplasts from Daudi cells that lack mitochondria [153]. Microscopic analysis of cells and cell dilution experiments after anti-CD20 mAb binding revealed that the potency of death induced was positively correlated to homotypic cellular adhesion [153]. Recently, the CLL11 trial (NCT01010061) demonstrated that obinutuzumab combined with chlorambucil significantly prolonged PFS from 15.2 to 26.7 months, in comparison to rituximab combined with chlorambucil [170].

It has been reported that compared to type II anti-CD20 mAb, type I mAb evoke rapid CD20 internalization in vitro and in vivo [161]. Two mechanisms have been proposed to explain this phenomenon: The first one is antigenic modulation (internalisation), a cis-mechanism accelerated by inhibitory FcγRII engagement. Type I anti-CD20 mAb bound

to CD20 on the target B cells can also cross link to FcγRII on the same cell through its Fc domain [171] (Figure 7). This results in internalisation of the tripartite complexes [171]. The importance of FcγRII in antigenic modulation has been demonstrated by using FcγRII blocking mAb(AT10) that supressed modulation, and thereby enhanced the retention of CD20 surface expression and mAb opsonisation [172]. In a xenograft lymphoma model, compared to rituximab alone, co-administration with AT10 markedly promoted the anti-tumour response [173]. The other mechanism purported to lead to a loss of CD20 and target mAb from the cell surface is antigenic shaving (trogocytosis) mediated by activatory FcγR expressing effector cells in a trans-manner. It is postulated that in certain conditions, for example when macrophages are saturated or exhausted, that instead of inducing phagocytosis, engagement of opsonised target cells by activatory FcγRs on macrophages leads to the plucking of parts of the cell membrane:target antigen complex from the target cell surface [174]. As a result, target cells become invisible to macrophages, and escape from ADCP (Figure 7).

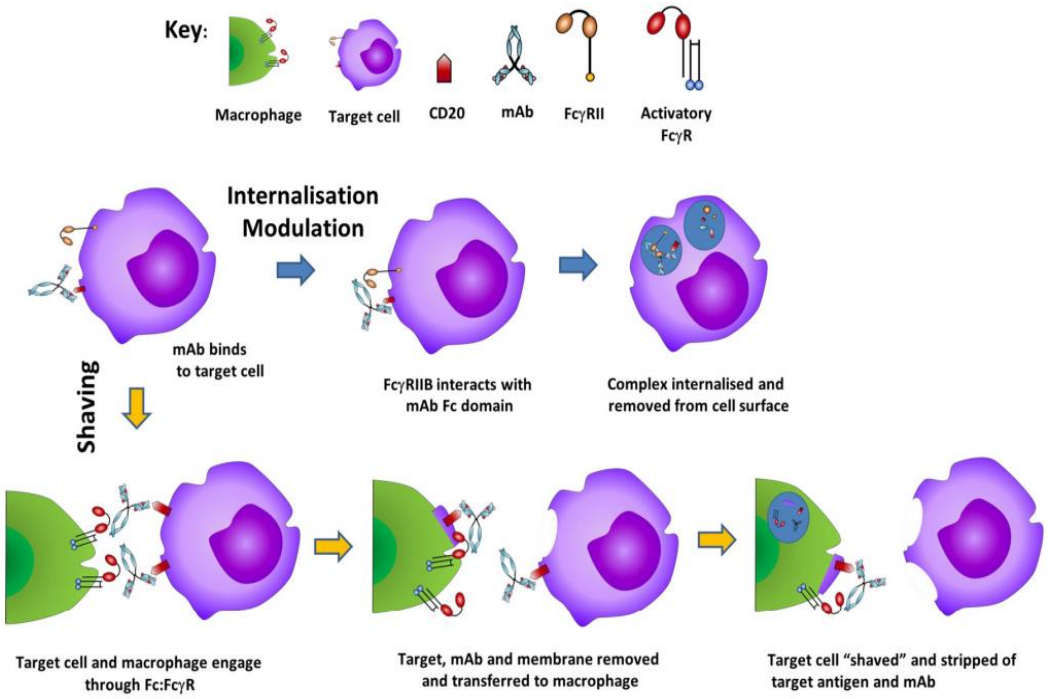

Figure 7: Potential Mechanisms that inhibit anti-CD20 mAb function. Two key models have been proposed, antigenic modulation and antigenic shaving. In antigenic modulation, type I CD20 antibody binding to CD20 also engages with FcγRII by Fc domain. The tripartite complexes are then removed from cell surface via internalisation. Antigenic shaving is proposed to occur in certain situations, such as when macrophages are saturated. Rather than deleting the target cell through phagocytosis, macrophages rip antigen-antibody immune complexes from the target cell in an activatory FcγR dependent manners (This figure is cited from [171]).

Trastuzumab (Herceptin) targets HER2 which belongs to human epidermal growth factor receptor family, and has been documented to be overexpressed in approximately 20-25% of invasive breast cancers [150]. By binding to the extracellular subdomain IV of HER2, trastuzumab stops its dimerization and can suppress cell growth and proliferation through inhibiting HER2 mediated MAPK and PI3K/Akt pathways[152]. In addition, trastuzumab mediated cytotoxic activity is impaired in mice deficient in activating Fc gamma receptors demonstrating that trastuzumab may eliminate tumour cells through ADCC or ADCP [160]. In 1998, the FDA approved trastuzumab for the treatment of HER2-positive metastatic breast cancer. In a large study, in comparison to chemotherapy alone, combination of trastuzumab with standard chemotherapy (Doxorubicin or epirubicin plus cyclophosphamide or paclitaxel) has been shown to increase overall response rate from 32 percent to 50 percent, and median survival from

20.3 months to 25.1 months in patients with progressive metastatic breast cancer that overexpressed HER2 [175].

1.10.2 Antibody-drug conjugates

Antibody-drug conjugates are designed for the targeted delivery of potent anti-cancer drugs with the aim of overcoming many of the non-specific side effects associated with traditional cancer chemotherapy [169]. Brentuximab vedotin consists of chimeric anti-CD30 mAb and antimitotic agent Monomethyl auristatin E [169]. Brentuximab binds to CD30 expressed on malignant cells, delivering Monomethyl auristatin E (MMAE), an antimitotic agent specifically to tumour cells, this stops tumour cell division by blocking the polymerisation of tubulin [169]. In 2011, Brentuximab vedotin was approved by the FDA for treatment of relapsed or refractory Hodgkin's lymphoma [169]. In a phase 1 trial, brentuximab vedotin was administrated to Hodgkin lymphoma and anaplastic large cell lymphoma (ALCL) patients once every 3 weeks, 36/42 (86%) patients showed tumour regression [176]. In a phase II study, 102 patients with relapsed and refractory Hodgkin lymphoma after autologous stem cell transplantation were treated with brentuximab vedotin [177]. Overall responses were observed in 75% of patients and 34% of patients showed a complete response [177]. In second phase II study, 58 systemic ALCL patients were treated with brentuximab vedotin with 50 out of 58 patients (86%) showing an objective response and 57% achieving a complete response [178]. Despite the fact that substantial positive results have been observed on brentuximab vedotin treated patients, serious adverse effects for example pulmonary toxicity and peripheral neuropathy have also been reported. These treatment toxicities are a major barrier to wider use antibody-drug conjugates therapy [179]. In a phase I study, 7 of 19 patients developed pulmonary toxicity after treating with brentuximab vedotin plus doxorubicin, bleomycin, vinblastine, and dacarbazine [179]. Recently, eight patients were reported to have developed pancreatitis after treatment with brentuximab vedotin, two of them died [180]. Because of

these side effects, a boxed warning was added to brentuximab vedotin by the FDA [179]. These adverse effects may be solved in the future through a better understanding of conjugate chemistry, for example, generating conjugates with more stable linkage molecules that are resistant to degradation.

1.10.3 Immunomodulatory mAb

Immunomodulatory mAb aim to activate immunological pathways that are essential in cancer immune surveillance [148]. In general, immunomodulatory mAbs are divided into agonists and checkpoint inhibitors [181] (Figure 8). To fully activate T cells, three signals are required: The first is provided by the cognate T cell receptor recognizing specific antigenic peptides presented by MHC expressed on APCs, such as DC and B cells. The second is provided by costimulatory signals, for example ligation of CD28 on T cells to B7 family proteins (CD80, CD86) on APCs, binding of CD40 ligand (CD154) on T cells to CD40 on APC, and association of 4-1BB expressed on T cell to its ligand etc. Together these signals are able to trigger naïve T cell proliferation [15, 26]. However, these T cells survive poorly, show limited effector function and do not generate a responsive memory population in the absence of the third signal that comes from inflammatory cytokines [182]. It has been demonstrated that IL-12 and IFNα/β activate the third signal which promotes CD8+ T cells clonal expansion and enhances effector function including IFNγ production and cytolytic activity [183]. Whilst, IL-1 acts directly on CD4+ T cells providing a crucial third signal that is able augment Ag-driven expansion and Th1 differentiation in vivo [184].

The T cell activation process is tightly regulated through a balance of activatory and inhibitory signals. One well studied inhibitory signal is the ligation of the cytotoxic T-lymphocyte-associated protein 4 (CTLA-4) to its ligand. CTLA-4 is a member of the immunoglobulin superfamily that is expressed on the surface of various T cells including T helper cells [185]. CTLA-4 and CD28 shares the B7 ligand, however compare to CD28,

CTLA-4 binds B7 with a higher avidity [186]. Thus CTLA-4 works as a competitive antagonist of CD28:B7-mediated co-stimulation [186]. In addition, it has been shown that CTLA-4 binding to B7 family proteins on APC may inhibit the PI3K/Akt signaling pathway that is important in triggering T cell activation [185, 186].

In order to activate T cells fully, it is necessary to suppress inhibitory signals whilst delivering the three activatory signals these fully activated T cells can then start producing autocrine interleukin-2 that is able to trigger T cell proliferation [15, 26]. Ipilimumab is a fully human 'checkpoint blocking' mAb that targets CLTA-4 to block the inhibitory signal, and potentiate T cell activation and responses to tumour antigen [148]. The FDA approved ipilimumab for late-stage melanoma treatment in 2011. In late-stage (metastatic) melanoma, compared to control group who received experimental vaccine alone, the overall survival of patients who received ipilimumab was prolonged from 6.5 months to 10 months [187]. Additionally, in a phase II study chemotherapy-naïve non-small cell lung carcinoma (NSCLC) patients treated with ipilimumab combined with first line therapy paclitaxel plus carboplatin demonstrated improved progression-free survival compared to those treated with paclitaxel plus carboplatin alone [131].

Agonistic or immunostimulatory mAb are another type of immunomodulatory mAb being developed. These mAb target costimulatory molecules, for example those of the tumor necrosis factor receptor (TNFR) superfamily, 4-1BB (CD137) [188], CD40 and OX40 [189]. Predominantly, 4-1BB and OX40 are expressed by CD8+ and CD4+ T cells [188, 189]. Ligation to their ligand is able to provide a costimulatory signal to T cells and induce T cell proliferation and activation [188, 189]. Anti-OX40 (9B12) has been in Phase I trials, outcomes demonstrated that 9B12 treatment increased the anti-tumor reactivity of T and B cells in patients with melanoma [190]. In a Phase I trial, a fully human anti-CD137 antibody from Pfizer and Bristol-Myers Squibb has demonstrated some anti-tumour efficacy (100) [191].

CD40 has been demonstrated to be expressed on a wide range of cells including all APC, epithelial and endothelial cells. CD154, the natural ligand for CD40, is a type II transmembrane protein that is predominantly expressed on activated Th cells [192]. CD40-CD40L ligation recruits the adapter protein TRAF, which activates several signaling pathways, such as MAPK, PI3K and NFκB [193]. In humoral immune responses, CD40 expressed on B cells binds to CD40L on activated T helper cells and has been demonstrated to be important in maintaining B cell survival, proliferation and differentiation [25]. Stimulating CD40 expressed on DC by CD40L activates and licenses DC to prime CD8 T cell response bypassing the need for CD4 help [194]. The stimulatory anti-mCD40 mAb 3/23 is able to induce strong cytotoxic CD8+ T cell responses that stop tumour growth in syngeneic murine BCL_1 lymphomas [195]. To date, the clinical development of agonistic/immunostimulatory mAb have trailed behind checkpoint inhibitors. There are several potential reasons for the slower progression of immunostimulatory mAb one of which may be that priming strong immune responses like starting a car, through applying the 'accelerator' in the form of agonistic mAb may not be enough, releasing the "brake" by checkpoint blockade may also be necessary to induce a productive response. The other possibility is that checkpoint inhibitors promote T cell activation and proliferation through blocking inhibitory receptors, which is a relatively simple process, whilst agonistic mAb stimulate T cells by a complex system that involves efficient FcγR dependent crosslinking.

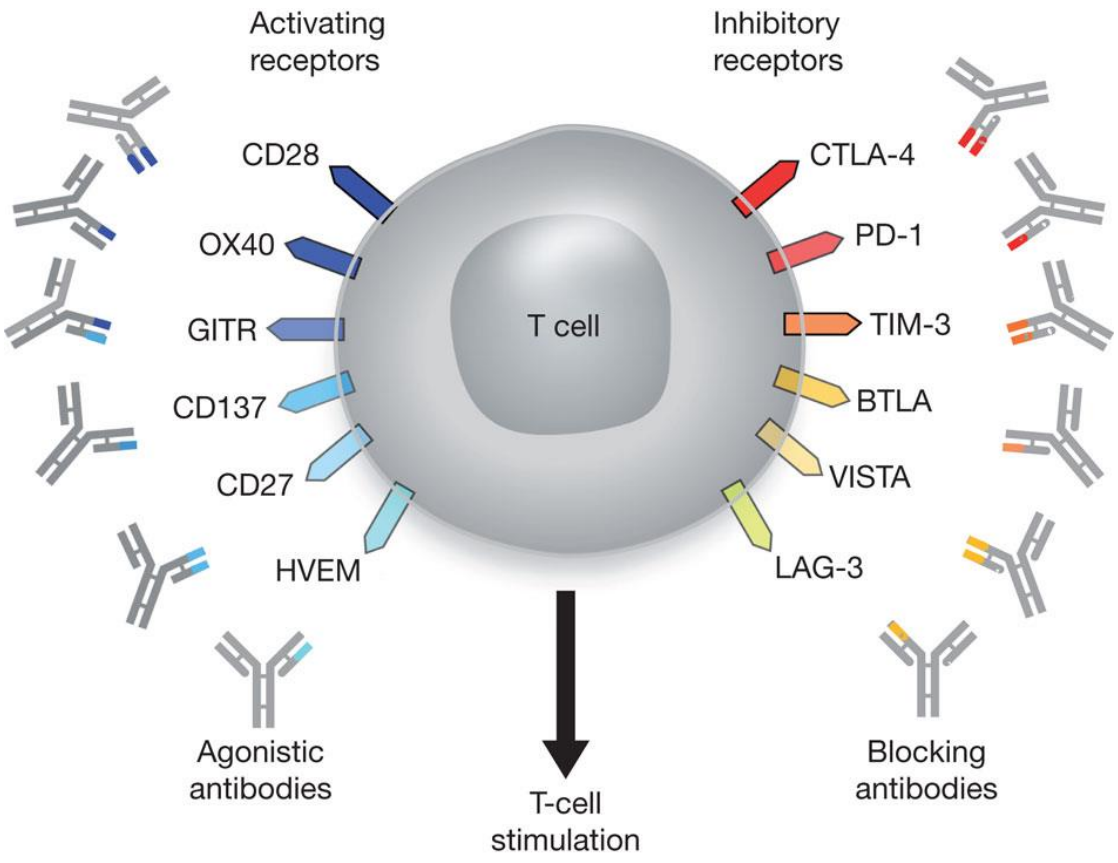

Figure 8: Target of immunomodulatory mAb. Apart from binding to specific antigen: T-cell activation is controlled by a balance of positive and negative signals. Agonistic mAb bind to co-stimulatory receptors (blue): CD28, OX40, glucocorticoid induced tumour necrosis factor receptor (GITR), CD137 (4-1BB), CD27, Herpesvirus entry mediator (HVEM), inducing important signals for T cell activation. Checkpoint inhibitor mAb bind to and block target receptors (red): cytotoxic T lymphocyte-associated antigen-4 (CTLA-4), Programmed cell death protein 1 (PD-1), T-cell immunoglobulin and mucin-domain containing-3 (TIM-3), B- and T-lymphocyte attenuator (BTLA), V-domain Ig suppressor of T cell activation (VISTA), and Lymphocyte-activation protein 3 (LAG-3), transducing inhibitory signals that suppress T cell activation. (This figure is cited from [181])

1.11 Antibody dependent cellular phagocytosis is one of the most important killing mechanisms mediated by anti-CD20 mAb rituximab

B-cell lymphomas are divided into Hodgkin's lymphomas and non-Hodgkin lymphomas (NHL), most of which express CD20 [196]. CD20 is a non-glycosylated phosphoprotein expressed on the surface of both normal and malignant B cells [162, 167]. CD20 is encoded by the MS4A1 gene in humans and so far no known natural ligand has been identified [162, 167]. The anti-CD20 mAb, rituximab has been shown to efficiently treat a variety of NHL [197]. Several mechanisms of action have been proposed for anti-CD20

mAb including complement-dependent cytotoxicity (CDC), induction of PCD, ADCC and ADCP [156] (Section 1.10.1, page 28). Despite the fact that FcγR are widely expressed on hematopoietic stem cell progenitors, several lines of evidence show that macrophages are the dominant FcγR expressing effector cells, and that rituximab primarily acts through ADCP to deplete target lymphoma cells [160, 198]. In a human xenograft tumour model, mouse deficient in activatory FcγR show remarkably decreased antibody mediated anti-tumour activity [160]. In the same model, antibody potency is increased in inhibitory FcγRII knock out mice [160]. In addition, in the syngeneic immunocompetent Eμ-Myc lymphoma mouse model, anti-CD20 mediated lymphoma depletion is reduced in activatory FcγR deficient mice, and increased in FcγRIIKO mice [198]. A clinical study comparing rituximab therapeutic activity between NHL patients with different FcγRIIIA polymorphisms, demonstrated that patients with FcγRIIIa-158V, a polymorphism bestowing higher affinity to IgG1 antibody responded better to rituximab treatment [199]. By using intravital imaging, it has been demonstrated that antibody-dependent phagocytosis by macrophages is the primary mechanism of anti-CD20 therapy [200, 201]. These pre-clinical and clinical studies suggest the Fc:FcγR interactions are crucial in mediating therapeutic potency for a range of mAb, including anti-CD20 and that the ratio of activatory:inhibitory FcγRs on macrophage may correlate with mAb treatment outcome.

However, it has been reported that other FcγR expressing effector cells, such as monocytes in blood [202] and neutrophils [203] are also involved in ADCP against cancer cells. Monocytes are generated in the bone marrow and then migrate to the blood [204]. Although blood-borne monocytes have a short half-life, research using low-dose clodronate to selectively deplete Ly6C low monocytes in the blood strongly inhibited anti-CD20 mAb mediated B cell deletion [202]. Circulating monocytes can be found to infiltrate into peripheral tissues including tumours and it has been shown that these inflammatory monocytes may be the precursors of TAMs [205]. Similar to monocytes,

neutrophils are produced in the bone marrow then released into circulation [206]. Neutrophils infiltrate into inflammatory tissues before monocytes [206]. In a short term (7 days) pre-clinical model, neutrophils have been shown to be necessary for anti-gp75 mAb therapy of melanoma [203]. This implies that neutrophils could be the effectors of ADCP in the very early stages of cancer. After tumour progression, tumour infiltrated neutrophils are switched to tumour associated neutrophils that may lose phagocytotic activity and enhance cancer cell growth, invasion and metastasis [207]. Therefore, it's possible that all of these effectors are involved to some extent in ADCP and that the recruitment of effectors to cancer cells are determined by the location and stage of tumour [208].

ADCC induced by NK cells is another potential mechanism of action for direct targeting mAbs. Although the data from murine studies strongly favour myeloid dependent ADCP as the dominant mechanism in vivo, It's still debated which mechanism is more important for mAb therapy in humans, ADCC or ADCP. Which of these mechanisms predominates could be determined by what therapeutic mAbs are used, as glycoengineering and alteration of isotypes can affect mAb mechanisms [209]. An in vivo study has demonstrated that anti-CD20 mAb (rituximab and tositumomab) mediated B cell depletion was largely abrogated when monocytes/macrophages were deleted with clodronate liposomes [161]. Moreover, clinical prognosis to rituximab therapy is correlated with polymorphisms of human FcγRIIa that is restricted to myeloid populations, but not expressed NK cells [210]. Taken together, these data would suggest that ADCC evoked by NK cells is likely not the dominant mechanism for rituximab therapy.

1.12 Repolarizing tumour associated macrophages to enhance mAb immunotherapy for cancer treatment

To date, a considerable amount of effort has been put in to improving antibody-FcγR interactions through glycoengineering and amino acid mutagenesis of antibody Fc. For example, the third-generation, humanized anti-CD20 antibody obinutuzumab (GA101), contains a glycoengineered Fc region which increases antibody binding to FcγRIIIA [211]. Another humanized anti-CD20 mAb veltuzumab, has a single amino acid change compared to rituximab, having aspartic acid instead of asparagine at the 101st position in CDR3 of the variable heavy chain. Based on in vitro results, the mutation lowered the off-rate of veltuzumab and increased its potency in Daudi lymphoma xenograft models compare to rituximab [212]. Although these mAb directed approaches have improved mAb function and efficacy, this approach is unlikely to overcome any inherent deficiencies in the resident effector population, for example through depletion, exhaustion or direct inhibition as a result of tumour microenvironment [213, 214]. TLR ligands have been shown to activate DC, NK cells and macrophages [108]. Currently a large number of TLR agonist clinical trials are on-going to evaluate their anti-tumour function, either as monotherapies or in combination with other therapies, such as radiation and cytotoxic chemotherapy [108]. The majority of these trials are based around TLR agonist mediated activation of DC and NK cells. Although there is a considerable amount of effort being put in to modifying antibodies to improve treatment outcome, the understanding of how we might manipulate macrophage function using TLR agonists to enhance mAb efficacy is still poor. In this project, we have utilised a range of agonists to polarize macrophages to a pro-inflammatory (M1-like) activated phenotype and investigated their therapeutic potential in combination with mAb treatment.

1.12 Hypothesis

The balance of activatory:inhibitory FcγR on macrophages is important in mediating anti-cancer mAb function. Tumour associated macrophages typically have a phenotype that is suboptimal for mediating anti-tumour effects. Repolarising macrophages into a pro-inflammatory phenotype with agonists will generate macrophages with a higher FcγR A:I and will enhance anti-cancer mAb efficacy.

1.13 Aims

1. Characterise the potential of TLR agonists and STING to polarize macrophages in vitro and in vivo to enhance their FcγR mediated mAb effector functions.

2. Determine the therapeutic potential of the combination of TLR agonists and STING with direct targeting anti-CD20 mAb in lymphoma model.

   .

3. Characterise the mechanism of action of the anti-4-1BB mAb LOB 12.0 and evaluate the therapeutic potential of using TLR agonists with LOB12.0 against carcinoma.

(11578 words)

Chapter II - Materials and Methods

2.1 Animals

Mice were bred and maintained in local facilities. Genetically altered strains used were human CD20 transgenic (Tg) C57BL/6 mice, described previously (126); γ-chain knockout (KO) BALB/c [215], FcγRII KO BALB/c [216], FcγR null mice (γ-chain knockout (KO) cross with FcγRII KO) were obtained by cross-breeding with genotypes confirmed by PCR and/or flow cytometry. CCR2 knock out C57BL/6 were obtained from Dr. Diego Gomez-Nicola [217], blood and spleen from CCR2 KO mice were verify by flow cytometry. Animal experiments were cleared through the local ethical committee and were performed under Home Office licenses PPL30/2451 and PPL30/2964.

Genetically modified mice	Background	Description
CCR2 KO mice	C57BL/6	CCR2 is a chemokine that specifically mediates monocyte chemotaxis. In CCR2 KO mice, monocytes fail to migrate into theblood, and remain trapped in the bone marrow [218].
HuCD20Tg mice	C57BL/6, BALB/c	A transgenic mouse carrying the human CD20 gene. Human CD20 is mainly expressed on mature B lymphocytes in this strain [219]. Murine CD20 is also expressed on mature B lymphocytes.
FcγRII KO mice	BALB/c	Genetically modified mouse carry inactivated FCGR2 gene, therefore this strain does not express inhibitory FcγRII.
γ-chain KO mice (FcRgamma KO mice)	BALB/c	Fc receptor common gamma-chain deficient mice. Activatory Fc gamma receptors require the gamma-chain to trigger the ITAM signalling pathway. Fc gamma receptor mediated ITAM signalling and thereby effector function is disabled in this strain.

FcγR null mice	BALB/c	γ-chain KO crossed with FcγRII KO mice. This strain effectively has no functioning Fcγ Receptors.

2.2 Reagents and materials

2.2.1 Antibodies

Antibodies for flow cytometry	Clone	Company
Anti-mouse CD19 APC	eBio1D3	ebioscience
Anti-mouse CD4 efluor 450	GK 1.5	ebioscience
Anti-mouse Foxp3 APC	FJK-16s	ebioscience
Anti-mouse CD11b PE	M1/70	ebioscience
Anti-mouse Ly6C Percp.Cy5.5	HK1.4	ebioscience
Anti-mouse Ly6G PE.Cy7	RB6-8C5	ebioscience
Anti-Mouse EOMES Alexa Fluor 488	Dan11mag	ebioscience
Anti-Mouse Ki67 APC	B56	BD Pharmingen
Anti-mouse F4/80 APC	MCA497APC	SeroTec
Anti-human CD206	19.2	BD bioscience
Anti-mouse BCL_1 Idiotype FITC	MC106A5	In house
Anti-mouse FcγR I $F(ab')_2$ FITC	AT152-9	In house
Anti-mouse FcγR II (AT130-2) N297A FITC	AT130-2	In house
Anti-mouse FcγR III (AT154-2) $F(ab')_2$ FITC	AT154-2	In house
Anti-mouse FcγR IV (AT137) $F(ab')_2$ FITC	AT137	In house
Anti-mouse CD86 FITC	GL1	In house
Antibody for experiments in vivo		
Anti-mouse Ly6G	1A8	Bio X Cell
Anti-mouse IL10 receptor (blocking)	1B1.3A	Bio X Cell
Anti-mouse CD8(depletion) Rat IgG2b	YTS169	In house
Rituximab mIgG2a		In house
BHH2 mIgG2a		In house
Anti-mouse CD20 mIgG2a	18B12	In house
Anti-mouse 4-1BB mIgG1	LOB12.0	In house
Anti-mouse 4-1BB mIgG2a	LOB12.0	In house

2.2.2 Reagents

Reagent	Company
2-Mercaptoethanol	Sigma-Aldrich

293fectin™	Invitrogen
α-Isonitrosopropiophenone	Sigma-Aldrich
Aprotinin	Sigma-Aldrich
Anti-Mouse/Rat Foxp3 Staining Set	Ebioscience
Bovine serum albumin	Europa
Mouse B cell isolation kit	Miltenyi
Carboxyfluorescein succinimidyl ester	Ebioscience
CPG ODN 1826	Invitrogen
CPG ODN 1826 CTL	Invitrogen
DMEM	Life Technologies
DMXAA	Sigma-Aldrich
Ethanol	HAYMAN
Fetal bovine serum	Sigma- Aldrich
Hydrochloric acid	VWR Chemicals
IL4	PeproTech
IL13	PeproTech
L-arginine	Sigma-Aldrich
L929	Sigma-Aldrich
L-glutamate	Life Technologies
LPS	Sigma-Aldrich
Lymphoprep™	STEMCELL
$MnCl_2$	Sigma-Aldrich
N-(1-naphthyl) ethylenediamine dihydrochloride	Sigma-Aldrich
Pepstain A	Sigma-Aldrich
Percoll	GE Healthcare Life Sciences
Phenylmethanesulfonyl fluoride	Sigma-Aldrich
Phosphoric acid	Sigma-Aldrich
Platinum® Quantitative PCR SuperMix-UDG	Invitrogen
Poly(I:C)	Sigma-Aldrich
Primers and probe for FcγR (See table below)	Sigma-Aldrich
Pyruvate	Life Technologies
R848	Invitrogen
RPMI	Life Technologies
RNeasy Mini Kit	QIAGEN
Superscript III first strand cDNA synthesis kit	Invitrogen
Sulfuric acid	VWR Chemicals
Sulphanilamide	Sigma-Aldrich
STING DMXAA	InvivoGen
Tris-Hcl	Sigma-Aldrich
Triton X-100	Flukka
Trypsin-EDTA	Life Technologies

Urea	Sigma-Aldrich

2.2.3 qPCR primers

Target	Type	Sequence 5'-3'
FcγR I	Probe	[6FAM]CCACCGACTGGAACCCAAAGTAGCAGA[TAM]
FcγR I	Forward	GGAGATGACATGTGGCTTCTAACA
FcγR I	Reverse	GCCTTGGTGGCATTAACCA
FcγR II	Probe	[6FAM]CAATTGTCAATACTGGTAAAGACCTGCT[TAM]
FcγR II	Forward	CTGTCCAAGGGCCCAAGTC
FcγR II	Reverse	GCGACAGCAATCCCAGTGA
FcγR III	Probe	[6FAM]AAAAGCAAACAGCAGCAGAATT[TAM]
FcγR III	Forward	CAATGGCTACTTCCACCACTGA
FcγR III	Reverse	AGAGCTGCACTCTGCCTGTCT
FcγR IV	Probe	[6FAM]ACTTAGTGGTCTGAAGCAATAGCCAGCCCA[TAM]
FcγR IV	Forward	ACCCAGTGCAACTAGAGGTCCAT
FcγR IV	Reverse	GGGTCCCCCTCCTGGAA

FACS wash buffer: 70.1 g NaCl, 7.9g KH_2PO_4, 34.4g Na_2HPO_4,6.5g Sodium azide,100g bovine serum albumin in 5L deionised water.

2.3 Bone marrow derived macrophage cell culture

2.3.1 Preparing L929 media

The L929 cell-line was originally derived from the normal adipose tissue of a 100 days old male C3H/An mouse. It has been shown that L929 media is a convenient and economical source of murine MCSF that is required for BMDM maturation and differentiation in vitro [220]. To collect L929 media for BMDM culture, L929 cells were maintained in RPMI media containing 10% FCS, glutamate/pyruvate and

penicillin/streptomycin. Media was collected (L929 media) when L929 cells were around 80% confluent. An endotoxin and mycoplasma test were performed for each new stock of L929 media to ensure that they were endotoxin and mycoplasma free. Our data showed that the best differentiation and maturation of BMDM was observed when using 20% L929 (Stephen Beers, data not shown). Therefore, 20% L929 media was used for all BMDM cultures.

2.3.2 BMDM culture

C57BL/6 or BALB/c mice were sacrificed and hind legs (femur/tibia) harvested under sterile conditions. Tissues were removed, being careful not to crush the bone in order to reduce contamination from other cells. The end of each bone was cut off using sterile scissors and using a 0.5x16 mm needle and 10 ml syringe containing media (RPMI 1640 with 10% FCS, glutamate/pyruvate, penicillin/streptomycin (Invitrogen) and 2mM 2-Mercaptoethanol) the bone marrow expelled into a 50ml tube. The bone marrow suspension was passed through a 100 µm cell strainer into a petri dish and particulates homogenised with the stopper from a sterile 1ml syringe and washed through the strainer into a 50ml tube using a Pasteur pipette to obtain a single cell suspension. Cell suspensions were washed twice in media, with centrifugation at 300g for 5 mins. Cells were resuspended at $1x10^6$ cells/ml, and 4 ml of cells added to each well of a 6 well-plate. 1 ml L929 media (20%,1ml L929+4ml complete media) [220] as a source of macrophage colony-stimulating factor was added to each well, to promote proliferation, differentiation, and survival of monocytes and macrophages. Cells were cultured in a humidified atmosphere at 37^{o}C, 5% CO_2, culture media was changed on days 1, 3 and 5. Cultured cells were observed by microscopy every other day, more than 90% of cultured cells became BMDM (elongated and adherent). BMDM were stimulated by different treatments at day 7, and harvested for NO and arginase assays, flow cytometry and qPCR at day 8. To harvest BMDM, media was replaced with 2 ml ice-cold PBS and incubated on ice for 15 minutes. Then gentle pipetting was used to detach the adherent

BMDM and each well checked under a microscope to ensure >90% of the cells were detached.

2.4 Arginase and NO assay

At Day 7-10, BMDM were harvested from 6 well plates and transferred to 96 well plates, with each well containing $2.5x10^5$ cells. BMDM were then left to adhere in a tissue culture incubator 37°, 5% CO_2 for at least 3 hours. BMDM were then stimulated with different TLR agonists and cytokines, LPS/ IFNγ 100/2 ng/ml, IL4/13 10/10 ng/ml, R848 1 µM, Poly(I:C) 40 µg/ml and CPG 1826 1 µg/ml (final concentration), and returned to the incubator. After 24 hours to allow sufficient time for activation, 100 µl of supernatant from each well was transferred to an ELISA plate and used for the nitric oxide assay. The cells were then used for the arginase assay.

NO assay:

A standard curve of $NaNO_3$ in complete 10% RPMI was prepared in duplicate, with the range from 250 µM quartering down to 0 µM. Equal volumes of Griess reagent (1:1 0.1% N-(1-naphthyl) ethylenediamine dihydrochloride (NED) in deionised H_20 and 1% sulphanilamide in 5% phosphoric acid) was added to each well of the ELISA plate containing culture supernatant. Then the plate was incubated at room temperature in the dark for 10 minutes for the colour to develop and the plate read on a Dynatech MR400 microplate at 570 nm absorbance [221].

Arginase assay:

BMDM were lysed in 96 well plates by addition of 25 µl 0.1% Triton x-100, 50 mM Tris-HCl containing 0.1 mg/ml each of pepstain A, aprotinin and 2 µl phenyl-methyl-sulphonyl fluoride (PMSF) (1000x dilution). Micropipette tips were used to scrape each well to harvest the lysates. To activate arginase, 25 µl Tris-HCl (50 mM; pH 7.5) containing 10 mM MnCl2 was added to each well. Macrophage arginase was then activated by heating

the plates at 55–60°C for 10 min. Arginase activity is monitored as the hydrolysis of L-arginine to L-ornithine and urea by arginase and this was carried out by incubating the mixture containing activated arginase with 50 µl of L-arginine (0.5 M; pH 9.7) at 37°C for 1 h. The reaction was stopped by adding 400 µl of the acid solution mixture (H_2SO_4:H_3PO_4:H_2O 1:3:7). Standard curves were made up in 1.5ml microcentrifuge tubes with doubling dilution of urea from 300 µg/100 µl to 2.34 µg/100 µl. For colorimetric determination of urea, a-isonitrosopropiophenone (25 µl, 9% in absolute ethanol) was then added, and the mixture was heated at 100°C for 45 min. After placing the samples in the dark for 10 min at room temperature, the urea concentration was determined by assaying the absorbance at 550 nm using a spectrophotometer (Dynatech MR400 microplate reader). The amount of the urea produced was used as an index for arginase activity.

2.5 qPCR assay

An optimised qPCR assay protocol came from colleague Matthew J. Carter. Briefly, after stimulation, RNeasy Mini Kit from Qiagen was used to purify BMDM RNA. About 1 x 10^6 cells from 6 well plates were harvested, and spun once at 300g for 5 minutes. To disrupt and homogenize the cells, buffer RLT was added, the lysate was then passed through a 20-gauge (0.9 mm) needle attached to a sterile plastic syringe at least 5–10 times. Ethanol was then added to the lysate, allowing binding of RNA to the RNeasy membrane. The sample was then applied to the RNeasy Mini spin column. Contaminants are efficiently washed away, while purified high-quality RNA is eluted in RNase-free water. RNA concentration was measured by Nano Drop 1000, the absorbance at 260/280 was measured and this value taken to represent the purity of RNA. A value of 2 reflects pure RNA, in the project, only sample with value > 2 is selected for future use. Additionally, a 260/230 ratio is measured to determine the level of solvent contamination, particularly

isothiocyanates that are a constituent from the RNA isolation kits. Again, a value of 2 reflects clean RNA, only sample with value > 2 were selected for future use in the project. Then 500 ng RNA was immediately reverse transcribed to cDNA by using Superscript III first strand cDNA synthesis kit from Invitrogen. Platinum® Quantitative PCR SuperMix-UDG from Invitrogen was used for TaqMan qPCR assay. In this assay, A TaqMan probe is constructed with a fluorescent reporter dye (here we used FAM) bound to the 5′ end and a quencher on the 3' end. The probe is intact before primers recognise their specific sequences, and the quencher acts to greatly reduce the fluorescence emitted by the reporter dye. After binding to their specific sequences, the probes anneal between primer sites and this separates the reporter dye from the quencher, thus increasing the reporter dye signal. In addition, removal of the probe from the target strand also allows primer extension to continue to the end of the template strand. In the project, we triplicated each qPCR reaction to ensure robust and reliable results.

Data from qPCR assays were analysed using the $2^{-\Delta\Delta C}{}_T$ method [222]. The CT reading is produced by the qPCR device and this value represents the number of amplifications required to reach the threshold cycle which is shown as a straight blue line on figure 14a (Section 3.2.3 page 70). For example, to calculate the fold change of FcγRI expression of stimuli A treated BMDM, FcγRI ΔCTA = the CT value of FcγRI stimuli A treated BMDM - the CT value of housekeeping of stimuli A treated BMDM. FcγRI ΔCTB= the CT value of FcγRI of non-treated BMDM - the CT value of housekeeping of non-treated BMDM. ΔΔCT=ΔCTA - ΔCTB, fold change= 2-ΔΔCT.

2.6 293F Transfection

The following protocol was used to transfect 293-F cells (Invitrogen). Ten ml 293-F cells at $1x10^6$cells/ml were incubated with 10 µg mouse FcγR cDNA (generated by Claude H.T Chan) and 20 µL 293fectin™ at 37º with shaking. After 48 hours, cells were

harvested, stained with different anti-mouse FcγR antibodies (see method 2.2) and analysed by flow cytometry.

2.7 Adoptive transfer

On Day 0, the same number of wild type (WT) and human CD20 transgenic C57BL/6 spleens were harvest and dissociated separately. Briefly, the fur was wet on the left side of the mouse using 70% ethanol, the abdominal cavity was opened up and the spleen removed using sterilized scissors and forceps. The spleen was placed into a cell strainer and using the plunger end of a 1 ml syringe the cells passed through the cell strainer into a petri dish. Single cell suspension was then transferred from the petri dish into 20 ml universal tubes. Cells were then spun at 400 g for 5 minutes, the supernatant discarded and the cells re-suspended to $2x10^7$ cells/ml. To distinguish these two populations, target huCD20 Tg cells were labelled as Carboxyfluorescein succinimidyl ester (CFSE) high by adding 50 µM CFSE. Non-target WT cell were labelled as CFSE low through addition of 5 µM CFSE. Flow cytometry analysis was used to assess the differential CFSE staining, and ensure that the target and non-target cells were mixed 1:1. Mixed cells were then intravenously (i.v.) injected via the tail vein into recipient C57BL/6. At Day 1, 10 µg LPS, 100 µg poly(I:C), 2.5 µg R848 or 300µg DMXAA were intraperitoneally injected into mice. A second dose of the same amount of poly(I:C) and R848 were given by I.P on day 2 in the morning. 50 µg rituximab m2a,10 µg BHH2 m2a or WR17 (irrelevant control) m2a were injected i.v. into mice on day 2 in the afternoon. Mice were sacrificed on Day 3 (18 hours post mAb injection) in the morning. Spleens were harvest for flow cytometric analysis (Figure 9).

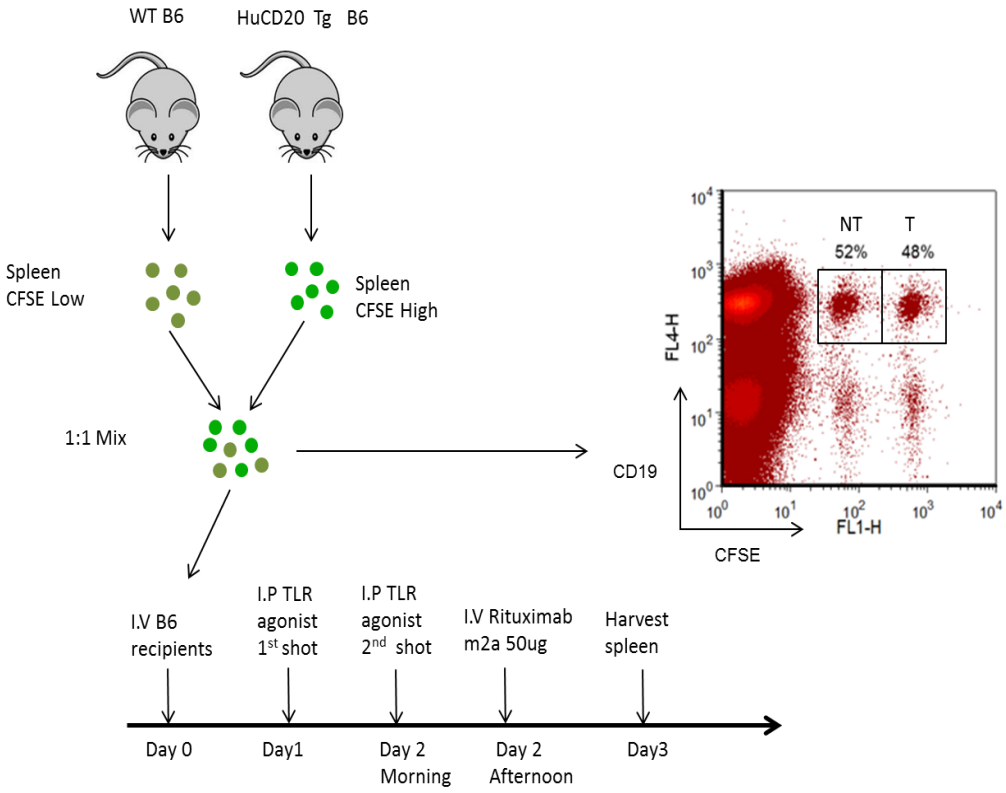

Figure 9: Human CD20 Tg adoptive transfer B cell depletion model. At Day 0, WT and human CD20 transgenic C57BL/6 spleens were harvest and labelled. Human CD20Tg cells are target cells and labelled CFSE high. WT cells are non-target cells and labelled CFSE low. Flow cytometric analysis was used to confirm CFSE staining (T=target, NT= non-target, here), and to ensure target and non-target are 1:1. Mixed cells were then i.v. injected into C57BL/6. On day 1, 10 µg LPS, 100 µg Poly(I:C), 2.5 µg R848 were i.p. injected into mice. The same amount of Poly(I:C) and R848 were given i.p. on day 2 morning. 50 µg rituximab m2a or WR17 m2a were injected i.v. on day 2 in the afternoon. Mice were sacrificed on day 3. Spleens were harvested for flow cytometry (see method 2.9) analysis

To calculate T:NT ratio, CD19+, CFSE+ adoptive transferred B cells (Gate NT+T on figure 9) were gated on from the FSC/SSC lymphocyte gate. CD19+ CFSE high (Gate T on figure 9) population represents target B cells, and CD19+ CFSE low (Gate NT on figure 9) represents non-target B cells. The T:NT ratio= percentage of target B cells/percentage of non-target B cells. Normalised T:NT ratio= T:NT ratio of mice treated with Ritm2a / T:NT ratio of correlated mice treated with isotype control.

2.7.1 BCL_1 adoptive transfer

On day 0, $1x10^4$ BCL1 lymophoma cells (see BCL1 tumour model section later, 2.12) were i.v injected into BALB/c mice. CFSE labelled HuCD20 Tg splenic cells were injected

into tumour bearing mice on day7. 100 µg poly(I:C), was injected i.p. into mice at day 8 and day 9 in the morning. 300 µg DMXAA, 800 µg CP, 100 µg rapamycin or 250 µg anti-IL10 receptor blocking mAb 1B1.3A were i.p injected to mice on day 8. On day 9 afternoon, 10 µg WR17 (isotype), 10 µg rituximab mIgG2a (Rit), 10 µg Bhh2 mIgG2a (Bhh2) were given to mice by i.v injection. Spleens were harvested at day 10 and analysed by flow cytometry.

2.8 Tissue digestion

To release target cells from connective tissues the DL liberase digestion enzyme mixture (Roche) was used. DL liberase consists of highly purified collagenase and neutral protease enzymes. DL liberase can efficiently dissociate collagen, a key component of the animal extracellular connective tissue, and allow target cell isolation [223].

Tissues harvested from mice were cut into small cubes (about $1mm^2$), then digested by DL liberase (final concentration 1 unit/ml) for 20 minutes at 37^o with shaking. After digestion, cells were passed through a 100 µm cell strainer and washed at least once before antibody staining.

To investigate tumour infiltrating Treg cells (Figure 47), tumour cells were dissociated by the tissue digestion protocol described above. After homogenisation cells were spun at 300 g for 5 minutes and re-suspended into 40% percoll. Tumour cells in 40% percoll were then layered on top of 70% percoll and spun at 900x g for 20 minutes. This step separates the tumour infiltrating lymphocytes from tumour cells. Tumour infiltrating lymphocytes were then collected in a 20ml universal and washed once before antibody staining.

To investigate tumour infiltrating lymphocytes (Figure 43), tumour cells were dissociated by the tissue digestion protocol described above. After homogenisation cells were collected in a 20ml universal and washed once before antibody staining. To record total

number of tumour cells and lymphocytes, percol separation method was not used in this experiment.

2.9 Flow cytometry

Surface staining: For primary labelling, to avoid non-specific binding $1x10^6$ cells were stained with 1 µg specific antibody for 30 minutes on ice. For secondary labelling, primary labelled cells were washed once with FACS buffer and stained with 1 µg secondary mAb for 30 minutes on ice. After staining, ex vivo samples or samples which would not be run immediately were fixed using AbD SeroTec Erythrolyse Red Blood cell lysis buffer. Samples were washed once with FACS buffer, and run on either a BD FACSCanto II or FACSCalibur and the data analysed using FCS Express. FSC-A vs FSC-H plot was used for doublet discrimination.

Intracellular staining: After surface staining (as described above), after the last wash, the supernatant was discarded and the sample pulse vortexed to completely dissociate the pellet. Typically, about 100 µl residual volume remains. The cells were fixed by adding 100 µl of intracellular (IC) Fixation Buffer (from BD anti-Mouse/Rat Foxp3 Staining Set) and pulse vortexed. The samples were then incubated in the dark at room temperature for 20-60 minutes. Without washing, 2 ml of 1X permeabilization buffer was added (diluted from BD anti-Mouse/Rat Foxp3 Staining Set) to each tube. Samples were spun at 300-400x g at room temperature for 5 minutes, the supernatant discarded, and this was repeated once. Then the recommended amount (1 µg mAb for 1 million cells) of intracellular staining antibody was added and incubated in the dark at room temperature for 20-60 minutes. 2 ml of 1X permeabilization buffer was then added to each tube and samples spun at 300-400x g at room temperature for 5 minutes and the supernatant discarded. Finally, 2 ml of FACs wash buffer was added to each tube and the samples spun at 300-400x g at room temperature for 5 minutes and then resuspended in their own volume.

2.10 In vitro T cell proliferation

Spleens from Foxp3-GFP mice were sorted to exclude GFP+ cells (-Treg cells; 99% of Treg cells removed; data not shown) or null sorted and plated at 1 x 105 cells/well with 0.1 µg/ml anti-CD3 and a range of LOB12.0 anti-4-1BB mAb concentrations as indicated. 1 µCi/well [3H]-thymidine was added 56 hours later and plates harvested after a further 16 hours culture. (This experiment was done by Dr Sarah Buchan)

2.11 BMDM phagocytosis assay

On day 1, BMDMs were differentiated and cultured as describe in section 2.3. To harvest BMDM at day 7, pre-warmed TE was used. Briefly, cells were washed with PBS once, then 2 ml TE was added to each well and the plates left in 37º, 5% CO2 incubator for 15 minutes. Cells were harvested using a cell scraper and re-suspended in complete media.

$5x10^4$ BMDM cells/well were plated into 96 well plates in 200 µl. To polarize BMDM, LPS/IFNγ 100/2 ng/ml (final concentration, same for the rest of reagents here), IL4/13 10/10 ng/ml, R8481µM, CPG 1 µg/ml or poly(I:C) 40 µg/ml were added and left for at least 24 hours to allow activation before incubation with opsonized target cells.

On day 8, to prepare target cells, a spleen from a HuCD20 Tg mouse was harvest and B cells isolated using a negative B Cell Isolation Kit from Miltenyi according to the manufacturer's instructions. To label target cells, HuCD20 Tg target B cells were incubate with 5µM CFSE (1/1000 dilution with 5mM stock) for 10 minutes at room temperature (Figure 10a). Equal volume of FCS was added to labelled cells to stop the reaction. To opsonise target cells, labelled cells were incubated either with Ritm2a (10 µg/ml final concentration) or WR17 (irrelevant, 10µg/ml) at 4º for 20 minutes (Figure 10a).

Opsonised cells were washed once with complete RPMI media and re-suspended at 2.5 x 10^6 cells/ml.

2.5 x 10^5 opsonised target cells were added to macrophage plates to achieve a 5:1 target:effector ratio. The plates were then incubated at 37^o for 30 minutes (Figure 10a). Afterwards, co-cultured cells were stained with 1µl F4/80 APC, then incubated in the dark at room temperature for 15 minutes (Figure 10a). Cells were then washed once and resuspended in 200 µl ice cold FACs buffer and incubated on ice for a further 10 minutes. Cells were transfered from 96 well plates to FACs tube by pipette (wells were scraped four time vertically, horizontally and then in a circular motion with a P200 pipette and tip and the sample drawn up) and the samples run on a BD FACSCanto II.

To measure the percentage of phagocytosis, BMDMs were identified and gated as FSC High and SSC high (Figure 10, gate 2). Among BMDMs, BMDMs which had phagocytosed target B cells were defined as F4/80 positive and CFSE positive (Figure 10, gate 3), while non-phagocytosed BMDMs were identified as F4/80 positive and CFSE negative (Figure 10, gate 4). Percentage of phagocytosis = Percentage of phagocytosed BMDMs (Gate 3) of all BMDM (Gate 2).

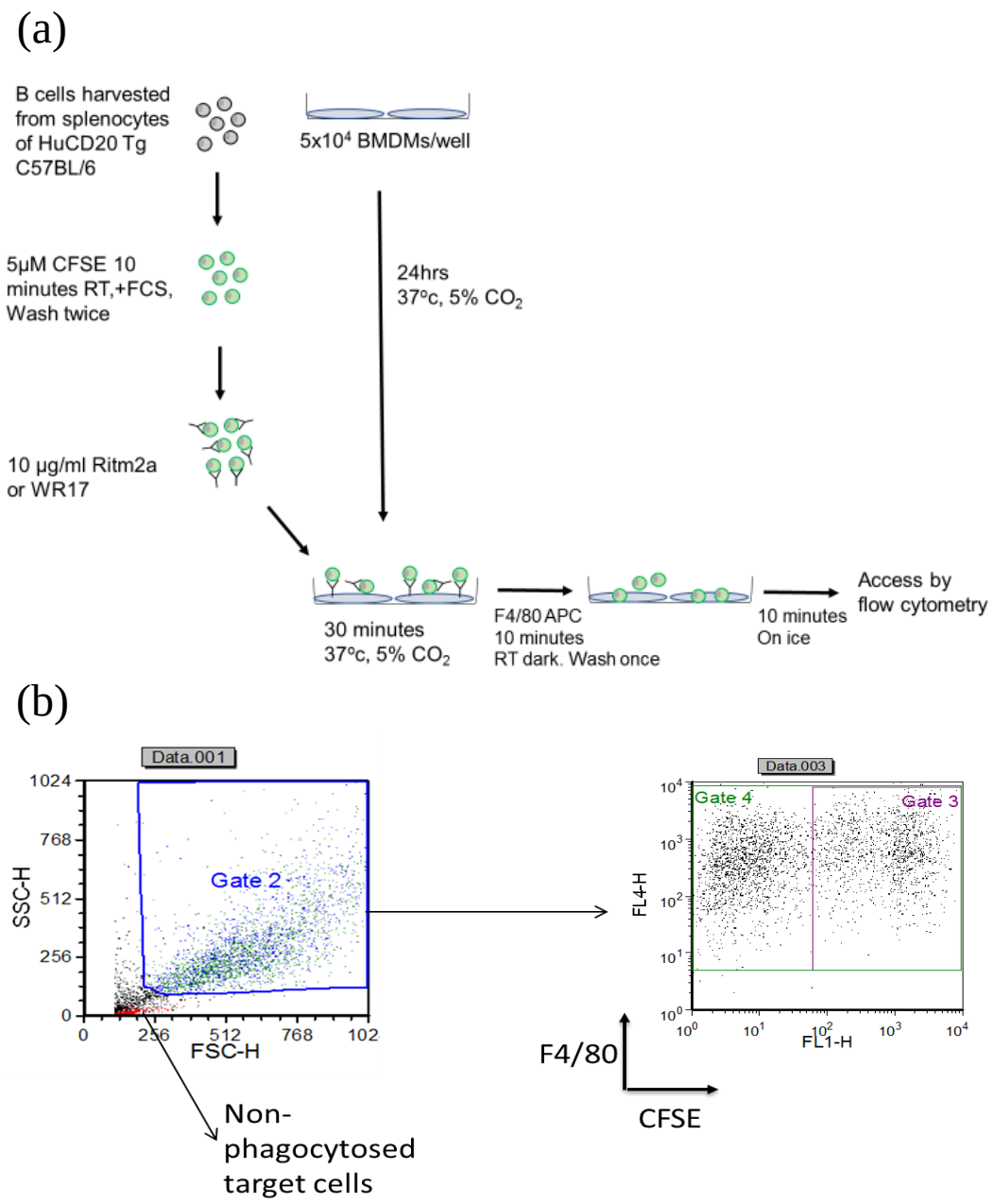

Figure 10: BMDM phagocytosis assay. (a) Phagocytosis assay design (b) All BMDMs (phagocytosed BMDM+ non-phagocytosed BMDM) were gate out as FSC high and SSC high (Gate 2). Under all BMDM gate, phagocytosed BMDMs were identified as F4/80 positive and CFSE positive (gate 3), while non-phagocytosed BMDMs were defined as F4/80 positive and Carboxyfluorescein succinimidyl ester (CFSE) (negative (Gate 4). Percentage of phagocytosis = Percentage of phagocytosed BMDMs (Gate 3) of all BMDM (Gate 2).

2.12 Tumour models

BCL_1 lymphoma

BCL_1 is an in vivo passaged lymphoma cell line that resembles human prolymphocytic leukemia [224]. This cell line was originally described by Slavin and Stroberused as a spontaneous B-cell lymphoma [225]. It's characterised by early splenomegaly and later leukaemia [225]. The advantages of using BCL_1 include: (a) carrying immunoglobulin idiotype as a clonal marker, therefore tumour cells can be identified by anti-idiotype mAb [225]. (b) Tumour grows rapidly and accumulates predominantly in the spleen [225], therefore it can be detected and staged for humane end-point easily by palpation. BCL_1 in this project was from historical frozen stocks and maintained by in vivo i.p passage through BALB/c mice for 6 months, then returning to stocks to maintain growth characteristics and therapy response. Spleens from terminal BCL_1 passaged mice were harvested. Spleens were then passed through a 100 µM cell strainer, resuspended in 20 ml of PBS and layered onto 10 ml lymphoprep solution. Cells were then centrifuged at 400 g for 15 minutes with the brakes off. Mononuclear cells forming an interface layer (mid layer) were collected by pasteur pipette into 50 ml falcon tubes. Cells were washed once by PBS and counted by coulter counter (Beckman Coulter). At day 0, $1x10^4$ cells were i.v injected into BALB/c mice. For BCL_1 therapy model, 300 µg DMXAA was i.p injected into mice on day 6 and 13. On day 7 and 14, 200 µg anti-CD20 mAb 18B12 were given to mice by i.v injection. Spleens size were monitored to humane end point by an independent animal technician blinded to the experimental groups.

Colon Tumor #26 (CT26)

The CT26 tumour model [226] is a colorectal carcinoma cell line that shares characteristics of aggressive, refractory human colorectal carcinoma. This cell line was developed in 1975 by exposing BALB/c mice to N-nitroso-N-methylurethane [227]. The

CT26 cell line used in this project were from historical stocks and maintained in DMEM media with 10% FCS, glutamate/pyruvate, penicillin/streptomycin. The CT26 cells were passaged at 80% confluent, and to maximise the reproducibility of experiments, cells were passaged once before s.c injection. To harvest the cells, the culture medium was removed from the flask, cells were then washed with 20ml PBS, then 10ml Trypsin-EDTA was added and the flask transferred into 37ºC 5% CO_2 humidified incubator for 5 minutes. To stop the reaction, dissociated cells were transfer into a 20 ml universal containing 10 ml culture media and centrifuged for 5 minutes at 300 g. The supernatant was discarded and the resuspended cells washed with 20 ml PBS at least once. Cells were set out to rest for one minute in a tissue culture hood, suspension cells were collected for later injection. To investigate the mechanism of action of the agonistic immunomodulatory anti-4-1BB mAb LOB12.0, $5x10^4$ CT26 cells were injected s.c. into age matched BALB/c females at day 0. Anti-4-1BB mAb LOB12.0 mouse IgG1 or IgG2a isotypes were administrated to mice by i.v when tumours were palpable, then i.p every other day for three further administrations, in total 200µg. Tumour sizes were measured by calliper 3 times per week until day 100. To investigate intra-tumoural CD4+Foxp3+ Treg cell depletion, CD8+ T cells were depleted by injecting 500 µg CD8 depletion mAb YTS169 [228] i.p on day -1, 1 and 4. $5x10^4$ CT26 cells were s.c injection in BALB/C females at day 0. In total 200 µg anti-4-1BB mAb LOB12.0 was given to mice by i.v on day 6, and i.p on day 8, 10, 12. Tumours were harvested from these mice for flow cytometry analyze on day 13. Similar protocol was used to explore the agonistic activity of anti-4-1BB LOB12.0 mAb. In this experiment, we were interested in CD8+ T cell, thus CD8 depletion mAb was not used. In addition, to investigate the role of FcγRs in LOB12.0 therapy, γ-chain knockout (KO) and FcγRII KO, FcγR null (γ-chain knockout (KO) cross with FcγRII KO) BALB/c were used (Section 2.1, page 44).

EG7 thymoma (Sarah L Buchan)

E.G7 thymoma cell was C57BL/6 (H-2 b) mouse lymphoma cell line EL4 (ATCC TIB-39) transfected with the neomycin resistance gene and a complete copy of chicken ovalbumin mRNA [229]. Thus, ovalbumin epitopes are overexpressed in this cell line.

The EG7 cells were maintained in complete RPMI 1640 medium at 5% CO2 and 37 °C and were passaged every 2 to 3 days. To inoculate EG7 thymoma, sex matched C57BL/6 mice were challenged with 5 x 10^5 EG7 s.c. on day 0. On days 3, 5 and 7 mice received 200 µg LOB12.0 mAb or PBS control i.p. as indicated. Tumour sizes were measured by calliper 3 times per week until day 100 and mice were culled when mean tumour area exceeded 225 mm^2.

NXS2 neuroblastoma (Stuart N Dunn)

NXS2 cell line comes from NX31T28 cell line that was created by hybridization of murine dorsal root ganglional cells from C57BL/6J mice with the GD 2 negative C1300 murine neuroblastoma cell line (A/J background) [230]. NXS2 cell was produced by selection of NX31T28 cells that express high level of GD 2. This is achieved by stained NX31T28 cells with anti-GD 2 mAb 14G2a and microbeads, then sorted GD 2 high populations with fluorescence and magnetic-activated cell sorting [230]

NXS2 cell line was maintained in Dulbecco's minimal essential medium with 10% FCS at 5% CO2 and 37 °C. The cell line was passaged every 4 to 5 days. To inoculate NXS2 neuroblastoma, sex matched A/J mice were challenged with 2 × 10^6 NXS2 cells s.c. and received 200 µg anti-41BB mAb or isotype control mAb i.p. when tumor was palpable. A second dose of 200 µg was given 3 days later. Tumour sizes were measured by calliper 3 times per week until day 100 and mice were culled when mean tumour area exceeded 225 mm^2.

2.13 Fc gamma receptor A:I ratio calculation

Fc gamma receptor A:I binding ratio in vitro and in vivo were calculated according to the expression of Fc gamma receptor and isotype control on the cell surface as detected by flow cytometry. The expression of Fc gamma receptors was quantified by using the geometric mean of mean fluorescence intensity (MFI) that was acquired by flow cytometry. To ensure accurate measurements the background, geometric MFI of isotype control was subtracted from that of Fc gamma receptors.

Activatory Fc gamma ratio= MFI of FcγRI x FcγRIII x FcγRIV

Inhibitory Fc gamma ratio=MFI of FcγRII

A:I ratio= Activatory Fc gamma ratio / Inhibitory Fc gamma ratio

$A:I_{NT}$=A:I ratio of NT macrophage

The results presented were obtained from several independent experiments and the baseline levels detected in these experiments were variable. Thus, to normalize these results, each test condition were divided by $A:I_{NT}$ so that non-treated macrophages received a ratio of 1.

Chapter III - TLR agonists polarize macrophages to a pro-inflammatory phenotype in vitro

3.1 Introduction

Macrophages are highly plastic cells, which can be skewed/polarised to different phenotypes in response to external stimuli [231, 232]. Macrophages can broadly be classified into a classically activated, M1 pro-inflammatory phenotype or an alternatively activated, M2 anti-inflammatory phenotype [44]. Although it's becoming clear that the M1-M2 paradigm is too simplistic, it is widely agreed that pro-inflammatory and anti-inflammatory phenotypes represent two extreme states of macrophage phenotypic activation states [233].

Pro-inflammatory macrophage activation has been demonstrated to be linked to the Th1 response and Th1-derived IFN-γ [234] hence the M1 nomenclature. The classic M1 stimuli LPS/IFN-γ polarizes macrophages into a pro-inflammatory phenotype which is characterised by the production of IL12, IL6, TNFα and NO [44, 233]. In contrast, macrophages can be polarized to anti-inflammatory phenotype by Th2 cytokines IL4/IL13 [44, 45, 233] and the M2 designation. In addition, it has been shown in vitro that stimulating human monocyte-derived macrophages (MDM) with classic M1 stimuli LPS/IFN-γ induces morphological changes, the MDM take on a "fried egg" morphology [235]. Whereas activated by M2 stimuli, IL4/IL13, causes MDM to elongate and form a "spindle-like" cell morphology [235]. It has been suggested that the shape of the macrophage itself can modulate macrophage phenotypes. The expression of M2 marker arginase-1 is higher in macrophages that have been seeded onto micropatterned (20 μm wide lines) surfaces than on unpatterned when treated with low doses of IL-4/IL-13 for 24 hours [236]. These observations support the contention that macrophages are perhaps uniquely sensitive to an array of microenvironmental queues and that they can adapt rapidly to adopt suitable phenotypes in response to those queues.

Macrophages are able to remove dead cells, cellular debris and pathogens via phagocytosis [20]. This process is mediate by Fc and FcγR interaction [15]. FcγR can be classified into activatory or inhibitory according to their response to ligation [30]. In mouse, activatory FcγRs including, FcγRI, FcγRIII, FcγRIV and inhibitory FcγRII [30]. In human FcγRI, FcγRIIa, FcγRIIIa and FcγRIIIb are activatory FcγRs, and FcγRII is inhibitory [30]. It has been documented that the balance between activatory FcγR and inhibitory FcγR is important in mediate ADCP efficacy. In the B16 melanoma model, the potency of therapeutic mIgG2a anti-gp75 TA99 is remarkably impaired in common gamma chain KO mice which lack all activatory FcγR, and enhanced in FcγRII KO mice which lack the inhibitory FcγR [160]. In a xenograft human breast cancer (BT474M) model, anti- Receptor tyrosine-protein kinase erbB-2(HER2) mAb 4D5 loses its ability to prevent tumour growth in common gamma chain KO mice [160]. In the same xenograft model, 4D5 therapeutic efficacy is greatly enhanced in FcγRII KO mice [160]. Additionally, anti-CD20 mAb were less efficient at deleting tumour cells in FcγRIII KO and FcγRI/III double KO mice in the syngeneic Eμ-Myc lymphoma (BL3750) model [198].

Macrophages have been shown to express the majority of TLRs, including extracellular TLR1, TLR 2, TLR4, TLR 5, TLR 6 and intracellular TLR 3, TLR 7, TLR 8, TLR 9, TLR 11, TLR 13 [6] (Figure 5, page 22). To data, it has been documented that TLR agonists such as poly(I:C) [237], R848 [238] and CPG [239] have the potential to polarize macrophages to a pro-inflammatory phenotype. Thus, we first aimed to recapitulate these results in vitro. We stimulated BMDM with different TLR agonists and compared their morphology, function and phenotypic markers to classic pro-inflammatory and anti-inflammatory phenotypes. Then we established the correlation between the phenotype of macrophage and their expression of FcγRs, and then determined the impact of this on their ability to mediate antibody effector function in the form of ADCP.

3.2 Results

3.2.1 TLR agonists R848 and poly(I:C) stimulation polarizes BMDM, inducing morphological changes and increases nitric oxide production

Pre-clinical data has demonstrated that TLR agonists for example R848, Poly IC and CpG can inhibit tumour growth via activating DC and NK cells (Section 1.8, page 22). Thus, we first investigated the phenotypes of well-studied murine bone marrow derived macrophages (BMDM) stimulated by these TLR agonists and compared them to published literature. LPS/IFNγ and IL4/IL13 are well defined polarizing reagents for BMDM [42]. In vitro, LPS/IFNγ stimulation polarized BMDM to a classically activated, pro-inflammatory phenotype [44], while IL4/IL13 treated macrophages become alternatively activated, anti-inflammatory phenotype [44]. In macrophages, L-arginine metabolism is controlled by the enzymes arginase I (Arg1) [52] and inducible NO synthase (iNOS), these two enzymes compete with each other to catalyse L-arginine [47]. Macrophages with a pro-inflammatory phenotype express high levels of iNOS and low levels of Arg1, high levels of iNOS will promote hydrolysis of L-arginine, resulting in increased nitric oxide (NO) production [47, 240, 241]. A range of tumour cells of differing origins, for example ovarian cancer [240], melanoma [241] and renal carcinoma [242] can be eliminated by high concentrations of NO. Several NO mediated mechanisms have been proposed for anti–tumour function, including direct damage of DNA, inhibition of DNA synthesis and induction of apoptosis [240, 241]. In contrast, M2 macrophages express low levels of iNOS and high levels of Arg1 that enhances the hydrolysis L-Arginine into urea and L-ornithine [52], the latter able to promote the proliferation of tumour cells. In these experiments, we attempted to define the plasticity of BMDMs. Cells were isolated from bone marrow and cultured in vitro for 7 days with complete RPMI media contain 20% L929 [220](Chapter 2.3, page 47). On Day 7 cells were stimulated for 48 hours with several well characterised, clinically relevant TLR agonists; TLR 3 agonist

poly(I:C) [237], TLR7/8 agonist R848 [238] and TLR 9 agonist CpG [239]. In these initial studies, we began by comparing morphological and functional changes in the form of NO and arginase production with non-treated cells and those treated with the classic M1 and M2 polarising agents LPS/IFNγ and IL4/IL13 respectively.

In comparison to NT macrophages LPS/IFNγ, poly(I:C), R848 and CPG polarised BMDM to a phenotype where cells appeared rounded and clumped together (Figure 11). In contrast, IL4/IL13 polarized BMDM and formed 'spindle like' structures (Figure 11).

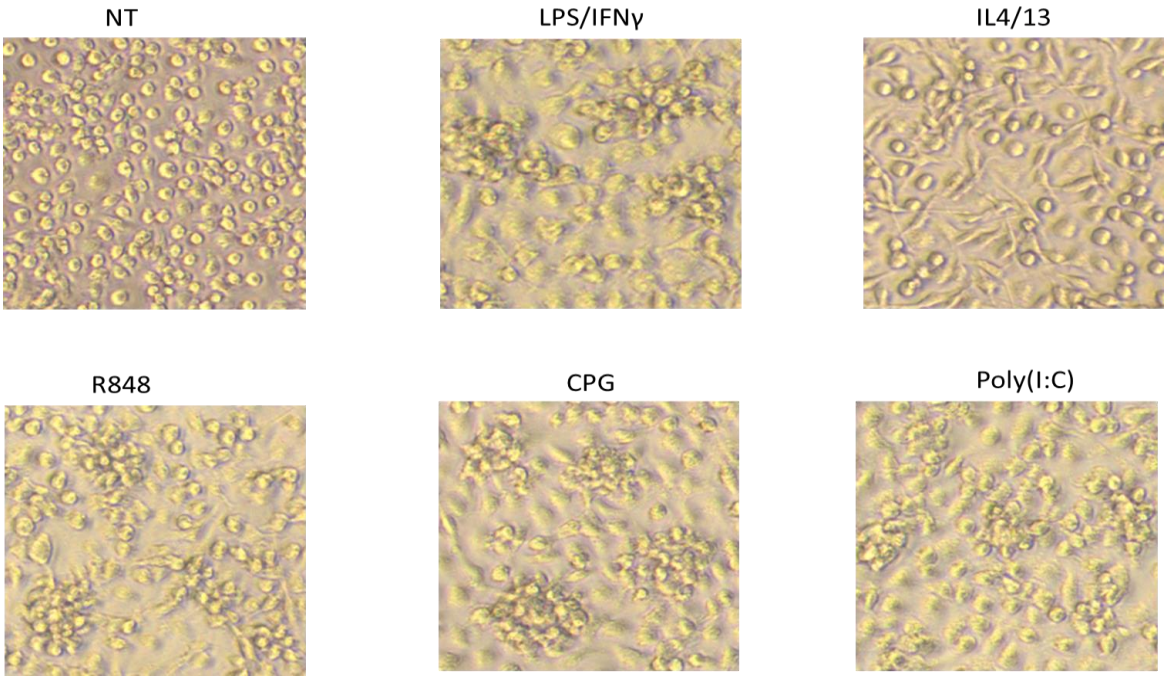

Figure 11: In vitro, TLR agonist stimulation induces BMDM morphologic changes. Bone marrow derived macrophages (BMDMs) at 1x106 cells/well were cultured for 7 days in media (RPMI with 10% FCS, GP, PS, 2ME and 20 % L929). BMDM were then stimulated with different reagents. LPS/IFNγ 100/2 ng/ml (final concentration, same for the rest of reagents here), IL4/13 10/10 ng/ml, R8481 µM, CPG 1 µg/ml or poly(I:C) 40 µg/ml were given to BMDM at day 7. After 48 hours, BMDMs were observed by Olympus CKX41 Microscopy, objective lens (10x). Representative images shown from four independent experiments.

Having established that, in keeping with the published literature [44], we could activate BMDM in vitro with typical morphological changes we sought to confirm that these reagents also induced functional changes. To this end, we performed NO and arginase assays on BMDMs stimulated with classic M1 stimuli LPS/IFNγ, M2 stimuli IL4/IL13 and

TLR agonists poly(I:C), R848, CpG [42, 243]. The production of NO is greatly increased on LPS/IFNγ, R848 and poly(I:C) treated BMDM and to a lesser extent with CpG activated cells (Figure 12a). As expected, stimulation by IL4/IL13 increased the production of arginase from BMDM (Figure 12b). None of the TLR agonists assayed here strongly augmented arginase production like IL4/IL13 (Figure 12b). The NO and arginase assay results combined with the morphological changes demonstrate that the TLR agonists R848 and poly(I:C) polarized BMDMs to an activatory phenotype similar to M1.

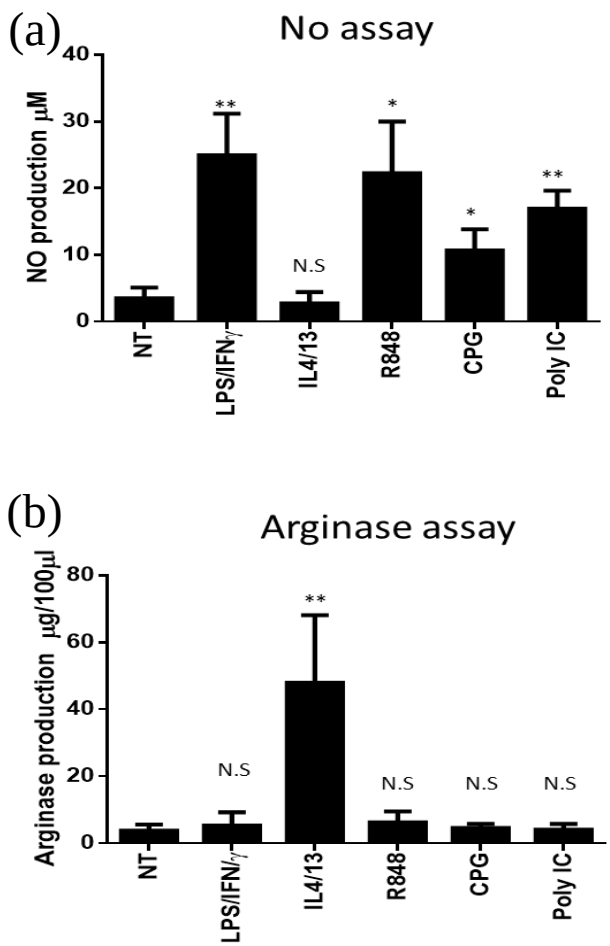

Figure 12：TLR agonist stimulation increased production of nitric oxide from BMDM. Bone marrow derived macrophages (BMDMs) were cultured with RPMI 1640 contain 10% FCS, GP, PS, 2ME and 20% L929. At day 7, $2.5x10^5$ cells were re-plated to each well of flat-bottomed 96 well plate, and left at least 8 hours to adhere before being given TLR agonists. After 24 hours of stimulation by LPS/IFNγ 100/2 ng/ml (final concentration, same for the rest of reagents here), IL4/13 10/10 ng/ml, R848 1 µM, CPG 1 µg/ml or pIC(poly(I:C)) 40 µg/ml, supernatants were harvested for nitric oxide assay (a) and cells were used for arginase assay (b). LPS/IFNγ, R848 or poly(I:C) activation largely increase NO production by BMDM (a). None of these reagents is able to induce arginase release by BMDM, except IL4/13 (b). A one-tailed nonparametric student T test was performed to analyse significant differences between NT group and various reagents treated group. * represents significance of $P<0.05$, ** represents $P<0.01$ and N.S indicates that the result is not significant (n=4).

3.2.2 Stimulation with LPS/IFNγ or TLR 3 agonist poly(I:C) changes phenotypic markers on BMDM

We started by investigating classic macrophage activation markers on the BMDM using the pro-inflammatory marker CD86 [244] and anti-inflammatory marker CD206 [45] when stimulation by different TLR agonists. We found that LPS/IFNγ and poly(I:C) were able to significantly increase the expression of co-stimulatory protein CD86 on BMDM (Figure 13b, c). While stimulated by IL4/13, R848 and CPG didn't alter CD86 expression on BMDM (Figure 13b, c). Although it's not significant, there is a trend that IL4/13, R848 and CpG stimulation increased the expression of mannose receptor CD206 (Figure 13b, c). The expression of CD206 on BMDM is not changed when polarized by LPS/IFNγ or poly (I:C) (Figure 13b, c).

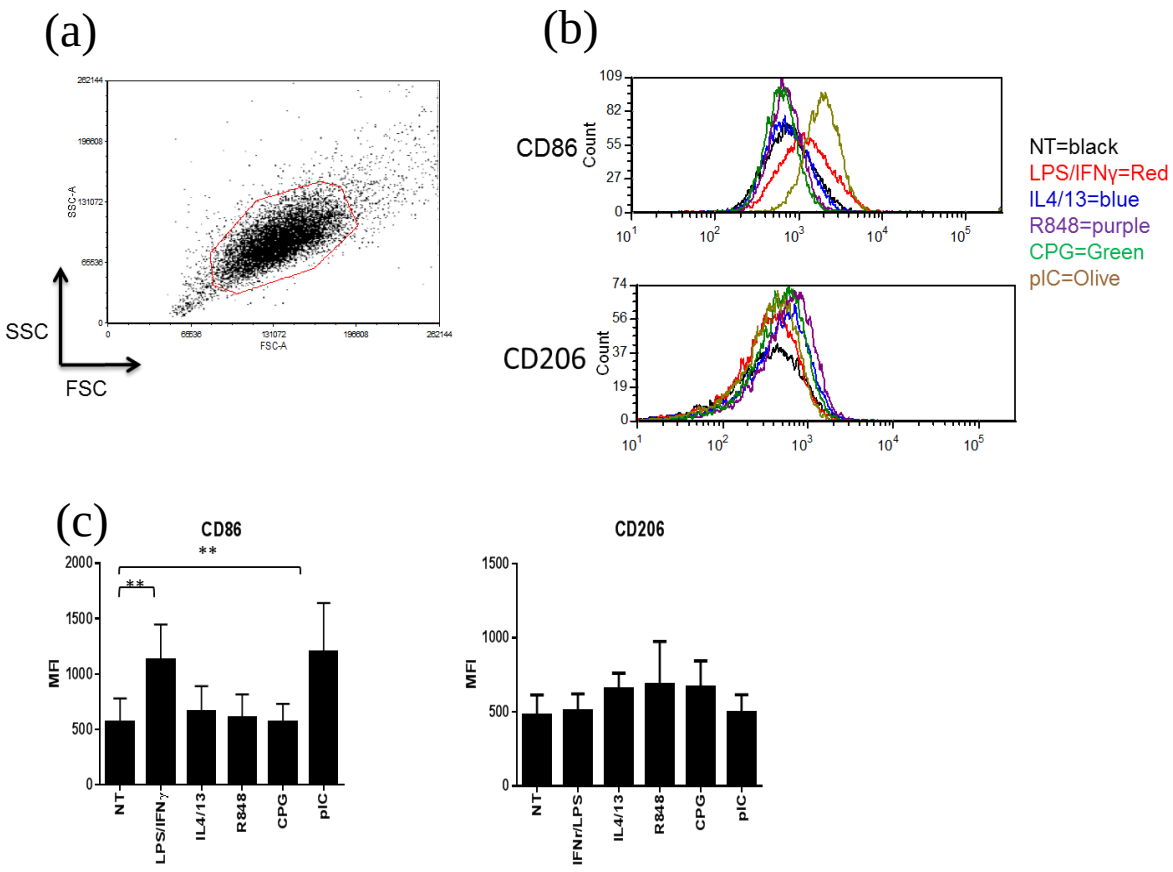

Figure 13: Phenotype markers expression on polarized BMDM. After 48 hours activation with LPS/IFNγ 100/2 ng/ml (final concentration, same for the rest of reagents here), IL4/13 10/10 ng/ml, R848 1 µM, CPG 1826 1 µg/ml or pIC 40 µg/ml, bone marrow derived macrophages (BMDMs) were harvested and analysed by flow cytometric analysis for expression of phenotype markers CD86 and CD206. (a) Gating strategy of BMDM. (b) Histogram of CD86 and CD206 expression on BMDM treated with different stimuli. (c) Summary of CD86 and CD206 expression on polarized BMDM. A one-tailed unpaired nonparametric T test was performed to analyse significance between NT and different treated groups (n=3). *represent a significance of P<0.05, ** represent a significance of P<0.01.

3.2.3 Stimulation of murine macrophages with LPS/IFNγ or TLR 3 agonist poly(I:C) increases the expression of FcγRI and IV in vitro

FcγR expressed on macrophages are important in mediating macrophage function [30]. To date, the FcγR expression on TLR agonist activated macrophages have not been well documented. To investigate the FcγR expression in response to different TLR agonist stimulation we performed a qPCR assay on BMDM after 24 hours stimulation (Figure 15) and attempted to correlate this to protein expression as assayed by flow cytometry at 48 hours (Figure 17). For qPCR assay, RNA was extracted from stimulated BMDM and reverse transcribed to cDNA immediately, the final product was used for qPCR assay

(Section 2.5, page 50). To calculate the FcγR gene expression between non-treated and stimuli treated BMDM, the $2^{-\Delta\Delta C_T}$ method was used [222] (See Chapter II 2.5 section).

To determine a suitable housekeeping gene to use for these experiments, we compared the gene expression of hypoxanthine-guanine phosphoribosyltransferase (HPRT) to GAPDH (Glyceraldehyde 3-phosphate dehydrogenase) in response to classic M1 skewer LPS/IFNγ and M2 stimuli IL4/13 stimulation. We found that compared to non-treated BMDM, LPS/IFNγ stimulation strongly changed the expression of GAPDH, 1.3-2.9-fold increases have been observed (Figure 14). While the expression of HPRT is more stable when treated with LPS/IFNγ (1.4 - 1.45-fold increase, Figure 14). Our results show that HPRT is more stable and reliable than GAPDH, thus HPRT was used as the housekeeping gene for our subsequent qPCR assays.

(a)

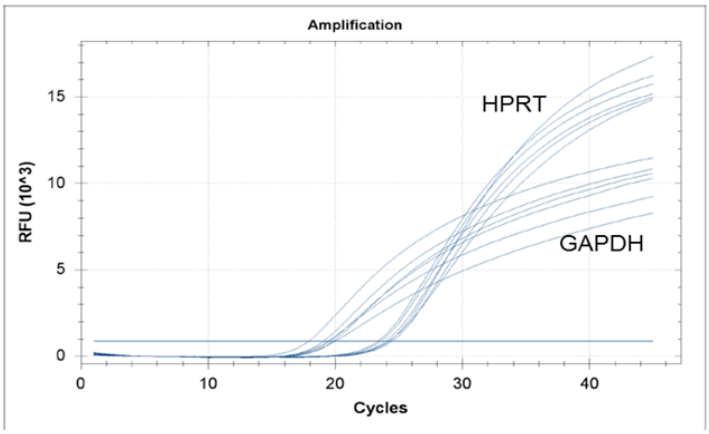

(b)

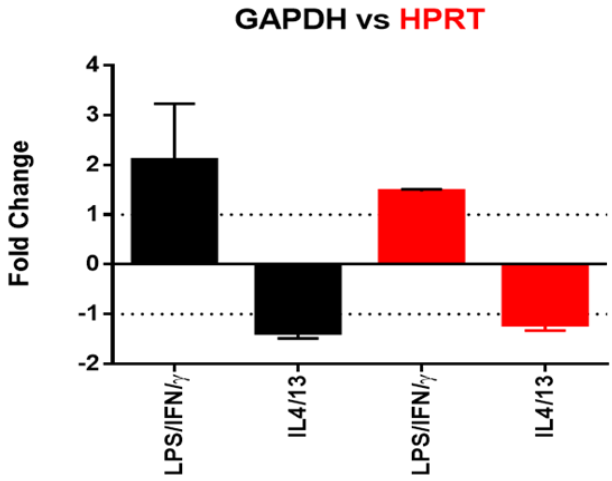

Figure 14: Determining the suitable housekeeping gene, GAPDH vs HPRT. RNA was extracted from non-treated, LPS/IFNγ, and IL4/13 treated bone marrow derived macrophage (BMDM). These RNAs were synthesized to cDNA, which was then used for the qPCR assay. (a) Raw data, number of amplification cycles required to reach threshold cycles. RFU= Relative fluorescence units. (b) The gene expression of glyceraldehyde 3-phosphate dehydrogenase (GAPDH) (black) and hypoxanthine-guanine phosphoribosyltra--nsferase (HPRT)(red) with LPS/IFNγ and IL4/13 treated BMDM. Data is normalised to non-treated BMDM. Data from qPCR assays were analysed by 2(-ΔΔC(T)) method. HPRT is more stable than GAPDH in BMDM. Representative results shown from two independent experiments.

After 24h stimulation, compared to non-treated BMDM, FcγRI and FcγRIV gene expression in LPS/IFNγ, poly(I:C), R848 and CpG treated BMDM were significantly increased. The most striking increase was observed on LPS/IFNγ and poly(I:C) activated BMDM with approximately 5 and 12-fold increase for FcγRI, 15 and 7-fold increase for FcγRIV respectively (Figure 15). In contrast, stimulation with IL4/13 reduced the gene expression of FcγRI (Figure 15). In keeping with its inhibitory role compared with

activatory FcγRI and FcγRIV, LPS/IFNγ, poly(I:C), R848 and CpG activation remarkably reduced the gene expression of FcγRII, and IL4/13 polarization slightly enhanced FcγRII mRNA expression (Figure 15).

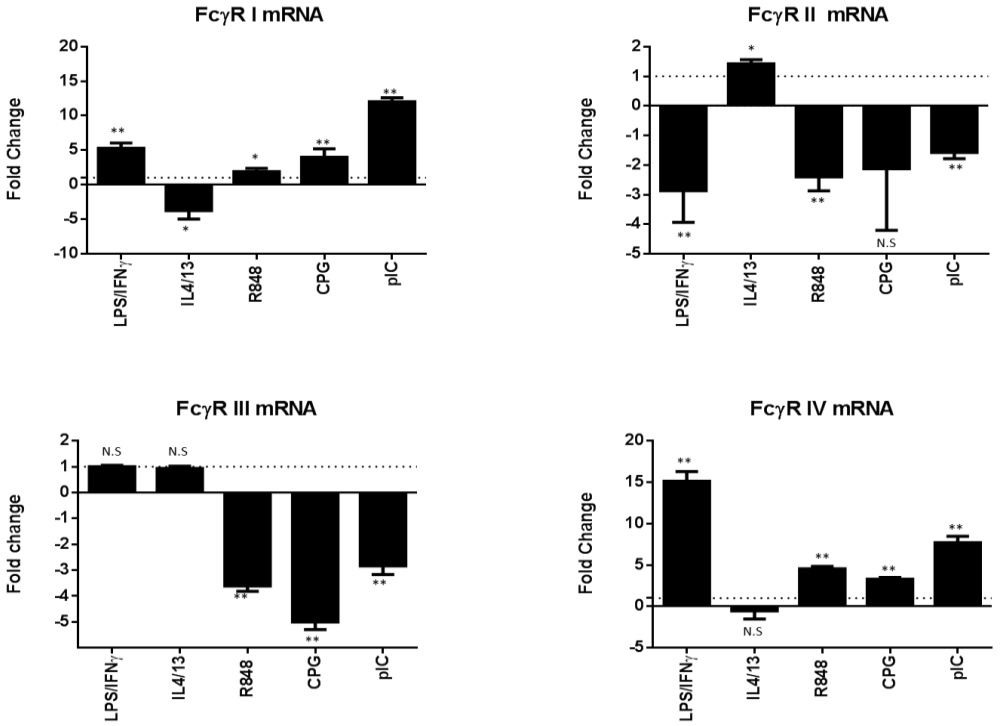

Figure 15: The gene expression of FcγR on polarized BMDM. After 24h stimulation with LPS/IFNγ 100/2 ng/ml (final concentration, same for the rest of reagents here), IL4/13 10/10 ng/ml, R848 1 µM, CPG 1826 1 µg/ml or pIC 40 µg/ml, bone marrow derived macrophages(BMDMs) were harvested for qPCR. Gene expression of FcγR on stimulated BMDM are shown, results are normalised to fold change of NT BMDM using the 2(-Delta Delta C(T)) method to minimise the variation between each experiment. One-fold equals no change in gene expression here. A one-tailed unpaired nonparametric T test was performed to analyse significance between NT and different treated groups (n=3). *represent a significance of P<0.05, ** represent a significance of P<0.01. Results are from two independent experiments.

3.2.4 Anti-mouse FcγR mAb titration

To avoid the cross reactivity of anti-mouse FcγR mAbs, we digested these in-house produced IgGs into $F(ab')_2$ fragments, and labelled them with fluorescein isothiocyanate (FITC) (Alison Tutt). For anti-mouse FcγRII (mFcγRII) IgG, Claude H.T Chan from our lab, substituted an asparagine at position 297 to an alanine. This N297A substitution

prevents the n-linked glycosylation of the Fc and prevents Fc:FcγR interactions. In order to verify the specificity of these anti-mFcγR mAb, the FreeStyle™ 293-F cell was used. 293-F is a permanent cell line derived from primary embryonic human kidney. This cell line was transformed with sheared human adenovirus type 5 DNA, which allowed cells to produce very high levels of recombinant proteins. Activatory mFcγRs, CD64 (FcγRI), CD16 (FcγRIII) and FcγRIV were co-transfected with mouse gamma chain, while CD32 (FcγRII) was transfect to 293F cells alone. After 48 hours, transfected cells were harvested and checked by flow cytometry (Method 2.9). To titrate FITC conjugated anti-mFcγR mAb, different concentration (final concentration) of mAb were used: 0, 2, 5, 10 and 20 µg/ml.

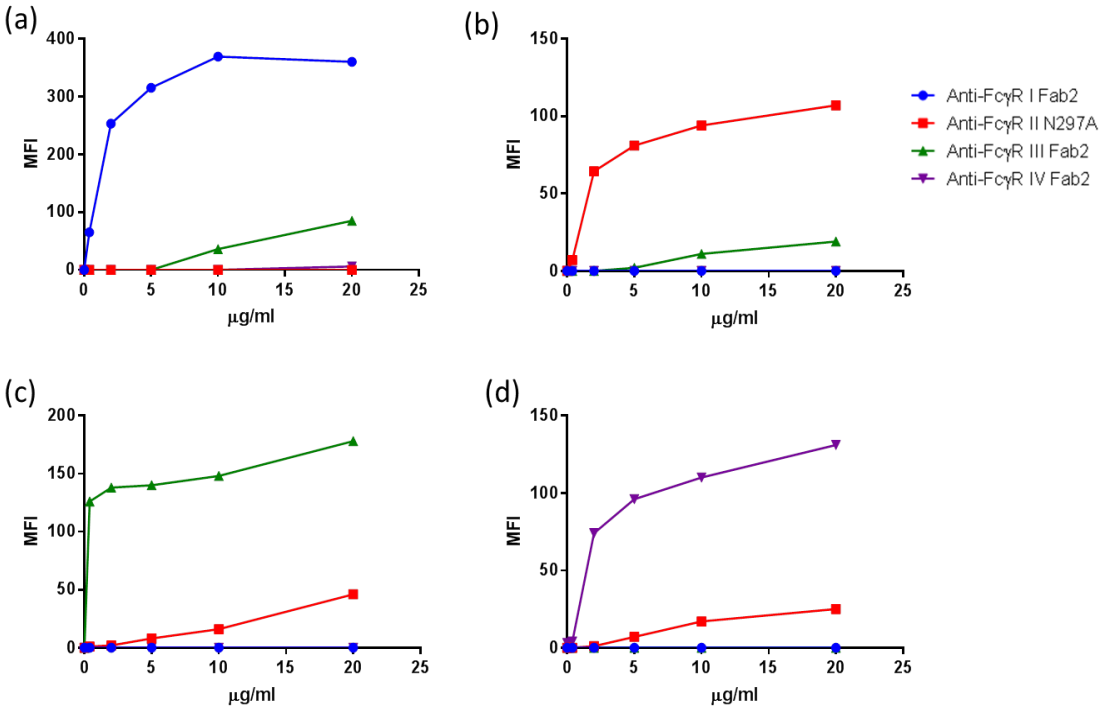

Figure 16: Anti-mouse FcγR F(ab')2 titration on transfected 293F cells. On day 0, 293F cells were transfected with different mFcγR, CD64 (FcγRI) (a), CD32 (FcγRII) (b), CD16 (FcγRIII) (c) and FcγRIV (d). Activatory mFcγR I, III and IV were co-transfected with mouse gamma chain. 48 hours after transfection, cells were harvested and stained by anti-mFcγRI F(ab')2 (blue), anti-mouse FcγRII N297A (red), anti-mouse FcγRIII F(ab')2 (green) and anti-mouse FcγRIV F(ab')2 (purple). The result are representative data from 3 different experiments.

The result suggested that anti-mFcγR I, II and IV are saturated at 10 μg/ml (Figure 16a, b,d), while the anti-mFcγR III saturated at much lower concentration around 1 μg/ml. All anti-mFcγR F(ab')2 and N297A mutation antibodies are highly specific. Although there is a small amount of cross binding by anti-mFcγRII N297A (Figure 16c, d) and anti-mFcγRIII (Figure 16a) but this is likely a consequence of the 293-F transfection system where the mFcγR are highly overexpressed at non-physiological levels.

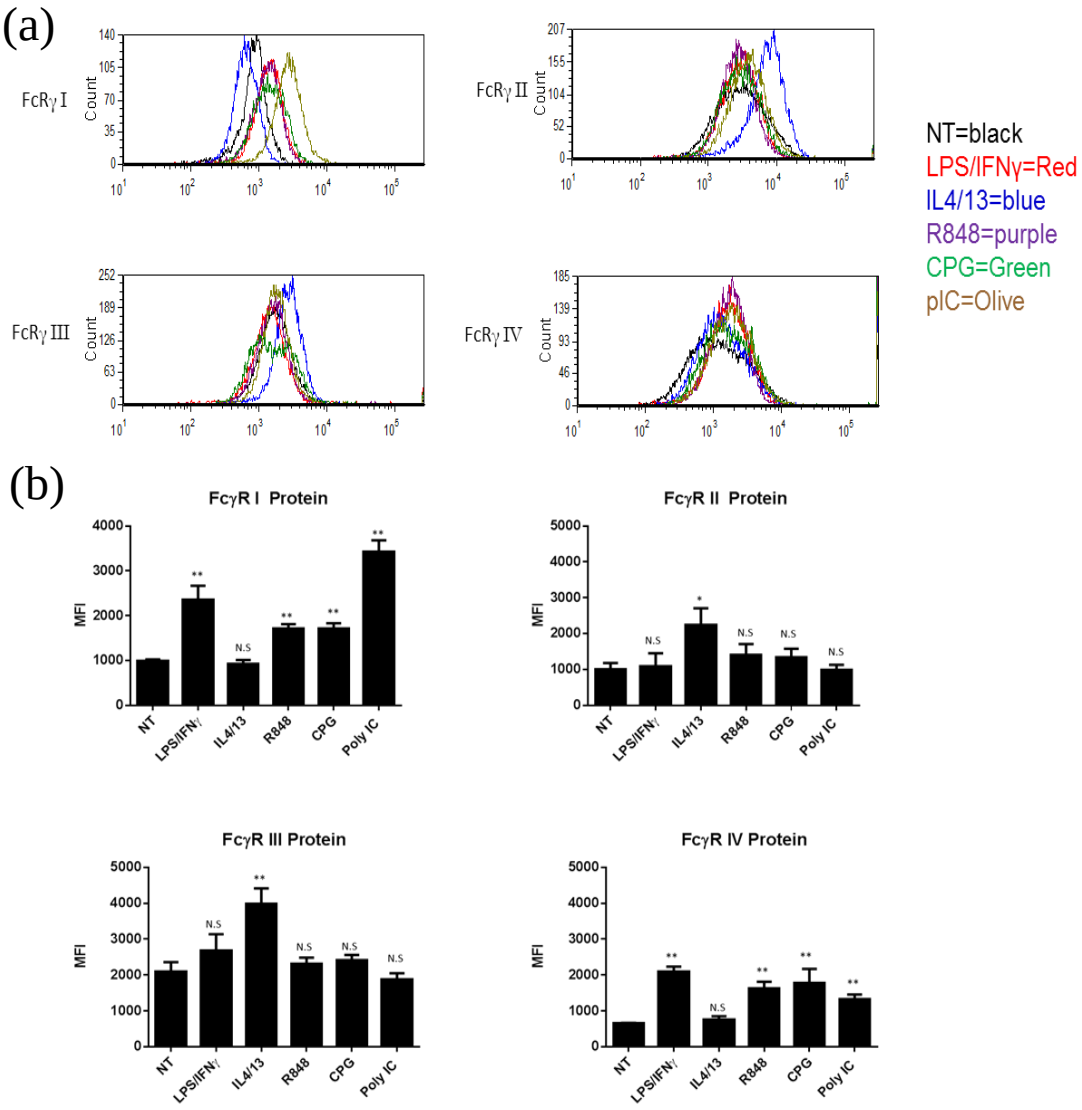

Figure 17: FcγR expression on polarized BMDM. After 48h stimulation with LPS/IFNγ 100/2 ng/ml (final concentration, same for the rest of reagents here), IL4/13 10/10 ng/ml, R848 1 µM, CPG 1826 1 µg/ml or pIC 40 µg/ml, cells were collected for flow cytometry analysis. (a) Representative data of FcγR expression on BMDM. (b) Surface expression of FcγR on polarized BMDM. Results are from three independent experiments. A one-tailed unpaired nonparametric T test was performed to analyse significance between NT and different treated groups (n=3). *represent a significance of P<0.05, ** represent a significance of P<0.01.

To confirm our qPCR results at the protein and cell surface expression level, we also analysed the BMDMs after 48h stimulation by flow cytometry using verified anti-mouse FcγR mAb (Figure 16). After 48h stimulation, a remarkable increase in FcγRI expression was observed with LPS/IFNγ, poly(I:C) and, to lesser extent on R848 and CPG treated BMDM (Figure 17a, b). IL4/13 activation didn't alter FcγRI expression (Figure 17a, b). Most of the reagents used didn't change FcγRII expression apart from IL4/13, which

significantly promote FcγRII expression on BMDM surface (Figure 17a, b). The same trend was observed for FcγRIII expression in that IL4/13 is the only stimuli to change it (Figure 17a, b). LPS/IFNγ, poly(I:C), R848 and CPG activation dramatically increased FcγRIV expression on BMDM (Figure 17a, b). Taken as a whole and potentially more importantly for functional activity, activation/polarization by LPS/IFNγ, poly(I:C), R848 or CpG significantly increased the FcγR activatory to inhibitory ratio (Figure 18) (Method 2.13), which has been shown to be important in regulating ADCP [160, 198].

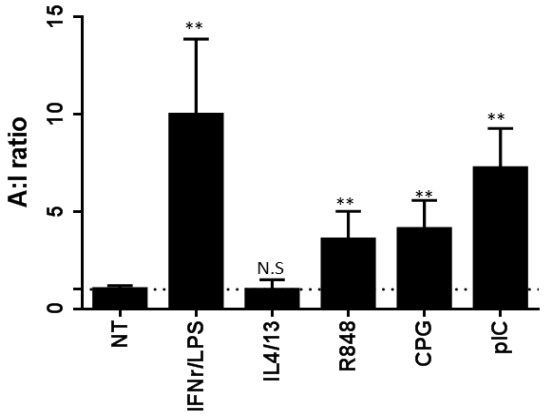

Figure 18: BMDM polarization alters FcγR A:I ratio. Activatory to inhibitory ratio of FcγR is calculated based on the MFI value from Figure 15b. Activatory FcγR = FcγR I x FcγR III x FcγR IV. Inhibitory FcγR= FcγR II. A one-tailed unpaired nonparametric T test was performed to analyse significance between NT and different treated groups (n=3). *represent a significance of P<0.05, ** represent a significance of P<0.01.

Although IL4/13 stimulation slightly increased the mRNA expression of FcγRII (Figure 15), it strongly promoted FcγRIII protein expression on BMDM (Figure 17b). BMDM activated by LPS/IFNγ, poly(I:C), and R848 inhibited the expression of FcγRII at the mRNA level (Figure 15), but didn't change the expression of FcγRII on the cell surface (Figure 17b). These data imply that polarization by classic M1 stimuli, M2 stimuli or the TLR agonists R848 and poly(I:C) may alter FcγR recycling. Immune complex (IC) bind to FcγRII induces internalisation, which then recycles FcγRII to the cell membrane both with or without IC [245] [246]. IL4/13 stimulation may strongly promote this process, thus

more cytosolic FcγRII will recycle to the cell membrane, and this may increase the FcγRII expression on cell surface.

3.2.5 Polarizing BMDM by LPS/IFNγ or poly(I:C) promotes antibody dependent cellular phagocytosis in vitro.

Having established that polarising macrophages with different stimuli changes FcγR expression we sought to confirm that these changes had a functional consequence for ADCP in vitro. Using time lapse microscopy, we showed that macrophages can ingest opsonised cells and eliminate them through ADCP (Figure 19). To quantify the ADCP, BMDM phagocytosis assay was used (Method 2.11). Briefly, BMDM cells were cultured in complete media RPMI with L929 supplementation [220] (Method 2.3) for 7 days. LPS/IFNγ, IL4/13, R848 or poly(I:C) were added to BMDM, 24 hours after stimulation BMDM were transferred into 96 well plates and incubated with CFSE labelled human CD20Tg B cells (5:1 target cell:effector ratio) opsonised with 10 μg/ml Ritm2a for the phagocytosis assay (described in Section 2.11) (Figure 20).

In our phagocytosis model, non-treated BMDM had taken up ~45% of anti-huCD20 opsonised B cells (Figure 20a, b). Stimulation by LPS/IFNγ or poly(I:C) strongly increased the percentage of phagocytosis to 80% and 75% respectively. However, compared to none treated BMDM, IL4/13 or R848 stimulation didn't change the percentage of deleted B cells (Figure 20b). Despite the fact that previous data had demonstrated R848 as a potent agonist for M1 polarization able to increase FcγR A:I ratio, and further enhance ADCP for human MDM [238] our data demonstrated that R848 can promote FcγR A:I ratio but that it failed to enhance ADCP (Figure 18, 20b). This may be due to the fact that R848 is a TLR7/8 agonist in humans [238] but that it

only binds to TLR7 in mice [247]. Thus, ligation and activation through TLR7 by R848 in mice may not be enough to fully polarize macrophages to an effective M1-like phenotype.

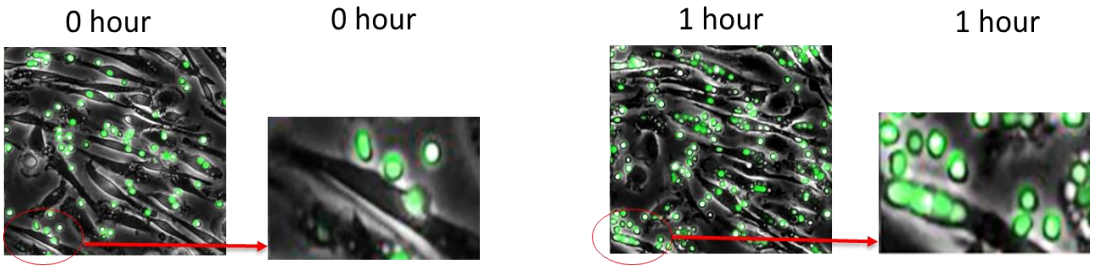

Figure 19: Macrophage eliminate opsonised target via antibody dependent cellular phagocytosis in vitro.. Time lapse microscopy demonstrates that macrophages are able to phagocytose opsonised target cells. (Effector: human monocyte-derived macrophages, target:CLL), left imagine 0 hour, opsonised with rituximab, right imagine 1 hour, opsonised with rituximab (Stephen Beers).

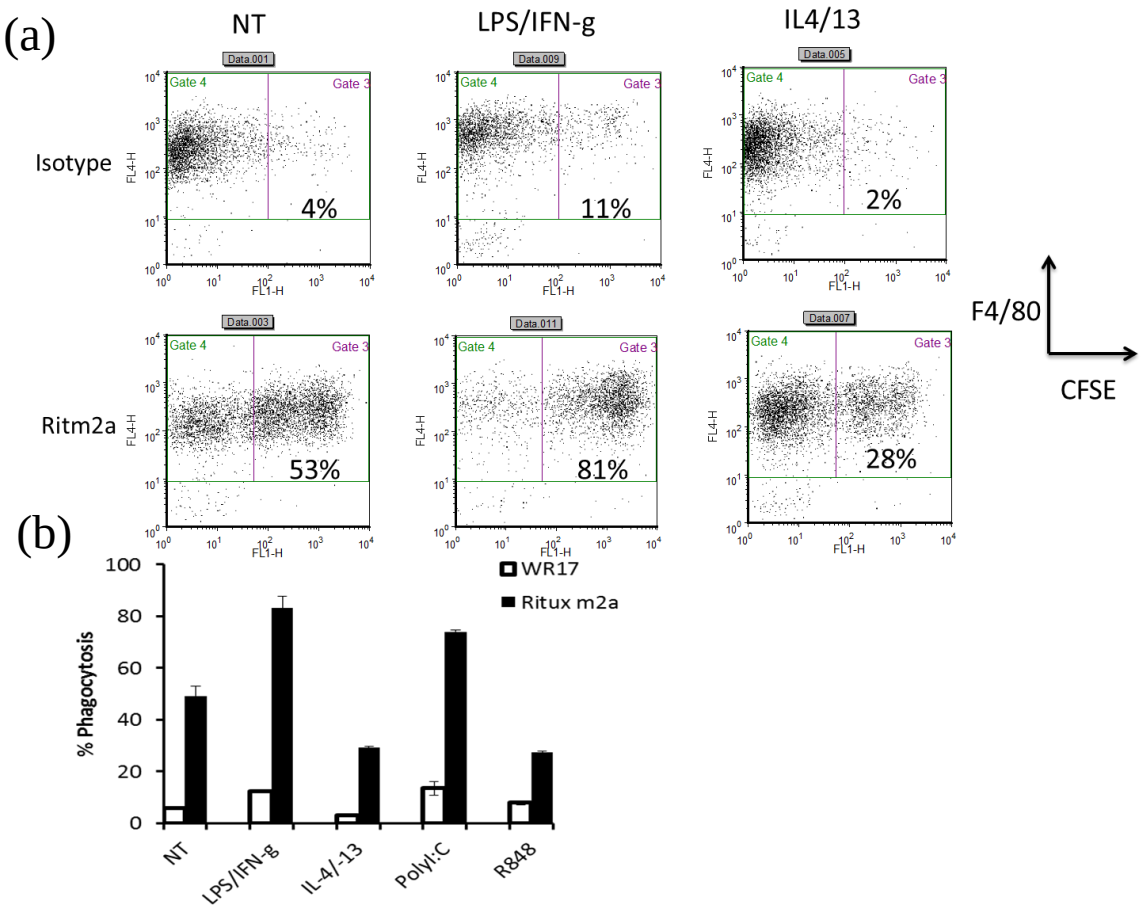

Figure 20: M1 stimuli promote antibody dependent cellular phagocytosis in vitro. Bone marrow cells from mice femurs were harvested and cultured in complete RPMI with 20% L929 media for 7 days (Method 2.3). LPS/IFNγ 100/2 ng/ml (final concentration, same for the rest of reagents here), IL4/13 10/10 ng/ml, R848 1 μM or pIC 40 μg/ml were added to BMDM on day 7. Cells were harvested and transferred to 96 well plates for the phagocytosis assay (Method 2.11) on day 8. (a) Representative data. X axis FL1, Carboxyfluorescein succinimidyl ester (CFSE). Y axis, FL4, F4/80-APC, macrophage marker. Double positive cells = portion macrophages taking up target cells. (b) Percentage of phagocytosis of non-treated, LPS/IFNγ, IL4/13, R848 and poly(I:C) stimulated BMDMs. Black Bar, HuCD20 Tg B cell opsonised with Ritm2a. White bar, HuCD20 Tg B cell opsonised with irrelevant WR17m2a. Representative data from at least two independent experiments carried out by L.N.Dahal.

3.3 Discussion

In this chapter, we stimulated murine BMDM with classic M1 (LPS/IFNγ), M2 stimuli (IL4 and IL13) and different TLR agonists, investigating the morphology, phenotype and function of these polarized BMDM. We found that stimulation by poly(I:C), R848 or CpG induced BMDM 'clumping' which resembled the morphology of M1 macrophages (Figure 11). In contrast polarizing BMDM with IL4/13 caused the cells to elongate and form spindle like shapes (Figure 11) [44]. Consistent with published literature [44, 235], stimulation with M1 stimuli, LPS/IFNγ, significantly increased NO production and release

(Figure 12), whilst in contrast polarizing BMDM to an M2 phenotype with IL4/13 increased arginase production (Figure 12). Poly(I:C), R848 or CpG stimulation increased NO, but not arginase release (Figure 12). This suggested that poly(I:C), R848 or CPG are more like M1 skewers rather than M2. In addition, only BMDM polarized by LPS/IFNγ or poly(I:C) increased the expression of M1 phenotypic marker CD86 (Figure 13)[233]. Although it's not significant, IL4/13, R848 and CPG stimulation showed a slight promotion in the expression of M2 marker CD206 (Figure 13).

At the same time, by using verified mAb (Figure 16), we found that the expression of FcγR is changed along with BMDM polarization at both the gene (Figure 15) and protein level (Figure 17). The gene and protein expression of FcγRI is greatly increased in response to LPS/IFNγ or poly(I:C) stimulation (Figure 15,16a, b), and a similar if less profound increase was also observed in response to R848 and CPG stimulation. Polarization by LPS/IFNγ, poly(I:C), R848 or CPG increased FcγRIV expression at the gene and protein level (Figure 15, 16a, b). IL4/13 is the only stimuli that promoted the gene and protein expression of inhibitory FcγRII (Figure 15, 16a, b). Further, R848 or CPG polarization increased the FcγR activatory to inhibitory ratio on BMDM, but not as much as LPS/IFNγ or poly(I:C) stimulation (Figure 18). Since the FcγR activatory to inhibitory ratio is closely related to the function of macrophage [198], we then investigated whether polarized BMDM by different reagents will alter ADCP or not. We found that LPS/IFNγ or poly(I:C) stimulation greatly enhanced ADCP in vitro, the percentage of phagocytic macrophages is increased from about 45% on NT BMDM to around 80% on LPS/IFNγ or poly(I:C) treated BMDM (Figure 20b). Although R848 has been shown to promote ADCP of monocytes isolated from human peripheral blood [238], our data reveals that R848 didn't enhance ADCP with mouse BMDM (Figure 20b). The distinct observation may due to that fact that R848 is a TLR 7 and 8 agonist in human [238], while it only activates TLR 7 in mice [248]. Indeed, R848 stimulation increased the FcγR A:I ratio on BMDM (Figure 18), but not as much as LPS/IFNγ or poly(I:C)

stimulation. Thus we propose that FcγR A:I ratio may have to increase to a certain threshold to alter ADCP of BMDM although this may well be target specific.

Chapter IV Polarizing macrophages in vivo to enhance anti-CD20 mAb activity

4.1 Introduction

Over the last 30 years, monoclonal antibody therapy against cancer has advanced considerably. The anti-CD20 mAb rituximab combined with different chemotherapy/radiotherapy has significantly promoted the survival statistics for follicular [196] and diffuse large B-cell lymphoma (DLBCL) patients [134]. In the MabThera (Rituximab) international trial, 824 DLBCL patients were treated with either standard CHOP alone (Cyclophosphamide + Hydroxydaunorubicin + Oncovin + Prednisone) or rituximab plus CHOP (R-CHOP). After a 3-year follow up period, patients treated with R-CHOP achieved 79% progression-free survival compared to 59% for patients who received CHOP alone [249].

Generally, based on their unique characteristics and potential mode of action, therapeutic mAb can be classified into three types; direct targeting mAb, antibody-drug conjugates and immunomodulatory mAb. Direct targeting mAb recognise antigen expressed on the target cell specifically, as a result, target cells are eliminated largely by the recruitment of innate effector mechanisms; ADCP, ADCC and complement [156]. Rituximab is one of the best studied direct targeting mAb and recognises the CD20 antigen, which is expressed on the majority of normal B cells and nearly all malignant B cells [167]. In this chapter, we will focus on means to enhance the activity of direct targeting anti-CD20 mAb, and we will discuss immunostimulatory mAb in other chapters.

The mechanisms of action of anti-CD20 mAb have been extensively studied for several decades. Based on in vitro data four mechanisms of action have been proposed: ADCP, ADCC, complement and PCD (Figure 6, page 31) [156]. Recent in vivo research in pre-

clinical models has demonstrated that rituximab primarily depletes target cells through macrophage mediated ADCP (Section 1.10.1).

Anti-CD20 mAb can be classified into type I (rituximab-like) or type II (tositumomab-like) based on their functional difference in vitro [156]. Type I anti-CD20 mAb can induces potent complement [168], but fails to induce PCD [156]. In contrast, type II anti-CD20 can evoke strong PCD, but are unable to efficiently activate complement [156]. The other key difference that has been observed between type I and II mAb is that after binding to CD20, type I anti-CD20 mAb can effectively drive CD20 loss from the target cell surface in vitro [171] and in vivo [161]. Two mechanisms have been proposed to explain this process, antigenic modulation and antigenic shaving (Figure 7) [171]. Although the role of antigenic shaving in this process is still controversial, it's clear that type II anti-CD20 mAb don't cause antigenic modulation in vitro [161]. In a recent phase II study the second-generation type II anti-CD20 mAb, obinutuzumab combined with CHOP achieved 95% overall response rates for untreated advanced-stage follicular lymphoma patients [250] this is comparable to RCHOP therapy with 96% overall response rates [251].

Over recent years a great deal of academic and industrial research effort has been focused on optimising mAb activity. For example, the third generation, anti-CD20 mAb GA101 has been glycoengineered to increase binding to FcγRIIIA for enhanced effector cell function [133]. Veltuzumab contains an aspartic acid instead of an asparagine at 101st position compared to rituximab, this mutation increases the half-life and therefore bioavailability of veltuzumab [134]. These methods have indeed enhanced antibody activity in vitro, however it is unclear of what benefit these modifications have made in patients to date. Potentially these engineered mAb may still be hindered in delivering a full therapeutic effect as they may still be unable to overcome any inherent deficiencies in patients' effector populations.

It has been demonstrated that therapeutic response of mAb therapy is impaired in chronic lymphocytic leukemia [252] and acute lymphoblastic leukemia [253]. In the latter research, using short hairpin RNA to target the inhibitory FcγRII promoted alemtuzumab-dependent macrophage-mediated phagocytosis in vitro and in vivo [253]. These observations suggest that mAb therapy-resistance in the tumour microenvironment is due, at least in part, to a decrease in the FcγR A:I ratio on macrophages. Based on our in vitro results from chapter III, here we aimed to enhance rituximab activity through manipulation of macrophage FcγR in vivo.

4.2 Results

4.2.1 Poly(I:C) stimulation promotes rituximab induced B cell depletion in vivo

To evaluate the therapeutic potential of TLR agonists, we set up a series of adoptive transfer experiments to compare rituximab mouse IgG2A (Ritm2a) mediated B cell depletion in non-treated or TLR agonist treated WT C57BL/6 mice [219]. Briefly, human CD20 transgenic and WT C57BL/6 splenic cells were CFSE labelled as high and low respectively and mixed 1:1 before adoptive transfer into WT C57BL/6 recipients (Method 2.7, figure 9). Results shown are pooled from 8 independent experiments where the background ratio of target:non-target are variable between each experiments. Thus, to reduce data redundancy, the results presented here are normalised to isotype controls from each individual experiment. The target:non target ratio was calculated according to the method in section 2.7. Poly(I:C) stimulation significantly ($P<0.0001$) promoted rituximab mediated depletion of adoptively transferred hCD20 Tg B cells in the spleen (Figure 21a, b), the target:non-target ratio, in average falling from 0.57 in untreated mice to 0.37 when rituximab was combined with Poly(I:C) (Figure 21b). Both the TLR4 agonist LPS ($P=0.569$) and TLR7 agonist R848 ($P=0.104$) showed a trend towards improved B

cell depletion (Figure 21b), but statistical analysis suggested the differences are not significant (Figure 21b).

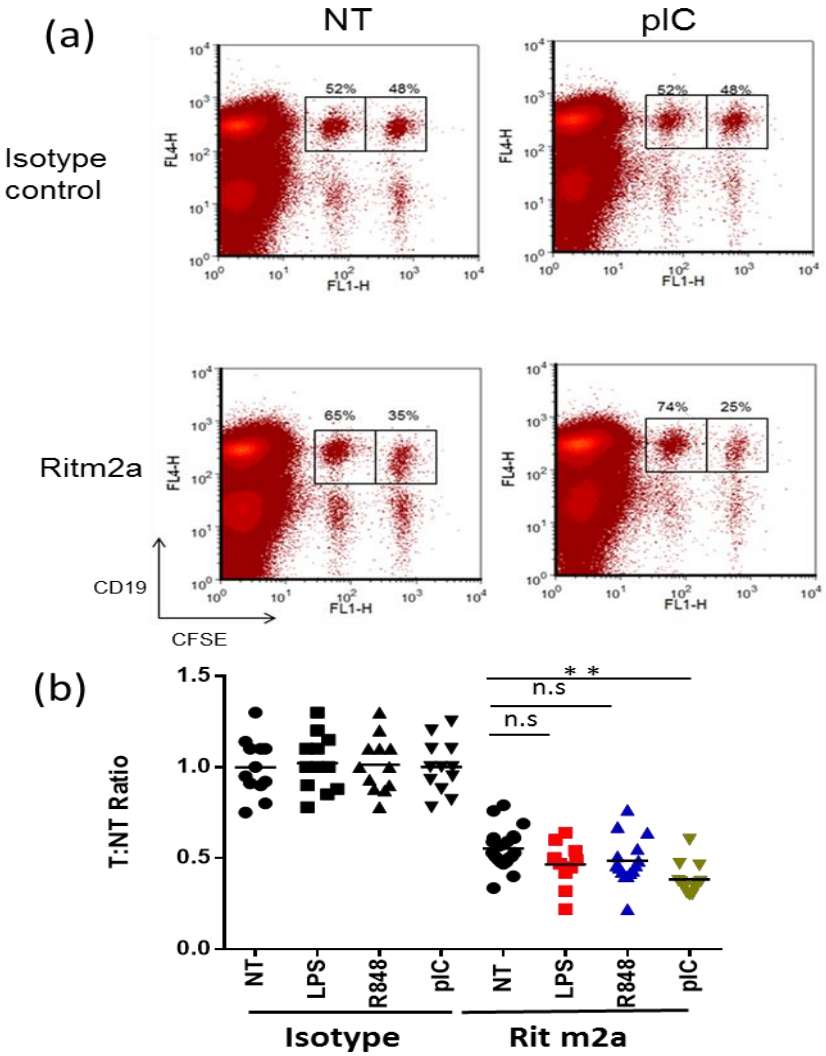

Figure 21: Poly(I:C) enhances Ritm2a induced hCD20 B cell depletion in vivo. Human CD20 transgenic and WT C57BL/6 splenic cells were CFSE labelled and injected i.v. into wild type C57BL/6 recipients at day 0. Day 1, 10 µg LPS, 100 µg poly(I:C) (pIC), or 2.5 µg R848 were injected i.p. A second dose of poly(I:C) and R848 were given i.p. on day 2 (a.m). 50 µg Ritm2a or isotype control mIgG2a (clone WR17) were injected i.v day 2 (p.m). Mice were sacrificed on day 3 and the spleens harvested and stained for flow cytometry. (a) Representative data of isotype and Ritm2a treated mice spleens. CD19+ CFSE high population represents target HuCD20 expression B cells.CD19+CFSE low population represent non-target HuCD20 negative B cells. (b) The target:non-target ratio (section 2.7) of adoptive transferred B cells in spleen. Data from Ritm2a treated sample are normalised to correlated isotype control to minimise the variation between experiments. Results are combined from 5 independent experiments (n=12), each symbol represents one mouse. A one-tailed nonparametric student T test was performed to analyse significant differences between NT and TLR agonist stimulated groups. ** represent a significance of P<0.01.

4.2.2 Percentage of inflammatory monocytes is increased in the tissue of poly(I:C) treated mice

We postulated that some of the differences in response observed in 4.2.1, Figure 21 may have been due to differences in the inflammatory response that these adjuvants elicited in the mice. Potentially, a highly inflamed microenvironment could promote accumulation of myeloid derived suppressor cells that have been shown to inhibit macrophage function [254]. In addition, infiltrating myeloid cells can induce the release of IL10, an immune suppressive cytokine that is able to inhibit macrophage function [255].

Here we examined the inflammatory infiltrates in different compartments in response to adjuvant administration. To distinguish these inflammatory populations, cells were stained with CD11b, F4/80, Ly6C and Ly6G, CD11b intermediate F4/80+ cells represent splenic macrophages, CD11b high Ly6C+ cells represent inflammatory monocytes, CD11b high, Ly6G+ cells represent neutrophils (Figure 25a). We found that stimulation with poly(I:C) significantly ($P < 0.0001$) increased the infiltration of CD11b+ Ly6C+ inflammatory monocytes in the spleen (Figure 25b). There was also a trend for increased neutrophil numbers in the tissues, whilst the percentage of macrophages does not change (Figure 25b). The results demonstrate that the increased depletion of B cell we observed in the spleen was not due to the expansion of macrophages in the tissues. However, the enhanced recruitment of Ly6C+ inflammatory monocytes to the tissues could potentially explain the increased activity observed.

At the same time, we observed that administration of LPS or R848 didn't increase the recruitment of Ly6C+ inflammatory monocytes to the spleen (Figure 25b). We also observed that somewhat unexpectedly activation with the TLR 4 agonist LPS did not significantly improve rituximab activity in vivo (Figure 21). We found that LPS stimulation did however induce a large infiltration of neutrophils, a sign of a highly inflammatory

environment (Figure 22a,25b). In addition, stimulation by LPS for 24 hours greatly enhanced CD11b expression on splenic macrophages (Figure 22a, b), CD11b expression was further increased after 48 hours LPS stimulation (Figure 22a, b). While the expression of CD11b on R848 (Figure 23) or poly(I:C) (Figure 24) treated splenic macrophage was not changed. These data suggest that unlike LPS, mice treated with R848 or poly(I:C) didn't trigger such a large inflammatory response.

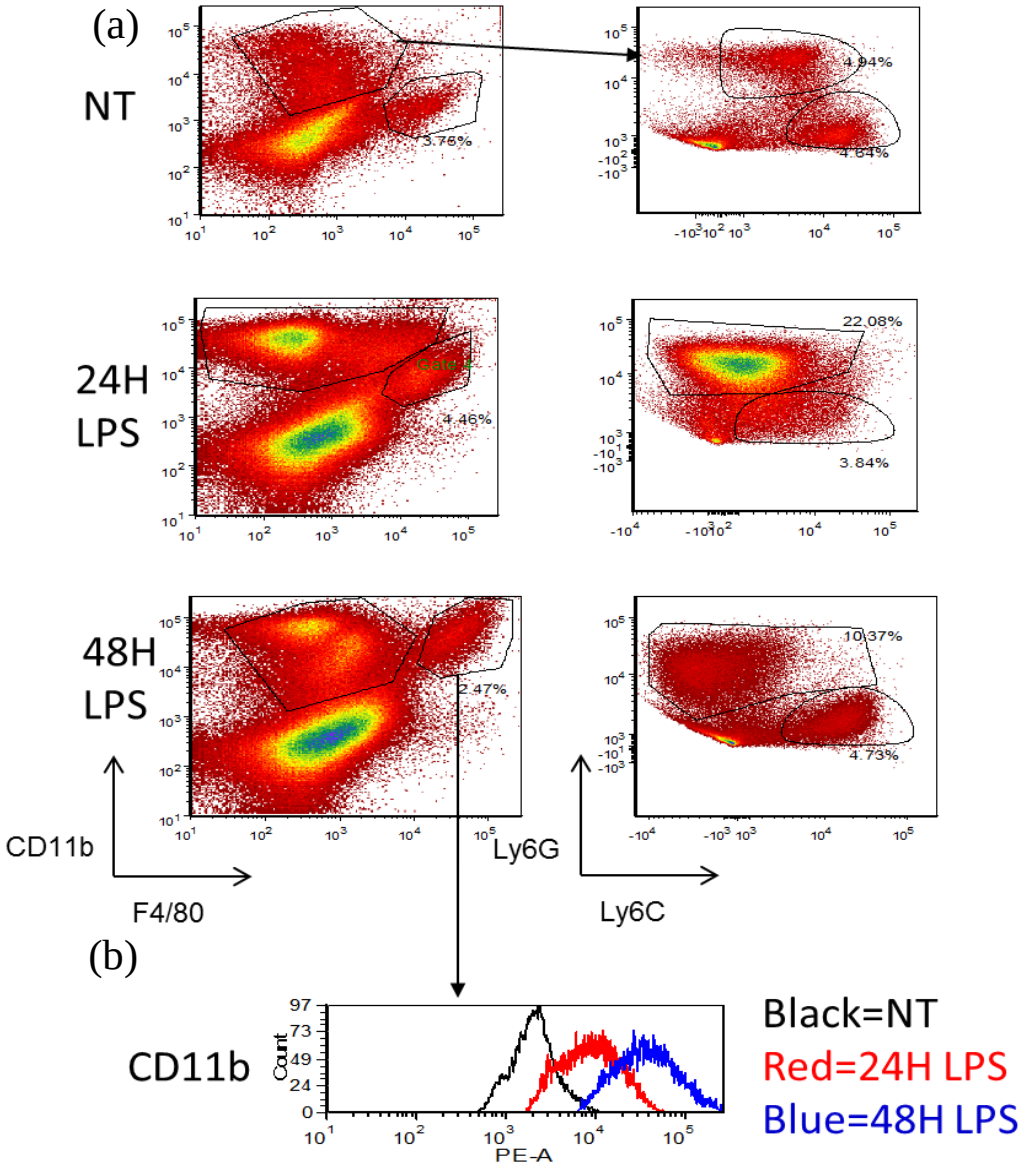

Figure 22: LPS stimulation induces neutrophil infiltration to the spleen. LPS (10 µg) was administered i.p. to C57BL/6 on day 1 (48h stimulation) or day 2 (24h stimulation), spleens were harvested and analysed by flow cytometry on day 3. (a) Representative data, CD11b intermediate, F4/80+ represent splenic macrophages. CD11b high population are gated upon, and further sorted by expression of Ly6C and Ly6G. Ly6G+ represents neutrophils and Ly6C+ monocytes. (b) Histogram of CD11b expression on splenic macrophages.

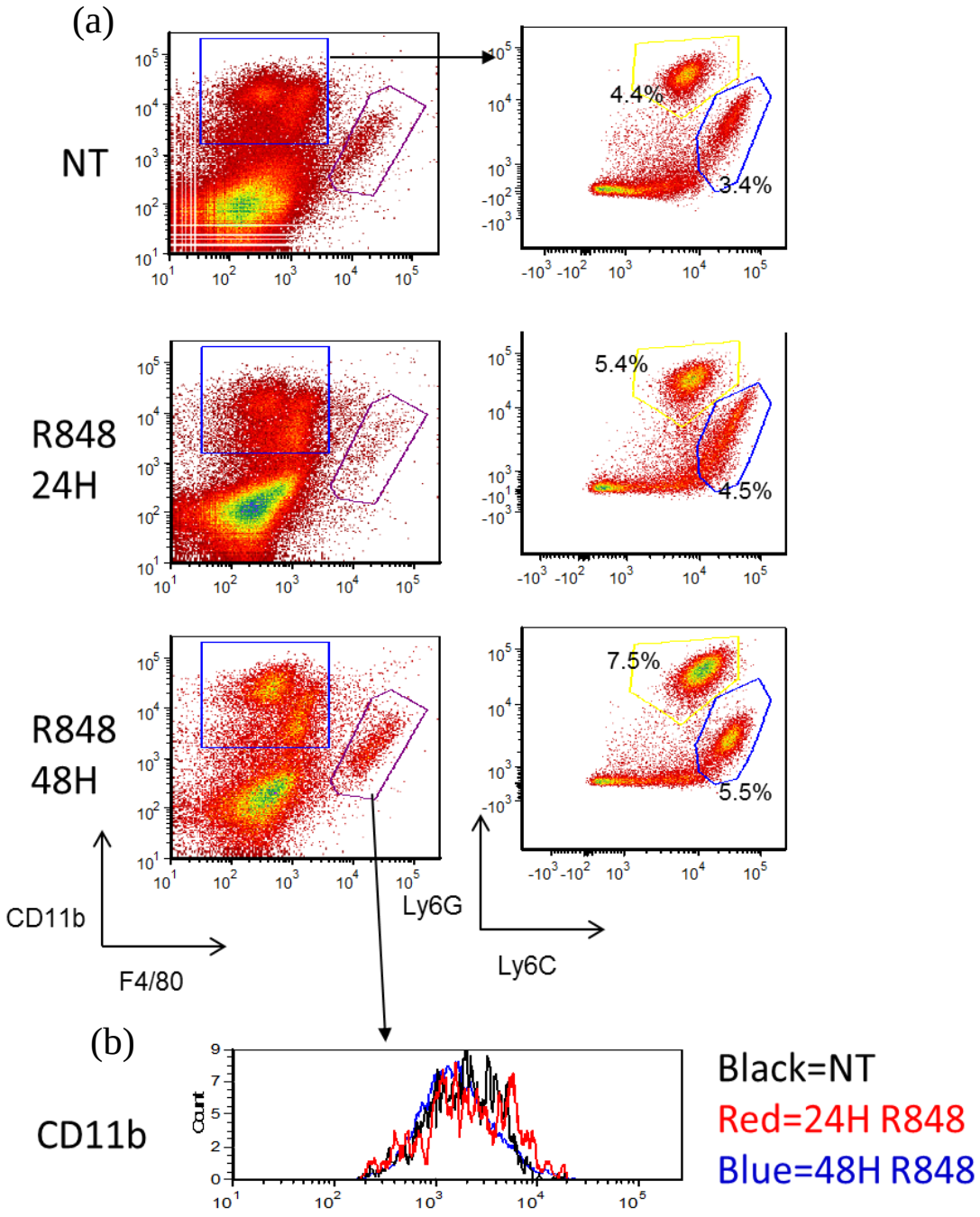

Figure 23: Splenic myeloid populations of R848 stimulated C57BL/6.R848(2.5 µg) was administered i.p. to C57BL/6 on day 1 (48h stimulation) or day 2 (24h stimulation), spleens were harvested and analysed by flow cytometry on day 3. (a) Representative data, CD11b intermediate, F4/80+ represent splenic macrophages. CD11b high population are gated upon and further sorted by expression of Ly6C and Ly6G. Ly6G+ represents neutrophils and Ly6C+ monocytes. (b) Histogram of CD11b expression on splenic macrophages.

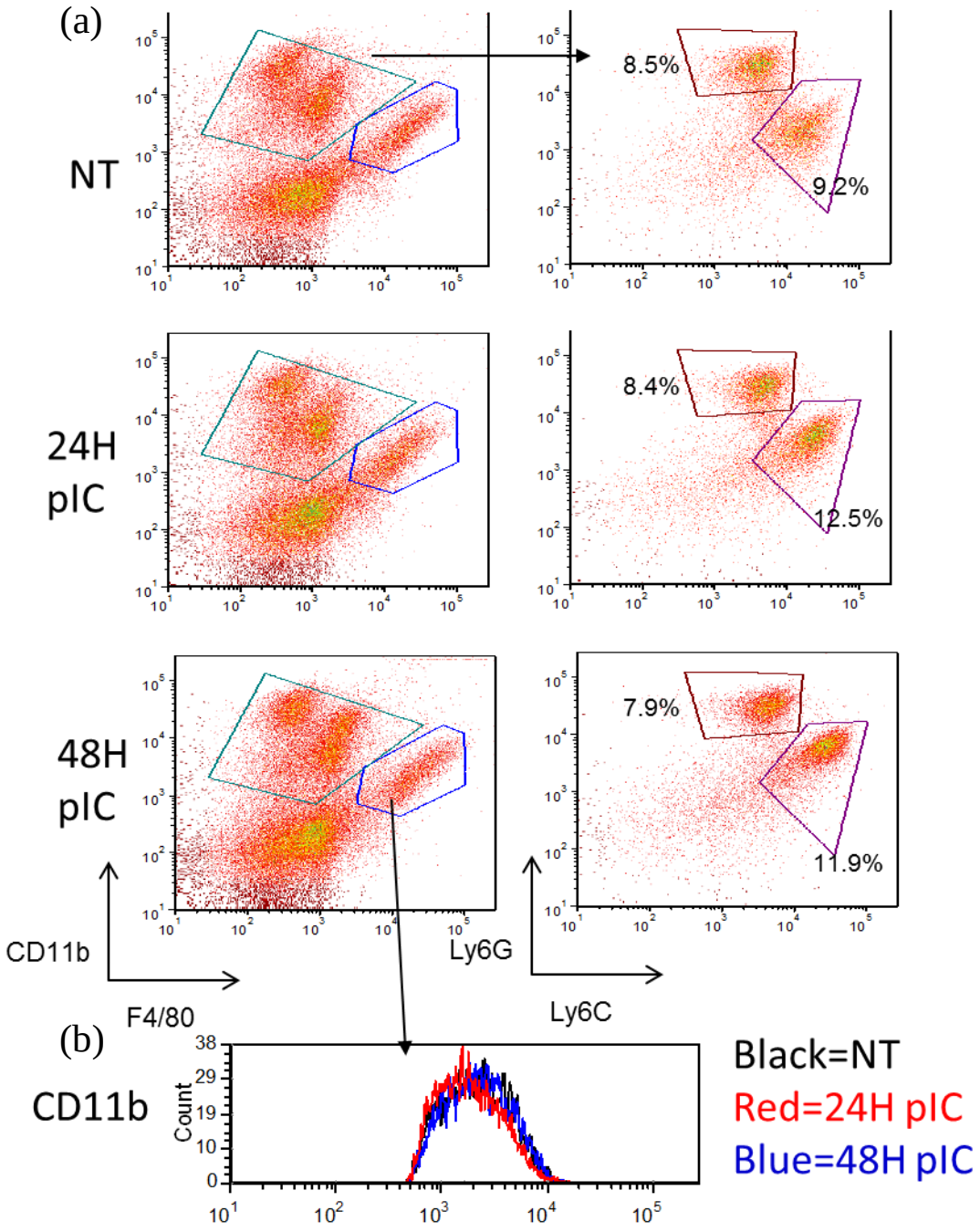

Figure 24: Splenic myeloid populations of pIC treated C57BL/6. Poly(I:C) (pIC) (100 µg) was administered i.p. to C57BL/6 on day 1 (48h stimulation) or day 2 (24h stimulation), spleens were harvested and analysed by flow cytometry on day 3. (a) Representative data, CD11b intermediate, F4/80+ represent splenic macrophages. CD11b high population are gated upon, and further sorted by expression of Ly6C and Ly6G. Ly6G+ represents neutrophils and Ly6C+ monocytes. (b) Histogram of CD11b expression on splenic macrophages.

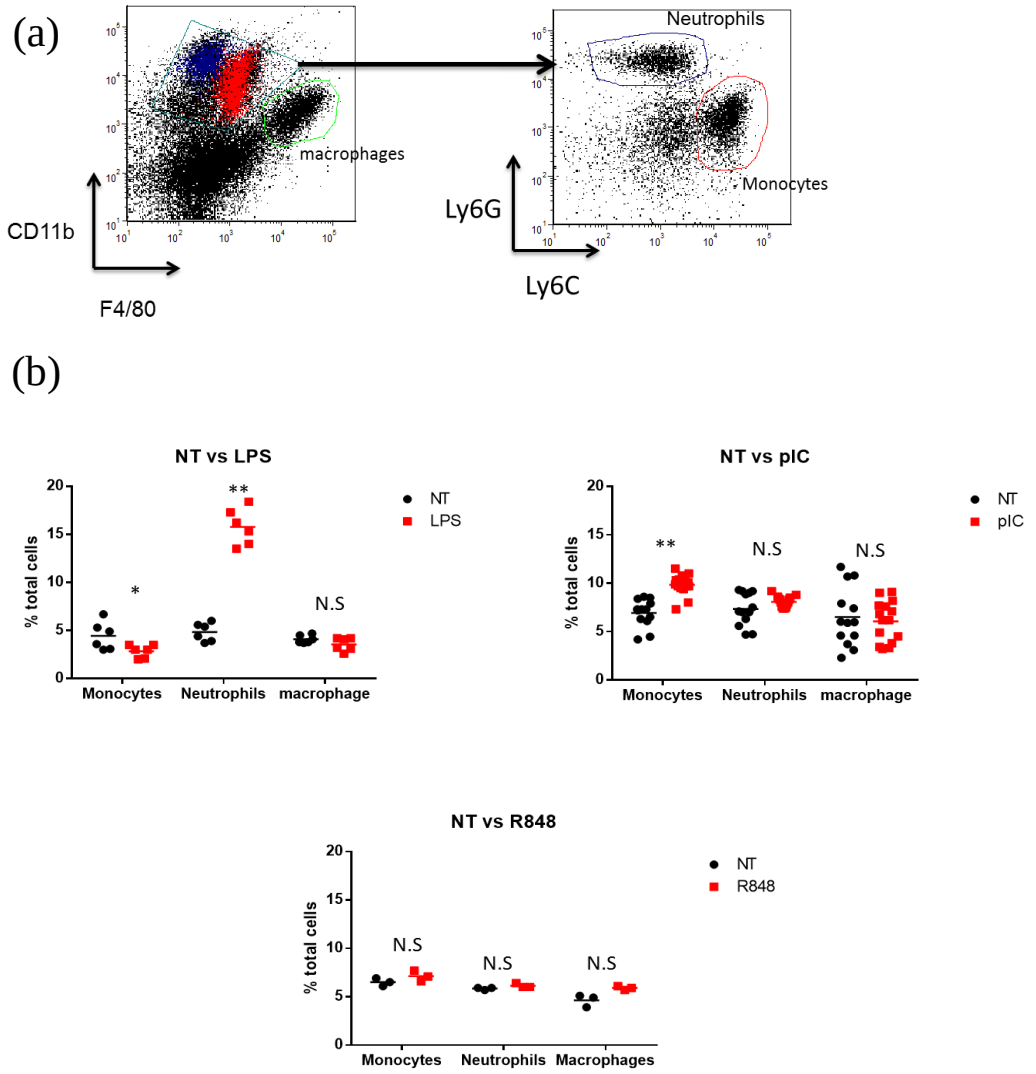

Figure 25: Percentage of splenic myeloid cells in NT and TLR agonist treated C57BL/6 mice. A single dose of 10µg LPS was given to mice on day 1, 100 µg poly(I:C) (pIC), or 2.5 µg R848 were administered i.p. to C57BL/6 on day 1 and 2. On day 3, spleens were harvested and analysed by flow cytometry. (a) Gating strategy, CD11b intermediate, F4/80+ represent splenic macrophages. CD11b high populations are gated upon, and further sorted by expression of Ly6C and Ly6G. Ly6G+ subpopulation represents neutrophils and Ly6C+ monocytes. (b) Percentage of myeloid cells in spleen. The overall results come from several independent experiments, each symbol represents one mouse (LPS stimulated mice n=6, R848 stimulated mice n=3, pIC stimulated mice n=12). A two-tailed nonparametric student T test was performed to analyse significance between NT and pIC treated group. ** represents a significance of P<0.01

4.2.3 The promotion of B cell depletion by poly(I:C) is independent of monocyte recruitment to the spleen

As poly(I:C) had significantly enhanced B cell depletion and this was also the adjuvant that increased monocyte numbers in the spleen, here we sought to investigate the possible role of monocytes in this augmented activity. To exclude a role for inflammatory monocytes in poly(I:C) promoted B cell depletion, we used the C-C chemokine receptor type 2 (CCR2) knock out mouse model. Here the majority of monocytes remain trapped in the bone marrow [218], because they do not express CCR2 which binds to chemokine monocyte chemoattractant protein-1 (MCP-1) mediating monocyte efflux [218]. Thus, there are no or very few circulating monocytes in the CCR2 KO mouse ($P<0.0001$) (Figure 26a, b). Despite this lack of monocytes, we found that Ritm2a can delete B cells from the spleens CCR2 KO mice as well as it can in WT (Figure 26c). The augmentation of B cell depletion induced by rituximab plus poly(I:C) was also comparable (No significant difference) between wild type and CCR2 KO mice (Figure 26c). These results support the contention that monocytes are not the primary effector cells for anti-CD20 mAb mediated deletion and further that the promotion of B cell depletion observed in response to poly(I:C) administration was not due to the infiltration of inflammatory monocytes.

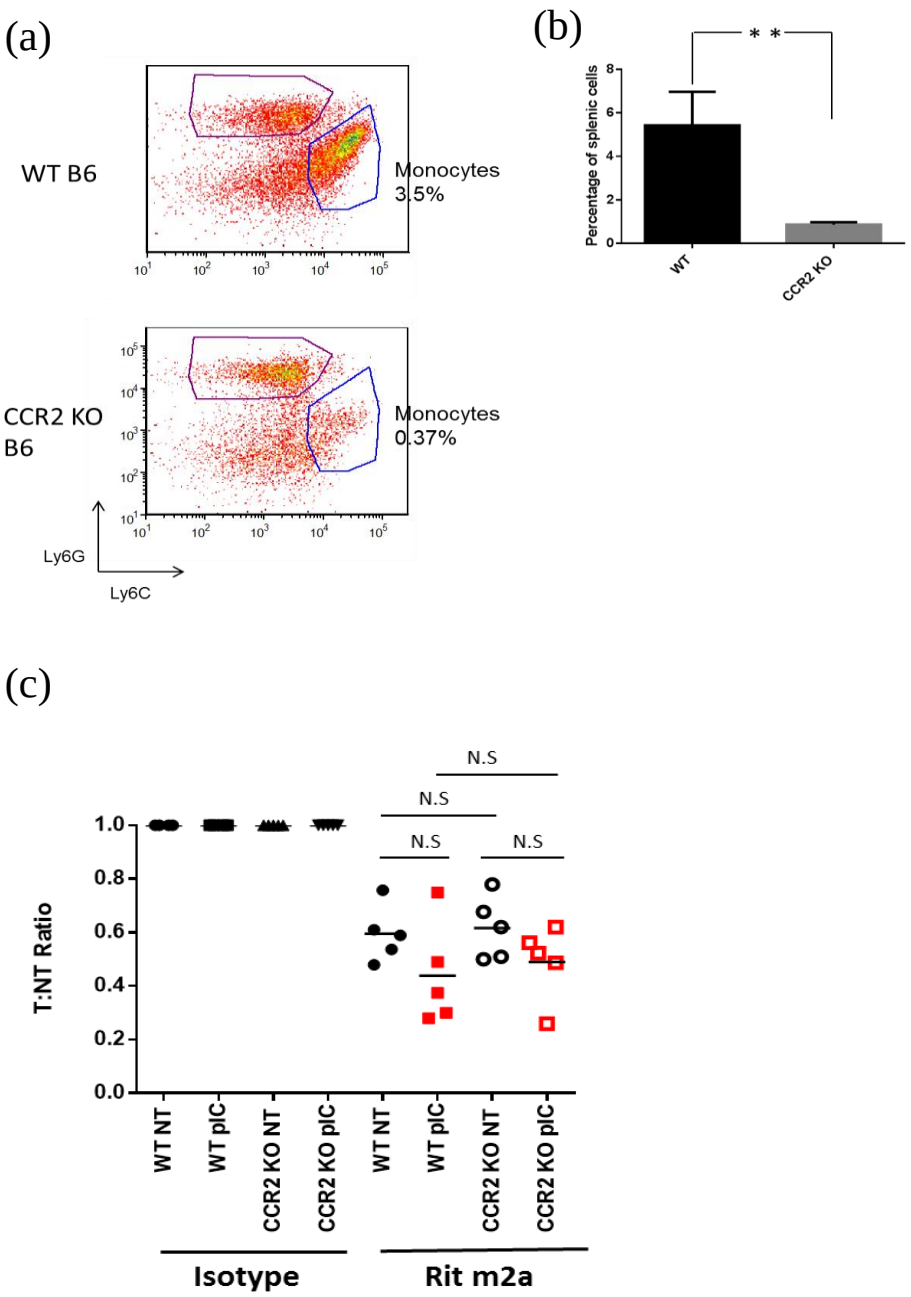

Figure 26: The promotion of B cell depletion by poly(I:C) is independent of monocyte recruitment to the spleen. Human CD20 Tg B cells were adoptively transferred into WT or CCR2 KO recipient mice on day 0. Poly(I:C) (pIC)(100µg) was given i.p. on day 1 and day 2 (a.m.). Day 2 (p.m.), 50 µg Ritm2a or isotype control (clone WR17) was given i.v. On day 3, spleens were harvested and analysed by flow cytometry. (a) Representative data of inflammatory monocytes in the spleen. (b) The percentage of splenic monocytes in WT and CCR2 KO mouse. (b) The target:non-target ratio of adoptively transferred B cells in the spleen, normalised data (n=5) . A two-tailed student nonparametric T test was performed to analyse significantly (n=3). ** represents significance P<0.01, and NS indicates not significant.

4.2.4 Neutrophil depletion does not alter poly(I:C) promoted B cell deletion

Although not significant, there is a trend in section 4.2.2, Figure 25b for poly(I:C) stimulation to also increase the number of neutrophils present in the spleen. Thus, to establish the role of neutrophils in our model, we used the Ly6G specific antibody 1A8 to deplete neutrophils [256] and compared the B cell depletion result with non-neutrophil depleted, wild type mice. After 96 hours, 1A8 treatment efficiently depleted neutrophils in the spleen (Figure 27a, b), the percentage of neutrophils in the spleen dropped from about 3% in non-treated to around 0.5% in 1A8 treated mice (Figure 27a, b). In contrast the percentage of macrophages in the spleen did not change (Figure 27b). Interestingly, poly(I:C) stimulation not only augmented CD20 mediated B cell depletion (Figure 21), but also enhanced 1A8 mediated neutrophil deletion ($P<0.05$) (Figure 27a, b). Percentage of neutrophils in spleen is further reduced from 0.5% in 1A8 treated to 0.2% in 1A8 plus poly(I:C) administered (Figure 27b). These data imply that the 1A8 mAb depletes neutrophils through a similar mechanism to that for Ritm2a and B cells and that the effector cell population responsible is unlikely to be neutrophils. Indeed, the percentage of monocytes in mice receiving 1A8 after poly(I:C) administration were significantly increased compared to non-treated (Figure 27b). This is likely because as the number of neutrophils, expressed as a percentage of the CD11b gate, is reduced (Figure 27b), the percentage of unaffected monocytes will increase proportionately.

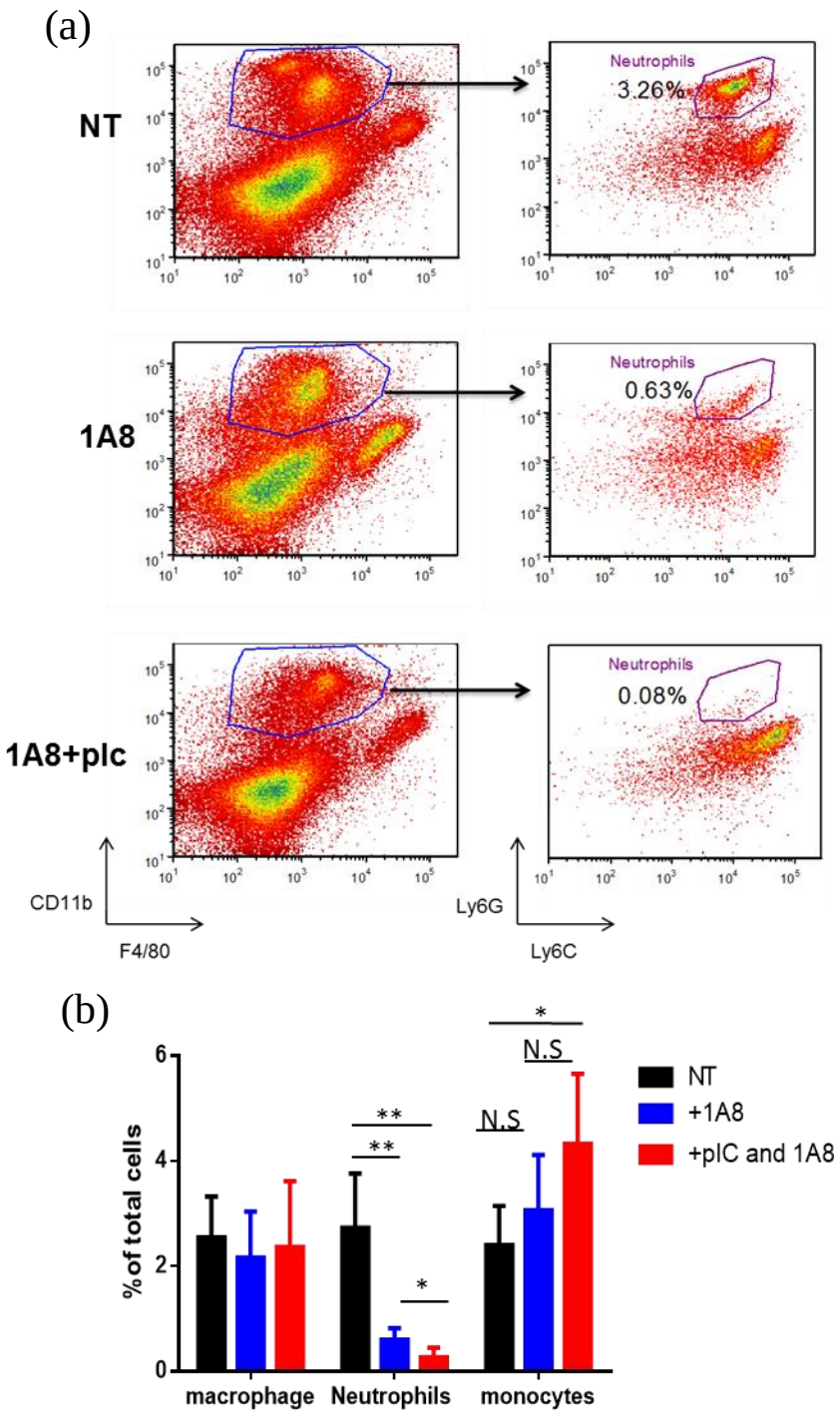

Figure 27: Depletion of neutrophils by Ly6G specific 1A8 mAb. A single administration (500 µg) of Ly6G depleting antibody 1A8 was given to mice. After 96 hours spleens were harvested and analysed by flow cytometry. (a) Representative data of 1A8 depletion in spleen. (b) Percentage of splenic myeloid cells in NT and 1A8 treated mouse. (c) The target:non-target ratio of adoptively transferred B cells in spleen, data are normalised. A two-tailed nonparametric student T test was performed to analyse significance (n=5). * represents significance of P<0.05, ** represents P<0.01, NS indicates the result is not significant.

We found that depletion of neutrophils by 1A8 didn't change the ability of Rim2a to deleted hCD20 Tg B cells, both non-treated and 1A8 treated mice are able to delete ~50%

of hCD20 Tg B cells (Figure 28). In addition, stimulation with poly(I:C) enhanced the Ritm2a mediated depletion in both non-treated and 1A8 treated mice (Figure 28). In summary, these data suggesting that neutrophils are not required for Ritm2a mediated deletion of target B cells.

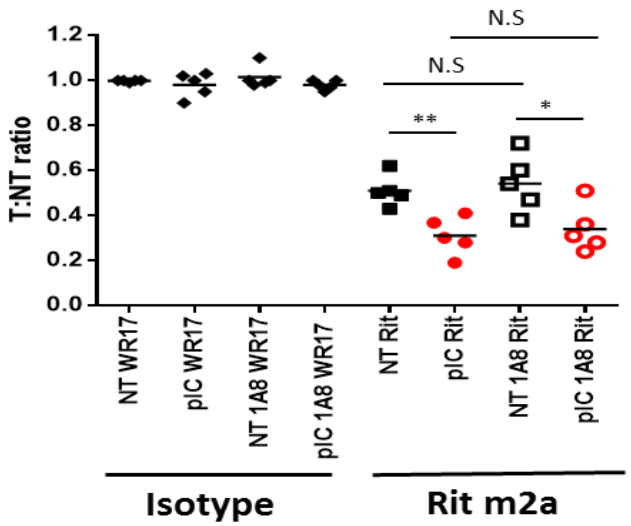

Figure 28: Depletion of neutrophils does not effect Poly(I:C) promoted B cell depletion. Human CD20 Tg B cell were adoptively transferred into NT or 500 µg 1A8 treated C57BL/6 on day 0 100 µg poly(I:C) (pIC) was given to mice i.p. on day 1 and the morning of day 2. Day 2 afternoon, 50 µg Ritm2a or isotype WR17 mIgG2A were given to mouse i.v. On day 3, spleens were harvested and analysed by flow cytometry. The target:non-target ratio of adoptively transferred B cells in the spleen, data are normalised. A one-tailed non parametric student T test was performed to analyse significance (n=5). * represents significance of P<0.05, ** represents P<0.01, NS indicates the result is not significant.

4.2.5 Deleting neutrophils in monocyte deficient mice does not alter anti-CD20 mediated B cell depletion

In the previous experiments, we demonstrated that in monocyte deficient or neutrophil depleted mice, poly(I:C) is still able to improve rituximab efficacy. However, there may be redundancy in these inflammatory effectors that might affect rituximab activity. Thus, we repeated the B cell depletion experiments in monocyte deficient (CCR2 KO) mice where we also depleted neutrophils. We found that poly(I:C) stimulation still improved rituximab activity in these doubly deficient mice (Figure 29). Combined with the data from CCR2

KO and neutrophil depleted experiments, we suggest that poly(I:C) enhances rituximab efficacy in a manner that is independent of monocytes and neutrophils.

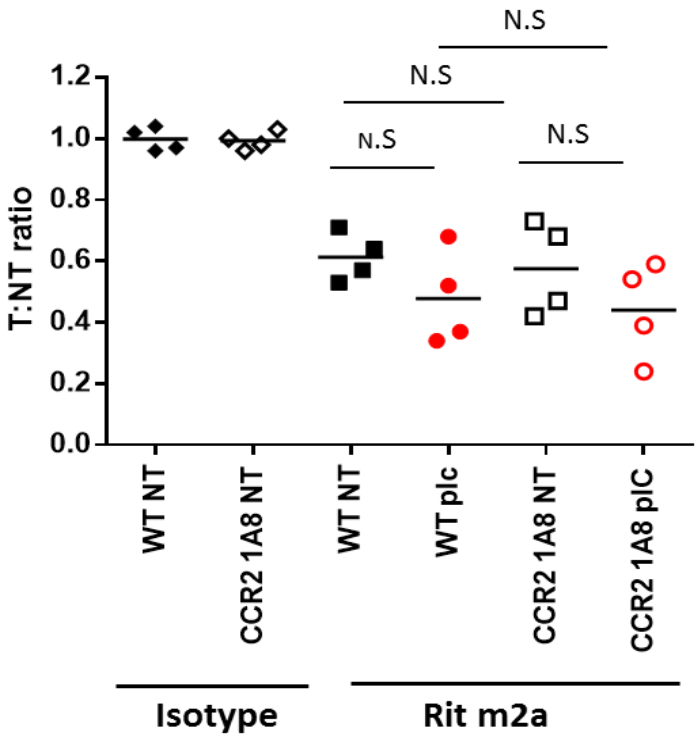

Figure 29: Deleting neutrophils in monocyte deficient mice does not alter Poly(I:C) promoted B cell deletion. A single shot (500 µg) of Ly6G depleting antibody was i.p injected to CCR2 KO C57BL/6 48h before the adoptive transfer experiment. CFSE labelled HuCD20 Tg splenocytes were adoptive transfer into NT or 1A8 treated CCR2 KO on day0.100 µg poly(I:C) (pIC) was given to mice i.p. on day 1 and day 2 morning. Day 2 afternoon, 50µg Ritm2a or isotype WR17 mIgG2A were given to mouse i.v. On day 3, spleens were harvested and analysed by flow cytometry. A two-tailed nonparametric student T test was performed to analyse significance (n=4). NS indicates the result is not significant.

4.2.6 Poly(I:C) enhances rituximab efficacy through increasing the A:I ratio of FcγR on tissue resident macrophages

The activity of rituximab has been shown to be correlated to the FcγR activatory to inhibitory ratio in several pre-clinical models [160, 198] and to FcγR polymorphisms in clinical studies [199]. To investigate how poly(I:C) stimulation augments Ritm2a activity in vivo we analysed the FcγR expression on F4/80+ macrophages in the spleen,

peritoneal cavity and lung. We found that the expression of FcγRI ($P=0.026$ in spleen, $P<0.001$ in peritoneal cavity) and FcγRIV ($P=0.0057$ in spleen, $P<0.001$ in peritoneal cavity) was greatly increased on F4/80+ macrophages in spleen and peritoneal cavity, whilst the expression of FcγRII and III largely remained unchanged (Figure 30b). Overall these changes led to a significant increase in the activatory:inhibitory ratio of FcγR on splenic ($P=0.01$) and peritoneal macrophages ($P<0.001$) (Figure 31). In addition, poly(I:C) stimulation does not change the expression of FcγR on alveolar macrophage in the lung (Figure 30). Although TLR3 is expressed in murine alveolar macrophages, in contrast to peritoneal macrophages, activating TLR3 in alveolar macrophages does not induce the production of type I IFN-β which is important in regulating STAT1 phosphorylation [257]. The phosphorylation of STAT1 has been shown to be crucial for expression of the activatory FcγR, particularly FcγRI [258]. Taken together, these results demonstrate that poly(I:C) augments Ritm2a efficacy through an increase in the FcγR A/I ratio on tissue resident macrophages, which is consistent with our in vitro data that poly(I:C) promoted ADCP via enhancing FcγR A/I ratio on BMDM (Figure 17-20, page 76-80).

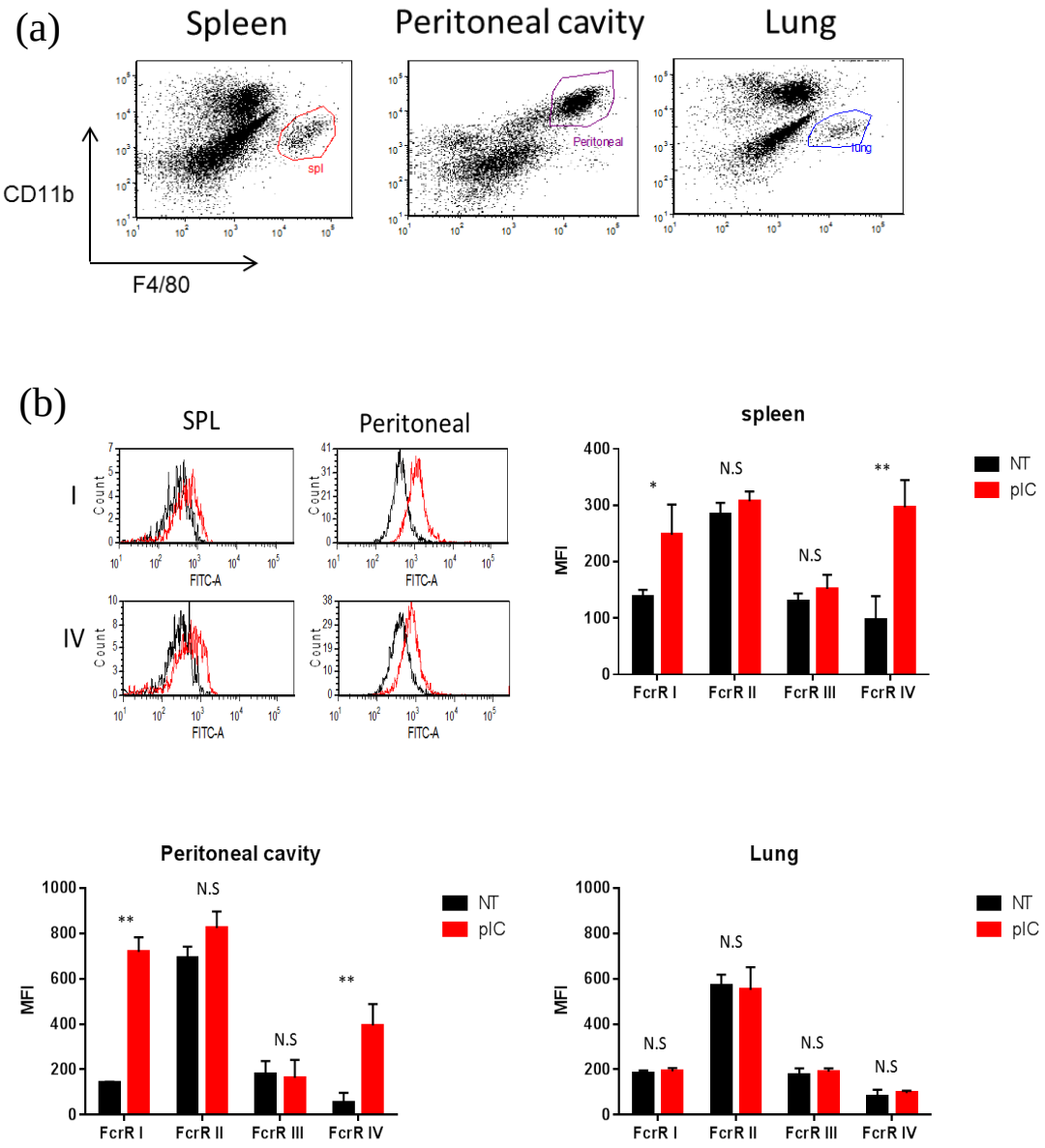

Figure 30: In vivo, poly(I:C) stimulation increased FcγRI and FcγRIV expression on macrophage in the spleen and peritoneal cavity. Poly(I:C) (pIC) (100 µg) was given i.p. to C57BL/6 at day 0 and day 1. Spleen, lung, peritoneal cavity cells were harvested at day 2 for flow cytometric analysis. (a) Gating strategy for splenic macrophages, alveolar macrophages and peritoneal macrophages. (b) Representative histograms showing FcγR expression (I= FcγRI, IV= FcγRIIV), black line= NT, red line= poly(I:C) stimulated. The column graphs show the summary of FcγR expression on macrophages in mouse spleen, peritoneal cavity and lung. A one- -tailed nonparametric student T test was performed to analyse significance (n=3). * represents significance of P<0.05, ** represents P<0.01 and NS indicates that the result is not significant. This experiment was repeated once, and the same result observed.

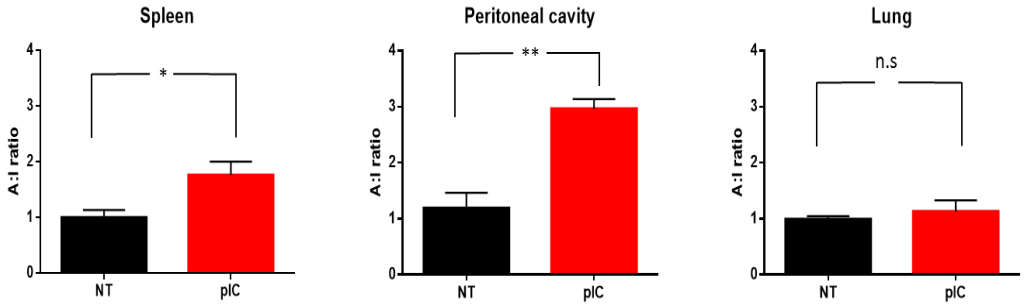

Figure 31: In vivo, poly(I:C) stimulation increased FcγR A:I ratio on macrophage in the spleen and peritoneal cavity. Poly(I:C) (pIC) (100 µg) was given i.p. to C57BL/6 at day 0 and day 1. Spleen, lung, peritoneal cavity cells were harvested at day 2 for flow cytometry analysis. The activatory:inhibitory ratio of FcγR on macrophage in spleen, peritoneal cavity and lung are shown. A two-tailed nonparametric student T test was performed to analyse significance (N=3). * represents significance of P<0.05, ** represents P<0.01 and NS indicates that the result is not significant. This experiment has been repeated once, and the same result observed.

4.2.7 The BCL_1 tumour microenvironment supresses the direct targeting function of type I anti-CD20 mAb

We have already demonstrated that TLR3 agonist poly(I:C) can efficiently polarize macrophages in vivo, which in turn significantly promoted Ritm2a induced B cell depletion in tumour free mice. Next, we investigated the therapeutic potential of poly(I:C) to augment antibody therapy in BCL_1, a well-established syngeneic BALB/c mouse lymphoma model [219, 224]. Mice were inoculated with 1 x 10^4 BCL_1 cells at day 0. At day 10, 0.8% of splenocytes were BCL_1 lymphoma cells (CD19+ Idiotype B cell receptor+), which had further expanded to 6.4% by Day 17 (Figure 32a). The increasing weight of harvested BCL_1 spleens at different time points demonstrated that the BCL_1 tumour progressed rapidly from day 10 (Figure 32b). These data showed that the BCL_1 tumour is still at an early stage on day 10 when we started our adoptive transfer experiments and that they represented a small proportion of the splenocytes. Notably, using clodronate containing liposomes [259](Stephen Beers) to deplete monocytes/macrophages inhibited tumour growth demonstrating the importance of tumour associated macrophage in tumour development and progression and illustrating

that this, often used, strategy for determining the role of macrophages could not be used in our functional in vivo assays (Figure 32b).

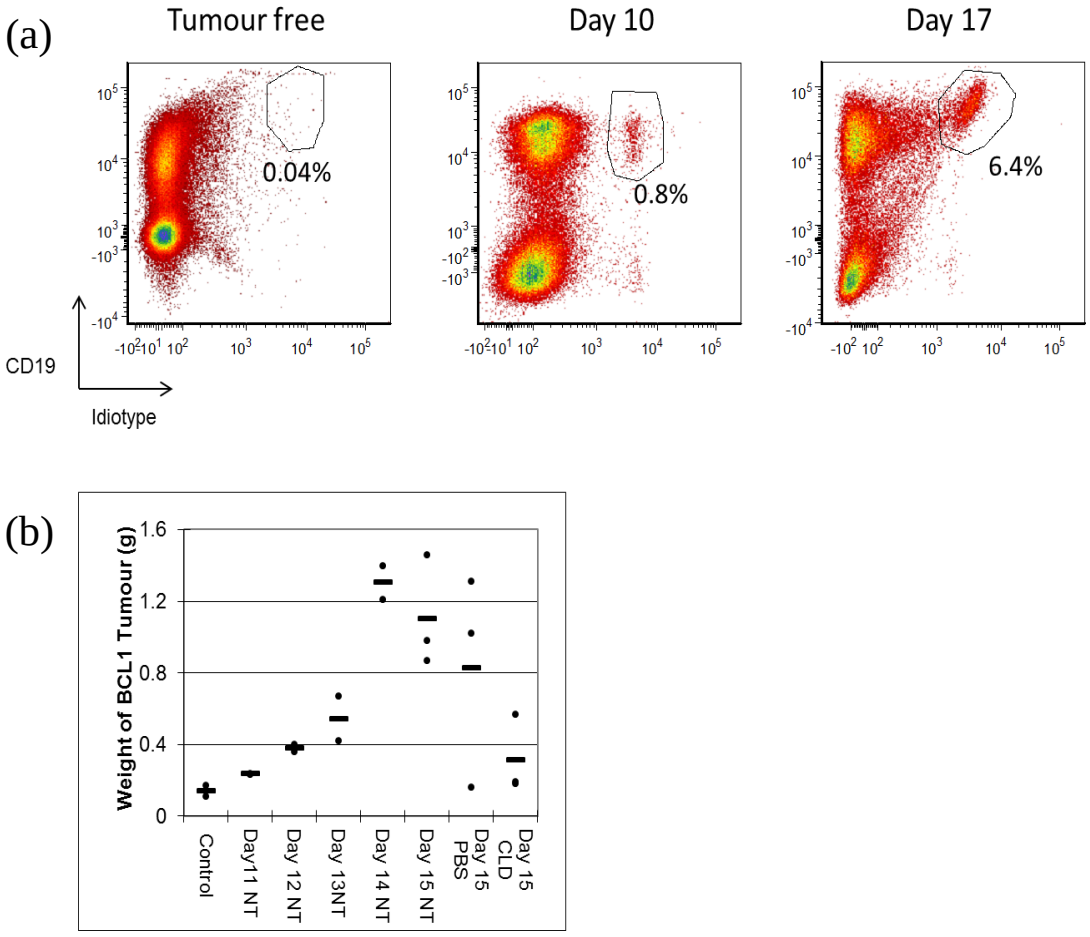

Figure 32: BCL_1 tumour cell growth and kinetics in BALB/c. Wild type BALB/c female mice were inoculated with $1x10^4$ BCL_1 cells i.v at day 0. (a) Percentage of BCL_1 cells in spleens of tumour free or BCL_1 bearing BALB/c. This experiment has been repeated once, similar results were observed. (b) The weight of BCL_1 mice spleens with tumour progression and macrophage depletion. PBS = i.v inject PBS to mice 3 days after tumour inoculation. CLD= i.v inject clodronate containing liposomes (Stephen Beers) to mice 3 days after tumour inoculation. (Each dot represents one mouse (n=3)).

We then sought to study the effects of the tumour environment on our adoptive transfer model. It is noteworthy that in this model the target cells were still normal HuCD20 Tg B cells, this allowed us to study the effects of tumour environment without the complication of having lymphoma target cells. In these adoptive transfer experiments, we found that Ritm2a mediated B cell depletion was completely inhibited in BCL_1 bearing mice at day 10 after tumour inoculation (Figure 33). This inhibition could be partially, but not fully,

recovered by increasing the dose of Ritm2a administered to 50 µg (Figure 33). It's notable that in marked contrast to Ritm2a, the type II anti-CD20 mAb Bhh2m2a was still able to delete target cells in BCL_1 bearing mice (Figure 33). There are two potential explanations for this discrepancy, one is that this simply reflects that type II anti-CD20 mAb are more potent than type I anti-CD20 mAb. [167]. Another explanations was that the BCL_1 microenvironment accelerates type I anti-CD20 regulated antigenic modulation, and CD20 on target B cells is rapidly decreased, thus supressing the type I anti-CD20 mAb activity, while type II anti-CD20 mAb activity is not affected by antigenic modulation in vitro [167].

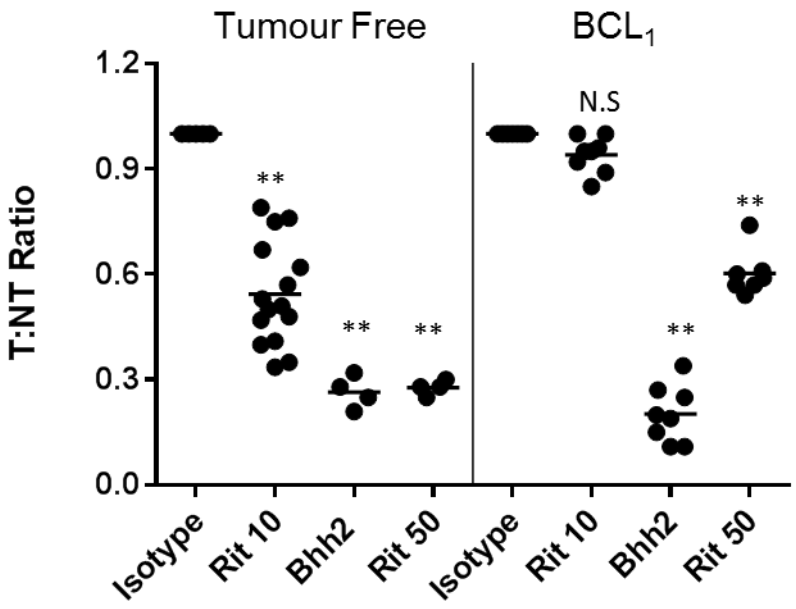

Figure 33: In vivo, BCL_1 tumour microenvironment supresses Ritm2a function. On day 0, $1x10^4$ BCL_1 cells were i.v injected into wild type BALB/c females. Carboxyfluorescein succinimidyl ester(CFSE) labelled HuCD20 Tg splenocytes cell were adoptive transferred into BCL_1 inoculated BALB/c or tumour free BALB/c at day 7. 10µg WR17 (isotype), 10 µg rituximab mIgG2a (Rit 10), 10 µg Bhh2 mIgG2a (Bhh2) or 50 µg rituximab mIgG2a (Rit 50) were given to mice by i.v injection on day 9 afternoon. Spleens were harvested, stained and analysed by flow at day 10. Adoptive transferred B cell depletion in tumour free or BCL_1 bearing BALB/c. The overall results come from 3 independent experiments, each symbol represents one mouse, n=15 for tumour free Rit 10 group, n=4 for tumour free Bhh2 and Rit 50 group. n=8 for Bcl_1 Rit 10, Bhh2 and Rit 50 group. A one-tailed nonparametric student T test was performed to analyse significance between mice receiving isotype or anti-CD20 mAb. * represents significance of $P<0.05$, ** represents $P<0.01$ and N.S indicates that the result is not significant.

4.2.8 BCL_1 microenvironment does not enhance type I anti-CD20 mediated antigenic modulation

To investigate whether the BCL_1 tumour microenvironment inhibits type I CD20 mAb function through accelerating mAb mediated antigenic modulation, we assessed CD20 expression on splenic B cells from our adoptive transfer mice. We found that, 18 hours after mAb injection, the CD20 expression on the target B cell surface decreased dramatically in both tumour free and BCL_1 bearing mice (Figure 34 a, b). The remaining CD20 expressed on adoptively transferred huCD20 Tg splenic B cells was comparable between type I anti-CD20 Ritm2a treated and type II anti-CD20 Bhh2 m2a treated BCL_1 bearing mice. Similar results have been observed in tumour free mice (Figure 34b). These results suggested that the BCL_1 microenvironment may not inhibit rituximab activity directly through downregulated target CD20 expression. However, it's possible that BCL_1 lymphoma inhibits Ritm2a function indirectly, for example perhaps prolonging the time taken for macrophage to interact with and make productive contact with opsonised target cells.

In WT (both tumour free and BCL_1 bearing) mice, administered with either Ritm2a or Bhh2m2a markedly reduced CD20 expression on target cells (HuCD20+ adoptively transferred B cells) (Figure 34b). Similarly, to WT mice, Ritm2a greatly decreased CD20 expression on target cells in non-depleting gamma chain KO mice (Figure 34b), supporting previous observations from the group [161] that activatory FcγRs are not involved in this process. In contrast, there was more CD20 remaining on the target cell surface from type II anti-CD20 mAb Bhh2 m2a treated gamma chain KO mice than Bhh2 m2a treated WT mice (Figure 34b), in keeping with previous results. Taken together these results imply that in vivo type II anti-CD20 mAb modulate target CD20 expression by two mechanisms: Predominately by shaving [160], an activatory Fc gamma receptor

dependent mechanism that we observe as a product of the phagocytic process. Additionally, the activatory FcγR independent, FcγRII enhanced antigenic modulation was also observed [161].

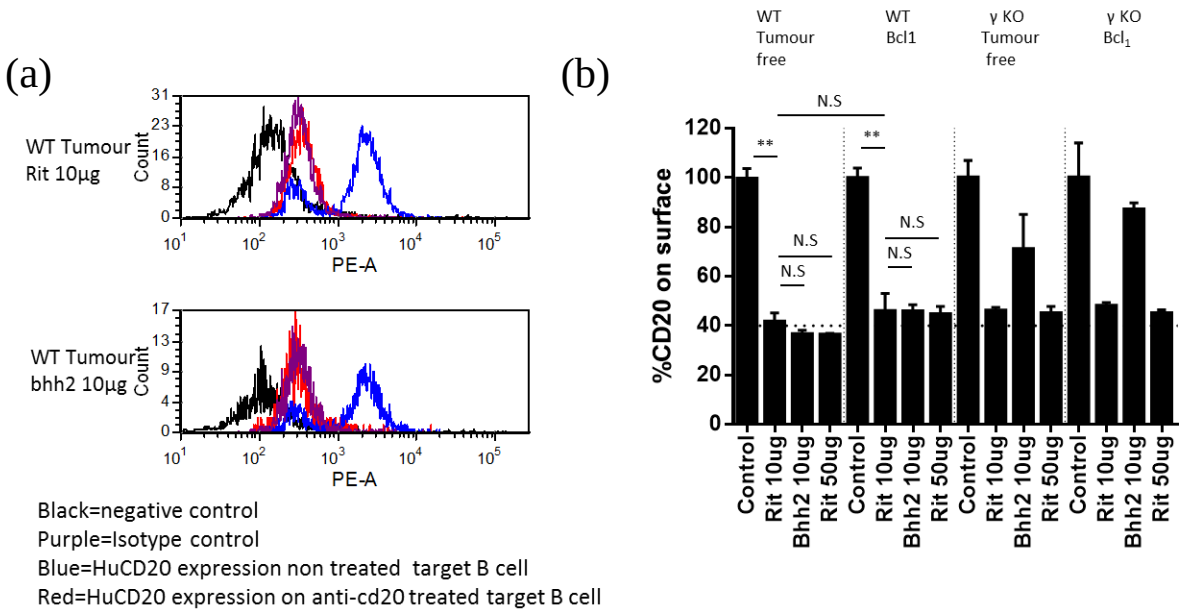

Figure 34: Antigenic modulation in tumour free and BCL_1 bearing mice. On day 0, 1x10 (4) BCL_1 cells were injected i.v in to wild type age matched BALB/c females. Carboxyfluorescein succinimidyl ester (CFSE) high and low labelled HuCD20 Tg and WT splenic B cells were adoptive transferred into wild type tumour free, wild type BCL_1, gamma chain K.O tumour free or gamma chain KO BCL_1 bearing BALB/C mice on day 7. On the day 9 afternoon, 10µg WR17 (control), 10 µg Ritm2a (Rit 10), 10 µg Bhh2 m2a (Bhh2, 10) or 50 µg Ritm2a (Rit 50) were given to mice by i.v injection. Spleens were harvested, stained and analysed by flow cytometry on day 10. (a) HuCD20 expression on adoptively transferred B cells in wild type mice, representative data. (b) Percentage HuCD20 expressed on adoptively transferred B cells in different groups of mice. HuCD20 on non-treated target B cells is represented as 100% and HuCD20 expression on the rest of the data shown are normalised to this value. A two-tailed nonparametric student T test was performed to analyse significance in wild type mice (n=4). * represents significance of $P<0.05$, ** represents $P<0.01$ and N.S indicates that the result is not significant. There is no statistical analysis carried out on gamma chain knock mice groups, as there are only 2 mice in each group.

4.2.9 Poly(I:C) alone or combined with other inhibitors can't overcome a suppressive tumour microenvironment

Our results showed that in WT, tumour free mice poly(I:C) stimulation improved Ritm2a mediated B cell depletion (Section 4.2.1, page 85). Thus, next we combined poly(I:C) with Ritm2a in an attempt to overcome BCL_1 suppression. We found that in tumour free mice, stimulation with poly(I:C) significantly increased Ritm2a activity with the T:NT ratio

reducing from ~0.52 in Ritm2a treated to ~0.37 in Ritm2a plus poly(I:C) treated mice (Figure 35). However, neither Ritm2a as a monotherapy nor in Ritm2a combination with poly(I:C) were able to induce target cell depletion in the presence of BCL_1 (Figure 35). This demonstrated that stimulation with poly(I:C) was not effective at overcoming tumour suppression of Ritm2a activity. Our phenotyping data showed that the BCL_1 microenvironment decreased the FcγR A:I ratio on splenic F4/80+ macrophage (Figure 40). Although poly(I:C) did show signs of activation of macrophages and a small increase in the FcγR A:I ratio, it appears to not be enough to restore the A:I ratio back to original non tumour levels (Figure 40).

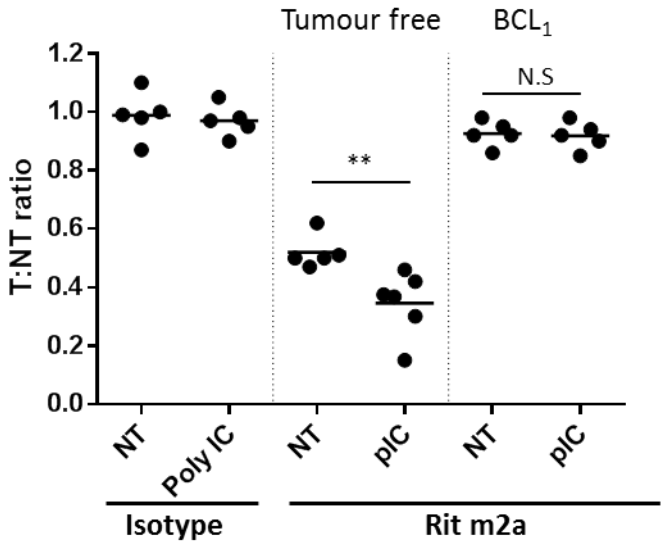

Figure 35: Poly(I:C) alone did not overcome tumour inhibition of Ritm2a activity. On day 0, $1x10^4$ BCL_1 cells were injected i.v in to wild type BALB/c females. Carboxyfluorescein succinimidyl ester(CFSE) High and low labelled HuCD20 Tg and WT splenic B cell, respectively, were adoptively transferred into BCL_1 inoculated or wild type tumour free BALB/c on day 7. On day 8 and day 9 morning, 100 µg poly(I:C) (pIC), was injected I.P in to mice. On day 9 afternoon, 10 µg WR17 (isotype), 10 µg Ritm2a (Rit), 10 µg Bhh2 mIgG2a (Bhh2) or were given to mice by i.v injection. Spleens were harvested, stained and analysed by flow cytometry at day 10, (n=5). A one-tailed nonparametric student T test was performed to analyse significant differences between treatment groups and isotype controls. * represents significance of $P<0.05$, ** represents $P<0.01$ and N.S indicates that the results are not significant.

The above data suggested that, poly(I:C) alone is not enough to overcome the immunosuppressive environment produced by BCL_1, therefore next we investigated

whether inhibitors of likely ongoing suppressive signalling pathways may permit poly(I:C) to repolarise the tumour associated macrophages. It has been well documented that stimulating macrophages via IL10 or IL4/13 in vitro polarizes macrophages into suppressive, anti-inflammatory, TAM-like phenotypes [260]. Elevated IL-10 levels have been observed in a majority of B cell lymphomas [261]. IL4/13 stimulation polarise macrophages into anti-inflammatory phenotype by triggering Janus kinase 3(JAK3) pathway [262]. In addition, Chen W et al. found that the mammalian target of rapamycin (mTOR) pathway is important in mediating monocyte differentiation to TAM [263]. Thus, we used suitable concentration (according to the literature) of IL10 receptor blocking antibody 1B1.3A [264], JAK3 inhibitor CP-690550 [265] or mTOR inhibitor [263] rapamycin with poly(I:C) in an attempt to enhance Ritm2a B cell depletion in BCL_1 bearing mice. As seen above, Ritm2a induced effective target cell depletion (T:NT ratio average 0.6) in tumour free mice and this is completely supressed (T:NT ratio average 1) in BCL_1 bearing mice (Figure 35). Poly(I:C) combined with IL10 receptor blocking antibody (T:NT ratio average 1) or rapamycin (T:NT average 1.1) were ineffective at reversing the inhibition (Figure 36). Poly(I:C) however, in combination with CP-690550 did show some potential to counter the tumour inhibitory effect, although the effect was limited and not significant (T:NT ratio average 0.9) (Figure 36). These results indicated that none of these combinations in isolation could efficiently overcome BCL_1 tumour environment potentially indicating the multi-faceted nature of immune suppression in the complex tumour environment.

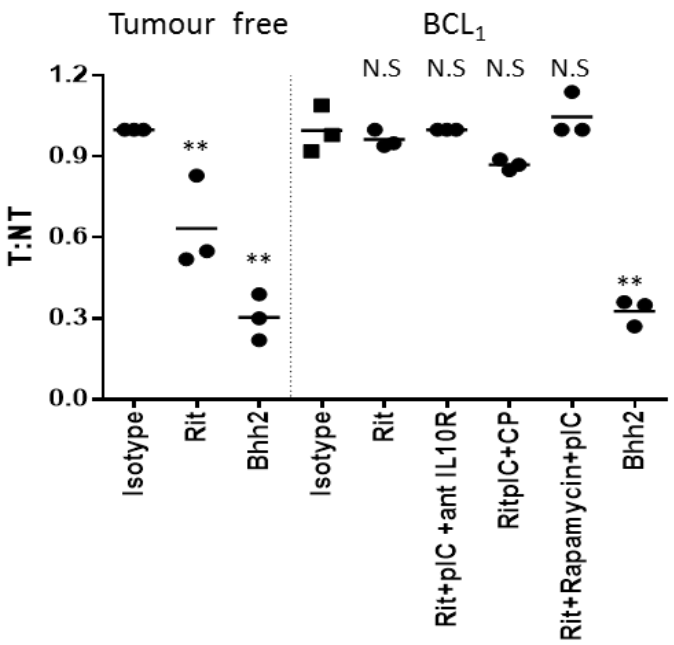

Figure 36: Poly(I:C) combined with signalling inhibitors cannot reverse tumour inhibition of Ritm2a activity. On day 0, $1x10^4$ BCL_1 cells were injected i.v in to wild type BALB/c females. Carboxyfluorescein succinimidyl ester(CFSE) labelled HuCD20 Tg and WT splenic B cells were adoptively transferred into BCL_1 bearing or wild type tumour free BALB/c on day 7. On day 8 and day 9 morning, 100 µg poly(I:C) (pIC), was I.P injected in to mice. On day 8, 800 µg CP, 100 µg rapamycin or 250 µg anti-IL10 receptor blocking mAb 1B1.3A were i.p injected in to mice. On day 9 afternoon, 10 µg WR17 (isotype), 10 µg rituximab mIgG2a (Rit), 10 µg Bhh2 mIgG2a (Bhh2) or were given to mice by i.v injection. Spleens were harvested, stained and analysed by flow cytometry on day 10, (n=3). A one-tailed nonparametric student T test was performed to analyse significant difference between different treatment groups and isotype controls. * represents significance of P<0.05, ** represents P<0.01 and N.S indicates that the result is not significant.

4.2.10 STING ligand DMXAA enables Ritm2a to overcome BCL_1 suppression

The data above demonstrated that the IRF3 activator poly(I:C) was not potent enough to overcome the immune suppression in BCL_1 bearing mice even at the low levels of tumour (~1% of splenocytes) present in this set up. We next sought to investigate STING ligands, a relatively new class of immune adjuvant, to see if it was a potentially more efficacious class of agonist in our lymphoma models. In order to do this, we used the murine STING ligand DMXAA that was originally described as a tumour-vascular disrupting agent but has now been shown to specifically bind STING leading to its activation. STING binding by its ligands leads to the recruitment and phosphorylation of TBK1 and subsequently to the enhancement of IRF-3 phosphorylation and consequently

type I interferon genes transcription (Section 1.9, page 24) [125]. We began by investigating STING effects in our in vitro BMDM system. Our in vitro polarization data shows that both poly(I:C) and DMXAA are able to enhance the expression of activatory FcγRs I and IV on BMDM (Figure 37a, b). Notably, neither of these agents increased inhibitory FcγRII expression (Figure 37a, b). These data demonstrate, at least in vitro, that DMXAA is as good as poly(I:C) in polarizing macrophages and manipulating of FcγR expression. Therefore, DMXAA may be a good candidate to polarize macrophages to a pro-inflammatory phenotype in vivo.

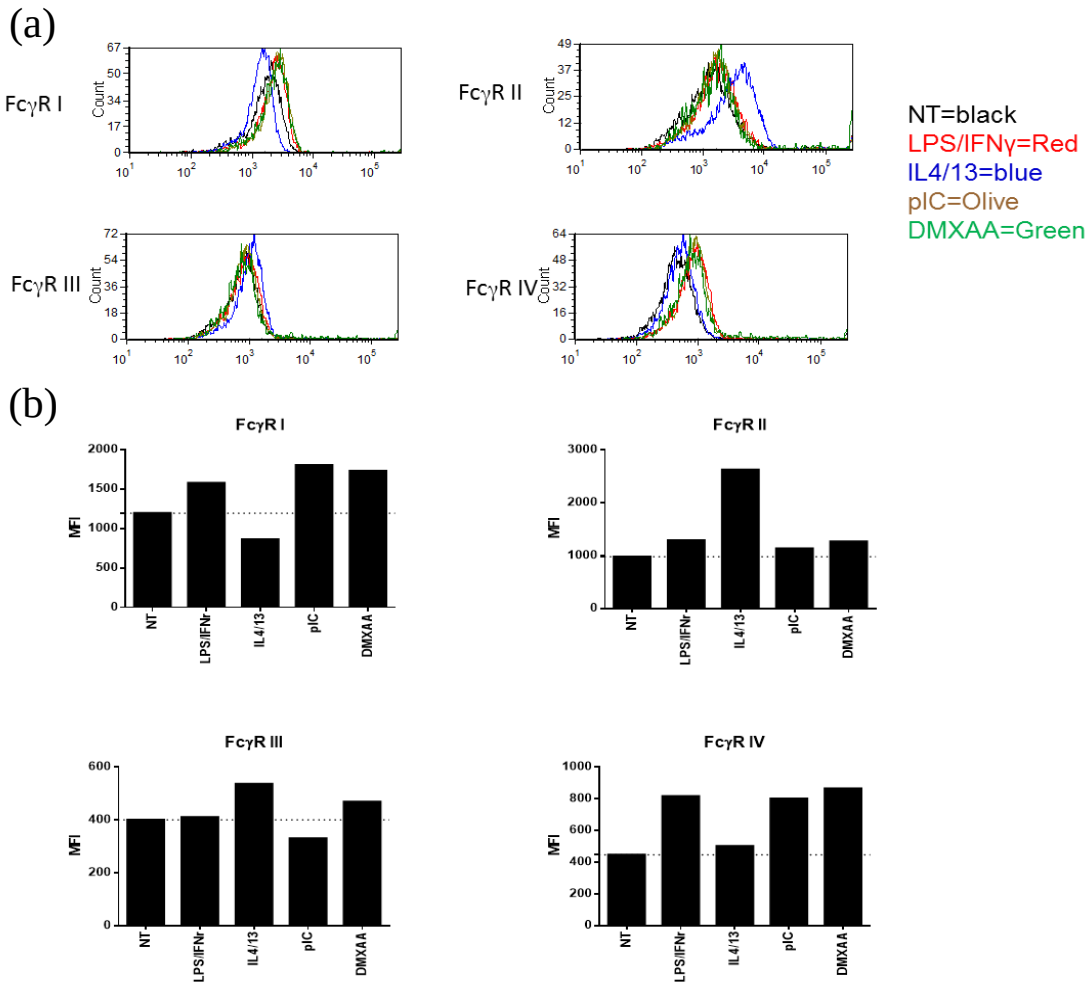

Figure 37: FcγR expression on DMXAA polarized BMDM. After 48h stimulation withLPS/IFNγ 100/2 ng/ml (final concentration, same for the rest of reagents here), IL4/13 10/10 ng/ml, poly(I:C) (pIC) 40 µg/ml or DMXAA 10 µg/ml, cells were harvested for flow cytometry analyses. (a) Histograms of FcγR expression on BMDM. (b) Summary of FcγR expression on BMDM following the indicated treatments. Results are from a single experiment. This experiment has been repeated by L.N.Dahal and the same results were observed.

We used the STING ligand DMXAA combined with Ritm2a in attempt to overcome the BCL_1 tumour microenvironment, a setting where the most effective TLR agonist poly(I:C) had failed previously. Notably, DMXAA combined with Ritm2a fully recovered the B cell depleting effect of this mAb in BCL_1 bearing mice (Figure 38). By using gamma chain KO mice where all depleting effect was abrogated, we have demonstrated that the recovery in huCD20 Tg B cell depletion from the combination of DMXAA with Ritm2a is entirely dependent on activatory FcγR and therefore a mAb mediated phenomenon (Figure 38).

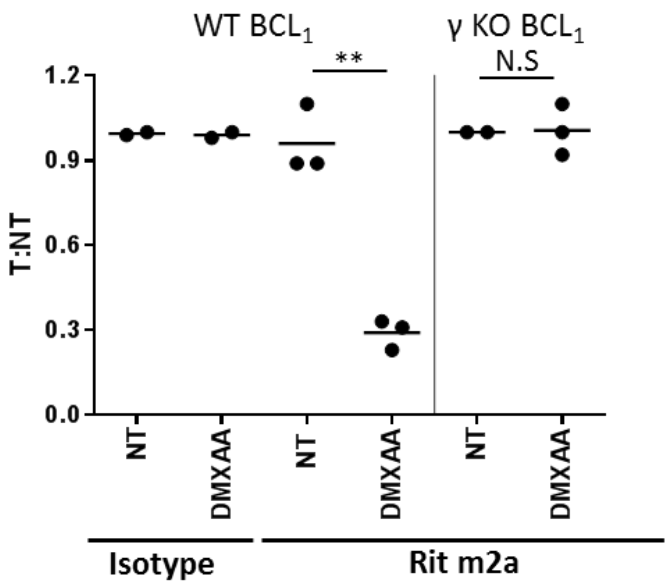

Figure 38: Sting ligand DMXAA enables Ritm2a to overcome BCL_1 tumour suppression. On day 0, $1x10^4$ BCL_1 cells were i.v injected in to wild type BALB/c females. CFSE labelled HuCD20 Tg and WT splenic B cell were adoptively transferred into BCL_1 inoculated or wild type tumour free BALB/c on day 7. On day 8, 300 µg DMXAA was injected I.P in to mice. On day 9 afternoon, 10 µg WR17 (isotype) or 10 µg Ritm2a (Rit 10) were given to mice by i.v injection. Spleens were harvested, stained and analysed by flow cytometry on day 10. Results are combined from 2 independent experiments and each symbol represents one mouse(n=3). A one-tailed nonparametric student T test was performed to analyse data. ** represents P<0.01.

Our in vivo polarization data demonstrated that the BCL_1 tumour microenvironment strongly inhibited the expression of activatory FcγRI, III and IV (Figure 39). Stimulation with poly(I:C) partially reversed this BCL_1 inhibition, but the expression of activatory FcγRs, especially FcγRI was still far below the level that is observed in WT mice (Figure 39). In marked contrast to this treatment with DMXAA completely reversed the suppression of activatory FcγRs that arise as a result of the BCL_1 tumour microenvironment (Figure 39). Indeed, the expression of FcγRIV is even higher in DXMAA treated BCL_1 bearing mice than that observed in WT mice (Figure 39).

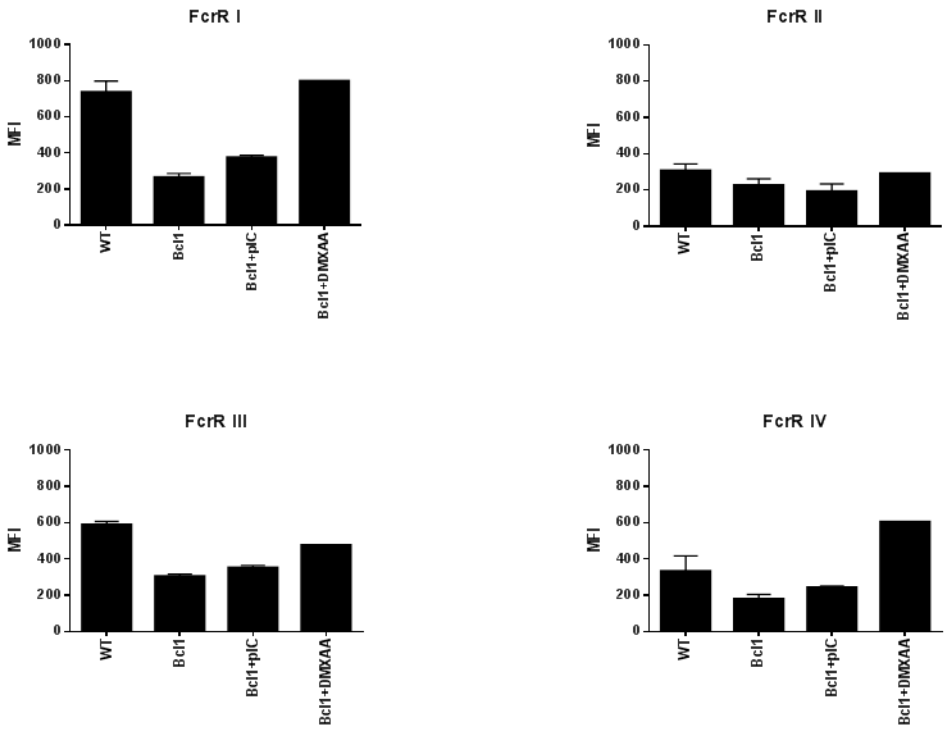

Figure 39: In vivo, stimulation with DMXAA changes splenic macrophage FcγR expression. On day 0, $1x10^4$ BCL_1 cells were injected i.v in to wild type BALB/c females. On day 8, 300 µg DMXAA was injected I.P in to mice. Spleens were harvested, stained and analysed by flow cytometry on day 10. FcγR expression on non-treated, poly(I:C), or DMXAA treated WT and BCL_1 mice. Results were from a single experiment. These experiments have been repeat by L.N.Dahal and similar results were observed.

These effects are also reflected by the overall FcγR A:I ratio (MFI of FcγRI x FcγRIII x FcγRIV / FcγRII) on splenic macrophages where the A:I ratio in DMXAA treated mice is about 5-fold higher than that in poly(I:C) treated mice (Figure 40). In summary, these date show that DMXAA is more potent than poly(I:C) in repolarizing tumour associated macrophages in BCL_1 mice.

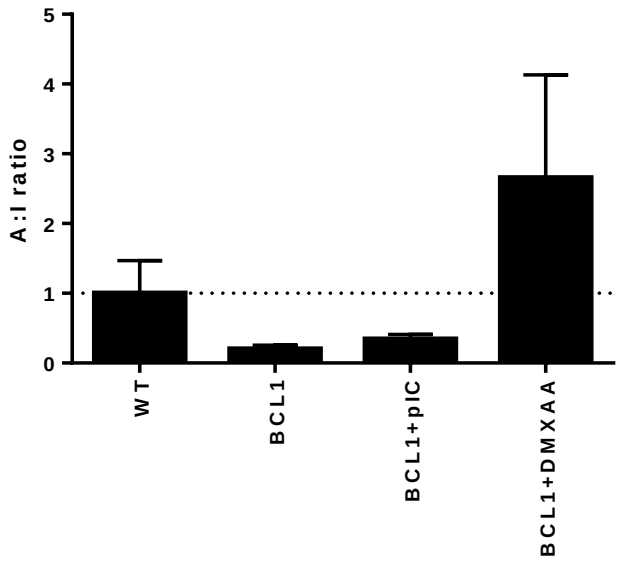

Figure 40: In vivo, stimulation with DMXAA changes FcγR A:I ratio on macrophage. On day 0, $1x10^4$ BCL_1 cells were injected i.v in to wild type BALB/c females. On day 8, 300 µg DMXAA were I.P injected to mice. Spleens were harvested, stained and analysed by flow cytometry on day 10. Summary of FcγR activatory to inhibitory ratio (MFI of FcγRI x FcγRIII x FcγRIV / FcγRII) on wild type, BCL_1 mice, BCL_1 mice treated with poly(I:C) (pIC) and BCL_1 treated with DMXAA. Results are from a single experiment. This experiments has been repeat by L.N. Dahal, and similar results obtained.

After establishing the potency of the STING ligand DMXAA in our adoptive transfer model, we evaluated the potential of using DMXAA as an adjuvant to anti-CD20 mAb therapy in the BCL_1 therapy model. To polarize macrophages, DMXAA was given to mice on day 6 and 13 after BCL_1 inoculation. In this syngeneic model system, we are unable to use Ritm2a as it doesn't target murine CD20, therefore we used mIgG2a anti-mouse CD20 mAb 18B12 in our therapy model. 18B12 was administered to mice on day 7 and day 14. In this setting the combination of DMXAA with CD20 mAb completely inhibited tumour progression, effectively 'curing' mice to day 100 (Figure 41a). As monotherapies both reagents had a modest effect on survival (~10 days) compared to control, non-treated mice (Figure 41a). These results suggest that the combination effect is more likely to be synergistic rather than additive. Notably, and in line with control mice, all mice from the combination therapy groups reached their humane endpoint ~20 days after rechallenge with BCL_1 cells at day 100 (Figure 41b). This would suggest that no

long term adaptive memory response was generated as result of the combination treatment but rather that tumour cell killing by antibody mediated mechanisms were augmented.

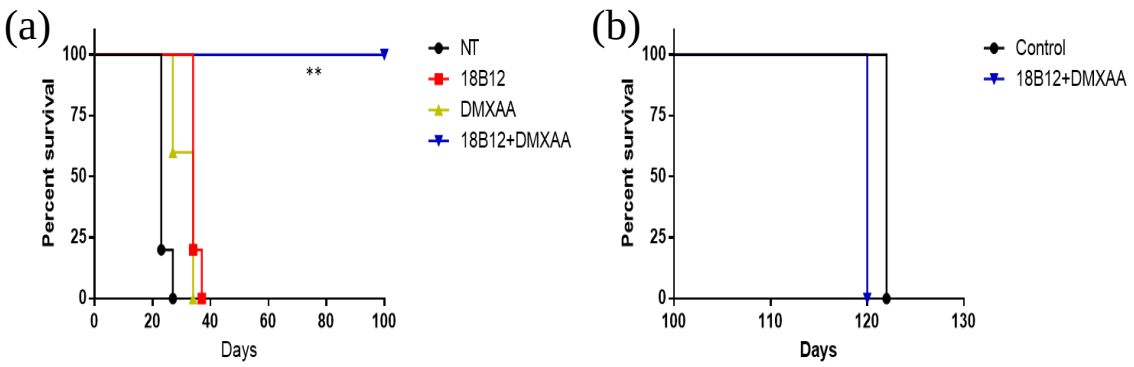

Figure 41: STING ligand DMXAA combined with anti-CD20 therapy prolongs the survival of BCL_1 bearing mice. On day 0, $1x10^4$ BCL_1 cells were injected i.v in to wild type BALB/c females. On days 6 and 13, 300 µg DMXAA was i.p injected in to mice. On day 7 and 14, 200 µg of anti-CD20 mIgG2a mab, 18B12, was administered to mice. (a) The survival curves of non-treated, 18B12, DMXAA and DMXAA+18B12 treated BCL_1 bearing mice. (b) On day 100, surviving mice from (a) were re-challenged with $1x10^4$ BCL_1 cells. Controls represent WT untreated mice challenged with the same dose of tumourBCL1. Figure (a) and (b) results were from a single experiment with each symbol representing one mouse (n=5). A one-tailed nonparametric student T test was performed to analyse data. ** represents P<0.01 This experiment has been repeated once with similar results observed.

4.3 Discussion

In this chapter, we first evaluated the potential of using TLR agonists; LPS, R848 and poly(I:C) as adjuvants for Ritm2a, a murinised version of rituximab, in vivo. In an adoptive transfer model, we found that poly(I:C) stimulation significantly promoted rituximab mediated HuCD20 transgenic B cell depletion in vivo (Figure 21). Consistent with in vitro results (Figure 20b), R848 didn't improve rituximab mediated B cell depletion in vivo (Figure 21). Notably, LPS didn't augment rituximab mediated B cell depletion in vivo (Figure 21), although it outperformed the other TLR agonists in vitro (Figure 20b). We observed that in mouse spleens stimulated with LPS there was a large increase in the number of infiltrating neutrophils a clear sign of inflammation (Figure 22,25). In addition, stimulation by LPS promoted an increase in the CD11b expression on F4/80+ splenic macrophages (Figure 22). CD11b is one subunit of the heterodimeric integrin

alpha-M beta-2 (αMβ2) molecule that is important in regulating cell adhesion and migration [266]. It has been demonstrated that CD11b indirectly regulates inflammation through control of cell adhesion and migration [266].Thus, it's possible that the highly inflammatory environment induced by LPS inhibits rituximab activity. In contrast, these inflammatory responses were not observed in R848 and poly(I:C) treated mice (Figure 25). In addition, stimulation with R848 (Figure 23) and poly(I:C) (Figure 24) didn't change CD11b expression on splenic macrophages. Instead, stimulation by poly(I:C) increased the infiltration of CD11b+Ly6C+ monocytes in mouse spleens (Figure 25).

To access the role of different myeloid populations in rituximab mediated B cell deletion. We used Ly6G specific mAb 1A8 [256] to delete neutrophils and CCR2 KO mice which are deficient in circulating monocytes [218]. We found that loss of CD11b+Ly6C+ monocytes (Figure 26) and CD11b+Ly6G+ neutrophils (Figure 27, 28) alone or together (Figure 29) did not change rituximab activity. This suggested that these myeloid populations are not necessary for rituximab mediated deletion in vivo. The potency of rituximab is closely related to the expression of FcγR in vivo [160, 198, 199]. Thus, we investigated the FcγR expression on macrophages from different compartments. We found that poly(I:C) stimulation significantly increased activatory FcγR I and IV expression on splenic and peritoneal macrophages (Figure 30). More importantly, poly(I:C) stimulation enhanced FcγR activatory to inhibitory ratio on splenic and peritoneal macrophages (Figure 31), the A:I ratio of FcγRs has been shown to be important in regulating ADCP in different pre-clinical models (Section 1.11,page 39). However, poly(I:C) stimulation didn't alter the FcγR expression and activatory to inhibitory ratio on alveolar macrophages. This observation may be because it has been shown that activating TLR3 on alveolar macrophages doesn't induce the phosphorylation of STAT1 which is important in mediating the expression of activatory FcγR, especially FcγRI [257, 258]. Together, we surmised that poly(I:C) promoted rituximab activity

through enhancing the FcγR activatory to inhibitory ratio on macrophages and thereby their phagocytic capacity and effector function.

Next, we assessed whether poly(I:C) was able to promote rituximab activity in a suppressive tumour microenvironment where macrophages may possess an anti-inflammatory M2-like phenotype and consequently may have reduced phagocytic capacity as we observed in vitro. In our adoptive transfer model, mice were inoculated with BCL_1 lymphoma cells 9 days before injecting rituximab. BCL_1 cells although low in number were detectable in the spleen by this stage (Figure 32a) and progressed rapidly from this point forward (Figure 32b). Deleting monocytes/macrophages with clodronate containing liposomes[259] stopped tumour growth demonstrating that tumour associated macrophage are crucial for tumour progression (Figure 32b). This also demonstrated that we could not deplete macrophages in this tumour model to determine directly their role in mediating mAb effector function. It was striking to observe that rituximab mediated B cell depletion was completely abolished in mice bearing established BCL_1 lymphoma (Figure 33). This inhibition could be partially, but not fully recovered by increasing rituximab dose by fivefold (Figure 33). Additionally, we observed that the activity of type II anti-CD20 mAb Bhh2 was not affect by the BCL_1 environment (Figure 33). One potential explanation for this discrepancy may be that the activity of type I anti-CD20 mAb is inhibited by antigenic modulation, whilst type II anti-CD20 mAb is not affect by this mechanism [161]. Thus, the tumour microenvironment may enhance antigenic modulation or increase the time taken for macrophage to engage with opsonised target cells, either of which may contribute to reduced rituximab function. To verify this possibility, we investigated the expression of CD20 on target B cells in vivo. After 18 hours, the CD20 level on rituximab treated B cells was similar to that of Bhh2 treated (Figure 34). This suggested that both type I and type II anti-CD20 mAb can induce rapid loss in the expression of CD20 on target cells (Figure 34). Using gamma chain knock out mice, we demonstrated that in vivo, rituximab induced CD20 loss is independent of

activatory FcγR, thus likely mediated by antigenic modulation (Figure 34)[161]. In contrast, Bhh2 mediated CD20 reduction depended on activatory FcγR, and hence the active depletion process and this loss may be regulated primarily by antigenic shaving (Figure 34). Indeed, both antigenic modulation and antigenic shaving are dynamic processes, investigating CD20 expression at one-time point, as done here, is not enough and further experiments to assess CD20 expression at different points post mAb administration and during the depletion process will be required.

BCL_1 is a mice lymphoma cell line, after inoculation, lymphoma cells develop massively enlarged spleens, then migrate to blood [224]. To overcome the BCL_1 tumour inhibition of Ritm2a activity, we used poly(I:C) alone (Figure 35) or poly(I:C) plus different TAM signal inhibitors (Figure 36) as adjuvants for rituximab, however none of these combinations was able to efficiently restore rituximab function in the BCL_1 lymphoma environment (Figure 35, 36). Finally, we assessed a new class of adjuvant, STING ligands, which was as good as, if not better than poly(I:C) in vitro at activating BMDM (Figure 36). Further, we found that the murine specific STING ligand DMXAA was able to restore rituximab function in BCL_1 mice (Figure 38). In vivo phenotyping data demonstrated that the BCL_1 microenvironment remarkably reduced the expression of activatory FcγR, particularly FcγRI expression on splenic CD11b+F4/80+ macrophages (Figure 39). DMXAA outperformed poly(I:C) in re-polarizing FcγR expression (Figure 39) and the FcγR A:I ratio (Figure 40) to levels comparable to that observed in WT mice.

It was striking that in the therapy model, DMXAA plus anti-CD20 mAb completely prevented BCL_1 tumour growth and effectively cured all mice in that group (Figure 41a). It appeared that the combination effect was synergistic rather than simply additive as mAb or DMXAA alone produced a minimal survival effect (Figure 41a). It has been shown that the STING ligand DMXAA can trigger CD8+ T cell responses to eliminate tumour cells [128]. Thus, we investigated whether the protective response we observed was due to adaptive T cell responses. We found that surviving mice had not generated a

protective adaptive immune response against tumour rechallenge (Figure 41b), suggesting that no long-term memory response was produced during the therapy, at least under the conditions tested here. Thus, we suggest that the combination of anti-CD20 mAb and STING ligand eliminates tumour cells through enhanced antibody regulated humoral immunity. To confirm this contention, my colleague L.N.Dahal has repeated these therapy experiments in mice treated with CD8 depletion mAb (YTS169). In the absence of CD8 T cells he obtained the same results; with DMXAA plus anti-CD20 mAb combination completely inhibited BCL_1 progression but the surviving mice were not protected from re-challenge. Both poly(I:C) and DMXAA are IRF3 activators, but in vivo phenotyping data suggests that DMXAA is significantly better than poly(I:C) at increasing FcγR activatory to inhibitory ratio on macrophages (Figure 40). This may be because poly(I:C) and DMXAA activate the IRF3 pathway through different pathways. Stimulation by poly(I:C) activates TIR-domain-containing adapter-inducing interferon-β(TRIF) adapter that in turn phosphorylates TBK1 and IRF3[6]. However, STING ligand DMXAA can muster IRF3 and TBK1 to its C-terminal region, thus promoting IRF3 phosphorylation by TBK1 [125].

In this chapter, a pre-clinical lymphoma model BCL_1 has been used. The BCL_1 cells are first observed in the blood, then migrate and accumulate in the spleen. After 21 days when the splenomegaly has established, the BCL_1 cells start metastasizing to bone marrow and liver [224]. In this project where the BCL_1 tumour were harvested at day 9, the BCL_1 cells were primary located in the blood and spleen.

Recent literature using MMTV-PyMT tumour model demonstrated that TAMs are derived from inflammatory CCR2+ Ly6C+ monocytes, and are distinct from tissue resident macrophages according to phenotypic markers and function [205]. It may be the same scenario for the BCL_1 tumour, TAMs originating from CCR2+ Ly6C+ monocytes may combine with other regulatory populations such as Treg cells and myeloid derived suppressive cells to form a suppressive niche that may further inhibit the function of

tissue resident macrophages in the spleen. Notably, in the literature CD11b against MHC II marker was used to distinguish TAMs from tissue resident macrophages [205]. Although we haven't used the MHCII as a marker in this project, it has been shown that both monocyte derived TAM and tissue resident macrophages express high level of F4/80 [205], thus the macrophage gate used here covers all F4/80+ macrophages and therefore may represent a mixture of monocyte derived TAM and tissue resident macrophages in BCL_1 bearing mice. Therefore, DMXAA may polarize both monocyte derived TAMs and tissue resident macrophages in the BCL_1 tumour. To confirm this contention, adding anti-MHC II mAb in the macrophage staining panel and repeating the DMXAA polarization experiments will be required in the future.

We have shown that in the adoptive transfer model, deletion of neutrophils didn't affect rituximab activity, as Ly6G is a conventional marker for both neutrophils and myeloid derived suppressive cells in mouse [267], using Ly6G specific deletion mAb may not suitable for BCL_1 model, as depletion of myeloid derived suppressive cells may inhibit tumour progression. Therefore, exploring a new method to specific delete neutrophils in tumour is required in the future. Published literature has demonstrated that CCR2+Ly6C+ monocytes are precursors for TAMs [205], in agreement with this finding, we showed that using clodronate containing liposomes to delete monocytes/macrophages strongly inhibit BCL_1 tumour growth (Figure 32). Thus, we suggest that rather than effectors, CCR2+Ly6C+ inflammatory monocytes are more like the precursor for tumour associated macrophages in BCL_1 tumour. In adoptive transfer and the pre-clinical BCL_1 model, NK cells can delete target cells via FcγRIII mediated ADCC. However, NK cells doesn't express TLR3 [266], moreover poly(I:C) activation were unable able to increase FcγRIII expression on macrophages in vitro (Figure 17) and in vivo (Figure 30). In contrast, DMXAA pathway can be found on murine NK cells [268], and we have demonstrated that stimulation with DMXAA increases FcγRIII expression on BMDMs in vitro (Figure 37). Therefore, we conclude that poly(I:C) stimulation may

only enhance ADCP, while DMXAA stimulation can potentially promote both ADCP and ADCC. This could offer an alternative explanation as to why DMXAA is more potent than poly(I:C) on augmenting anti-CD20 mAb activity in vivo.

Chapter V Characterisation and evaluation of the therapeutic potential of dual mechanism mAb

5.1 Introduction

Immunomodulatory mAb target effector cells or APC that are important in cancer immune surveillance [148]. Immunomodulatory mAb that enhance anti-cancer immunity via blockade of inhibitory signals are known as checkpoint inhibitors, for example mAb targeting CTLA4 [269]. To fully activate T cells, three signals are required, the first one comes from ligation of T cell receptor to antigenic peptide presented in the context of MHC [15]. The second signal, also called the costimulatory signal, is antigen nonspecific. The third signal are provided by inflammatory cytokines, such as IL1, IL12 and IFNα/β [182, 183]. Several costimulatory signals have been discovered [15]. One of the best character costimulatory signals is from binding of CD28 on the T cell to a B7 family protein on APC, for example CD80 or CD86 [15]. The co-stimulatory signal is crucial for T cell differentiation, proliferation and survival [15]. In the absence of a co-stimulation signal, ligation of the TCR may cause T cell deletion or anergy [15]. Activation of T cells is strictly regulated by the immunoglobulin superfamily molecule CTLA4, which is also expressed on T cells [269]. CTLA4 binds to B7 family protein on APC preventing the ligation of CD28 to B7 family protein and thus inhibiting the costimulatory signal. Ipilimumab, a checkpoint inhibitor that augments T cell response via blockade of CTLA4 has been approved by the U.S. FDA for the treatment of melanoma [269]. In a randomized phase III trial, anti-CTLA4 mAb ipilimumab alone improved overall survival of previously treated melanoma patients, increasing the median overall survival from 6.4 to 10.1 months [269]. Additionally, several clinical trials are ongoing to evaluate the potential of using ipilimumab against NSCLC [131], bladder cancer and prostate cancer.

Agonistic mAb promote anti-cancer immunity through delivery of co-stimulatory signals to effectors or APC. CD40 is a TNF-receptor superfamily member protein that is expressed

on a wide range of cells including all APC, epithelial and endothelial cells. Activating CD40 by CD40 ligand expressed on T helper cells enhances B cell survival, proliferation and differentiation [25]. It has been demonstrated that anti-mCD40 mAb, clone 3/23, can induce strong CD8+ T cell responses and completely stop tumour growth in the pre-clinical BCL_1 lymphoma model [195]. Cross-linking with FcγRII is required for anti-CD40 mAb to mediate anti-tumour activity. In vitro experiments showed that CD40 mediated CD8+ T cell proliferation is greatly reduced in FcγRII knock out mice [270]. In addition, anti-CD40 mIgG1 performs better than other isotypes to enhance CD8 response in vitro [270] and in vivo [270] consistent with mIgG1 possess higher affinity for FcγRII and therefore greater crosslinking ability.

4-1BB is another member of the TNFR superfamily, and expressed on a wide range of cells, including DC, NK and activated T cells [15]. 4-1BB binds with its ligand providing a costimulatory signal to T cells, thereby enhancing T cell proliferation and survival [15]. Anti-4-1BB mAb has been shown promote anti-tumour activity in pre-clinical cancer models via activating T cells, to a larger extent CD8 than CD4 T cells [271].

Recently, it has been demonstrated that anti-CTLA4 can augment antitumor immunity through deleting intratumoral regulatory T cells in mice [272] and humans [273]. In preclinical models, anti-CTLA4 mIgG2a mediated Treg cell depletion in an activatory FcγR dependent manner, with Treg deletion completely abolished in gamma chain knock out mice [272]. In patients with metastatic melanoma, ipilimumab responders were shown to possess fewer tumour infiltrating Treg cells post therapy compared to non-responders likely demonstrating deletion [273]. Similarly intratumoral regulatory T dells depletion has been demonstrated for anti-GITR [274] and anti-OX40 [275] mAb in preclinical models. Based on the fact that 4-1BB is a downstream target of the Treg lineage-defining transcription factor Foxp3, is expressed on resting Treg cells and is upregulated on Treg activation [276], it is possible that anti-4-1BB mAb LOB12.0 might also work in part through depletion of intratumoral Tregs as well as direct costimulation.

CT26 tumour model was used to investigate the mechanism of anti-4-1BB mAb LOB12.0 for 2 reasons: Firstly, CT26 is very well characterized and has been used in more than 500 studies [227]. Secondly, one important aim of this project is to study the potential for Treg deletion by anti-4-1BB mAb, CT26 tumours have been described as containing a high number of CD4+Foxp3+ suppressive Treg cells and are responsive to their deletion [227], and is therefore an ideal model to use. In this chapter, we investigated the mechanisms of action anti-4-1BB mAb in solid tumours and then we attempted to enhance anti-4-1BB mAb therapeutic activity via manipulation of FcγR expression through macrophage polarization,

5.2 Results

5.2.1 In vitro agonistic activity of anti-4-1BB mAb is determined by isotype

TNFR superfamily immunomodulatory mAb, for example anti-CD40 mAb require cross-linking with inhibitory FcγRII to induce anti-tumour immunity [270]. To investigate if this requirement similarly applied to anti-4-1BB we generated mIgG1 and mIgG2a chimeric versions of the rIgG2a anti-4-1BB mAb (LOB12.0 generated in-house by antibody discovery group [277]). These mAbs were then analysed by surface plasmon resonance (C. Ian Mockridge), a technology routinely used to characterise protein - protein interactions. The results obtained demonstrated that these isotypes switched mAb bound mouse FcγR with the characteristic, distinct profiles with mIgG2a possessing a high activatory to inhibitory FcγR ratio (high affinity to FcγR I and IV, medium affinity to FcγR III) and mIgG1 a low ratio (medium affinity to FcγR II, and low affinity to FcγR III) (Appendix figure 1a). A construct encoding the extracellular and transmembrane region of murine 4-1BB was stably transfected to a human cell line (Sarah L Buchan). To compare anti-4-1BB mAbs binding, anti-4-1BB mIgG1 and anti-4-1BB mIgG2a were incubated with transfected cell line either independently (Appendix figure 1b) or mixed

with their parent anti-4-1BB rIgG2a (Appendix figure 1c). The binding data shows that both anti-4-1BB mAb mIgG1 and mIgG2a isotype achieve saturation at 1 µg/ml the same as their parent anti-4-1BB rIgG2a isotype (Appendix figure 1b). In addition, both mAb were equally able to block anti-4-1BB rIgG2a binding (Appendix figure 1c), demonstrated that anti-4-1BB mIgG1, anti-4-1BB mIgG2a and anti-4-1BB rIgG2a are binding equivalently to the same epitope of 4-1BB. In summary, although anti-4-1BB mIgG1 and mIgG2a binds to mouse FcγR with different profiles, they are similar to their parent anti-4-1BB rIgG2a for binding to 4-1BB.

Once we had established that the mIgG1 and mIgG2a versions of LOB12.0 behaved as expected we carried out an in vitro T cell co-stimulation assay to investigate the agonistic activity of anti-4-1BB mAb. We found that only the mIgG1 isotype and not the mIgG2a demonstrated appreciable agonistic activity (Figure 42) and this result was in good agreement with other published literature [270, 278]. Furthermore, the agonistic activity of mIgG1 was independent of Treg cells in the T cell co-stimulation assay (Figure 42), demonstrating that anti-4-1BB mIgG1 mediates its agonistic effects via targeting 4-1BB on effector T cells.

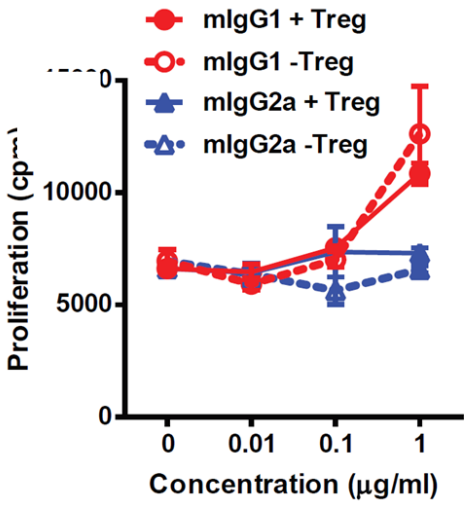

Figure 42: Anti-4-1BB mIgG1 exerts agonistic activity in vitro. Splenocytes from Foxp3-GFP mice either sorted to remove GFP+ cells (-Treg) or not (+Treg) were incubated with 0.1 µg/ml anti-CD3 and the indicated concentrations of either anti-4-1BB (LOB12.0) mIgG1 or mIgG2a as indicated. Incorporation of [3H]-thymidine was measured during the last 16 hours of a 72-hour culture. This experiment was performed by Sarah L Buchan.

5.2.2 Agonistic activity of anti-4-1BB mAb is determined by isotype in vivo

To establish the isotype dependence of anti-4-1BB mAb (LOB12.0) agonistic activity in vivo, we investigated serval activation makers expressed on tumour infiltrating CD8+ T cells in the CT26 colon carcinoma model [277]. On day 0, $5x10^4$ CT26 cells were s.c. into wild type BALB/c, 50 µg anti-4-1BB mAb mIgG1 or mIgG2a were given on day 6 by i.v, then 50 µg i.p every other day, until day 12. Spleens were harvested on day 13 for flow cytometry analysis. We found that both LOB12.0 mIgG1 and mIgG2a were able to increase the percentage of tumour infiltrating CD8+ T cell that expressed the proliferation marker Ki-67, however, LOB12.0 mIgG1 was significantly more potent than LOB12.0 the mIgG2a (Figure 43). Eomesodermin (Eomes) is a T-box transcription factor that is important in regulating CD8 differentiation [279] and anti-tumour activity [280]. Stimulation with LOB12.0 mIgG1 strongly promoted the percentage of intratumoural CD8+ T cells that expressed Eomes, whilst administration of the LOB12.0 mIgG2a version failed to do so (40). Taken together we suggested that whilst both LOB12.0 mIgG1 and mIgG2a possess agonistic activity the LOB12.0 mIgG1 is more potent than the LOB12.0 mIgG2a at activating CD8+ T cells.

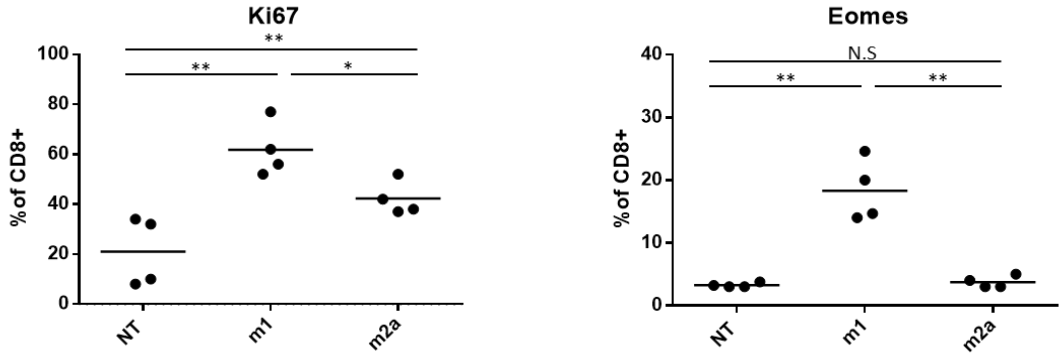

Figure 43. In vivo agonistic activity of anti-4-1BB mAb. Wild type BALB/c mice were inoculated with $5x10^4$ CT26 cells s.c. on day 0. Anti-4-1BB mAb mIgG1 (m1) or mIgG2a (m2a) were given on days 6 by i.v, 8 i.p,10 i.p, and 12 i.p, 200 µg in total. Mice were sacrificed on day 13 and spleens and tumour analysed by flow cytometry. (a) Percentage of tumour infiltrated CD8+ T cell express Eomes. (b) Percentage of tumour infiltrated CD8+ T cell express Ki67, each symbol representing a mouse. (n=4). One-tailed nonparametric student T test was performed to analyse data. * represents significance of P<0.05, ** represents P<0.01 and N.S indicates that the result is not significant.

5.2.3 Isotype and CD8+ T cells dependent therapeutic activity of anti-4-1BB mAb

Having characterised the agonistic activity of LOB12.0 anti-4-1BB mIgG1 and mIgG2a, we tested the therapeutic activity of these mAb LOB12.0 against three established solid tumour models; CT26 colon carcinoma (Figure 43a), EG7 thymoma [229] (Figure 43b) (performed by Sarah L Buchan) and NXS2 neuroblastoma[281] (Figure 43c) (performed by Stuart N Dunn). We found that in all three models it was the anti-4-1BB mIgG2a isotype mAb (high A:I ratio) which was able to efficiently inhibit tumour growth (~80% long term survival) (Figure 43 a,b,c), whilst the mIgG1(Low A:I ratio) showed little anti-tumour activity (0%-20% survival) (Figure 43 a,b,c). These results are in marked contrast to our previous data (42,43), as well as the published data that agonistic anti-CD40 [270] and anti-DR5 [282] perform better as a mIgG1 isotype. Hence, it was possible that in this setting anti-4-1BB mAb most effectively mediated anti-tumoural immune responses through an alternative mechanism than direct agonism that does not require efficient cross-linking with FcγRII.

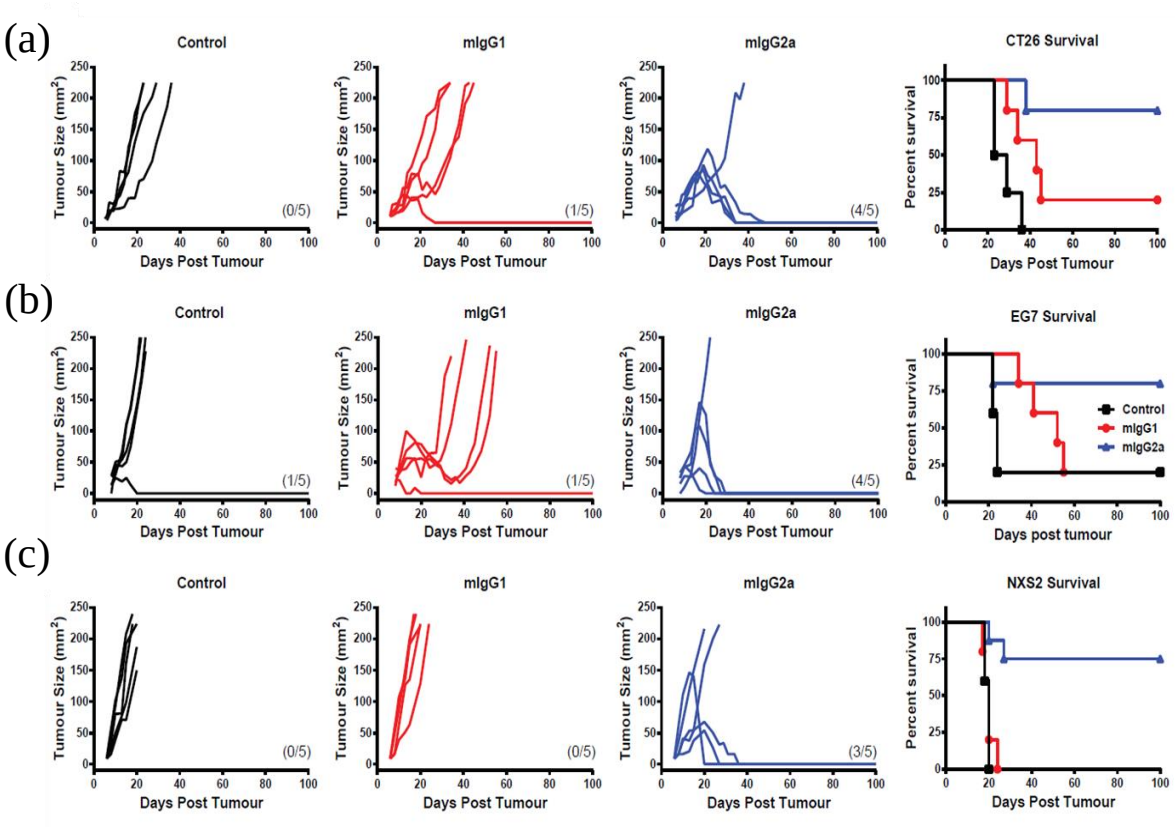

Figure 44: Anti-4-1BB mIg2a but not mIgG1 provides effective tumour protection in solid tumour models. (a) BALB/c females were inoculated with $5x10^4$ CT26 cells by on day 0. Anti-4-1BB mIgG1(mIgG1) or mIgG2a(mIgG2a) were given to mice by i.v when tumour was palpable, then another 3 shots of antibody were given i.p every other day. In total, we gave 200 µg for each antibody. (B) Groups of C57BL/6 mice were challenged with $0.5x10^6$ EG7 tumour cells s.c. on day 0 prior to 200 µg of anti-4-1BB mAb or PBS control i.p. on days 3, 5 and 7. (C) Groups of A/J mice were challenged with $2x10^6$ NXS2 cells s.c. and received 200 µg anti-4-1BB mAb or isotype control mAb i.p. when tumour was palpable. A second dose of 200 µg was given 3 days later. For all three experiments tumour growth was monitored 3 times per week using calipers, n=5. Control=non-treated, mIgG1= anti-4-1BB mIgG1 treated, mIgG2a= anti-4-1BB mIgG2a treated These experiments have been repeated at least once with similar results observed.

In the CT26 model, pre-treating mice with anti-CD8 mAb YTS169 to deplete CD8+ T cells [228] strongly abrogating therapeutic activity of anti-4-1BB m2a (Figure 45). These results demonstrate the therapeutic activity of anti-4-1BB m2a still required an adaptive CD8+ T cell response.

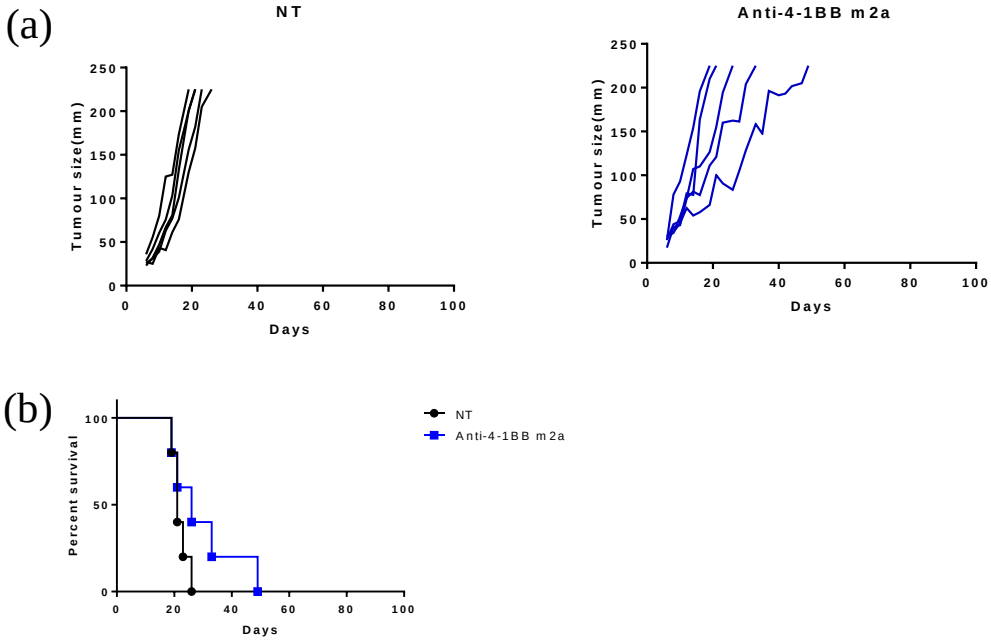

Figure 45: Anti-4-1BB m2a eliminates solid tumour CT26 in CD8+ T cells dependent manner. On day -1, 1 and 4 500 µg CD8 depletion mAb YTS169 were given to mice i.p. Mice were inoculated with $5x10^4$ CT26 cells s.c. on Day 0. Anti-4-1BB mAb mIgG2a were given on day 6 by i.v, 8 i.p,10 i.p, and 12 i.p, 200 µg in total (n=5). (a) Growth kinetics of NT and anti-4-1BB treated CT26. (b) Survival curve of NT and anti-4-1BB treated CT26.

5.2.4 Dual mechanism of anti-4-1BB mAb

Recent publications have demonstrated that several immunomodulatory mAb; CTLA-4 [272], GITR [274] and OX40 [275] act, at least in part, by deleting Treg cells rather than through checkpoint blockade or agonistic activity. Given that it was the mIgG2a isotype of LOB12.0 anti-4-1BB (Figure 44, page 126) which was effective at treating tumour bearing mice and this isotype is optimal for depletion we investigated whether the same mechanism could be operating here. We began by confirming the expression of 4-1BB on different cell populations and in different compartments in the CT26 and EG7 (data not shown) tumour models. We found that 4-1BB was expressed primarily on tumour-infiltrating Treg cells with only low level expression on a minority CD4 and CD8 effector T cells (Figure 46). In addition, 4-1BB was absent on splenic CD8 and CD4+Foxp3- cells with only low level expression on a small fraction of splenic Treg cells (Figure 46).

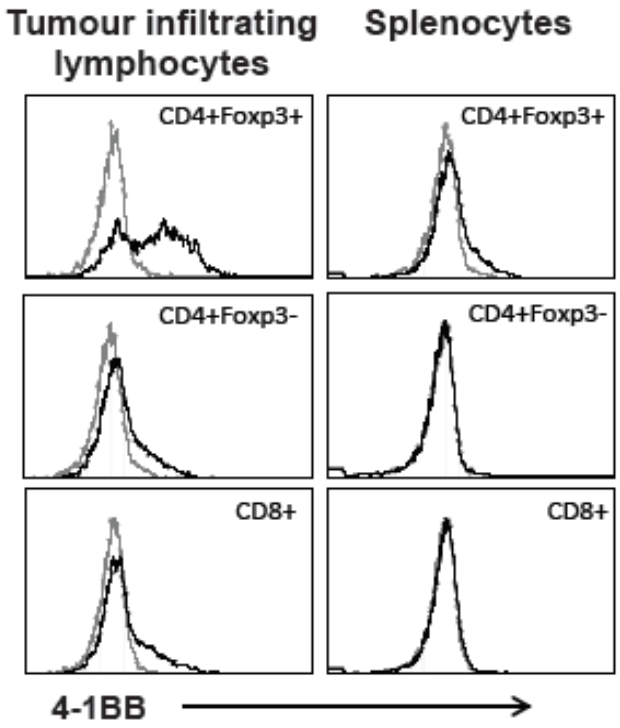

Figure 46: 4-1BB is expressed on tumour resident Treg cells. (a) The expression of 4-1BB on T cell subsets from TILs (inset left panels) and splenocytes (inset right panels). The expression of 4-1BB (black line) on CD4+Foxp3+ (inset top panels), CD4+ Foxp3- (inset middle panels) and CD8+ T cells (inset bottom panels), isotype control staining is shown by the grey histograms. Cells were isolated from mice bearing CT26 tumour. Representative data shown from 3 separate experiments. Results shows with kind permission of Jane Willoughbyi.

The presence of CD8+ T cells will effectively dilute the CD4+ T cells pool, thus as they expand they may lead to a change in the percentage of CD4+ Foxp3+ Treg cells in the tumour in the absence of depletion. To avoid the possible disturbance to our investigations that may arise from changing levels CD8+ T cells, we depleted CD8+ cells using YTS169 mAb [283] before we gave CT26 tumour. 50 µg anti-4-1BB mAb mIgG1 or mIgG2a were given on day 6 by i.v, then 50 µg i.p every other day, until day 12. On day 13 after tumour inoculation and one day after the final mAb administration, we found that anti-4-1BB mIgG2a efficiently deleted intra-tumoural Treg whilst the mIgG1 variant was ineffective (Figure 47). Notably, this depletion effect was restricted to the tumour, and was absent in the spleen (Figure 47a,b), because 4-1BB was predominately expressed on CD4+Foxp3+ Treg cells in tumour, and only a small fraction was found on splenic

CD4+Foxp3+ Treg cells (Figure 46) [284]. These data support the contention that anti-4-1BB mAb is able to elicit a therapeutic response through intratumoural Treg deletion.

To further assess the mechanism of action and FcγR requirements of the anti-4-1BB isotypes, we repeated our tumour infiltrating lymphocyte experiments in FcRgamma KO mice and FcγRII KO mice (Figure 47b). Anti-4-1BB mIgG2a mAb mediated intra-tumoural Treg depletion was abolished in FcR gamma KO mice, demonstrating that anti-4-1BB mIgG2a mAb deplete Treg cells in an activatory FcγR dependent manner (Figure 47a, b). Unexpectedly, in gamma KO mice, anti-4-1BB m1 stimulation significantly increase percentage of Treg cells in the tumour (Figure 47b). It has been suggested that Treg cells are unstable and might switch to T effector cells in context of tumour [285, 286]. Thus, we hypothesized that in gamma KO mice, tumour infiltrated Treg cells were switched to effector T cells, which start proliferating upon stimulation with agonistic anti-4-1BB mIgG1 (Figure 47b). Notably, anti-4-1BB mIgG1 mAb was able to induce intra-tumoural Treg depletion in FcγRII KO mice (Figure 47b). This observation can be explained by the fact that by knocking out the inhibitory FcγRII we have effectively increased the A:I ratio of the mIgG1 isotype making it an effective depleting mAb.

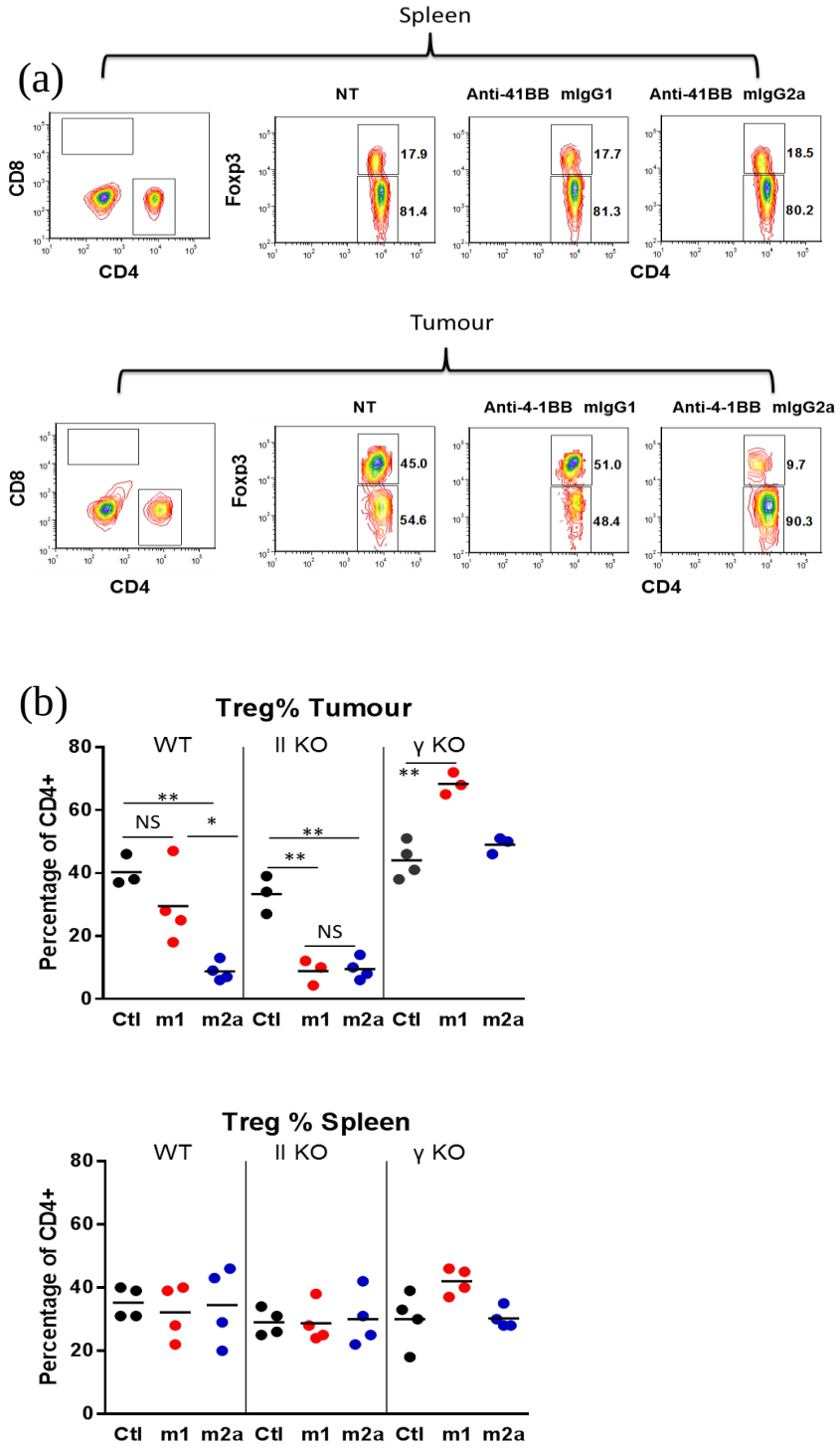

Figure 47: Anti-4-1BB m2a specifically depletes Treg in CT26 tumours in an FcγR dependent manner. On day -1, 1 and 4 500 µg CD8 depletion mAb YTS169 were given to mice i.p. Mice were inoculated with $5x10^4$ CT26 cells s.c. on Day 0. Anti-4-1BB mAb mIgG1 (m1) or mIgG2a (m2a) were given on day 6 by i.v, 8 i.p,10 i.p, and 12 i.p, 200 µg in total. Mice were sacrificed on day 13 and spleens and tumour analysed by flow cytometry. (a) Representative data of Treg deletion in spleen and tumour. (b) Summary data, each symbol representing a mouse. (n=4) WT=wild type mice, II KO= FcγR II KO mice, γ KO= FcγR common gamma chain KO mice. One-tailed nonparametric student T test were performed to analyse data. * represents significance of P<0.05, ** represents P<0.01 and N.S indicates that the result is not significant. This experiment has been repeated once, similar results were observed.

In the CT26 model, anti-4-1BB mIgG1 mediated anti-tumour activity is improved in FcγRII KO mice (Figure 48), this is consistent with previous data that mIgG1 induced intra-tumoural Treg deletion is enhanced in FcγRII KO mice (Figure 47b). In addition, the activity of anti-4-1BB mIgG2a is maintained in γ chain KO mice (Figure 48), suggesting that Treg cell depletion alone may not fully account for its therapeutic activity. These findings suggested that in absence of competitive activatory FcγR, anti-4-1BB mAb are able to deliver costimulatory signals to T cells through cross-linking with FcγRII. Thus, Anti-4-1BB mAb are able to mediate anti-tumour immunity through two mechanisms, activatory FcγR dependent Treg depletion and inhibitory FcγR dependent agonistic activity. This contention is supported by the observation that therapeutic activity of anti-4-1BB mAb is completely lost in FcγR null (γ chain KO x FcγRII KO) mice (Figure 48). More importantly, these results imply that there is the potential to control and potentially to enhance mAb activity through manipulation of FcγR expression.

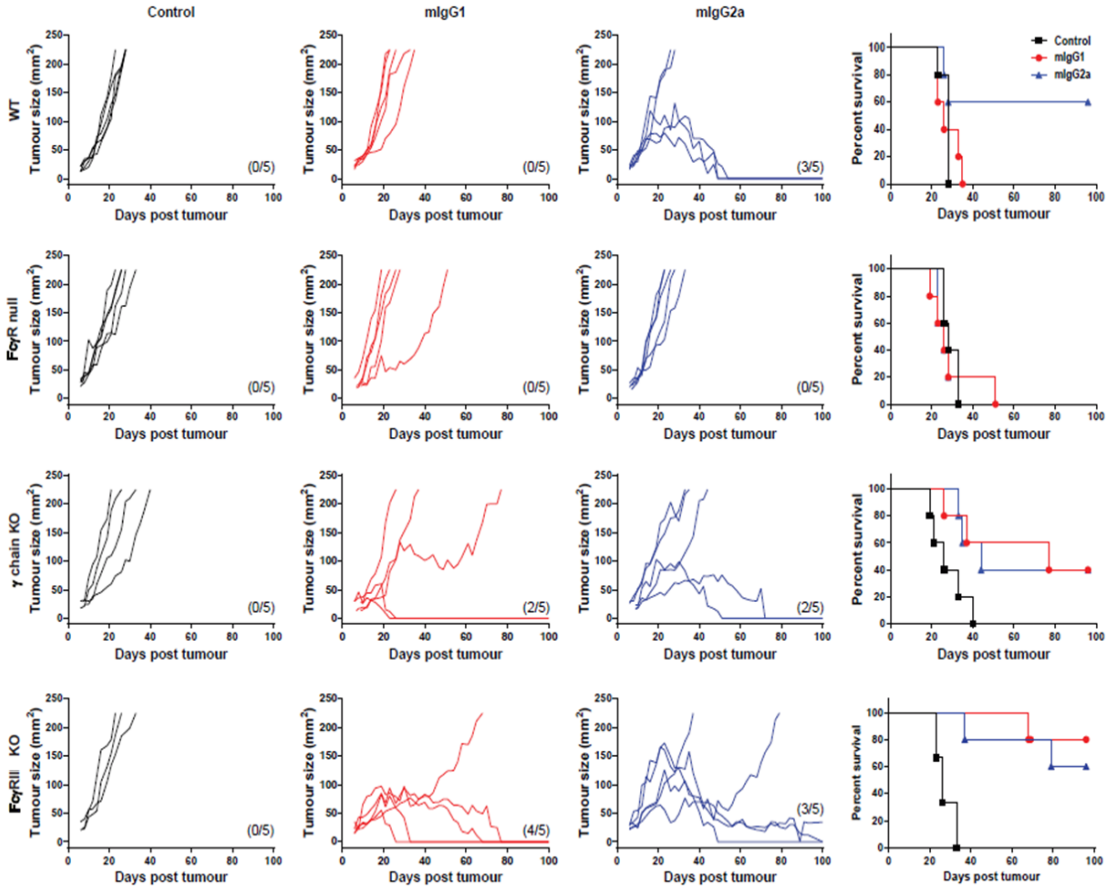

Figure 48:The primary mechanism of anti-4-1BB mAb therapy in solid tumours is dependent on antibody isotype and FcγR availability. Groups of WT, FcγR null mice (γ chain KO x FcγRII KO), γ chain KO, or FcγRII KO BALB/c mice were challenged with 5 x 10^4 CT26 cells s.c on day 0. Anti-4-1BB mIgG1 (mIgG1) or mIgG2a (mIgG2a) were given to mice i.v when tumour was palpable, then another 3 doses of antibody were given i.p every other day (200 µg total). Tumour growth was monitored and mice culled when mean tumour area exceeded 225 mm^2. Data are expressed as tumour area (mm^2) on the days after tumour challenge as indicated, each line represents an individual mouse. Control=non-treated, mIgG1= anti-4-1BB mIgG1 treated, mIgG2a= anti-4-1BB mIgG2a treated. Panels on the right show percentage survival to the humane end-point. Data represents examples of at least 2 experiments where n = 5 mice per group.

5.2.5 Optimising anti-4-1BB activity by combination of mIgG1 and mIgG2a isotype

Having demonstrated that anti-4-1BB mAb can deliver therapeutic responses through two mechanisms of action with differing FcγR requirements we sought to determine if we could combine both mechanisms to better therapeutic effect. We began by testing whether altered scheduling could promote therapeutic activity (Figure 49a). We found that injecting mIgG2a followed by mIgG1 showed promising therapeutic activity (Figure 49b, c). In comparison to anti-4-1BB mIgG2a treatment, mIgG2a-mIgG1 scheduled

therapy reduced the average tumour size from ~100 mm^2 to ~50 mm^2 (Figure 49b). Importantly, there are more tumour free mice in the mIgG2a-mIgG1 scheduled treatment group than anti-4-1BB mIgG2a treated group by day 100 (4/5 tumour free vs 3/5 tumour free) (Figure 49c). These results suggest that there is the potential to improve anti-4-1BB mAb efficacy by combining different isotypes of anti-4-1BB mAb. Using anti-4-1BB mAb mIgG2a to delete Treg cells in the first instance and then activating CD8 T cells with the mIgG1 isotype combined to substantially inhibit tumour growth.

(a)

	Tumour Palpable Day 0	Tumour Palpable Day 2	Tumour Palpable Day 4	Tumour Palpable Day 6
Anti-4-1BB mIg2a	50µg mIgG2a i.v	50µg mIgG2a i.p	50µg mIgG2a i.p	50µg mIgG2a i.p
mIgG2-mIgG1 scheduled	50µg mIg2a i.v	50µg mIg2a i.p	50µg mIgG1 i.p	50µg mIgG1 i.p

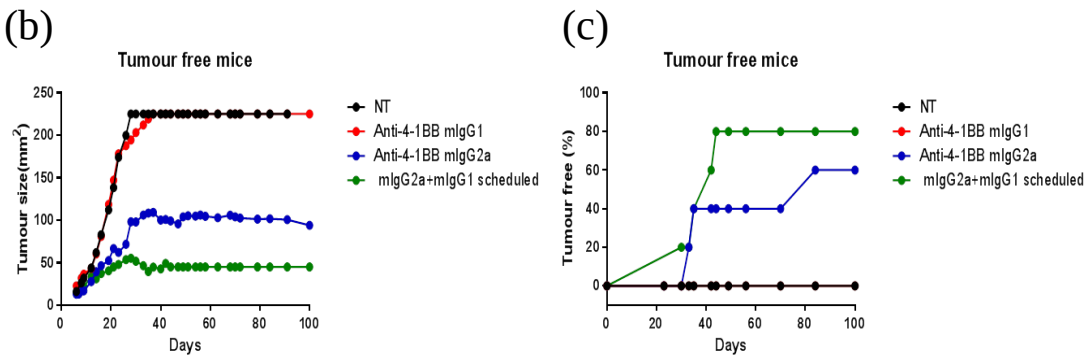

Figure 49: Combination of anti-4-1BB mIgG1 and mIg2a. BALB/c females were inoculated with $5x10^4$ CT26 cells by on day 0. Anti-4-1BB mIgG1 or mIgG2a were given as shown in (a.), NT=non-treated, mIgG1=LOB12.0 mIgG1 and mIgG2a = LOB12.0 mIgG2a. (b) Average tumour size until day 100 of non-treated, mIgG2a and mIgG2a-mIgG1 scheduled treatment BALB/c. (c) Percentage of tumour free mice of non-treated, mIgG2a and mIgG2a-mIgG1 scheduled treated BALB/c. n=4-5.

5.2.6 Evaluated therapeutic potential of using TLR agonist with anti-4-1BB mIgG2a

Having established that the anti-tumour activity of anti-4-1BB is dependent on the profile of FcγR in the CT26 colorectal model, next we attempted to enhance the therapeutic activity of the mIgG2a isotype through augmentation of its depleting activity by combining this mAb with poly(I:C) as we have done for Ritm2a (see chapter 4.2.1 page 85). We have already demonstrated that poly(I:C) stimulation is able to increase the FcγR activatory to inhibitory ratio on splenic and peritoneal macrophages (Figure 30,31). Although we found that anti-4-1BB mIgG2a alone is enough to prevent the majority of mice succumbing to tumour, the response is relatively slow with only 1/5 mouse completely regressed by day 50 (Figure 50b, c). In this tumour model combining poly(I:C) with anti-4-1BB mIgG2a treatment markedly changed the kinetics of tumour growth with 4/5 mice showing tumour regression by day 50 (Figure 50b). This was supported by the finding that before day 50, the average size of tumour in the combination treated mice was smaller than that with anti-4-1BB alone (Figure 50c). Interestingly, one mouse receiving poly(I:C) alone showed complete regression of its tumour. This may be due to other non-antibody mediated anti-tumour effects of poly(I:C) itself through the direct activation of immune cells, such as macrophages, NK and DC [108] [109]. These other potential mechanisms will be the subject of future investigations.

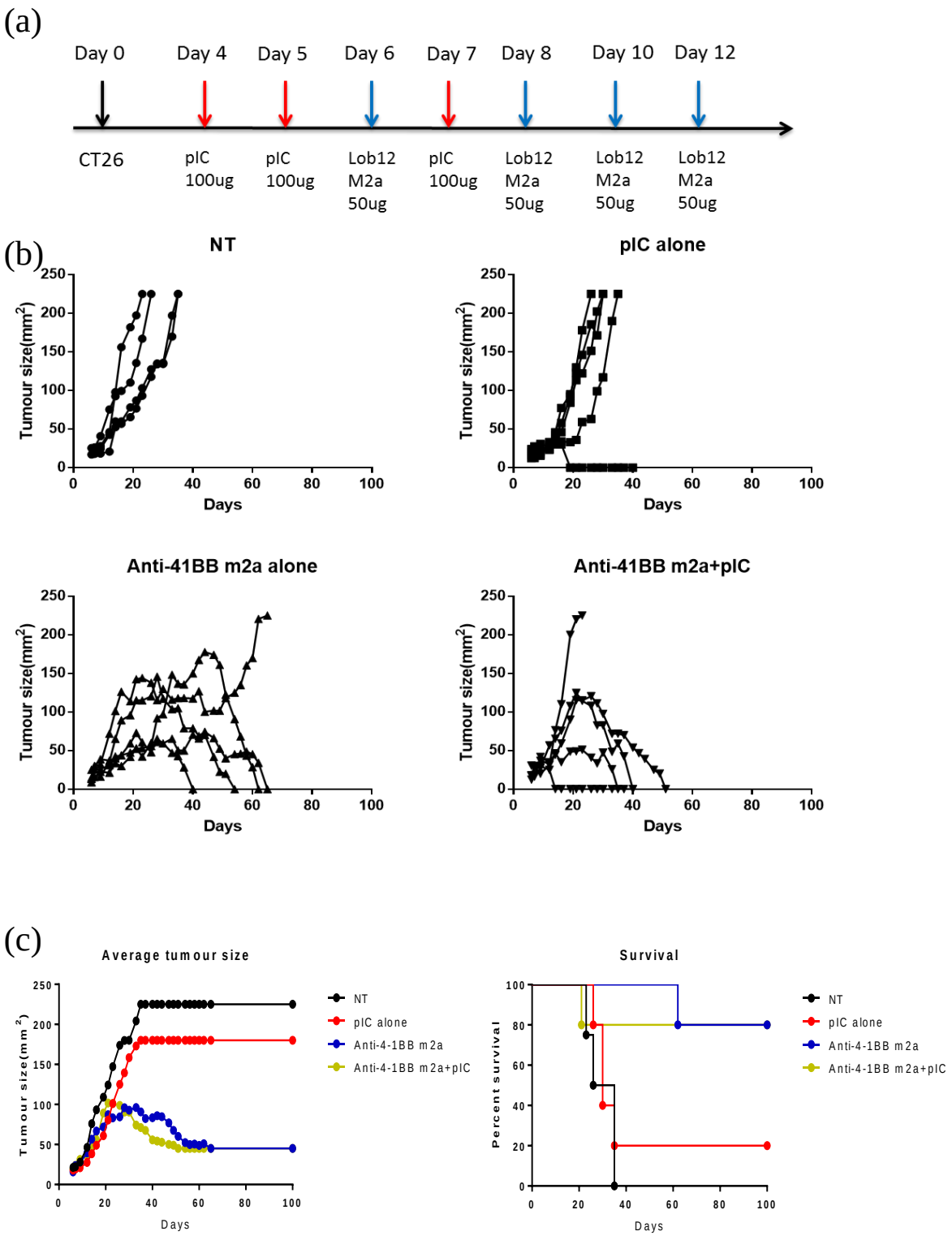

Figure 50: Poly(I:C) enhanced anti-4-1BB mIgG2a efficacy in the CT26 tumour model. (a) Experimental plan, $5x10^4$ CT26 cells were given s.c to WT BALB/c on day 0. 100 µg poly(I:C) (pIC) was administered to mice on day 4, 5 and 7 i.p. Anti-4-1BB mIgG2a antibody was given to mice i.v on day 6, and i.p on day 8, 10, 12. In total, we gave 200 µg. Tumours were monitored by calliper 3 times per week until day 100 and growth plotted. (b) CT26 tumour growth kinetics until day 100. (c) Average tumour size and survival curve. (n=5)

5.3 Discussion

It has been well document that anti-TNFR superfamily mAb require efficient cross-linking to induce their anti-tumour immunity and that for most mAb this is best provided by inhibitory FcγR engagement [189, 270]. However, recent research has demonstrated that mAb targeting CTLA-4, OX40 and GITR are able to enhance anti-tumour activity through intra-tumoural Treg depletion [272, 274]. Thus, the therapeutic mechanism of anti-TNFR superfamily mAb are still controversial. Here we first investigate the mechanism of action of LOB12.0, a mAb targeting the TNFR superfamily molecule 4-1BB, in the setting of solid tumours.

We found the therapeutic activity of anti-4-1BB mAb is dependent on mAb isotype and further, their affinity to FcγRs. We investigated three solid tumour settings and in all found that anti-4-1BB mIgG2a, with high affinity for activitory FcγRs evoked strong anti-tumour activity (Figure 44). In contrast, anti-4-1BB mIgG1 which preferentially binds to inhibitory FcγRs induced poor anti-tumour immunity (Figure 44). These results are in contrast to our previous data that anti-4-1BB mIgG1 is more potent than mIgG2a on activating CD8 T cells in vitro (Figure 43) and in vivo (Figure 44). Our data suggested this may be because anti-4-1BB mIgG2a stops tumour progression via an alternative mechanism from agonism, that is deletion of intra-tumoural Treg cells (Figure 47) whilst mIgG1 isotype was unable to delete intra-tumoural Treg cells in same setting (Figure 47). Importantly, pre-treated mice with CD8+ T cells deletion mAbs YTS169 strongly reduced anti-4-1BB mIg2a activity (Figure 45). This demonstrates that depleting Treg cells is not enough to stop tumour growth, stimulating CD8+ T cells is crucial for therapeutic activity of anti-4-1BB mAb. In addition, we found that the activity of both anti-4-1BB mIgG1 and mIgG2a was retained in γ chain knock out mice (Figure 48), suggested that anti-4-1BB mAb mediated anti-tumour activity through two mechanisms. One is agonistic activity via activating CD8 T cells, another one is deleting intra-tumoural Treg cells. Consistent with this conclusion, we found that anti-4-1BB mAb completely lost its therapeutic activity in

FcγR null mice (Figure 48). Compared to anti-4-1BB mIgG2a treatment alone, scheduling the injection of anti-4-1BB mIgG2a and mIgG1 (Figure 48a) strongly decreased average tumour size and promoted the percentage of tumour free mice by day 100 (Figure 48b, c). These data demonstrate that it may be possible to use the same mAb specificity to in turn delete suppressive intra-tumoural Treg followed by agonistic activation of CD8 cells and that such a strategy can remarkably supress tumour growth.

In FcγRII knock out mice anti-4-1BB mIgG1 gained activity through augmented depletion of intra-tumoural Treg cells (Figure 47,48). Further, both anti-4-1BB mIgG1 and anti-4-1BB mIgG2a were able to prevent tumour progression and cure a proportion of mice in FcγRII knock out setting (Figure 48). This implies that there is potential to mediate anti-4-1BB therapeutic activity through manipulation of FcγR expression. In the previous chapter, we showed that the TLR3 agonist poly(I:C) is able to promote activatory FcγR expression on splenic and peritoneal macrophages (Figure 30). In attempt to enhance anti-tumour activity, we combined poly(I:C) with anti-4-1BB mIgG2a therapy. Although combination with poly(I:C) didn't improve overall survival at day 100, it did change the kinetics and extent of tumour growth. In the combination therapy group, 4/5 mice were completely regressed by day 50 compared to 1/5 in those receiving mAb alone (Figure 50b, c). Interestingly, one mouse from the poly(I:C) monotherapy group regressed at day 20 (Figure 50b), demonstrating that the poly(I:C) itself has some anti-tumour activity. Thus, further work is required to determine whether combination effects observed were synergistic or additive.

Chapter VI Discussion

6.1 Poly(I:C) stimulation skew BMDMs into M1 like phenotype in vitro

The A:I ratio of FcγRs on macrophages has been shown correlate to therapeutic efficacy of direct targeting mAb [160, 198, 199]. In this project, we attempted to polarize macrophages to a pro-inflammatory phenotype possessing a higher FcγRs A:I ratio. We hypothesised that with this approach we could improve the therapeutic activity of direct targeting mAb.

We have characterized the changes in murine macrophage phenotype and function in response to stimulation by different reagents; the classic M1 agents, LPS/IFNγ, classic anti-inflammatory cytokines IL4/13 and different TLR agonists, TLR3 agonist poly(I:C), TLR7 agonist R848 and TLR9 agonist CpG. Microscopy images showed that all of these TLR agonists are able to polarize macrophages to an M1-like phenotype that is defined by cell clumping and a rounded morphology (Figure 11) [235]. IL4/13 treated macrophages looked different, they formed spindle-like structures which is typical and indicative of M2 macrophages (Figure 11) [235]. We then investigated the function of these activated BMDMs. We found that LPS/IFNγ, R848 and poly(I:C) stimulation greatly increased NO release from BMDM whilst CpG stimulation only had a slight impact (Figure 12a). In contrast, only the classic anti-inflammatory skewing cytokine combination of IL4/13 augmented arginase activity in BMDM (Figure 12b). These results suggest that TLR agonists poly(I:C), R848 and CpG reprogramme BMDM to a pro-inflammatory phenotype in vitro.

We also observed that the FcγR expression pattern on BMDM was changed along with polarization. LPS/IFNγ, poly(I:C), R848 and CpG stimulation strongly increased both gene and surface expression of activatory FcγRI and IV on BMDM (Figure 15,16). IL4/13 in contrast slightly increased the level of FcγRII mRNA and strongly promoted FcγRII

protein expression on the BMDM plasma membrane (Figure 15,16). Additionally, LPS/IFNγ, poly(I:C) or R848 stimulation inhibited the expression of FcγRII on BMDM at the mRNA level (Figure 15,16), however this didn't alter the expression of FcγRII on BMDM surface (Figure 15,16). This suggests that polarization with these reagents may change FcγR expression through changes in recycling as well as transcriptionally. Further experiments will be required to confirm this hypothesis. It is notable that LPS/IFNγ and poly(I:C) activation also increased the expression of CD86 on BMDM (Figure 13). This suggests that LPS/IFNγ and poly(I:C) stimulation may improve BMDM antigen presentation function [287]. Activation by IL4/13, R848 and CPG moderately increase the expression of the mannose receptor (CD206) on BMDM (Figure 13), suggesting that these reagents may augment macrophage mediated pathogen and viral defence. Apart from CD86 and CD206, we also investigated other well documented macrophage phenotype marker such as Dendritic cell-specific ICAM-3–grabbing nonintegrin (DC-SIGN) [288]. Although, the expression of DC-SIGN altered with TLR agonist stimulation (Data not shown), these changes were not consistent with published literature. This implies that certain macrophage phenotypic markers such as DC-SIGN, which works quite well in human may not be suited for use in mouse models and therefore that interpretation and extrapolation between systems needs to be carefully considered. Our in vitro phagocytosis results showed that stimulated by LPS/IFNγ and poly(I:C) improved B cell depletion mediated by macrophages (Figure 20b). Taken together, these in vitro data suggest that M1 and M2 represent two distinct form of macrophages, however M1 and M2 macrophages are not opposite to each other, some phenotypes may share the phenotypic marker and function from both M1 and M2 macrophages (Figure 51). For example, BMDMs stimulated with R848 (Figure19) possessed some M1 function such as enhancing NO releasing (Figure 12a) and increasing FcγR expression (Figure 17), but not as good as the true M1 phenotype. However, they didn't promote M1 marker CD86 expression (Figure 13) and phagocytosis

(Figure 20b), instead they enhanced the expression of some M2 markers such as CD206 (Figure 13).

To date, murine M1 and M2 macrophages have been well documented with some papers suggesting that M1 and M2 are two distinct types of macrophage that are opposite to each other in terms of activation state and function [289]. Our in vitro data supports the contention that M1 and M2 phenotypes may represent two extreme forms of macrophages, with a spectrum of differential phenotypes of macrophages sitting between these 'classic' M1 and M2 macrophage activation states. These other, different macrophage phenotypes may share markers and functions from either M1, M2 or a combination of both of them reflecting a spectrum of activation states (Figure 51). BMDM polarized by poly(I:C) exhibited a phenotype that is almost identical to classically activated M1 macrophages, which is characterised by increased iNOS release, CD86 expression, activatory FcγRI and IV expression and enhanced ADCP. Stimulation by R848 or CPG polarized BMDM into a phenotype close to M1, with increasing iNOS and activatory FcγRI and IV expression although to a lesser extent compared to LPS/IFNγ and poly(I:C). However, these BMDM neither increased the expression of M1 marker CD86 nor enhanced ADCP. At the same time, they increased the expression of the M2 marker CD206. This suggests that these BMDM are subtly different in their activation state as compared to an M1 phenotype. They enhanced expression of CD206, thus they might possess some M2 function. The model we propose is in good agreement with Joachim L Schultze's multi-dimensional model, in which macrophage can be divided into a large number of different activation states in term of their transcriptional profiling [290].

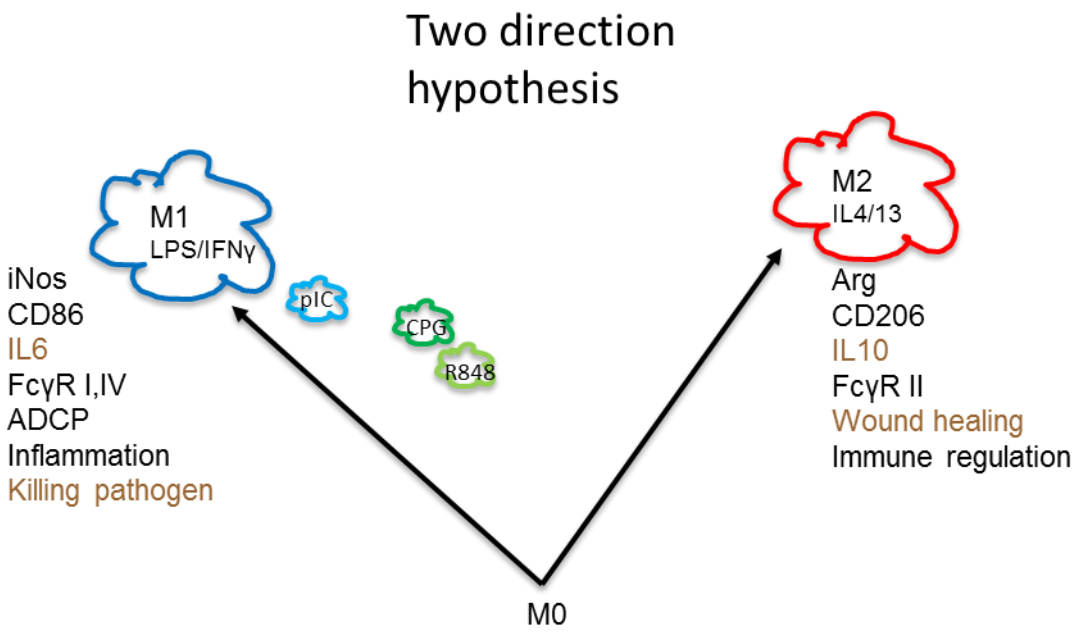

Figure 51: Macrophage M1-M2 activation models. Stimulation with LPS/IFNγ polarized BMDM into an M1 phenotype that is characterised by increased nitric oxide, CD86, IL-6 release and FcγRI and IV expression. IL4/13 stimulation polarized BMDM in M2 phenotype with increasing release of arginase, CD206, IL10 and FcγRII expression. Two models are proposed; the opposite model and two directional model. pIC = BMDM polarized by poly(I:C). CpG BMDM polarized by CPG. R848=BMDM polarized by R848. Brown colour characters= characters that have been documented in the literature, but not been shown in this project. Black colour characters= characters that have been reported in the literature and in this report.

In humans, based on our in vitro data [291] ,the TLR3 agonists poly(I:C) is a poor M1 skewer for human MDM in contrast to murine BMDM. To date little data on the antitumor effects of poly(I:C) in humans have been reported [108]. One explanation for this may be that poly(I:C) is rapidly inactivated in human systems [108, 292], stable derivatives of poly I:C, for example Poly-ICLC (Hiltinol) have therefore been developed to overcome this issue [108]. Poly-ICLC is stabilized with poly-lysine, and currently Poly-ICLC associated with DCs and radiation therapy are being studied in phase II trials for solid tumours [292]. Whether Poly-ICLC is a potent adjuvant for mAb therapy has not been well studied, therefore further investigation to understand the potential of Poly-ICLC on human MDM polarization is required.

6.2 Poly(I:C) enhances Ritm2a activity in vivo via polarization of macrophage into an M1-like phenotype

In light of our in vitro BMDM findings, we evaluated the therapeutic potential of TLR3 agonist poly(I:C), TLR 4 agonist LPS and TLR7/8 agonist R848 in combination with direct target antibodies in vivo. In our adoptive transfer model, we found that poly(I:C) stimulation significantly increased the depleting abilities of a murine version of rituximab, Ritm2a (Figure 21). Unexpectedly, LPS stimulation didn't improve rituximab activity in this model (Figure 21). The enhancement in depletion observed was not due to the proliferation of macrophages in the spleen (Figure 25b). Indeed, we observed the infiltration of Ly6C+ monocytes in the spleen after poly(I:C) stimulation (Figure 25b). Using the CCR2 KO mouse, which lack circulating monocytes, we showed that Ritm2a can efficiently delete B cells in both WT and CCR2 KO mice (Figure 26c), suggesting that increases in infiltrating CD11b+Ly6C+ monocytes in response to poly(I:C) administration were not responsible for the depletion observed in our human CD20 Tg B cell adoptive transfer model. Recently, it was demonstrated that neutrophils were required for the therapeutic efficacy of mAb in a short-term subcutaneous mouse tumour model [203]. However, our data showed opposite results. We found that depletion of neutrophils by the Ly6G specific antibody 1A8 did not alter B cell depletion in the spleen (Figure 28). The distinct observations could be due to several reasons including differences in mouse models and specificity of the direct targeting mAb used. Further to this and in partial support of our observations, Markus Biburger and colleagues used a fluorescently labelled liposome model to demonstrate that Ly6C- monocytes were superior to Ly6G+ neutrophils in their capacity to take up fluorescently labelled liposomes in the peripheral blood [202]. At the same time, by using 1A8, a Ly6G specific antibody and MC21, a CCR2 specific antibody, they demonstrated that depleting neutrophils or CCR2+Ly6C+ monocytes did not affect CD20-specific IgG2a antibody

induced B cell killing in peripheral blood [202]. To address whether there was redundancy between monocytes and neutrophils activity that might affect rituximab efficacy, we depleted neutrophils in CCR2 KO mice. We showed that in mice devoid of both populations, rituximab was still able to mediate B cell depletion (Figure 29). Taken together, we suggest that Ly6C+ monocytes and Ly6G+ neutrophils were dispensable for rituximab activity in our B cell depletion model. To date, it is still controversial as to which is the predominant macrophage population mediating ADCP. Using intravital microscopy, Fabricio Montalvao et al demonstrated that kupffer cells (tissue resident macrophages of the liver) mediated ADCP is the primary mechanism for anti-CD20 therapy [200]. In our adoptive transfer model, very few HuCD20 Tg target B cells were observed in the mouse liver (data now shown). This may due to the fact that in our transfer model relatively few targets are transferred and/or that kupffer cells are very efficient phagocytes and are simply too good at clearing circulating cells that transferred target cells can't be seen to readily accumulate. Thus, determining the relative role of kupffer cells and other tissue macrophage populations in our depletion model will be a priority in the future.

Having established the likely role of macrophages as effectors in our depletion model, we sought to confirm whether poly(I:C) led to changes in macrophage FcγR expression in vivo. Our results showed that poly(I:C) stimulation led to significantly increased expression of activatory FcγRI and IV on splenic and peritoneal cavity F4/80+ macrophages (Figure 30) suggesting that these changes may play a role in the enhanced depletion observed in combination with anti-CD20 mAb. These changes in individual FcγR expression can be converted to an A:I ratio of FcγRs and when this is done, it can be seen that Poly(I:C) increased this ratio on splenic and peritoneal cavity F4/80+ macrophages (Figure 30) [293]. These results are consistent with our in vitro polarization results (Figure 17,18). Interestingly, stimulation with poly(I:C) didn't alter FcγR expression on alveolar macrophage (Figure 30,31). Published literature suggests that unlike peritoneal macrophages, stimulation through TLR3 on alveolar macrophage

doesn't induce the release of type I IFN-β that is essential for STAT1 activation [257]. STAT1 signalling has been shown to be important in mediating expression of activatory FcγRs, particularly FcγRI[258]. It is notable that poly(I:C) also promoted 1A8 mediated neutrophil depletion (Figure 27). This suggests that 1A8 also depletes neutrophils in an FcγR dependent manner and potentially through the same cell population. Poly(I:C) stimulation markedly increased the A:I ratio of FcγR on F4/80+ macrophages resulting in enhancement of the 1A8 mediated neutrophil depletion. Unexpectedly, given our in vitro results LPS did not significantly improve rituximab mediated B cell depletion. We observed that in vivo LPS stimulation induced a strong inflammatory response that is characterised by infiltration of CD11b+Ly6G+ neutrophils (Figure 22,25) and increased expression of CD11b (Figure 22) on macrophages, and we postulate that the highly inflammatory microenvironment created may actually inhibit macrophage function and further investigation will be required in future. Similar responses were not observed in R848 (Figure 23) or poly(I:C) (Figure 24) treated mice.

6.3 In a pre-clinical lymphoma model, STING ligand DMXAA, but not poly(I:C) promotes anti-CD20 mAb efficacy

To validate whether our in vivo experimental observations can be recapitulated in a tumour model, we repeated our adoptive transfer experiments in mice bearing the syngeneic BCL_1 lymphoma. We found that rituximab mediated B cell depletion could be completely supressed as early as day 10 after BCL1 inoculation (Figure 33). This suppression could be partially overcome by increasing the rituximab dose from 10 µg to 50 µg (Figure 33). It's interesting that in contrast the type II anti-CD20 mAb, Bhh2 was not inhibited in the BCL_1 model (Figure 33). One fundamental difference between type I and type II anti-CD20 mAb is antigenic modulation, CD20 expressed on target B cells is lost rapidly after binding with type I anti-CD20 mAb, while type II anti-CD20 mAb are not

affected by antigenic modulation in vitro [161]. Thus, we speculated that the tumour environment may supress anti-CD20 activity via enhanced antigenic modulation. To investigate whether tumour microenvironment affected antigenic modulation we looked at HuCD20 expression on target B cells in our adoptive transfer model, 18 hours after inject with mAb. We found that HuCD20 expression had decreased greatly after 18 hours (Figure 34), however levels remaining on the target B cells of rituximab or Bhh2 treated BCL_1 mice were comparable (Figure 34). This implies that the tumour microenvironment may not alter target CD20 expression. Type II anti-CD20 mAb Bhh2 outperformed the type I anti-CD20 Rituximab in the BCL_1 model, and this may simply reflect the fact that type II anti-CD20 mAb have been demonstrated to be more potent than type I mAb in vivo [161]. Type II anti-CD20 mAb are also able to induced an FcγR independent, homotypic cell adhesion dependent apoptosis (programmed cell death) in B-cell lymphomas [153]. It's possible that both type I and type II anti-CD20 mAb induced ADCP are inhibited in the context of BCL_1 lymphoma, however type II induced programmed cell death may work to compensate for this inhibition and help type II mAb delete target B cells. Thus, further work to investigate the potential role of programmed cell death in depleting normal B cells in the BCL_1 model would be interesting. Indeed, rituximab mediated B cell depletion is a rapid process [200] and it is possible that the tumour microenvironment may alter antigenic modulation at earlier time points than those investigated here (18 hours). A full kinetic analysis of HuCD20 expression on target B cells between 0 to 18 hours after mAb injection is needed to confirm our results suggesting that modulation does not contribute to the poor activity of type I mAb in the presence of lymphoma.

It was perhaps surprising that target HuCD20 expression also dropped in type II anti-CD20 mAb Bhh22 treated WT mice. This observation was not consistent with the in vitro data which showed that treatment with type II anti-CD20 mAb didn't induce target CD20 internalization [161]. Using non-depleting, gamma chain KO mice, we found that majority

of target HuCD20 was retained after administration of type II anti-CD20 mAb B2 (Figure 34). In marked contrast HuCD20 expression was still lost in rituximab treated gamma chain KO mice. Thus, we propose that type II anti-CD20 mAb Bhh2 reduce target antigen levels primarily via activatory FcγR dependent antigenic shaving [160],to lesser extent by inhibitory FcγRII enhanced antigenic modulation [167] in vivo.

In an attempt to restore rituximab B cell depletion function in the BCL_1 model, we first combined IRF3 activator poly(I:C) with rituximab. Although poly(I:C) was able to improve rituximab activity in WT tumour free mice (Figure 21), it failed to restore rituximab activity in the presence of lymphoma BCL_1 (Figure 35). Our phenotyping data suggested that poly(I:C) alone was not able to restore macrophage FcγR activatory to inhibitory ratio in lymphoma (Figure 40). Then we used poly(I:C) in combination with inhibitors that we hope to supress macrophages polarization towards a TAM phenotype, these inhibitors include IL10 receptor blocking antibody 1B1.3A, JAK3 inhibitor CP-690550 and mTOR inhibitor rapamycin. None of these combinations was able to recover rituximab function in the BCL_1 model (Figure 36). Finally, we tried another IRF3 stimulator, the STING ligand DMXAA, as an adjuvant to rituximab in the BCL_1 model. In vitro phenotyping data demonstrated DMXAA was as good as poly(I:C) at enhancing activatory FcγR expression (Figure 37). In the BCL_1 model, we found that DMXAA alone was enough to restore rituximab function (Figure 38). Using gamma chain KO mice, we showed that this response was FcγR dependent (Figure 38). We then phenotyped macrophages from BCL_1 spleens, and found that these TAMs expressed low levels of activatory FcγR, especially activatory FcγRI (Figure 39). Stimulation with DMXAA completely reversed suppression of the activatory FcγR expression back to levels observed in WT mice (Figure 39).

It was striking that DMXAA combined with anti-mCD20 mAb 18B12 eradicated tumour growth completely (Figure 41a). In combination treatment groups, 5/5 mice showed complete responses with all mice effectively ‘cured’ (survival beyond day 100) (Figure

41a). Whilst in the monotherapy groups, all mice were terminated between day 35 and day 38 (Figure 41a). This suggested that the combination response was synergistic rather than simply an additive effect. Seng-Ryong Woo et al found that the STING pathway was required for DC activation which then primed CD8+ T cells and inhibited tumour growth [186]. Thus, to understand the mechanism of action of DMXAA in the BCL_1 model, we re-challenged surviving mice BCL_1. Notably, the surviving mice were not protected and therefore had not produced a long term protective immune response (Figure 41b). It has been reported that DMXAA eradicate subcutaneous 344SQ-ELuc tumours via disrupting vascularization [127]. However, this effect was not observed in our lymphoma model. Thus, we would suggest that DMXAA plus anti-CD20 mAb eradicates tumour through antibody mediated humoral immunity. To verify this contention, my colleague L.N.Dahal repeated these therapy experiments in mice depleted of CD8 T cells and the same curative responses were observed.

Interestingly, both poly(I:C) and DMXAA activate IRF3 through the TBK-pathway, however they stimulate TBK-1 in a different manner [6, 125]. Poly(I:C) stimulation activates TIR-domain-containing adapter-inducing interferon-β (TRIF) adapter which in turn phosphorylates and activates IRF3 [6]. Whilst DMXAA works as a scaffold that brings TBK1 adapter to IRF3, therefore enhancing IRF3 phosphorylation [6, 125]. The relative impact of these differential activation pathways needs further investigation in order to better understand why one of the reagents is effective and the other not. Importantly though, our data does demonstrate that DMXAA is more potent than poly(I:C) at augmenting the macrophage FcγR activatory to inhibitory ratio in a tumour setting BCL_1 (Figure 39,40). So, although it is still unclear why poly(I:C) plus TAM signalling inhibitors can't recover rituximab function in the BCL_1 model it is clear that potent IRF3 activators such as the STING ligand DMXAA are able to enhance mAb activity in lymphoma BCL_1. Although our DMXAA data is promising this reagent is toxic to mice. In our experiments, high doses (400 µg for BALB/C and 800 µg for C57BL/6) DMXAA was

lethally toxic. This may be because STING ligands can also activate NFκB through the TRAF6-TAK1 pathway [130] which induces strong inflammation and tissue damage. Thus, we would propose to design small molecule adjuvants specifically targeting and restricted to the TBK-IRF3 pathway which could improve rituximab activity with less toxicity, thus bringing therapeutic benefit to poorly responding rituximab patients.

Despite the STING agonist DMXAA shows impressive effects in a lymphoma model, it failed in Phase III clinical trial [294]. Subsequent studies found that DMXAA is a ligand for mouse STING, and therefore cannot activate the human STING pathway [295]. A series of synthetic CDN derivatives have since been generated and demonstrated ability to activate all five human STING alleles [296]. These synthetic CDN derivatives combined with radiation therapy show promising effects against pancreatic tumours [296]. Our data shows that synthetic CDN derivatives can skew human MDMs into M1-like phenotypes, and subsequently enhances MDM ability to mediate ADCP in vitro [291]. Next, our group plan to evaluate the activity of these synthetic CDN derivatives in vivo by using a novel human STING KI mouse. Firstly, we will test the toxicity of these synthetic CDN derivatives. Then, we will compare the activity of human STING agonists (synthetic CDN derivatives) to murine STING agonist DMXAA in terms of myeloid cell infiltration, FcγR expression and type I IFN release. Lastly, we will inoculate STING KI mice with suitable tumour, and investigate the potency of synthetic CDN derivatives as adjuvants of anti-CD20 mAb.

Currently, it's still controversial as to which populations are the predominate effectors for antibody-dependent immunotherapy response in humans. In this project, we focussed on macrophages in the BCL_1 tumour model, and this is in agreement with published literatures that demonstrated macrophage mediated ADCP is the dominate mechanism for rituximab therapy [161, 201, 210]. Recent research has demonstrated the key effector cells mediating direct targeting mAb response was determined by tumour location [208], consistent with our results, this literature suggested that for the systemic tumour, such as

BCL_1, the prominent effectors are indeed macrophages although the contributions of monocyte derived versus tissue resident macrophages to TAM populations is still to be determined.

To date, few studies demonstrating the reprogramming TAMs have been published. One group found that the scavenger receptor MARCO is expressed on TAMs and that anti-MACRO mAb ED31 can reprogram TAMs to an M1-like phenotype and improve anti-CTLA4 activity against melanoma and colon carcinoma [297]. However, a strategy using mAb to polarize macrophages has limitations. Firstly, it's cost ineffective. Secondly, mAb binding to the macrophage surface may activate M2 macrophage and induce IL10 production via cross linking of FcγRs [298]. Despite success in pre-clinical studies, directly translation from mouse tumour models to human cancers is difficult, at least in part, due to the dissimilarities in surface markers, receptors, and the extreme heterogeneity of human macrophages [299]. A majority of clinical trials currently are focussed on altering the tumour environment to reduce TAM number. In a phase II trial, neutralising anti-IL-6 antibody siltuximab effectively inhibited TAM infiltration in patients with ovarian carcinoma [300]. Additionally, in a phase I trial, anti-MCSF (CSF-1) mAb RG7155 showed promising anti-tumour activity via deletion of TAMS in Diffuse-Type Giant Cell Tumour [301]. A problem with these strategies is that they are effectively incompatible with antibody therapy where macrophages are the desired effector cell population. There are a few trials evaluating the adjuvant effect of macrophage polarization for mAb therapy. It has been documented that patients with relapsed indolent NHL[302] and bulky indolent NHL[303] are partially resistant to rituximab monotherapy. In this project, we recapitulated the rituximab resistance in a mouse lymphoma model, and found that the resistance could be overcome by macrophage polarization through DXMAA. In combination with our now published human MDM polarization data that human STING agonist synthetic CDN derivatives can efficiently polarize MDM to M1-like macrophages with enhance phagocytotic activity [291], we

suggested that macrophage polarization may help patients with indolent NHL to overcome rituximab resistance. In addition, macrophage polarization strategies may also apply to human cancers that contain large numbers of infiltrating TAM, for example breast cancer. As TAM play multiple roles in breast cancer development, include: tumour growth [57], metastasis[98] and angiogenesis[91], therefore reagents that polarize TAMs to M1 like macrophages could be an ideal adjuvant for mAb therapy against HER2+ breast cancer.

6.4 Anti-4-1BB mAb LOB12.0 eradicates tumours through dual mechanisms

Our focus then switched to the anti-TNFR superfamily molecule 4-1BB mAb LOB12.0 which is able to activate CD8+ T cell to induce anti-tumour immunity. Our data demonstrated that anti-4-1BB mIgG1 was more potent than anti-4-1BB mIgG2a at enhancing activity of CD8+ T cells in vitro (Figure 43) and in vivo (Figure 44) through enhanced FcγRII dependent agonistic function. However, in three different solid tumour therapy models, anti-4-1BB mIgG2a was superior to anti-4-1BB mIgG1 at inhibiting tumour growth (Figure 44). About 80% of mice completely regressed after anti-4-1BB mIgG2a treatment compared to only ~20% survival after anti-4-1BB mIgG1 (Figure 44). This result was opposite to the CD8+ T cell agonism data, implying that an alternative mechanism was required for anti-4-1BB mIgG2a to supress tumour growth. Recently, it has been described that mAb targeting TNFR superfamily molecules such as GITR [274] and OX40 [275] inhibit tumour progression through deletion of intratumoral Treg cells. Thus, we assessed 4-1BB expression on tumour infiltrating T lymphocytes and splenocytes. We found that 4-1BB was highly expressed on CD4+Foxp3+ Treg cells in tumours (Figure 46). Furthermore, administration of anti-4-1BB mIgG2a, but not mIgG1 efficiently deleted intratumoral Treg cells in an activatory FcγR dependent manner

(Figure 47). These data suggest that in some settings the direct targeting and deletion of Treg cells is more important than co-stimulatory activity to eradicate tumours. This could explain why anti-4-1BB mIgG2a shows stronger anti-tumour activity in our solid tumour models (Figure 44). Published literature has demonstrated that mAb mediated, FcγR dependent Treg deletion was also observed in Ipilimumab treated melanoma patients [273]. These results suggest that Treg depletion mechanisms induced by immunomodulatory mAb may not be restricted to mice, but also apply to human supporting the translational potential of our studies.

Notably, the therapeutic activity of anti-4-1BB mIgG2a was maintained in γ chain knock out mice (Figure 48). Deletion of CD8+ T cells by specific mAb before mAb treatment greatly abolished the anti-4-1BB mIgG2a activity (Figure 45). These results demonstrate that the anti-cancer immune responses of anti-4-1BB mIgG2a requires CD8+ T cells. Additionally, neither anti-4-1BB mIgG1 nor anti-4-1BB mIgG2a were able to supress tumour growth in FcγR null mice (Figure 48), implying that FcγR engagement is crtically required for the therapeutic activity of anti-4-1BB mAbs. Our results are consistent with published work that demonstrate cross-linking with FcγR is important for agonistic activity of anti-TNFR superfamily receptor antibodies, such as CD40 [270, 304] and TRAILR2/DR5 [305]. Taken together, we suggest that anti-4-1BB mediated anti-tumour immunity can operate via two separate mechanisms, agonism through stimulating CD8+ T cells, and Treg cell depletion by specifically targeting tumour infiltrating Treg cells. FcγRs are required for both mechanisms, albeit differentially and thus play a central role in anti-4-1BB mediated anti-tumour responses.

6.5 Poly(I:C) can be used as an adjuvant to augment LOB12.0 activity

Based on our anti-4-1BB mAb characterisation data, we showed that the anti-4-1BB mAb activity can be manipulated through FcγR availablity. For example, anti-4-1BB mIgG1

was enhanced for intratumoral Treg depleting activity in FcγRII KO mice (Figure 47), and showed comparable anti-tumour activity to anti-4-1BB mIgG2a in this setting (Figure 48). Compared to anti-4-1BB mIgG2a that binds to activatory FcγRI and FcγRIV with high affinity, mIgG1 isotype does not bind to FcγRI, FcγRIV, (Appendices figure 1). We have demonstrated that poly(I:C) augments ADCP predominantly by promoting FcγRI and FcγRIV expression on macrophages in vitro (Figure 17) and in vivo (Figure 30). Thus, we decided to combine poly(I:C) with anti-4-1BB mIgG2a mAb in an attempt to further enhance depletion and therapeutic efficacy. Our hypothesis was that poly(I:C) treatment would act to increase the A:I ratio of FcγR on tumour associated F4/80+ macrophages which would then be better able to mediate intra-tumoural Treg depletion thereby changing the tumour microenvironment from one that is immunosuppressive to one that is activated. We found that compared to mAb alone, anti-41BB mIgG2a combined with poly(I:C) greatly changed the kinetics of tumour growth. 4/5 mice were completely regressed in the combination group, whilst only 1/5 regressed with anti-4-1BB mIgG2a alone at day 50 (Figure 50b). In addition, between days 20-50, the average tumour size in the combination group was significantly smaller than the monotherapy 4-1BB group (Figure 50c). It was disappointing that compared to the monotherapy LOB12.0 alone, combination with poly(I:C) didn't improve overall survival and this potentially could simply reflect that the LOB12.0 mIgG2a alone was enough to eradicate tumour cells. We will repeat the experiments with reduced dosing LOB12.0 mIgG2a in the future in an attempt to optimise this model.

In this project, we manipulated the FcγR expression on macrophages by polarizing macrophages into pro-inflammatory phenotypes. We showed that IRF3 activator poly(I:C) significantly promote ADCP by increasing A:I ratio of FcγR on macrophages in vitro and in vivo. In a pre-clinical lymphoma model, we found that new class IRF3 activator STING ligand DMXAA greatly enhanced rituximab activity by re-polarizing tumour associated macrophages (Low A:I ratio) into pro-inflammatory phenotypes (High A:I ratio).

Additionally, we demonstrated that in house made anti-4-1BB mAb LOB12.0 supressed tumour growth using two FcγR dependent mechanisms, intratumoral CD8+ T cell stimulation and intratumoral Treg cell deletion. Combination with poly(I:C) showed limited effect on improving anti-4-1BB mAb therapy. Thus, further work such as changing combination strategy and altering injection routes may be required to optimise adjuvant treatment.

References

1. van Furth, R. and Z.A. Cohn, *The origin and kinetics of mononuclear phagocytes.* J Exp Med, 1968. 128(3): p. 415-35.
2. Schulz, C., et al., *A lineage of myeloid cells independent of Myb and hematopoietic stem cells.* Science, 2012. 336(6077): p. 86-90.
3. Mikkelsen, H.B. and L. Thuneberg, *Op/op mice defective in production of functional colony-stimulating factor-1 lack macrophages in muscularis externa of the small intestine.* Cell Tissue Res, 1999. 295(3): p. 485-93.
4. Khazen, W., et al., *Expression of macrophage-selective markers in human and rodent adipocytes.* FEBS Lett, 2005. 579(25): p. 5631-4.
5. Apostolopoulos, V. and I.F. McKenzie, *Role of the mannose receptor in the immune response.* Curr Mol Med, 2001. 1(4): p. 469-74.
6. Kaisho, T. and S. Akira, *Toll-like receptor function and signaling.* J Allergy Clin Immunol, 2006. 117(5): p. 979-87; quiz 988.
7. Kanneganti, T.D., M. Lamkanfi, and G. Nunez, *Intracellular NOD-like receptors in host defense and disease.* Immunity, 2007. 27(4): p. 549-59.
8. Yoneyama, M., et al., *The RNA helicase RIG-I has an essential function in double-stranded RNA-induced innate antiviral responses.* Nat Immunol, 2004. 5(7): p. 730-7.

9. Ezekowitz, R.A., et al., *Uptake of Pneumocystis carinii mediated by the macrophage mannose receptor.* Nature, 1991. 351(6322): p. 155-8.
10. Marodi, L., H.M. Korchak, and R.B. Johnston, Jr., *Mechanisms of host defense against Candida species. I. Phagocytosis by monocytes and monocyte-derived macrophages.* J Immunol, 1991. 146(8): p. 2783-9.
11. Mogensen, T.H., *Pathogen recognition and inflammatory signaling in innate immune defenses.* Clin Microbiol Rev, 2009. 22(2): p. 240-73.
12. Svanborg, C., G. Godaly, and M. Hedlund, *Cytokine responses during mucosal infections: role in disease pathogenesis and host defence.* Curr Opin Microbiol, 1999. 2(1): p. 99-105.
13. Matsukawa, A., et al., *Chemokines and innate immunity.* Rev Immunogenet, 2000. 2(3): p. 339-58.
14. Unanue, E.R., *Antigen-presenting function of the macrophage.* Annu Rev Immunol, 1984. 2: p. 395-428.
15. Murphy, K., et al., *Janeway's immunobiology*. 8th ed. 2012, New York: Garland Science.
16. Flannagan, R.S., V. Jaumouille, and S. Grinstein, *The cell biology of phagocytosis.* Annu Rev Pathol, 2012. 7: p. 61-98.
17. Desjardins, M., et al., *Biogenesis of phagolysosomes proceeds through a sequential series of interactions with the endocytic apparatus.* J Cell Biol, 1994. 124(5): p. 677-88.
18. Vieira, O.V., et al., *Distinct roles of class I and class III phosphatidylinositol 3-kinases in phagosome formation and maturation.* J Cell Biol, 2001. 155(1): p. 19-25.
19. Simonsen, A., et al., *EEA1 links PI(3)K function to Rab5 regulation of endosome fusion.* Nature, 1998. 394(6692): p. 494-8.
20. Aderem, A. and D.M. Underhill, *Mechanisms of phagocytosis in macrophages.* Annu Rev Immunol, 1999. 17: p. 593-623.
21. Turk, B., D. Turk, and V. Turk, *Lysosomal cysteine proteases: more than scavengers.* Biochim Biophys Acta, 2000. 1477(1-2): p. 98-111.
22. Gordon, D.L. and J.L. Rice, *Opsonin-dependent and independent surface phagocytosis of S. aureus proceeds independently of complement and complement receptors.* Immunology, 1988. 64(4): p. 709-14.
23. Borghesi, L. and C. Milcarek, *From B cell to plasma cell: regulation of V(D)J recombination and antibody secretion.* Immunol Res, 2006. 36(1-3): p. 27-32.
24. Woyach, J.A., A.J. Johnson, and J.C. Byrd, *The B-cell receptor signaling pathway as a therapeutic target in CLL.* Blood, 2012. 120(6): p. 1175-84.
25. McHeyzer-Williams, L.J., L.P. Malherbe, and M.G. McHeyzer-Williams, *Helper T cell-regulated B cell immunity.* Curr Top Microbiol Immunol, 2006. 311: p. 59-83.
26. Cruse, J.M. and R.E. Lewis, *Atlas of immunology*. 3rd ed. 2010, Boca Raton, FL: CRC Press/Taylor & Francis. 940 p.
27. Woof, J.M. and D.R. Burton, *Human antibody-Fc receptor interactions illuminated by crystal structures.* Nat Rev Immunol, 2004. 4(2): p. 89-99.
28. Michaelsen, T.E., et al., *The four mouse IgG isotypes differ extensively in bactericidal and opsonophagocytic activity when reacting with the P1.16 epitope on the outer membrane PorA protein of Neisseria meningitidis.* Scand J Immunol, 2004. 59(1): p. 34-9.
29. Gould, H.J., et al., *The biology of IGE and the basis of allergic disease.* Annu Rev Immunol, 2003. 21: p. 579-628.
30. Nimmerjahn, F. and J.V. Ravetch, *Fcγ receptors as regulators of immune responses.* Nat Rev Immunol, 2008. 8(1): p. 34-47.
31. Bruhns, P., *Properties of mouse and human IgG receptors and their contribution to disease models.* Blood, 2012. 119(24): p. 5640-9.
32. Billadeau, D.D. and P.J. Leibson, *ITAMs versus ITIMs: striking a balance during cell regulation.* J Clin Invest, 2002. 109(2): p. 161-8.

33. Hulett, M.D. and P.M. Hogarth, *Molecular basis of Fc receptor function.* Adv Immunol, 1994. 57: p. 1-127.
34. García-García, E. and C. Rosales, *Signal transduction during Fc receptor-mediated phagocytosis.* Journal of Leukocyte Biology, 2002. 72(6): p. 1092-1108.
35. Fitzer-Attas, C.J., et al., *Fcgamma receptor-mediated phagocytosis in macrophages lacking the Src family tyrosine kinases Hck, Fgr, and Lyn.* J Exp Med, 2000. 191(4): p. 669-82.
36. Lennartz, M.R. and E.J. Brown, *Arachidonic acid is essential for IgG Fc receptor-mediated phagocytosis by human monocytes.* The Journal of Immunology, 1991. 147(2): p. 621-6.
37. Indik, Z., et al., *The molecular dissection of Fc gamma receptor mediated phagocytosis.* Blood, 1995. 86(12): p. 4389-4399.
38. Larsen, E.C., et al., *Differential requirement for classic and novel PKC isoforms in respiratory burst and phagocytosis in RAW 264.7 cells.* J Immunol, 2000. 165(5): p. 2809-17.
39. Bolland, S. and J.V. Ravetch, *Spontaneous autoimmune disease in Fc(gamma)RIIB-deficient mice results from strain-specific epistasis.* Immunity, 2000. 13(2): p. 277-85.
40. Schwab, I. and F. Nimmerjahn, *Intravenous immunoglobulin therapy: how does IgG modulate the immune system?* Nat Rev Immunol, 2013. 13(3): p. 176-89.
41. Suzuki, H., Forrest, A.R., van Nimwegen, E., Daub, C.O., Balwierz, P.J., Irvine, K.M., Lassmann, T., Ravasi, T., Hasegawa, Y., de Hoon, M.J., et al; FANTOM Consortium; Riken Omics Science Center., *The transcriptional network that controls growth arrest and differentiation in a human myeloid leukemia cell line.* Nat Genet, 2009. 41(5): p. 553-562.
42. Mantovani, A., et al., *Tumor-associated macrophages and the related myeloid-derived suppressor cells as a paradigm of the diversity of macrophage activation.* Hum Immunol, 2009. 70(5): p. 325-30.
43. Sica, A., et al., *Tumour-associated macrophages are a distinct M2 polarised population promoting tumour progression: potential targets of anti-cancer therapy.* Eur J Cancer, 2006. 42(6): p. 717-27.
44. Mills, C.D., et al., *M-1/M-2 macrophages and the Th1/Th2 paradigm.* J Immunol, 2000. 164(12): p. 6166-73.
45. Martinez, F.O., L. Helming, and S. Gordon, *Alternative Activation of Macrophages: An Immunologic Functional Perspective.* Annual Review of Immunology, 2009. 27(1): p. 451-483.
46. Xu, W., et al., *The role of nitric oxide in cancer.* Cell Res, 2002. 12(5-6): p. 311-20.
47. Fang, F.C., *Perspectives series: host/pathogen interactions. Mechanisms of nitric oxide-related antimicrobial activity.* J Clin Invest, 1997. 99(12): p. 2818-25.
48. Nathan, C., *Inducible nitric oxide synthase: what difference does it make?* The Journal of Clinical Investigation, 1997. 100(10): p. 2417-2423.
49. Scott, D.J., et al., *Lack of inducible nitric oxide synthase promotes intestinal tumorigenesis in the Apc(Min/+) mouse.* Gastroenterology. 121(4): p. 889-899.
50. Jenkins, D.C., et al., *Roles of nitric oxide in tumor growth.* Proc Natl Acad Sci U S A, 1995. 92(10): p. 4392-6.
51. Saraiva, M. and A. O'Garra, *The regulation of IL-10 production by immune cells.* Nat Rev Immunol, 2010. 10(3): p. 170-81.
52. Witte, M.B. and A. Barbul, *Arginine physiology and its implication for wound healing.* Wound Repair Regen, 2003. 11(6): p. 419-23.
53. Jetten, N., et al., *Anti-inflammatory M2, but not pro-inflammatory M1 macrophages promote angiogenesis in vivo.* Angiogenesis, 2014. 17(1): p. 109-118.
54. Sakaguchi, S., et al., *Implication of anti-inflammatory macrophages in regenerative moto-neuritogenesis: Promotion of myoblast migration and neural*

chemorepellent semaphorin 3A expression in injured muscle. The International Journal of Biochemistry & Cell Biology, 2014. 54: p. 272-285.
55. Golbar, H.M., et al., *Immunohistochemical analyses of the kinetics and distribution of macrophages, hepatic stellate cells and bile duct epithelia in the developing rat liver.* Experimental and Toxicologic Pathology, 2012. 64(1): p. 1-8.
56. Chen, J.J., et al., *Tumor-associated macrophages: the double-edged sword in cancer progression.* J Clin Oncol, 2005. 23(5): p. 953-64.
57. Lin, E.Y., et al., *The macrophage growth factor CSF-1 in mammary gland development and tumor progression.* J Mammary Gland Biol Neoplasia, 2002. 7(2): p. 147-62.
58. Wyckoff, J., et al., *A Paracrine Loop between Tumor Cells and Macrophages Is Required for Tumor Cell Migration in Mammary Tumors.* Cancer Research, 2004. 64(19): p. 7022-7029.
59. Ryder, M., et al., *Increased density of tumor associated macrophages is associated with decreased survival in advanced thyroid cancer.* Endocrine-related cancer, 2008. 15(4): p. 1069-1074.
60. Steidl, C., et al., *Tumor-associated macrophages and survival in classic Hodgkin's lymphoma.* N Engl J Med, 2010. 362(10): p. 875-85.
61. Kim, D.W., et al., *High tumour islet macrophage infiltration correlates with improved patient survival but not with EGFR mutations, gene copy number or protein expression in resected non-small cell lung cancer.* British Journal of Cancer, 2008. 98(6): p. 1118-1124.
62. Taskinen, M., et al., *A High Tumor-Associated Macrophage Content Predicts Favorable Outcome in Follicular Lymphoma Patients Treated with Rituximab and Cyclophosphamide-Doxorubicin-Vincristine-Prednisone.* Clinical Cancer Research, 2007. 13(19): p. 5784-5789.
63. Canioni, D., et al., *High Numbers of Tumor-Associated Macrophages Have an Adverse Prognostic Value That Can Be Circumvented by Rituximab in Patients With Follicular Lymphoma Enrolled Onto the GELA-GOELAMS FL-2000 Trial.* Journal of Clinical Oncology, 2008. 26(3): p. 440-446.
64. Qian, B.Z. and J.W. Pollard, *Macrophage diversity enhances tumor progression and metastasis.* Cell, 2010. 141(1): p. 39-51.
65. Whiteside, T.L., *The tumor microenvironment and its role in promoting tumor growth.* Oncogene, 2008. 27(45): p. 5904-12.
66. Ehlers, S., S.H. Kaufmann, and C. Participants of the 99 Dahlem, *Infection, inflammation, and chronic diseases: consequences of a modern lifestyle.* Trends Immunol, 2010. 31(5): p. 184-90.
67. Gallucci, S. and P. Matzinger, *Danger signals: SOS to the immune system.* Curr Opin Immunol, 2001. 13(1): p. 114-9.
68. Woo, E.Y., et al., *Regulatory CD4(+)CD25(+) T cells in tumors from patients with early-stage non-small cell lung cancer and late-stage ovarian cancer.* Cancer Res, 2001. 61(12): p. 4766-72.
69. Serafini, P., I. Borrello, and V. Bronte, *Myeloid suppressor cells in cancer: recruitment, phenotype, properties, and mechanisms of immune suppression.* Semin Cancer Biol, 2006. 16(1): p. 53-65.
70. Hsieh, C., et al., *Development of TH1 CD4+ T cells through IL-12 produced by Listeria-induced macrophages.* Science, 1993. 260(5107): p. 547-549.
71. Mantovani, A., et al., *Cancer-related inflammation.* Nature, 2008. 454(7203): p. 436-44.
72. Pang, B., et al., *Lipid peroxidation dominates the chemistry of DNA adduct formation in a mouse model of inflammation.* Carcinogenesis, 2007. 28(8): p. 1807-13.
73. Lluis, J.M., et al., *Dual role of mitochondrial reactive oxygen species in hypoxia signaling: activation of nuclear factor-{kappa}B via c-SRC and oxidant-dependent cell death.* Cancer Res, 2007. 67(15): p. 7368-77.

74. Malik, S.T.A., et al., *Paradoxical effects of tumour necrosis factor in experimental ovarian cancer.* International Journal of Cancer, 1989. 44(5): p. 918-925.
75. Harrison, M.L., et al., *Tumor Necrosis Factor α As a New Target for Renal Cell Carcinoma: Two Sequential Phase II Trials of Infliximab at Standard and High Dose.* Journal of Clinical Oncology, 2007. 25(29): p. 4542-4549.
76. Lee, E.C.Y., et al., *Antiandrogen-induced cell death in LNCaP human prostate cancer cells.* Cell Death Differ, 2003. 10(7): p. 761-771.
77. Leibovich, S.J., et al., *Macrophage-induced angiogenesis is mediated by tumour necrosis factor-[alpha].* Nature, 1987. 329(6140): p. 630-632.
78. Saccani, A., et al., *p50 nuclear factor-kappaB overexpression in tumor-associated macrophages inhibits M1 inflammatory responses and antitumor resistance.* Cancer Res, 2006. 66(23): p. 11432-40.
79. DeNardo, D.G., et al., *CD4(+) T cells regulate pulmonary metastasis of mammary carcinomas by enhancing protumor properties of macrophages.* Cancer Cell, 2009. 16(2): p. 91-102.
80. Rodriguez, P.C., et al., *Arginase I production in the tumor microenvironment by mature myeloid cells inhibits T-cell receptor expression and antigen-specific T-cell responses.* Cancer Res, 2004. 64(16): p. 5839-49.
81. Condeelis, J. and J.W. Pollard, *Macrophages: obligate partners for tumor cell migration, invasion, and metastasis.* Cell, 2006. 124(2): p. 263-6.
82. Wang, S., et al., *Disruption of the SRC-1 gene in mice suppresses breast cancer metastasis without affecting primary tumor formation.* Proceedings of the National Academy of Sciences of the United States of America, 2009. 106(1): p. 151-156.
83. Guweidhi, A., et al., *Osteonectin influences growth and invasion of pancreatic cancer cells.* Ann Surg, 2005. 242(2): p. 224-34.
84. Sangaletti, S., et al., *Macrophage-derived SPARC bridges tumor cell-extracellular matrix interactions toward metastasis.* Cancer Res, 2008. 68(21): p. 9050-9.
85. Egeblad, M. and Z. Werb, *New functions for the matrix metalloproteinases in cancer progression.* Nat Rev Cancer, 2002. 2(3): p. 161-74.
86. Vasiljeva, O., et al., *Tumor cell-derived and macrophage-derived cathepsin B promotes progression and lung metastasis of mammary cancer.* Cancer Res, 2006. 66(10): p. 5242-50.
87. Gocheva, V., et al., *IL-4 induces cathepsin protease activity in tumor-associated macrophages to promote cancer growth and invasion.* Genes Dev, 2010. 24(3): p. 241-55.
88. Kitamura, T., et al., *SMAD4-deficient intestinal tumors recruit CCR1+ myeloid cells that promote invasion.* Nat Genet, 2007. 39(4): p. 467-475.
89. Baeriswyl, V. and G. Christofori, *The angiogenic switch in carcinogenesis.* Seminars in Cancer Biology, 2009. 19(5): p. 329-337.
90. Zumsteg, A. and G. Christofori, *Corrupt policemen: inflammatory cells promote tumor angiogenesis.* Current Opinion in Oncology, 2009. 21(1): p. 60-70.
91. Lin, E.Y., et al., *Macrophages Regulate the Angiogenic Switch in a Mouse Model of Breast Cancer.* Cancer Research, 2006. 66(23): p. 11238-11246.
92. Kimura, Y.N., et al., *Inflammatory stimuli from macrophages and cancer cells synergistically promote tumor growth and angiogenesis.* Cancer Science, 2007. 98(12): p. 2009-2018.
93. Qian, B.-Z. and J.W. Pollard, *Macrophage Diversity Enhances Tumor Progression and Metastasis.* Cell. 141(1): p. 39-51.
94. Giraudo, E., M. Inoue, and D. Hanahan, *An amino-bisphosphonate targets MMP-9–expressing macrophages and angiogenesis to impair cervical carcinogenesis.* Journal of Clinical Investigation, 2004. 114(5): p. 623-633.
95. Kim, S., et al., *Carcinoma Produced Factors Activate Myeloid Cells via TLR2 to Stimulate Metastasis.* Nature, 2009. 457(7225): p. 102-106.
96. Kaplan, R.N., et al., *VEGFR1-positive haematopoietic bone marrow progenitors initiate the pre-metastatic niche.* Nature, 2005. 438(7069): p. 820-827.

97. Hiratsuka, S., et al., *MMP9 induction by vascular endothelial growth factor receptor-1 is involved in lung-specific metastasis.* Cancer Cell, 2002. 2(4): p. 289-300.
98. Qian, B., et al., *A Distinct Macrophage Population Mediates Metastatic Breast Cancer Cell Extravasation, Establishment and Growth.* PLoS ONE, 2009. 4(8): p. e6562.
99. Barton, G.M. and R. Medzhitov, *Toll-like receptors and their ligands.* Curr Top Microbiol Immunol, 2002. 270: p. 81-92.
100. Kawai, T. and S. Akira, *The role of pattern-recognition receptors in innate immunity: update on Toll-like receptors.* Nat Immunol, 2010. 11(5): p. 373-84.
101. Gilmore, T.D., *Introduction to NF-kappaB: players, pathways, perspectives.* Oncogene, 2006. 25(51): p. 6680-4.
102. Yamamoto, M., et al., *Essential role for TIRAP in activation of the signalling cascade shared by TLR2 and TLR4.* Nature, 2002. 420(6913): p. 324-329.
103. Yamamoto, M., et al., *TRAM is specifically involved in the Toll-like receptor 4-mediated MyD88-independent signaling pathway.* Nat Immunol, 2003. 4(11): p. 1144-1150.
104. Coley, W.B., *The Treatment of Inoperable Sarcoma by Bacterial Toxins (the Mixed Toxins of the Streptococcus erysipelas and the Bacillus prodigiosus).* Proceedings of the Royal Society of Medicine, 1910. 3(Surg Sect): p. 1-48.
105. Diamond, M.S., et al., *Type I interferon is selectively required by dendritic cells for immune rejection of tumors.* The Journal of Experimental Medicine, 2011. 208(10): p. 1989-2003.
106. Terunuma, H., et al., *Potential Role of NK Cells in the Induction of Immune Responses: Implications for NK Cell–Based Immunotherapy for Cancers and Viral Infections.* International Reviews of Immunology, 2008. 27(3): p. 93-110.
107. Fuertes, M.B., et al., *Host type I IFN signals are required for antitumor CD8(+) T cell responses through CD8α(+) dendritic cells.* The Journal of Experimental Medicine, 2011. 208(10): p. 2005-2016.
108. Pradere, J.-P., D.H. Dapito, and R.F. Schwabe, *The Yin and Yang of Toll-like Receptors in Cancer.* Oncogene, 2014. 33(27): p. 3485-3495.
109. Chin, A.I., et al., *Toll-like Receptor 3-mediated Suppression of TRAMP Prostate Cancer Demonstrates the Critical Role of Type I Interferons in Tumor Immune Surveillance.* Cancer research, 2010. 70(7): p. 2595-2603.
110. Chew, V., et al., *Toll-Like Receptor 3 Expressing Tumor Parenchyma and Infiltrating Natural Killer Cells in Hepatocellular Carcinoma Patients.* JNCI Journal of the National Cancer Institute, 2012. 104(23): p. 1796-1807.
111. Schon, M.P. and M. Schon, *TLR7 and TLR8 as targets in cancer therapy.* Oncogene, 0000. 27(2): p. 190-199.
112. Drobits, B., et al., *Imiquimod clears tumors in mice independent of adaptive immunity by converting pDCs into tumor-killing effector cells.* The Journal of Clinical Investigation, 2012. 122(2): p. 575-585.
113. Stary, G., et al., *Tumoricidal activity of TLR7/8-activated inflammatory dendritic cells.* The Journal of Experimental Medicine, 2007. 204(6): p. 1441-1451.
114. Geisse, J., et al., *Imiquimod 5% cream for the treatment of superficial basal cell carcinoma: results from two phase III, randomized, vehicle-controlled studies.* Journal of the American Academy of Dermatology. 50(5): p. 722-733.
115. Adams, S., et al., *Topical TLR7 agonist imiquimod can induce immune-mediated rejection of skin metastases in patients with breast cancer.* Clinical cancer research : an official journal of the American Association for Cancer Research, 2012. 18(24): p. 6748-6757.
116. Brignole, C., et al., *Therapeutic Targeting of TLR9 Inhibits Cell Growth and Induces Apoptosis in Neuroblastoma.* Cancer Research, 2010. 70(23): p. 9816-9826.

117. Heckelsmiller, K., et al., *Peritumoral CpG DNA Elicits a Coordinated Response of CD8 T Cells and Innate Effectors to Cure Established Tumors in a Murine Colon Carcinoma Model.* The Journal of Immunology, 2002. 169(7): p. 3892-3899.
118. Kortylewski, M., et al., *In vivo delivery of siRNA to immune cells by conjugation to a TLR9 agonist enhances antitumor immune responses.* Nat Biotech, 2009. 27(10): p. 925-932.
119. Krieg, A.M., *Development of TLR9 agonists for cancer therapy.* The Journal of Clinical Investigation, 2007. 117(5): p. 1184-1194.
120. Noack, J., et al., *TLR9 agonists induced cell death in Burkitt's lymphoma cells is variable and influenced by TLR9 polymorphism.* Cell Death & Disease, 2012. 3(6): p. e323.
121. Ochi, A., et al., *MyD88 inhibition amplifies dendritic cell capacity to promote pancreatic carcinogenesis via Th2 cells.* The Journal of Experimental Medicine, 2012. 209(9): p. 1671-1687.
122. Fabbri, M., et al., *MicroRNAs bind to Toll-like receptors to induce prometastatic inflammatory response.* Proceedings of the National Academy of Sciences of the United States of America, 2012. 109(31): p. E2110-E2116.
123. Ochi, A., et al., *Toll-like receptor 7 regulates pancreatic carcinogenesis in mice and humans.* The Journal of Clinical Investigation, 2012. 122(11): p. 4118-4129.
124. Burdette, D.L., et al., *STING is a direct innate immune sensor of cyclic di-GMP.* Nature, 2011. 478(7370): p. 515-518.
125. Tanaka, Y. and Z.J. Chen, *STING Specifies IRF3 phosphorylation by TBK1 in the Cytosolic DNA Signaling Pathway.* Science signaling, 2012. 5(214): p. ra20-ra20.
126. Baguley, B.C. and L.M. Ching, *Immunomodulatory actions of xanthenone anticancer agents.* BioDrugs, 1997. 8(2): p. 119-27.
127. Downey, C.M., et al., *DMXAA causes tumor site-specific vascular disruption in murine non-small cell lung cancer, and like the endogenous non-canonical cyclic dinucleotide STING agonist, 2'3'-cGAMP, induces M2 macrophage repolarization.* PLoS One, 2014. 9(6): p. e99988.
128. Wallace, A., et al., *The vascular disrupting agent, DMXAA, directly activates dendritic cells through a MyD88-independent mechanism and generates antitumor cytotoxic T lymphocytes.* Cancer Res, 2007. 67(14): p. 7011-9.
129. Jassar, A.S., et al., *Activation of Tumor-Associated Macrophages by the Vascular Disrupting Agent 5,6-Dimethylxanthenone-4-Acetic Acid Induces an Effective CD8+ T-Cell–Mediated Antitumor Immune Response in Murine Models of Lung Cancer and Mesothelioma.* Cancer Research, 2005. 65(24): p. 11752-11761.
130. Abe, T. and G.N. Barber, *Cytosolic-DNA-Mediated, STING-Dependent Proinflammatory Gene Induction Necessitates Canonical NF-κB Activation through TBK1.* Journal of Virology, 2014. 88(10): p. 5328-5341.
131. Lynch, T.J., et al., *Ipilimumab in Combination With Paclitaxel and Carboplatin As First-Line Treatment in Stage IIIB/IV Non–Small-Cell Lung Cancer: Results From a Randomized, Double-Blind, Multicenter Phase II Study.* Journal of Clinical Oncology, 2012. 30(17): p. 2046-2054.
132. Bryan, J. and G. Borthakur, *Role of rituximab in first-line treatment of chronic lymphocytic leukemia.* Therapeutics and Clinical Risk Management, 2011. 7: p. 1-11.
133. Hudis, C.A., *Trastuzumab — Mechanism of Action and Use in Clinical Practice.* New England Journal of Medicine, 2007. 357(1): p. 39-51.
134. Sehn, L.H., et al., *Introduction of Combined CHOP Plus Rituximab Therapy Dramatically Improved Outcome of Diffuse Large B-Cell Lymphoma in British Columbia.* Journal of Clinical Oncology, 2005. 23(22): p. 5027-5033.
135. Webster, R.G. and H.L. Robinson, *DNA vaccines: a review of developments.* BioDrugs, 1997. 8(4): p. 273-92.
136. Fioretti, D., et al., *DNA vaccines: developing new strategies against cancer.* J Biomed Biotechnol, 2010. 2010: p. 174378.

137. Song, K., Y. Chang, and G.J. Prud'homme, *IL-12 plasmid-enhanced DNA vaccination against carcinoembryonic antigen (CEA) studied in immune-gene knockout mice.* Gene Ther, 2000. 7(18): p. 1527-35.
138. Rice, J., C.H. Ottensmeier, and F.K. Stevenson, *DNA vaccines: precision tools for activating effective immunity against cancer.* Nat Rev Cancer, 2008. 8(2): p. 108-20.
139. Anderson, R.J. and J. Schneider, *Plasmid DNA and viral vector-based vaccines for the treatment of cancer.* Vaccine, 2007. 25 Suppl 2: p. B24-34.
140. Yuan, J., et al., *Safety and immunogenicity of a human and mouse gp100 DNA vaccine in a phase I trial of patients with melanoma.* Cancer Immun, 2009. 9: p. 5.
141. Rosenberg, S.A., *IL-2: the first effective immunotherapy for human cancer.* J Immunol, 2014. 192(12): p. 5451-8.
142. Dutcher, J., *Current status of interleukin-2 therapy for metastatic renal cell carcinoma and metastatic melanoma.* Oncology (Williston Park), 2002. 16(11 Suppl 13): p. 4-10.
143. Kantoff, P.W., et al., *Sipuleucel-T immunotherapy for castration-resistant prostate cancer.* N Engl J Med, 2010. 363(5): p. 411-22.
144. Fong, L., et al., *Dendritic cell-based xenoantigen vaccination for prostate cancer immunotherapy.* J Immunol, 2001. 167(12): p. 7150-6.
145. van de Laar, L., P.J. Coffer, and A.M. Woltman, *Regulation of dendritic cell development by GM-CSF: molecular control and implications for immune homeostasis and therapy.* Blood, 2012. 119(15): p. 3383-3393.
146. Lipowska-Bhalla, G., et al., *Targeted immunotherapy of cancer with CAR T cells: achievements and challenges.* Cancer Immunol Immunother, 2012. 61(7): p. 953-62.
147. Porter, D.L., et al., *Chimeric antigen receptor T cells persist and induce sustained remissions in relapsed refractory chronic lymphocytic leukemia.* Sci Transl Med, 2015. 7(303): p. 303-139.
148. Scott, A.M., J.D. Wolchok, and L.J. Old, *Antibody therapy of cancer.* Nat Rev Cancer, 2012. 12(4): p. 278-287.
149. Brennan, P.J., et al., *HER2/Neu: mechanisms of dimerization/oligomerization.* Oncogene, 2002. 21(2): p. 328.
150. Slamon, D.J., et al., *Human breast cancer: correlation of relapse and survival with amplification of the HER-2/neu oncogene.* Science, 1987. 235(4785): p. 177-82.
151. Vu, T. and F.X. Claret, *Trastuzumab: updated mechanisms of action and resistance in breast cancer.* Front Oncol, 2012. 2: p. 62.
152. Junttila, T.T., et al., *Ligand-Independent HER2/HER3/PI3K Complex Is Disrupted by Trastuzumab and Is Effectively Inhibited by the PI3K Inhibitor GDC-0941.* Cancer Cell. 15(5): p. 429-440.
153. Chan, H.T.C., et al., *CD20-induced Lymphoma Cell Death Is Independent of Both Caspases and Its Redistribution into Triton X-100 Insoluble Membrane Rafts.* Cancer Research, 2003. 63(17): p. 5480-5489.
154. Cragg, M.S. and M.J. Glennie, *Antibody specificity controls in vivo effector mechanisms of anti-CD20 reagents.* Blood, 2004. 103(7): p. 2738-2743.
155. Ivanov, A., et al., *Monoclonal antibodies directed to CD20 and HLA-DR can elicit homotypic adhesion followed by lysosome-mediated cell death in human lymphoma and leukemia cells.* The Journal of Clinical Investigation, 2009. 119(8): p. 2143-2159.
156. Glennie, M.J., et al., *Mechanisms of killing by anti-CD20 monoclonal antibodies.* Molecular Immunology, 2007. 44(16): p. 3823-3837.
157. Honeychurch, J., et al., *Antibody-induced nonapoptotic cell death in human lymphoma and leukemia cells is mediated through a novel reactive oxygen species-dependent pathway.* Blood, 2012. 119(15): p. 3523.
158. Lanier, L.L., *Natural killer cell receptor signaling.* Curr Opin Immunol, 2003. 15(3): p. 308-14.

159. Bryceson, Y.T., et al., *Synergy among receptors on resting NK cells for the activation of natural cytotoxicity and cytokine secretion.* Blood, 2006. 107(1): p. 159-166.
160. Clynes, R.A., et al., *Inhibitory Fc receptors modulate in vivo cytoxicity against tumor targets.* Nat Med, 2000. 6(4): p. 443-446.
161. Beers, S.A., et al., *Antigenic modulation limits the efficacy of anti-CD20 antibodies: implications for antibody selection.* Blood, 2010. 115(25): p. 5191-5201.
162. Tedder, T.F., et al., *Isolation and structure of a cDNA encoding the B1 (CD20) cell-surface antigen of human B lymphocytes.* Proceedings of the National Academy of Sciences of the United States of America, 1988. 85(1): p. 208-212.
163. Uchida, J., et al., *Mouse CD20 expression and function.* Int Immunol, 2004. 16(1): p. 119-29.
164. Walshe, C.A., et al., *Induction of Cytosolic Calcium Flux by CD20 Is Dependent upon B Cell Antigen Receptor Signaling.* Journal of Biological Chemistry, 2008. 283(25): p. 16971-16984.
165. Anderson, K.C., et al., *Expression of human B cell-associated antigens on leukemias and lymphomas: a model of human B cell differentiation.* Blood, 1984. 63(6): p. 1424-33.
166. Stashenko, P., et al., *Characterization of a human B lymphocyte-specific antigen.* J Immunol, 1980. 125(4): p. 1678-85.
167. Beers, S.A., et al., *CD20 as a Target for Therapeutic Type I and II Monoclonal Antibodies.* Seminars in Hematology. 47(2): p. 107-114.
168. Cragg, M.S., et al., *Complement-mediated lysis by anti-CD20 mAb correlates with segregation into lipid rafts.* Blood, 2003. 101(3): p. 1045-1052.
169. Firer, M.A. and G. Gellerman, *Targeted drug delivery for cancer therapy: the other side of antibodies.* Journal of Hematology & Oncology, 2012. 5: p. 70-70.
170. Goede , V., et al., *Obinutuzumab plus Chlorambucil in Patients with CLL and Coexisting Conditions.* New England Journal of Medicine, 2014. 370(12): p. 1101-1110.
171. Vaughan, A.T., M.S. Cragg, and S.A. Beers, *Antibody modulation: Limiting the efficacy of therapeutic antibodies.* Pharmacological Research, 2015. 99: p. 269-275.
172. Lim, S.H., et al., *Fc gamma receptor IIb on target B cells promotes rituximab internalization and reduces clinical efficacy.* Blood, 2011. 118(9): p. 2530-2540.
173. Roghanian, A., et al., *Antagonistic human FcγRIIB (CD32B) antibodies have anti-tumor activity and overcome resistance to antibody therapy in vivo.* Cancer Cell. 27(4): p. 473-488.
174. Beum, P.V., et al., *The Shaving Reaction: Rituximab/CD20 Complexes Are Removed from Mantle Cell Lymphoma and Chronic Lymphocytic Leukemia Cells by THP-1 Monocytes.* The Journal of Immunology, 2006. 176(4): p. 2600-2609.
175. Slamon , D.J., et al., *Use of Chemotherapy plus a Monoclonal Antibody against HER2 for Metastatic Breast Cancer That Overexpresses HER2.* New England Journal of Medicine, 2001. 344(11): p. 783-792.
176. Younes, A., et al., *Brentuximab vedotin (SGN-35) for relapsed CD30-positive lymphomas.* N Engl J Med, 2010. 363(19): p. 1812-21.
177. Younes, A., et al., *Results of a pivotal phase II study of brentuximab vedotin for patients with relapsed or refractory Hodgkin's lymphoma.* J Clin Oncol, 2012. 30(18): p. 2183-9.
178. Pro, B., et al., *Brentuximab vedotin (SGN-35) in patients with relapsed or refractory systemic anaplastic large-cell lymphoma: results of a phase II study.* J Clin Oncol, 2012. 30(18): p. 2190-6.
179. Ansell, S.M., *Brentuximab vedotin.* Blood, 2014. 124(22): p. 3197-3200.
180. Gandhi, M.D., et al., *Pancreatitis in patients treated with brentuximab vedotin: a previously unrecognized serious adverse event.* Blood, 2014. 123(18): p. 2895-7.

181. Mellman, I., G. Coukos, and G. Dranoff, *Cancer immunotherapy comes of age.* Nature, 2011. 480(7378): p. 480-489.
182. Mescher, M.F., et al., *Signals required for programming effector and memory development by CD8+ T cells.* Immunological Reviews, 2006. 211(1): p. 81-92.
183. Curtsinger, J.M., et al., *Inflammatory Cytokines Provide a Third Signal for Activation of Naive CD4+ and CD8+ T Cells.* The Journal of Immunology, 1999. 162(6): p. 3256-3262.
184. Pape, K.A., et al., *Inflammatory cytokines enhance the in vivo clonal expansion and differentiation of antigen-activated CD4+ T cells.* The Journal of Immunology, 1997. 159(2): p. 591-8.
185. Brunet, J.-F., et al., *A new member of the immunoglobulin superfamily[mdash]CTLA-4.* Nature, 1987. 328(6127): p. 267-270.
186. Carreno, B.M., et al., *CTLA-4 (CD152) Can Inhibit T Cell Activation by Two Different Mechanisms Depending on Its Level of Cell Surface Expression.* The Journal of Immunology, 2000. 165(3): p. 1352-1356.
187. Hodi, F.S., et al., *Improved Survival with Ipilimumab in Patients with Metastatic Melanoma.* New England Journal of Medicine, 2010. 363(8): p. 711-723.
188. Sica, G. and L. Chen, *Biochemical and immunological characteristics of 4-1BB (CD137) receptor and ligand and potential applications in cancer therapy.* Arch Immunol Ther Exp (Warsz), 1999. 47(5): p. 275-9.
189. Croft, M., *Control of Immunity by the TNFR-Related Molecule OX40 (CD134).* Annual review of immunology, 2010. 28: p. 57-78.
190. Curti, B.D., et al., *OX40 is a potent immune stimulating target in late stage cancer patients.* Cancer research, 2013. 73(24): p. 7189-7198.
191. Weiner, L.M., R. Surana, and S. Wang, *Antibodies and cancer therapy: versatile platforms for cancer immunotherapy.* Nature reviews. Immunology, 2010. 10(5): p. 317-327.
192. Grewal, I.S. and R.A. Flavell, *CD40 and CD154 in cell-mediated immunity.* Annu Rev Immunol, 1998. 16: p. 111-35.
193. Elgueta, R., et al., *Molecular mechanism and function of CD40/CD40L engagement in the immune system.* Immunological reviews, 2009. 229(1): p. 10.1111/j.1600-065X.2009.00782.x.
194. Schoenberger, S.P., et al., *T-cell help for cytotoxic T lymphocytes is mediated by CD40-CD40L interactions.* Nature, 1998. 393(6684): p. 480-483.
195. French, R.R., et al., *CD40 antibody evokes a cytotoxic T-cell response that eradicates lymphoma and bypasses T-cell help.* Nat Med, 1999. 5(5): p. 548-553.
196. Salles, G.A., *Clinical Features, Prognosis and Treatment of Follicular Lymphoma.* ASH Education Program Book, 2007. 2007(1): p. 216-225.
197. Lim, S.H., et al., *Anti-CD20 monoclonal antibodies: historical and future perspectives.* Haematologica, 2010. 95(1): p. 135-143.
198. Minard-Colin, V., et al., *Lymphoma depletion during CD20 immunotherapy in mice is mediated by macrophage FcγRI, FcγRIII, and FcγRIV.* Blood, 2008. 112(4): p. 1205-1213.
199. Treon, S.P., et al., *Polymorphisms in FcγRIIIA (CD16) Receptor Expression Are Associated With Clinical Response to Rituximab in Waldenström's Macroglobulinemia.* Journal of Clinical Oncology, 2005. 23(3): p. 474-481.
200. Montalvao, F., et al., *The mechanism of anti-CD20–mediated B cell depletion revealed by intravital imaging.* The Journal of Clinical Investigation, 2013. 123(12): p. 5098-5103.
201. Gul, N., et al., *Macrophages eliminate circulating tumor cells after monoclonal antibody therapy.* J Clin Invest, 2014. 124(2): p. 812-23.
202. Biburger, M., et al., *Monocyte subsets responsible for immunoglobulin G-dependent effector functions in vivo.* Immunity. 35(6): p. 932-944.
203. Albanesi, M., et al., *Neutrophils mediate antibody-induced antitumor effects in mice.* Blood, 2013. 122(18): p. 3160-3164.

204. Hamon, P., et al. *Tracking mouse bone marrow monocytes in vivo*. Journal of visualized experiments : JoVE, 2015. e52476.
205. Franklin, R.A., et al., *The Cellular and Molecular Origin of Tumor-associated Macrophages.* Science (New York, N.Y.), 2014. 344(6186): p. 921-925.
206. da Silva, F.M., A.M. Massart-Leen, and C. Burvenich, *Development and maturation of neutrophils.* Vet Q, 1994. 16(4): p. 220-5.
207. Moses, K. and S. Brandau, *Human neutrophils: Their role in cancer and relation to myeloid-derived suppressor cells.* Seminars in immunology, 2016. 28(2): p. 187-196.
208. Lehmann, B., et al., *Tumor location determines tissue-specific recruitment of tumor-associated macrophages and antibody-dependent immunotherapy response.* Science Immunology, 2017. 2(7).
209. Sylvia, H., et al., *Abstract 3631: Modulation of monocyte- and macrophage-mediated antibody-dependent cell phagocytosis and cytotoxicity (ADCP/ADCC) by Fc engineering of therapeutic antibodies.* Cancer Research, 2014. 74(19 Supplement): p. 3631.
210. Weng, W.-K. and R. Levy, *Two Immunoglobulin G Fragment C Receptor Polymorphisms Independently Predict Response to Rituximab in Patients With Follicular Lymphoma.* Journal of Clinical Oncology, 2003. 21(21): p. 3940-3947.
211. Mössner, E., et al., *Increasing the efficacy of CD20 antibody therapy through the engineering of a new type II anti-CD20 antibody with enhanced direct and immune effector cell–mediated B-cell cytotoxicity.* Blood, 2010. 115(22): p. 4393-4402.
212. Goldenberg, D.M., et al., *Properties and structure-function relationships of veltuzumab (hA20), a humanized anti-CD20 monoclonal antibody.* Blood, 2009. 113(5): p. 1062-1070.
213. Ostrand-Rosenberg, S., et al., *Cross-talk between myeloid-derived suppressor cells (MDSC), macrophages, and dendritic cells enhances tumor-induced immune suppression.* Seminars in cancer biology, 2012. 22(4): p. 275-281.
214. Pollard, J.W., *Tumour-educated macrophages promote tumour progression and metastasis.* Nat Rev Cancer, 2004. 4(1): p. 71-8.
215. Takai, T., et al., *FcR gamma chain deletion results in pleiotrophic effector cell defects.* Cell, 1994. 76(3): p. 519-29.
216. Takai, T., et al., *Augmented humoral and anaphylactic responses in Fc gamma RII-deficient mice.* Nature, 1996. 379(6563): p. 346-9.
217. Peters, W., M. Dupuis, and I.F. Charo, *A mechanism for the impaired IFN-gamma production in C-C chemokine receptor 2 (CCR2) knockout mice: role of CCR2 in linking the innate and adaptive immune responses.* J Immunol, 2000. 165(12): p. 7072-7.
218. Shi, C. and E.G. Pamer, *Monocyte recruitment during infection and inflammation.* Nat Rev Immunol, 2011. 11(11): p. 762-774.
219. Ahuja, A., et al., *Depletion of B cells in murine lupus: efficacy and resistance.* J Immunol, 2007. 179(5): p. 3351-61.
220. Weischenfeldt, J. and B. Porse, *Bone Marrow-Derived Macrophages (BMM): Isolation and Applications.* Cold Spring Harbor Protocols, 2008. 2008(12): p. pdb.prot5080.
221. Ding, A.H., C.F. Nathan, and D.J. Stuehr, *Release of reactive nitrogen intermediates and reactive oxygen intermediates from mouse peritoneal macrophages. Comparison of activating cytokines and evidence for independent production.* The Journal of Immunology, 1988. 141(7): p. 2407-12.
222. Livak, K.J. and T.D. Schmittgen, *Analysis of Relative Gene Expression Data Using Real-Time Quantitative PCR and the 2−ΔΔCT Method.* Methods, 2001. 25(4): p. 402-408.
223. Bond, M.D. and H.E. Van Wart, *Characterization of the individual collagenases from Clostridium histolyticum.* Biochemistry, 1984. 23(13): p. 3085-3091.

224. Muirhead, M.J., et al., *BCL1, a murine model of prolymphocytic leukemia. I. Effect of splenectomy on growth kinetics and organ distribution.* The American Journal of Pathology, 1981. 105(3): p. 295-305.
225. Slavin, S. and S. Strober, *Spontaneous murine B-cell leukaemia.* Nature, 1978. 272(5654): p. 624-626.
226. Brattain, M.G., et al., *Establishment of Mouse Colonic Carcinoma Cell Lines with Different Metastatic Properties.* Cancer Research, 1980. 40(7): p. 2142-2146.
227. Castle, J.C., et al., *Immunomic, genomic and transcriptomic characterization of CT26 colorectal carcinoma.* BMC Genomics, 2014. 15(1): p. 190.
228. Penttilä, J.M., et al., *Depletion of CD8(+) cells abolishes memory in acquired immunity against Chlamydia pneumoniae in BALB/c mice.* Immunology, 1999. 97(3): p. 490-496.
229. Moore, M.W., F.R. Carbone, and M.J. Bevan, *Introduction of soluble protein into the class I pathway of antigen processing and presentation.* Cell. 54(6): p. 777-785.
230. Lode, H.N., et al., *Targeted interleukin-2 therapy for spontaneous neuroblastoma metastases to bone marrow.* J Natl Cancer Inst, 1997. 89(21): p. 1586-94.
231. Murray, Peter J., et al., *Macrophage Activation and Polarization: Nomenclature and Experimental Guidelines.* Immunity. 41(1): p. 14-20.
232. Xue, J., et al., *Transcriptome-Based Network Analysis Reveals a Spectrum Model of Human Macrophage Activation.* Immunity. 40(2): p. 274-288.
233. Martinez, F.O. and S. Gordon, *The M1 and M2 paradigm of macrophage activation: time for reassessment.* F1000Prime Reports, 2014. 6: p. 13.
234. *Identification of interferon-gamma as the lymphokine that activates human macrophage oxidative metabolism and antimicrobial activity.* The Journal of Experimental Medicine, 1983. 158(3): p. 670-689.
235. Verreck, F.A.W., et al., *Phenotypic and functional profiling of human proinflammatory type-1 and anti-inflammatory type-2 macrophages in response to microbial antigens and IFN-γ- and CD40L-mediated costimulation.* Journal of Leukocyte Biology, 2006. 79(2): p. 285-293.
236. McWhorter, F.Y., et al., *Modulation of macrophage phenotype by cell shape.* Proceedings of the National Academy of Sciences of the United States of America, 2013. 110(43): p. 17253-17258.
237. Forghani, P. and E.K. Waller, *New Mechanism in Anti Tumor Activity of Poly (I:C): Modulation of Tumor-Associated Myeloid Derived Suppressor Cells in Murine Model of Breast Cancer.* Blood, 2014. 124(21): p. 2728-2728.
238. Butchar, J.P., et al., *Reciprocal regulation of activating and inhibitory Fcγ receptors by TLR7/8 activation: Implications for tumor immunotherapy.* Clinical cancer research : an official journal of the American Association for Cancer Research, 2010. 16(7): p. 2065-2075.
239. Shirota, B.Y., H. Shirota, and D.M. Klinman, *Intra-tumoral injection of CpG oligonucleotides induces the differentiation and reduces the immunosuppressive activity of myeloid-derived suppressor cells.* Journal of Immunology (Baltimore, Md. : 1950), 2012. 188(4): p. 1592-1599.
240. Xu, L., K. Xie, and I.J. Fidler, *Therapy of Human Ovarian Cancer by Transfection with the Murine Interferon β Gene: Role of Macrophage-Inducible Nitric Oxide Synthase.* Human Gene Therapy, 1998. 9(18): p. 2699-2708.
241. Xie K, H.S., Dong Z, Juang SH, Gutman M, Xie QW, Nathan C, Fidler IJ, *Transfection with the inducible nitric oxide synthase gene suppresses tumorigenicity and abrogates metastasis by K-1735 murine melanoma cells.* The Journal of Experimental Medicine, 1995. 181(4): p. 1333-1343.
242. Juang, S.-H., et al., *Suppression of Tumorigenicity and Metastasis of Human Renal Carcinoma Cells by Infection with Retroviral Vectors Harboring the Murine Inducible Nitric Oxide Synthase Gene.* Human Gene Therapy, 1998. 9(6): p. 845-854.

243. Sica, A., et al., *Tumour-associated macrophages are a distinct M2 polarised population promoting tumour progression: Potential targets of anti-cancer therapy.* European Journal of Cancer. 42(6): p. 717-727.
244. Kigerl, K.A., et al., *Identification of two distinct macrophage subsets with divergent effects causing either neurotoxicity or regeneration in the injured mouse spinal cord.* J Neurosci, 2009. 29(43): p. 13435-44.
245. Mousavi, S.A., et al., *Receptor-mediated endocytosis of immune complexes in rat liver sinusoidal endothelial cells is mediated by FcγRIIb2.* Hepatology, 2007. 46(3): p. 871-884.
246. Zhang, C.Y. and J.W. Booth, *Divergent Intracellular Sorting of FcγRIIA and FcγRIIB2.* Journal of Biological Chemistry, 2010. 285(44): p. 34250-34258.
247. Hemmi, H., et al., *Small anti-viral compounds activate immune cells via the TLR7 MyD88-dependent signaling pathway.* Nat Immunol, 2002. 3(2): p. 196-200.
248. Pham Van, L., et al., *Treatment with the TLR7 agonist R848 induces regulatory T-cell-mediated suppression of established asthma symptoms.* European Journal of Immunology, 2011. 41(7): p. 1992-1999.
249. Pfreundschuh, M., et al., *CHOP-like chemotherapy plus rituximab versus CHOP-like chemotherapy alone in young patients with good-prognosis diffuse large-B-cell lymphoma: a randomised controlled trial by the MabThera International Trial (MInT) Group.* The Lancet Oncology. 7(5): p. 379-391.
250. Czuczman, M.S., et al., *Chemoimmunotherapy with ofatumumab in combination with CHOP in previously untreated follicular lymphoma.* British Journal of Haematology, 2012. 157(4): p. 438-445.
251. Hiddemann, W., et al., *Frontline therapy with rituximab added to the combination of cyclophosphamide, doxorubicin, vincristine, and prednisone (CHOP) significantly improves the outcome for patients with advanced-stage follicular lymphoma compared with therapy with CHOP alone: results of a prospective randomized study of the German Low-Grade Lymphoma Study Group.* Blood, 2005. 106(12): p. 3725-3732.
252. Moreton, P. and P. Hillmen, *Alemtuzumab therapy in B-cell lymphoproliferative disorders.* Seminars in Oncology. 30(4): p. 493-501.
253. Pallasch, C.P., et al., *Sensitizing Protective Tumor Microenvironments to Antibody-Mediated Therapy.* Cell, 2014. 156(3): p. 590-602.
254. Mantovani, A., *The growing diversity and spectrum of action of myeloid-derived suppressor cells.* European Journal of Immunology, 2010. 40(12): p. 3317-3320.
255. Boyd, Z.S., et al., *Interleukin-10 Receptor Signaling through STAT-3 Regulates the Apoptosis of Retinal Ganglion Cells in Response to Stress.* Investigative Ophthalmology & Visual Science, 2003. 44(12): p. 5206-5211.
256. Daley, J.M., et al., *Use of Ly6G-specific monoclonal antibody to deplete neutrophils in mice.* Journal of Leukocyte Biology, 2008. 83(1): p. 64-70.
257. Gao, J.J., et al., *Autocrine/Paracrine IFN-αβ Mediates the Lipopolysaccharide-Induced Activation of Transcription Factor Stat1α in Mouse Macrophages: Pivotal Role of Stat1α in Induction of the Inducible Nitric Oxide Synthase Gene.* The Journal of Immunology, 1998. 161(9): p. 4803-4810.
258. Feldman, G.M., E.J. Chuang, and D.S. Finbloom, *IgG immune complexes inhibit IFN-gamma-induced transcription of the Fc gamma RI gene in human monocytes by preventing the tyrosine phosphorylation of the p91 (Stat1) transcription factor.* The Journal of Immunology, 1995. 154(1): p. 318-25.
259. Zeisberger, S.M., et al., *Clodronate-liposome-mediated depletion of tumour-associated macrophages: a new and highly effective antiangiogenic therapy approach.* Br J Cancer, 2006. 95(3): p. 272-281.
260. Mia, S., et al., *An optimized Protocol for Human M2 Macrophages using M-CSF and IL-4/IL-10/TGF-β Yields a Dominant Immunosuppressive Phenotype.* Scandinavian Journal of Immunology, 2014. 79(5): p. 305-314.

261. O'Garra, A., et al., *Production of cytokines by mouse B cells: B lymphomas and normal B cells produce interleukin 10.* Int Immunol, 1990. 2(9): p. 821-32.
262. Wang, N., H. Liang, and K. Zen, *Molecular Mechanisms That Influence the Macrophage M1–M2 Polarization Balance.* Frontiers in Immunology, 2014. 5: p. 614.
263. Chen, W., et al., *Macrophage-Induced Tumor Angiogenesis Is Regulated by the TSC2–mTOR Pathway.* Cancer Research, 2012. 72(6): p. 1363-1372.
264. Ueki, I., et al., *B cell-targeted therapy with anti-CD20 monoclonal antibody in a mouse model of Graves' hyperthyroidism.* Clinical and Experimental Immunology, 2011. 163(3): p. 309-317.
265. Kudlacz, E., et al., *The Novel JAK-3 Inhibitor CP-690550 Is a Potent Immunosuppressive Agent in Various Murine Models.* American Journal of Transplantation, 2004. 4(1): p. 51-57.
266. Solovjov, D.A., E. Pluskota, and E.F. Plow, *Distinct Roles for the α and β Subunits in the Functions of Integrin αMβ2.* Journal of Biological Chemistry, 2005. 280(2): p. 1336-1345.
267. Bronte, V., et al., *Identification of a CD11b(+)/Gr-1(+)/CD31(+) myeloid progenitor capable of activating or suppressing CD8(+) T cells.* Blood, 2000. 96(12): p. 3838-46.
268. Nakamura, T., et al., *Liposomes loaded with a STING pathway ligand, cyclic di-GMP, enhance cancer immunotherapy against metastatic melanoma.* Journal of Controlled Release, 2015. 216: p. 149-157.
269. Lipson, E.J. and C.G. Drake, *Ipilimumab: An Anti-CTLA-4 Antibody for Metastatic Melanoma.* Clinical cancer research : an official journal of the American Association for Cancer Research, 2011. 17(22): p. 6958-6962.
270. White, A.L., et al., *Fcγ Receptor Dependency of Agonistic CD40 Antibody in Lymphoma Therapy Can Be Overcome through Antibody Multimerization.* The Journal of Immunology, 2014. 193(4): p. 1828-1835.
271. Snell, L.M., et al., *T-cell intrinsic effects of GITR and 4-1BB during viral infection and cancer immunotherapy.* Immunological Reviews, 2011. 244(1): p. 197-217.
272. Selby, M.J., et al., *Anti-CTLA-4 Antibodies of IgG2a Isotype Enhance Antitumor Activity through Reduction of Intratumoral Regulatory T Cells.* Cancer Immunology Research, 2013.
273. Romano, E., et al., *Ipilimumab-dependent cell-mediated cytotoxicity of regulatory T cells ex vivo by nonclassical monocytes in melanoma patients.* Proc Natl Acad Sci U S A, 2015. 112(19): p. 6140-5.
274. Bulliard, Y., et al., *Activating Fc γ receptors contribute to the antitumor activities of immunoregulatory receptor-targeting antibodies.* The Journal of Experimental Medicine, 2013. 210(9): p. 1685-1693.
275. Marabelle, A., et al., *Depleting tumor-specific Tregs at a single site eradicates disseminated tumors.* The Journal of Clinical Investigation, 2013. 123(6): p. 2447-2463.
276. McHugh, R.S., et al., *CD4(+)CD25(+) immunoregulatory T cells: gene expression analysis reveals a functional role for the glucocorticoid-induced TNF receptor.* Immunity, 2002. 16(2): p. 311-23.
277. Taraban, V.Y., et al., *Expression and costimulatory effects of the TNF receptor superfamily members CD134 (OX40) and CD137 (4-1BB), and their role in the generation of anti-tumor immune responses.* European Journal of Immunology, 2002. 32(12): p. 3617-3627.
278. White, A.L., et al., *Interaction with FcγRIIB Is Critical for the Agonistic Activity of Anti-CD40 Monoclonal Antibody.* The Journal of Immunology, 2011. 187(4): p. 1754-1763.
279. Pearce, E.L., et al., *Control of Effector CD8+ T Cell Function by the Transcription Factor Eomesodermin.* Science, 2003. 302(5647): p. 1041-1043.

280. Galon, J., et al., *Type, Density, and Location of Immune Cells Within Human Colorectal Tumors Predict Clinical Outcome.* Science, 2006. 313(5795): p. 1960-1964.
281. Greene, L.A., et al., *Neuronal properties of hybrid neuroblastoma X sympathetic ganglion cells.* Proc Natl Acad Sci U S A, 1975. 72(12): p. 4923-7.
282. Li, F. and J.V. Ravetch, *Apoptotic and antitumor activity of death receptor antibodies require inhibitory Fcgamma receptor engagement.* Proc Natl Acad Sci U S A, 2012. 109(27): p. 10966-71.
283. Cobbold, S.P., et al., *Therapy with monoclonal antibodies by elimination of T-cell subsets in vivo.* Nature, 1984. 312(5994): p. 548-551.
284. Houot, R., et al., *Therapeutic effect of CD137 immunomodulation in lymphoma and its enhancement by T(reg) depletion.* Blood, 2009. 114(16): p. 3431-3438.
285. Sakaguchi, S., et al., *The plasticity and stability of regulatory T cells.* Nat Rev Immunol, 2013. 13(6): p. 461-467.
286. Addey, C., et al., *Functional plasticity of antigen-specific regulatory T cells in context of tumor.* J Immunol, 2011. 186(8): p. 4557-64.
287. Gordon, S. and P.R. Taylor, *Monocyte and macrophage heterogeneity.* Nat Rev Immunol, 2005. 5(12): p. 953-964.
288. Domínguez-Soto, A., et al., *Dendritic Cell-Specific ICAM-3–Grabbing Nonintegrin Expression on M2-Polarized and Tumor-Associated Macrophages Is Macrophage-CSF Dependent and Enhanced by Tumor-Derived IL-6 and IL-10.* The Journal of Immunology, 2011. 186(4): p. 2192-2200.
289. Clària, J., et al., *New Insights into the Role of Macrophages in Adipose Tissue Inflammation and Fatty Liver Disease: Modulation by Endogenous Omega-3 Fatty Acid-derived Lipid Mediators.* Frontiers in Immunology, 2011. 2.
290. Schmidt, S.V., et al., *The transcriptional regulator network of human inflammatory macrophages is defined by open chromatin.* Cell Research, 2016. 26(2): p. 151-170.
291. Dahal, L.N., et al., *STING Activation Reverses Lymphoma-Mediated Resistance to Antibody Immunotherapy.* Cancer research, 2017. 77(13): p. 3619-3631.
292. Ammi, R., et al., *Poly(I:C) as cancer vaccine adjuvant: Knocking on the door of medical breakthroughs.* Pharmacology & Therapeutics, 2015. 146: p. 120-131.
293. Nimmerjahn, F. and J.V. Ravetch, *Translating basic mechanisms of IgG effector activity into next generation cancer therapies.* Cancer Immunity, 2012. 12: p. 13.
294. Jr, P.N.L., et al., *Randomized Phase III Placebo-Controlled Trial of Carboplatin and Paclitaxel With or Without the Vascular Disrupting Agent Vadimezan (ASA404) in Advanced Non–Small-Cell Lung Cancer.* Journal of Clinical Oncology, 2011. 29(22): p. 2965-2971.
295. Conlon, J., et al., *Mouse, but not Human STING, Binds and Signals in Response to the Vascular Disrupting Agent 5,6-Dimethylxanthenone-4-Acetic Acid.* The Journal of Immunology, 2013. 190(10): p. 5216-5225.
296. Baird, J.R., et al., *Radiation therapy combined with novel STING-targeting oligonucleotides results in regression of established tumors.* Cancer research, 2016. 76(1): p. 50-61.
297. Georgoudaki, A.-M., et al., *Reprogramming Tumor-Associated Macrophages by Antibody Targeting Inhibits Cancer Progression and Metastasis.* Cell Reports. 15(9): p. 2000-2011.
298. Pander, J., et al., *Activation of Tumor-Promoting Type 2 Macrophages by EGFR-Targeting Antibody Cetuximab.* Clinical Cancer Research, 2011. 17(17): p. 5668.
299. Heusinkveld, M. and S.H. van der Burg, *Identification and manipulation of tumor associated macrophages in human cancers.* Journal of Translational Medicine, 2011. 9(1): p. 216.
300. Coward, J., et al., *Interleukin-6 as a Therapeutic Target in Human Ovarian Cancer.* Clinical Cancer Research, 2011. 17(18): p. 6083.

301. Ries, Carola H., et al., *Targeting Tumor-Associated Macrophages with Anti-CSF-1R Antibody Reveals a Strategy for Cancer Therapy.* Cancer Cell, 2014. 25(6): p. 846-859.
302. Maloney, D.G., et al., *IDEC-C2B8 (Rituximab) Anti-CD20 Monoclonal Antibody Therapy in Patients With Relapsed Low-Grade Non-Hodgkin's Lymphoma.* Blood, 1997. 90(6): p. 2188.
303. Davis, T.A., et al., *Single-Agent Monoclonal Antibody Efficacy in Bulky Non-Hodgkin's Lymphoma: Results of a Phase II Trial of Rituximab.* Journal of Clinical Oncology, 1999. 17(6): p. 1851-1851.
304. Li, F. and J.V. Ravetch, *Inhibitory Fcgamma receptor engagement drives adjuvant and anti-tumor activities of agonistic CD40 antibodies.* Science, 2011. 333(6045): p. 1030-4.
305. Wilson, N.S., et al., *An Fcgamma receptor-dependent mechanism drives antibody-mediated target-receptor signaling in cancer cells.* Cancer Cell, 2011. 19(1): p. 101-13.

Appendices

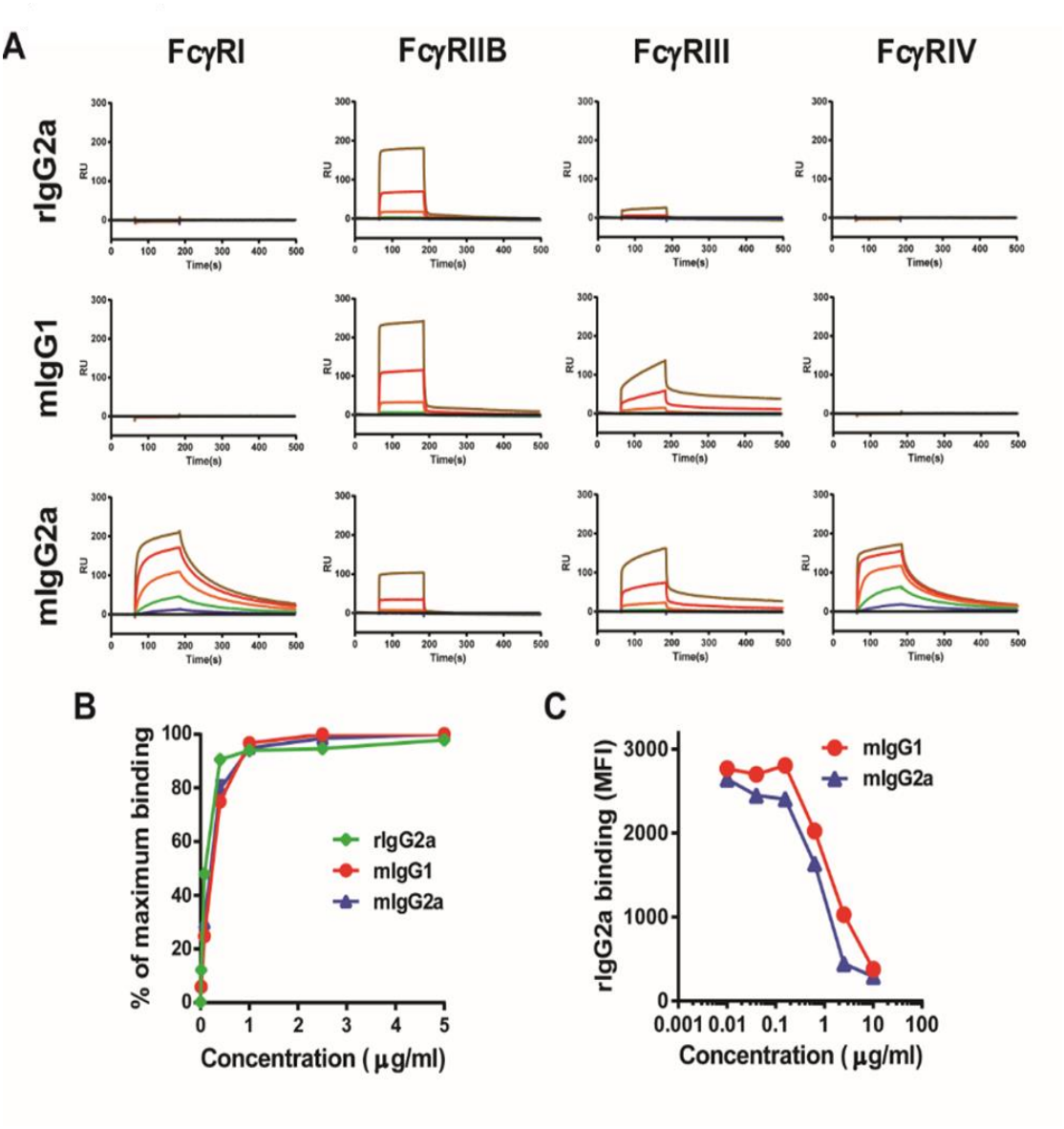

Figure 1: Surface plasmon resonance analysis on anti-4-1BB (LOB12.0) isotypes. (A) Analyses of anti-4-1BB mAb and soluble FcγR interactions were assayed using a Biacore T100 (GE Healthcare Life Sciences, Buckinghamshire, UK). Antibodies or BSA as a control were immobilized at 5000 resonance units [RU]) to the flow cells of CM5 sensor chips (GE Healthcare Life Sciences, Buckinghamshire, UK) by standard amine coupling according to the manufacturer's instructions. Soluble FcγR (R&D Systems, Abingdon, U.K.) were injected through the flow cell at 1500, 500, 166, 55, 18, and 6 nM in HBS-EP running buffer (GE Healthcare Life Sciences, Buckinghamshire, UK) at a flow rate of 30 µl/min. Soluble Fc receptor was injected for 2 min, and dissociation was monitored for 2 min. Background binding to the control flow cell was monitored automatically. Affinity constants were derived from the data by equilibrium binding analysis as indicated using Biacore Bioevaluation software (GE Healthcare Life Sciences, Buckinghamshire, UK) (This data is reproduced by the kind permission of my colleague C. Ian Mockridge). (B) A human cell line stably transfected with a construct encoding the extracellular and transmembrane region of murine 4-1BB was incubated with anti-4-1BB of mIgG1, mIgG2a isotype or with the parental rIgG2a mAb at a range of concentrations prior to staining with a PE-labelled secondary antibody. Data show mean fluorescence intensity at each concentration as a percentage of maximum. (C) Rat anti-4-1BB was mixed with mouse mIgG1 or mIgG2a anti-4-1BB mAb at the concentrations indicated, prior to incubation with a murine 4-1BB transfected cell line. Rat mAb binding was detected with an anti-rat secondary antibody and data are expressed as mean fluorescence intensity of the rat anti-4-1BB antibody relative to the concentration of competitive mouse anti-4-1BB.